An investigation of low-temperature off-axis hydrothermal systems using lithium isotopes and trace element geochemistry

by

Minasadat Seyedali
B.Sc., Amirkabir University of Technology, 2012
M.Sc., Amirkabir University of Technology, 2014

A Dissertation Submitted in Partial Fulfillment
of the Requirements for the Degree of

DOCTOR OF PHILOSOPHY

in the School of Earth and Ocean Sciences

© Minasadat Seyedali, 2020
University of Victoria

All rights reserved. This Dissertation may not be reproduced in whole or in part, by photocopy or other means, without the permission of the author.

Supervisory Committee

An investigation of low-temperature off-axis hydrothermal systems using lithium isotopes and trace element geochemistry
by

Minasadat Seyedali
B.Sc., Amirkabir University of Technology, 2012
M.Sc., Amirkabir University of Technology, 2014

Supervisory Committee

Dr. Laurence Coogan (School of Earth and Ocean Sciences)
Co-Supervisor

Dr. Kathryn Gillis (School of Earth and Ocean Sciences)
Co-Supervisor

Dr. Jay Cullen (School of Earth and Ocean Sciences)
Departmental Member

Dr. Alexandre Brolo (Department of Chemistry)
Outside Member

Abstract

This dissertation contributes to our understanding of the use of the Li-isotopic composition of seawater as a tracer of the earth system with a focus on the role of low-temperature hydrothermal systems within the lava section of the ocean crust. Experiments were conducted to study the exchange coefficient (D(Li/Ca)) and isotopic fractionation factor (α; $1000\ln(\alpha)=\Delta$) for lithium between inorganic calcite and an aqueous solution as a function of solution chemistry. These experiments show that, under the conditions used, D(Li/Ca) negatively correlates with solution H^+/Ca^{2+} ratio (and the solution pH) and Δ positively correlates with solution pH. The change in D(Li/Ca) with solution chemistry is interpreted as indicating that Li is incorporated into calcite as $LiHCO_3$, and hence depends on solution H^+/Ca^{2+}. A series of diffusion experiments were performed to test whether changes in pH led to changes in the aqueous Li speciation that would lead to changes in the relative diffusivity of the two Li-isotopes, but no such changes were observed. It is proposed that the change in Δ with changing solution pH may either reflect a kinetic or equilibrium isotope fractionation associated with changing solution chemistry. These results have important implications for interpreting the Li content of calcite that has undergone any diagenetic modification.

The Li-content and isotopic composition of rocks altered by low-temperature, off-axis hydrothermal systems in the upper oceanic crust were studied to better understand the role of these systems in controlling the Li-isotopic composition of seawater. Results of a detailed study of DSDP Holes 417A, 417D and 418A from 119 Myr Western North Atlantic Ocean basin show that the Li content of the lavas decreases with depth in the upper ~30 m below sediments while the Li-isotopic composition increases from a low value and then does not show systematic variation in deeper sections. No evidence was found to support a role for a change in mineralogy of alteration products to explain the observed variation in Li composition of lavas. There is also no evidence for the modification of the composition of hydrothermal fluid due to a mixture with sediment pore-fluid. Simple one-dimensional fluid flow and fluid-rock reaction models also cannot explain the observed variation. Instead, a model of free-circulation of seawater through the upper few tens of meters of the lavas, and leakage of modified fluid into the deeper portion of the lava pile seems to explain the observed variations best. To investigate the role of low-temperature off-axis hydrothermal systems on the Li content and isotopic composition of seawater from the Cretaceous to modern era, five DSDP/ODP holes with crustal age spanning from 13.6 to 95 Myr were studied in combination with results from previous studies. Results suggest that the average amount of Li added to the upper oceanic crust decreases, while its average Li-isotopic composition increases, from the Cretaceous to the modern. The simplest explanation for these variations may be a decrease in Li concentration and an increase in Li-isotopic composition, of seawater over this time interval.

Table of Contents

Supervisory Committee ii
Abstract iii
Table of Contents iv
List of Tables viii
List of Figures ix
Acknowledgments xvii
Dedication xviii
1. Introduction 1
1.1. Secular variation in seawater chemistry from Cretaceous to modern era 1
1.2. Proposed controls of seawater chemistry 3
1.3. Characteristics of low-temperature, off-axis hydrothermal systems 6
1.3.1. Controls and magnitude of off-axis hydrothermal circulation 6
1.3.2. Mineralogical and chemical changes of upper oceanic crust during low-temperature hydrothermal alteration 7
1.4. Li concentration and Li-isotopic composition of seawater as a tracer for the evolution of the Earth system 8
1.4.1. Record of Li concentration and Li-isotopic composition of paleo-seawater 8
1.4.2. Controls on sources and sinks of Li in seawater 10
1.4.3. Models to explain the increase in δ^7Li of seawater over the last 120 11
1.4.4. Previous work on Li elemental and isotopic exchange in off-axis hydrothermal systems 12
1.5. Thesis outline 13
1.5.1. Chapter 2: An assessment of the parameters controlling the accuracy and precision of Li-isotope measurements using single collector Inductively Coupled Plasma Mass Spectrometry (ICP-MS) 13
1.5.2. Chapter 3: The effect of solution chemistry on elemental and isotopic fractionation of lithium during precipitation of inorganic calcite 14
1.5.3. Chapter 4: Lithium and lithium isotopic exchange between seawater and off-axis oceanic crust: A case study from DSDP Holes 417A, 417D and 418A 14
1.5.4. Chapter 5: The role of low-temperature hydrothermal alteration of off-axis oceanic crust in controlling the Li concentration and isotopic composition of seawater over the past 120 Myrs 14
1.5.5. Chapter 6: Conclusions and future work 15
2. An assessment of the parameters controlling the accuracy and precision of Li-isotope measurements using single collector Inductively Coupled Plasma Mass Spectrometry (ICP-MS) 16
2.1. Introduction 16
2.2. Sample preparation 17
2.2.1. Sample digestion 17
2.2.2. Column chromatography 17
2.3. Parameters controlling the accuracy and precision of Li-isotopes measurements 19
2.3.1. Mismatching effect of acid concentration on precision and accuracy of Li isotopes measurements 19

2.3.2. Instrument condition and set up for Li-isotopic analysis 20
2.4. Impact of the matrix effect on precision and accuracy of the Li-isotopic measurements 22
2.5. NaCl wash method 24
2.5.1. Effect of NaCl wash on stability of $^{7}Li/^{6}Li$ ratio 24
2.5.2. Effect of NaCl wash on the matrix effect from Na and other trace metals 26
2.6. Summary 29
3. The effect of solution chemistry on elemental and isotopic fractionation of lithium during inorganic precipitation of calcite 30
3.1. Introduction 30
3.2. Experimental methods 32
3.2.1. Calcite growth experiments 32
3.2.2. Diffusion experiments 34
3.3. Analytical methods 34
3.4. Results 34
3.4.1. Mineralogy and fluid chemistry in calcite growth experiments 34
3.4.2. Lithium partitioning between calcite and solution 35
3.4.3. Lithium isotopic fractionation between calcite and solution 37
3.4.4. Relative diffusivity of ^{6}Li and ^{7}Li in different aqueous solutions 39
3.5. Discussion 42
3.5.1. Lithium incorporation into calcite 42
3.5.2. The lithium isotopic fractionation between calcite and solution 44
3.5.3. Li in biogenic calcite 46
3.5.4. Possible geological signals of the control of solution chemistry on Li in calcite 46
3.6. Conclusions 47
4. Lithium and lithium isotope exchange between seawater and off-axis oceanic crust: A case study from DSDP Holes 417A, 417D and 418A 48
4.1. Introduction 48
4.2. Study area and sample suite 49
4.3. Analytical methods 52
4.3.1. Silicate materials 52
4.3.2. Carbonates 54
4.3.3. X-Ray Diffraction (XRD) 54
4.4. Results 55
4.4.1. Lithium abundance in bulk samples 55
4.4.2. Lithium isotopic composition of bulk samples 57
4.4.3. Sub-sample analyses 59
4.5. Discussion 66
4.5.1. Controls on the behaviour of Li in Holes 417A, 417D and 418A 69
4.6. Conclusions 80
5. The role of low-temperature hydrothermal alteration of the upper oceanic crust in controlling the Li concentration in, and isotopic composition of seawater over the past 120 Myrs 81
5.1. Introduction 81
5.2. Study areas and sample suite 83

5.3. Results ... 86
5.3.1. Lithium abundances in lava samples ... 86
5.3.2. Lithium isotopic composition of lava samples ... 88
5.4. Discussion ... 89
5.4.1. Effect of crustal age, alteration temperature and sedimentation rate on Li uptake in off-axis oceanic crust ... 89
5.4.2. Lithium isotopic composition of bulk altered oceanic crust ... 93
5.4.3. Lithium-isotopic fractionation factors between altered crust and seawater over the past 120 Myrs ... 95
5.5. Conclusions ... 103
6. Conclusions ... 105
6.1. Summary and significance of findings ... 105
6.1.1. Sources of uncertainty during measurement of Li-isotopes using ICP-MS ... 105
6.1.2. The effect of solution chemistry on Li partitioning and isotopic fractionation between inorganic calcite and aqueous solution ... 105
6.1.3. Lithium concentration and isotopic composition of the upper lava section of the oceanic crust ... 106
6.1.4. The effect of low-temperature off-axis hydrothermal alteration within the oceanic crust in controlling the Li concentration and isotopic composition of seawater ... 106
6.2. Future work ... 107
6.2.1. Decoupling the effect of Ca^{2+} concentration and pH of solution on Li partitioning between inorganic calcite and solution ... 107
6.2.2. Effect of temperature on Li partitioning and isotopic fractionation between inorganic calcite and solution ... 107
6.2.3. Mechanism of Li-isotope fractionation between inorganic calcite and solution ... 108
6.2.4. Identifying the main controls on changes in Li uptake into the upper lava section of the oceanic crust ... 109
Bibliography ... 110
Appendix A: Additional analytical details for Chapter 3 ... 127
A.1. Sample preparation for chemical analysis ... 127
A.2. ICP-MS elemental analysis ... 127
A.3. Li-isotope analysis using ICP-MS ... 128
A.4. Total alkalinity measurements using an automated titrator ... 129
A.5. SEM images ... 130
A.6. XRD analysis results ... 134
Appendix B: Modeling of the evolution of the Li concentration and isotopic composition of altered oceanic crust during interaction with hydrothermal fluid at low temperatures ... 145
Appendix C: Additional analytical details ... 152
C.1. Lava samples ... 152
C.1.1. Crushing samples ... 152
C.1.2. Weighing samples ... 152
C.1.3. Sample dissolution ... 152

C.1.4. Sample preparation for trace and Li-isotopes analysis..... 153
C.2. Carbonate samples..... 155
C.2.1. Consumables required..... 155
C.2.2. Sample preparation for trace and Li-isotopes analysis..... 155
C.2.3. Column chromatography..... 156
C.2.3.1. Preparation of sample loader..... 156
C.2.3.2. Washing and conditioning columns..... 157
C.2.3.3. Loading samples and elution..... 157
C.3. Cleaning Teflon wares..... 158
Appendix D: Supplementary Tables..... 159

List of Tables

Table 2.1. The amount of Li collected in the pre- and post- aliquots collected for reference rock standards used in this study..... 18

Table 2.2. Instrumental conditions for Li-isotopic analyses..... 22

Table 2.3. The composition of IRMM-016 solutions used to test the NaCl washing method on the matrix effect. 27

Table 4.1. Summary of the key characteristics of DSDP Holes 417A, 417D and 418A.. 50

Table 4.2. Constituent parts of altered lava samples and proportion of detected minerals 61

Table 4.3. Averages of δ^7Li and Li added to the shallow and deeper intervals of oceanic crust in Holes 417A, 417D and 418A..... 68

Table 4.4. Parameters used to model Li concentration and isotopic composition of lava samples..... 74

Table 5.1. Key characteristics of DSDP/ODP sites for which Li-isotopic data for lavas exist. 85

Table 5.2. Lithium isotopic composition of altered crust in all studied areas. 94

Table 5.3. Properties of different study areas in the Troodos ophiolite..... 99

Table 5.4. Model results and parameters used to extract the Li-isotopic fractionation factor between seawater and altered oceanic crust. 101

Table A.1. Instrumental conditions for Li-isotope analyses. 129

Table B.1. Parameters used to calculate the diffusion reaction length and length of advection for Li..... 147

List of Figures

Figure 1.1. Mg^{2+}, Ca^{2+} and SO_4^{2-} concentrations of seawater reported by Horita et al. (2002) and Lowenstein et al. (2003) versus crustal age. Data show increasing trends of Mg^{2+} and SO_4^{2-} and decreasing trend of Ca^{2+} concentrations of seawater over the past 120 Myrs. 2

Figure 1.2. Cartoon of the global scale of hydrothermal fluid circulation through the upper oceanic crust. High-temperature hydrothermal fluid circulation is focused on the ridge axis, and low-temperature hydrothermal fluid circulation occurs away from the ridge axis, on the ridge flanks. The magnitude of fluid circulation decreases as the distance from the ridge axis increases and sediment thickness increases (from Coogan and Gillis, 2018)..... 6

Figure 1.3. Lithium isotopic composition of seawater over the past 120 Myrs. Circle symbols show the Li isotopic composition of seawater based on the Li isotopic composition of bulk foraminifera (Misra and Froelich, 2012) and triangles show the Li isotopic composition of seawater based on leaching of bulk sediments to extract the carbonate fraction (Pogge Von Strandmann et al., 2013; Lechler et al., 2015). In both cases the carbonate is assumed to have the same δ^7Li as the seawater it grew from. This data suggests an ~9 ‰ increase in the Li isotopic composition of seawater over the past 90 Myrs. 9

Figure 1.4. Cartoon of the global Li cycle showing the large uncertainty on the Li fluxes and isotopic composition of sources and sinks of Li to the seawater based on previously published data. f: flux; LT: low temperature; HT: high temperature; HF: hydrothermal fluid; sed: sediments; τ: residence time of Li in seawater. Sources of data: Stoffyn-Egli and Mackenzie (1984); Seyfried et al. (1984); Huh et al. (1998); Teng et al. (2004); Chan et al. (2006); Tomascak et al. (2008); Misra and Froelich (2012) and Gale et al. (2013). 11

Figure 2.1. The fraction of Li (molar) and Na (molar) in aliquots collected for column calibrations using a mixture of basalt samples. The Li peak is collected between 25 g and 75 g of eluant released. The Li recovery is higher than 99 %, and the amount of Na in the Li peak is nearly zero. 18

Figure 2.2. (a) The effect of acid concentration of matrix of solutions on ^{7}Li signal intensity and (b) measured ^{7}Li/^{6}Li of IRMM-016. The ^{7}Li signal intensity decreases with increasing concentration of nitric acid. The green circle is a 5 ppb IRMM-016 in 2% HNO_3, however, the 2% HNO_3 used to dilute this sample was made from a different batch of 2 % HNO_3 than the standard solution (open circles). Error bars showing the Relative Standard Deviation (RSD) of Li isotope measurements which accounts for minimum uncertainty of the measurements. 20

Figure 2.3. Plot of the room temperature in the ICP-MS lab over the course of three ICP-MS sessions. The green and red arrows show the time when the instrument was turned on and off respectively. About 1°C increase and decrease in the room temperature occurs during 80 minutes after turning the instrument on and off, respectively. 21

Figure 2.4. The $^{7}Li/^{6}Li$ of 10 ppb IRMM-016 with Li/Na ratio between 0.3 to 7.5 M/M versus run number. The Na/Li ratio ≤ 7.5 M/M in samples do not influence the precision and accuracy of the measurements and do not lead to significant matrix effect. 23

Figure 2.5. The Na/Li ratio of international reference rock solutions which were prepared for Li isotope analysis with 10 ppb Li concentration. The Na/Li ratio is less than 2 M/M for all international reference rock solutions. 24

Figure 2.6. (a) The ^{7}Li signal intensity of blank 2 % HNO_3, 10 ppb IRMM-016 before and after running the 5 wt% NaCl solution at run number 27. The NaCl washing method reduces the Li count rate of the background. (b) The $^{7}Li/^{6}Li$ ratio of IRMM-016 versus the run number before and after introducing the 5 wt% NaCl solution to the ICP. A large drift introduces after running the NaCl solution in $^{7}Li/^{6}Li$ ratio. (c) The $\delta^{7}Li$ of 10 ppb IRMM-016 solutions versus the run number showing that the precision of measurements is improved by ~0.5 ‰. 26

Figure 2.7. The $^{7}Li/^{6}Li$ ratio of 6 ppb IRMM-016 solutions with variable compositions versus the run number. The labeled numbers are showing the total molar concentrations of solutions (excluding Li). The 5 wt% NaCl solution was run at the beginning of the run (run number 1). The precision of measurements is disturbed after running the samples with Na ≥ 2.2 μM (Na/Li ≥ 2.4 M/M), showing the significant effect of Na in inducing matrix effects and inefficiency of the NaCl washing method in eliminating the induced matrix effect by increasing the Na content of matrix. 28

Figure 2.8. The Li isotopic composition of international reference rocks is plotted against their published values. Error bars showing 2 standard error of measurements. For an updated list of published values see http://georem.mpch-mainz.gwdg.de). 29

Figure 3.1. The (a) Li/Ca exchange coefficient, and (b) Li partition coefficient plotted against the pH of the final solution in the experiments. Symbol colour (this study and Fügar et al., 2019) reflects the solution Ca content. Large and small symbols, connected by a line, show the final and initial solution pH respectively; the pH variation was less than 0.1 unit for samples shown as a single symbol. Because of the experimental design the solution pH and Ca content inversely correlate. Uncertainties in the y-axis are smaller than the symbols. The data point surrounded by an open black circle has a much higher Ca concentration in its final solution compared to the other high-pH (≥ 9) experiments, which I interpret as due to contamination by calcite during separation of the solution from the calcite. The solid line shows a model for incorporation of Li in calcite as $LiHCO_3$ (see text for details). 36

Figure 3.2. The Li/Ca exchange coefficient plotted against the duration of experiments (left) and Li content of solution at the end of experiments (right). Symbol colour reflects the Ca content of solutions at the end of experiments. Both plots show that variation of the Li/Ca exchange coefficient is independent of the duration of experiments and Li content of solution. The data point surrounded by an open black circle has a much higher Ca concentration in its final solution compared to the other high-pH (≥ 9) experiments, which I interpret as due to contamination by calcite during separation of the solution from the calcite. 37

Figure 3.3. Variation in measured difference in Li isotopic composition of calcite and the solution it grew in (Δ) with solution pH. Symbol colour reflects the solution Ca content (this study only). Large and small symbols connected by a line show the final and initial solution pH respectively; the pH variation was less than 0.1 unit for samples shown as a single symbol. The data point surrounded by an open black circle has a much higher Ca concentration in its final solution compared to the other high-pH (≥ 9) experiments, which I interpret as due to contamination by calcite during separation of the solution from the calcite. 38

Figure 3.4. The measured Li isotopic fractionation factor (Δ) between calcite and the final solution plotted against the duration of experiments (left) and Li content of solution at the end of experiments (right). Symbol colour reflects the Ca content of solutions at the end of experiments. Both plots show that the Li isotope fractionation factor is independent of duration of experiments and Li content of solution. The data point surrounded by an open black circle has a much higher Ca concentration in its final solution compared to the other high-pH (≥ 9) experiments, which I interpret as due to contamination by calcite during separation of the solution from the calcite. 39

Figure 3.5. Li-isotopic composition of the source solution in the diffusion experiments as a function of the fraction of Li remaining in the source (f_{Li}). The curves are fit through data from each experimental time series performed at a different pH using a non-linear model (Eq. 3.3) weighted according to the uncertainty on the Li-isotope data (Supplementary Table D.1.2). Data for experiments in a DI matrix are from Richter et al. (2006) performed at 75°C (versus ~21°C in this study). 41

Figure 3.6. Calculated approximate equilibrium constant (K^*_{eq}) based on measured concentrations for Li incorporation into calcite as the Li_2CO_3, $LiNaCO_3$ and $LiHCO_3$ components (models A, B and C discussed in the text) plotted against the pH of the final solution in the experiment for both my study and that of Füger et al. (2019) which agree reasonably well with one another despite different experimental designs. Only for Li incorporation as $LiHCO_3$ is the calculated equilibrium constant similar for all experiments meaning that this is a plausible substitution mechanism and the others are not. The open symbols show a sample that has a higher Ca concentration in its final solution compared to the other high-pH (≥ 9) experiments, almost certainly due to calcite contamination during the separation of the solution from the precipitated calcite. 43

Figure 4.1. Cartoon showing the location of Holes 417A, 417D and 418A relative to each other. The stratigraphy of the drill holes and sediment types are taken from the DSDP preliminary reports (Donnelly et al., 1979a and Donnelly et al., 1979b). The gaps in the sediment sections are regions without recovery. 51

Figure 4.2. Li vs. Y concentration of lava samples. The black line shows a regression through MORB glass data interpreted as the magmatic differentiation trend (Gale et al., 2013). The altered lavas fall above the line, indicating Li uptake during low-temperature hydrothermal alteration of the upper lava section of the ocean crust. Numbers in brackets is the number of samples..... 56

Figure 4.3. Lithium concentration versus depth below sediments in Holes 417A, 417D and 418A. The solid symbols represent basalt samples. Basalt sample lithologies are shown with different colours and open circles show sediments. Open symbols with black

rims identify previously published data (triangles are composite samples and squares are basalt samples; Bouman et al., 2008). The gray band shows the range of Li concentrations of fresh MORBs at these sites. In general, Li concentration decreases from the top of crust to deeper levels. An elevated Li concentration of massive flow samples at the deepest levels of the Hole 418A might be due to longer residence time of hydrothermal fluid and hence longer fluid-rock interaction in low-permeable massive basalts with small input/output hydrothermal fluid flux. 57

Figure 4.4. Lithium isotopic composition versus depth below sediments in Holes 417A, 417D and 418A. The solid symbols represent basalts. Basalt sample lithologies are shown with different colours and open circles show sediments. Open symbols with black rims are taken from previously published data (triangles are composite samples and squares are basalt samples; Bouman et al., 2008). The gray band shows the range of Li isotopic compositions of fresh MORBs. In general, Li-isotopic composition increases from the uppermost part of crust to ~30 m below sediments, then fluctuates in deeper levels. I suggest that a high Li-isotopic composition of samples at deep levels (deeper than 475 m blow sediments) of the Hole 418A might be due to interaction of rocks with a highly evolved hydrothermal fluid with high Li-isotopic composition. Horizontal error bars represent ±2SDE on replicate analysis of δ^7Li of samples. 58

Figure 4.5. Lithium isotopic composition versus Li concentration at the Holes 417A, 417D and 418A. The solid symbols represent basalt samples and open circles show sediments. Symbols with black rims are taken from previously published data (triangles are composite samples and squares are basalt samples; Bouman et al., 2008). Vertical error bars represent ±2SDE on replicate analysis of δ^7Li of samples. 59

Figure 4.6. Calculated proportions of each secondary phase determined using XRD and chemical analysis data for the sub-samples. 62

Figure 4.7. XRD patterns for lava sample 418A-33R-2-14-17. Shifts in basal peak positions of groundmass (GM) and pseudomorph after plagioclase (psd plg) sub-samples after ethylene glycol vapor treatment are shown by arrows. The two sub-samples show different basal peak positions, the 0.11 nm difference in d-spacing indicates the presence of two different clay minerals (Supplementary Table D.2.6). 62

Figure 4.8. The lithium isotopic composition of three lavas with their separated parts versus their lithium concentration. It depicts that different altered parts (except the groundmass of 418A-33-2R-14-17 which is mainly identified fresh-see text for detail) of the same lava have the same lithium-isotopic composition regardless of the amount of lithium they have taken up. 63

Figure 4.9. Al versus Li contents of calcite samples hosted in the lava samples from variable depths in the Hole 417A. Two samples with the highest Al contents are assumed to be contaminated with silicates. Duplicate analysis of one sample (417A-29R-4-122-125) shows heterogeneity in the Li content in the picked chips of carbonate. Numbers next to each symbol shows the depth below sediment (m) of each sample. 66

Figure 4.10. Li-isotopic composition versus reciprocal Li concentration. Dredge samples and samples from Holes 504B/896A from 5.9 to 6.8 Myr old oceanic crust (Chan et al., 1992 and Chan et al., 2002) which are assumed to have interacted with modern-like

seawater (180 ppb Li and δ^7Li of 31 ‰) show that δ^7Li becomes heavier as Li is added to the rock. Fitting a line to published data starting from fresh MORB gives end-member altered rock δ^7Li of 16 ‰ and 24 ‰, for dredged samples and Holes 504B/896A samples, respectively. These suggest apparent Li isotopic fractionation factors of 15 ‰ and 7 ‰, respectively ($\Delta_{SW\text{-}lava}=\delta^7Li_{SW}-\delta^7Li_{lava}$). Observed correlation between 1/Li and δ^7Li of samples from Holes 504B/896A and dredge samples does not exist in samples from Holes 417A, 417D and 418A. Symbols with black rims are taken from published data (triangles are composite samples and squares are lava samples; Bouman et al., 2008). Open diamond symbol represents fresh MORB. Vertical error bars represent ±2SDE on replicate analysis of δ^7Li of samples..... 67

Figure 4.11. Depth distribution of clay minerals at Holes 417A, 417D and 418A is shown with different colours (right side of each panel). The vertical lines show the depth range for each clay mineral type and the horizontal lines on each vertical line identify the depths where each mineral was identified (published works; compiled mineral assemblage data from Holes 417A, 417D and 418A are reported by Coogan and Gillis, 2018). Comparison of the mineralogy with the δ^7Li of samples shows that variation of δ^7Li with depth is not obviously correlated with the type of secondary clay minerals. Open symbols with black rims are taken from previously published data (triangles are composite samples and squares are lava samples; Bouman et al., 2008). 70

Figure 4.12. Models (solid lines) for the evolution of Li concentration (top row) and Li-isotopic composition (bottom row) for three different fluid fluxes and four different N_D during vertical fluid flow. The Kd_{Li} and $\Delta_{s\text{-}f}$ are assumed to be constant at 300 and -25 ‰, respectively. Symbols show the measured Li concentration and δ^7Li of lava samples from Holes 417A, 417D and 418A. There does not seem to be a good fit for both Li concentration and δ^7Li of all three cores. Symbols with black rims are from previously published data (triangles are composite samples and squares are lava samples; Bouman et al., 2008). 73

Figure 4.13. Models of the evolution of Li concentration of lava samples during interaction with hydrothermal fluid flowing laterally at four different porosities and corresponding fluid fluxes with variable N_D of 0.1, 1, 10 and 100 (central panel; for model parameters and values see Table 4.4). The models assume a decrease in fluid flux and crustal porosity with depth (right panel). The general variation in Li concentration of lava samples with depth for Hole 417A can be explained with a model at a lateral distance of 20 m, if fluid fluxes decreases from 2 to 0.2 x10^7 kg/m^2 from top to ~60 m below sediments and a N_D of 10 (brown dashed line; left panel). Hole 417D and 418A are 450 and 6500 away from Hole 417A, respectively (lateral distances of the three holes relative to each other are marked on the plots of the central panel). At lateral location of 417D (~470 m), only a model with N_D of 0.1 (orange dashed line) shows slight variation in Li concentration at different fluid fluxes which does not fit the data from this hole. Gray dashed line shows predicted Li concentration for any N_D between 0.1 to 100 at Hole 418A. No model can explain the data from Holes 417D and 418A regardless of N_D and fluid flux (left panel). Symbols with black rims are from previously published data (triangles are composite samples and squares are lava samples; Bouman et al., 2008). .. 76

Figure 4.14. Models of the evolution of δ^7Li of lava samples during interaction with hydrothermal fluid flowing laterally at four different porosities and corresponding fluid

fluxes with variable N_D of 0.1, 1, 10 and 100 (Central panel; for model parameters and values see Table 4.4). The models assume a decrease in fluid flux and crustal porosity with depth (right panel). The model which explains Li concentration from Hole 417A (with N_D of 10 at lateral distance of 20 m) cannot explain δ^7Li of lava samples from this hole. Hole 417D and 418A are 450 and 6500 away from Hole 417A, respectively (lateral distances of the three holes relative to each other are marked on the plots of the central panel). At lateral location of 417D (~470 m), only a model with N_D of 0.1 (orange dashed line) shows variation in δ^7Li at different fluid fluxes which does not fit the data from this hole. Gray dashed line shows predicted δ^7Li for any N_D between 0.1 and 100 at Hole 418A. No model can explain the δ^7Li data from Holes 417A, 417D and 418A, regardless of N_D and fluid flux (left panel). Symbols with black rims are from previously published data (triangles are composite samples and squares are lava samples; Bouman et al., 2008). Horizontal error bars represent ±2SDE on replicate analysis of δ^7Li of samples..... 77

Figure 4.15. Calculated range of δ^7Li of hydrothermal fluid based on δ^7Li of lava samples from deeper than 30 m below sediments in Hole 417A, and assuming a constant Li-isotopic fractionation factor between altered crust and seawater of -22 ‰ throughout the entire core (gray shaded area). Black symbols show the measured δ^7Li of calcite samples from veins in Hole 417A. If samples were precipitated at pH~7, the δ^7Li of hydrothermal fluid would be ~7 ‰ heavier than the calcite (open symbols). Two symbols shown at the same depth are duplicates from the same sample, possibly suggesting heterogeneity of δ^7Li of calcite samples. 79

Figure 5.1. Carbonate formation temperature (circles) and estimated bottom seawater temperature (blue line) versus age of oceanic crust. Carbonate formation temperatures were obtained using the oxygen isotopic composition of precipitated carbonates (using the Kim and O'Neil (1997) thermometer). The average of carbonate temperatures at each age is colour coded based on the sedimentation rate. The estimate of bottom seawater temperature is from Cramer et al. (2011)..... 82

Figure 5.2. Approximate location of each studied site is shown on the map. Green stars show sites included in this study and red stars show those sites for which there is published data. 84

Figure 5.3. Li vs. Y concentration of lava samples. The black line shows a regression through MORB glass data interpreted as the magmatic trend for fresh glass (Gale et al., 2013). The altered lavas from most of the holes fall above the line, indicating Li uptake during low-temperature hydrothermal alteration. The number in brackets is the number of data. * Coogan et al. (2017); ** Gao et al. (2012). Published data for Holes 417A, 417D, 418A (Bouman et al., 2008), 504B/896A (Chan et al., 2002) and dredged samples (Chan et al., 1992) are not included in this plot due to lack of Y data. 86

Figure 5.4. Lithium added (ΔLi) to the lava samples versus depth below sediments for compiled data (with available Li and Y data; gray symbols) and sites studied here (Table 5.1; black symbols). Red crosses represent the average of ΔLi and the red solid lines indicate the depth interval that the average was calculated for. 87

Figure 5.5. Lava Li vs. K_2O (bottom) and Li vs. Rb (top) for Mesozoic (left) and Cenozoic (right) drill sites. There is no obvious correlation between Li and Rb or K_2O although some individual areas (e.g., Holes 417A, 417D and 418A; Chapter 4) do show

strong correlations between different proxies for extent of low-temperature hydrothermal alteration. The average MORB glass composition is from Gale et al. (2013). Number in brackets is the number of data.* Coogan et al. (2017). 88

Figure 5.6. Lava lithium isotopic compositions versus depth below the sediment-lava contact for Mesozoic (left) and Cenozoic (right) cores. The light gray shaded area shows the average lithium isotopic composition of fresh MORBs (3.7±0.4 ‰; Tomascak et al., 2008). *Coogan et al. (2017). **Gao et al. (2012). *** Chan et al. (2002). **** Chan et al. (1992). 89

Figure 5.7. Carbonate formation temperature versus depth below sediments at study areas with available Li-isotopic composition. Oxygen-isotopic composition of precipitated carbonates is used to calculate the carbonate formation temperature (using the Kim and O'Neil (1997) thermometer), which is assumed as temperature of alteration of lava samples (e.g., Gillis and Coogan, 2011; Gillis et al., 2015). Cretaceous study areas have 15°C to 20°C higher alteration temperatures compared with Cenozoic sites (except young oceanic crust from Holes 1256D, 504B and 896A which have experienced anomalously high temperatures of alteration due to restriction of fluid penetration into the crust as a result of rapid sedimentation rate (504B/896A)). 91

Figure 5.8. Calculated amount of Li added to the upper 100 m of the oceanic crust versus crustal age colour coded by alteration temperature (left) and sedimentation rate (right) for the compiled dataset (smaller symbols) and this study (larger symbols). The data are from: (a and d) upper 100 m below sediments, (b and e) averages at each study area, (c and f) averages of added Li (both compiled and this study) in 5 Myr crustal age intervals, showing positive correlation (r^2=0.3) between Li uptake into the oceanic crust and crustal age. Error bars on the Y-axis represents the SDE of the data. 92

Figure 5.9. (a) Weighted average Li-isotopic composition of bulk altered upper lava section of oceanic crust (δ^7Li_{crust}; temperature colour coded circles) and δ^7Li of seawater for the last 120 Myr (gray symbols; Hathorne and James, 2006; Misra and Froelich, 2012; Pogge Von Strandmann et al., 2013; Lechler et al., 2015) versus the crustal age. The δ^7Li of bulk altered crust is obtained based on weighted averages of δ^7Li of lava samples at each study area, and the averages ΔLi are used to weight the isotope data. (b) The apparent Li-isotopic fractionation factors ($\Delta_{sw\text{-}crust}$) versus the inverse of alteration temperature (crustal age colour coded). The calculated $\Delta_{sw\text{-}crust}$ are the difference between the δ^7Li of seawater and bulk altered upper ocean crust. The δ^7Li of Cretaceous seawater is assumed 21 ‰. Vertical error bars are 2SDE and they are calculated following the error propagation method. 95

Figure 5.10. Lava δ^7Li versus Li^{-1} for each study area. A mixing model (regression line) is shown based on the assumption that lavas compositions are binary mixtures of fresh rock (green circle) and secondary minerals. This model is used to extract the lithium-isotopic composition of altered crust end-member (red star). Only samples with lithium contents higher than fresh MORB are used to define the mixing line (black symbols). Linear kinetic models (pink curves) for two different N_D values are tested against the data at studied sites where variation in reacting fluid composition is possible (see Table 5.3 for model parameters and Chapter 4 for mathematics of the model). Published data is from: Chan et al. (1992), Chan et al. (2002), Bouman et al. (2008), Gao et al. (2012) and

Coogan et al. (2017). For the Dredged samples (Chan et al., 1992) only the transact basalts from the Mid-Atlantic Ridge older than 10 Myr (10 to 46 Myr) are included. These samples are old enough that their δ^7Li is overprinted by modern seawater composition. 97

Figure 5.11. Li concentration (left) and δ^7Li (right) of lava samples from four regions of the Troodos ophiolite versus depth below sediment. The Li and δ^7Li profiles are similar in all four studied regions despite their having different lithologies and sedimentation histories. Data is from Coogan et al. (2017). 99

Figure 5.12. The estimated Li-isotopic fractionation factor ($\Delta_{sw\text{-}crust}$) between the off-axis lava section of the oceanic crust and seawater using a binary mixing (triangles) and a linear kinetic model (i.e., vertical fluid flow; circles) versus the crustal age. The data is colour coded with alteration temperatures. There is no correlation between either crustal age or alteration temperature. Vertical error bars at each study area is representative of 2SDE. 103

Figure A.1. The measured alkalinity plotted against the calculated alkalinity of solutions which were simple mixtures of $NaHCO_3$ and $CaCl_2$. The measurements were made immediately after making the solutions. The dashed line shows 1:1 line and it demonstrates good agreement between measured and expected values. The maximum difference between the measured and calculated alkalinity is 14.0 % and the average is 4.7 %. 129

Figure B.1. Cartoon shows the conceptual model for the evolution of Li concentration and isotopic composition of hydrothermal fluid (*HF*) and altered mid ocean ridge basalt (*alt-BR*; *MORB* stands for fresh mid ocean ridge basalt). Mass (*M*) of basalt is assumed to stay unchanged but mass of hydrothermal fluid flowing through the fractures is assumed to decrease with depth. Fluid flows through fractures between parallel slabs of rocks with a thickness of *b*. Li exchanges between rock (with permeability of $K_{basalt,1}$ to $K_{basalt,n}$) and fluid while the linear kinetic processes of Li exchange rate and advection are limiting the exchange process. 148

Acknowledgments

I would like to express my most sincere gratitude to my supervisors, Dr. Laurence Coogan and Dr. Kathryn Gillis whose their consistent support, guidance, continued patience and encouragement were invaluable to me throughout this research. I would also like to specially thank Jody Spence, for his extensive assistance and guidance during lab works and operating the ICP-MS.

Finally, I wish to express my deepest appreciation to the dedicated support and great love of my mother, Mahboobeh; my brother, Mohsen and my husband, Babak. They kept me going on and this work would not have been possible without them.

Dedication

This dissertation is dedicated to the memory of 176 passengers of the Flight PS752 which was shot down on January 8, 2020. This tragedy caused insurmountable loss to the scientific community.

1. Introduction

1.1. Secular variation in seawater chemistry from Cretaceous to modern era

Over the course of Earth history, the chemistry of the ocean has evolved. The records of change in seawater chemistry over time provide important insights into the operation of the Earth System. These records come from numerous sources. The mineralogy of marine evaporites, and composition of fluid inclusions trapped in halite in these evaporites, provide information about paleo-seawater composition and aid our understanding of the chemical evolution of ancient seawater (Timofeeff et al., 2000; Lowenstein et al., 2001; Brennan et al., 2013). In addition, the composition of preserved carbonate minerals of biomineralizing organisms (e.g., Ivany et al., 2004; Fantle, 2010) and abiogenic hydrothermally precipitated calcium carbonate veins in low-temperature, off-axis oceanic crust (e.g., Coggon et al., 2010) were used to reconstruct the composition of paleo-seawater and records of seawater major, trace and isotopic compositions over time.

There is a general agreement on the patterns of the variation of the major ion chemistry of seawater, however, there is less certainty about the mechanisms that control the compositional changes. There are six ions which comprise the major composition of seawater: Na^+, K^+, Mg^{2+}, Ca^{2+}, Cl^- and SO_4^{2-} (Lyman and Fleming 1940; Pilson, 1998). The total alkalinity (TA) can be defined as a difference between concentration of proton acceptors and proton donors (Dickson, 1981). The charge difference between major cations and anions is defined as total alkalinity which also comprises largely the dissolved inorganic carbon species (HCO_3^-, CO_3^{2-}), borate ion ($B(OH)_4^-$) and hydroxide ion (OH^-):

$$TA=[Na^+]+[K^+]+2[Ca^{2+}]+2[Mg^{2+}]-[Cl^-]-2[SO_4^{2-}]=[HCO_3^-]+2[CO_3^{2-}]+[B(OH)_4^-]+[OH^-]-[H^+] \quad \text{Eq. 1.1}$$

Total alkalinity of the modern ocean is ~2.2 mM and it cannot change dramatically (e.g., Turchyn and DePaolo, 2019). This is because carbonate and bicarbonate ions provide the majority of the alkalinity of the ocean and a dramatic change in total alkalinity would lead to a major change in dissolved CO_2 concentration of ocean ($CO_2+H_2O \leftrightarrow HCO_3^-+H^+ \leftrightarrow CO_3^{2-}+2H^+$). This would result in a large change in the ocean pH and eventually the concentration of atmospheric CO_2, which would lead to major change in the Earth's surface temperature in a way that it has never been recorded (Ridgwell and Zeebe, 2005). Hence, explanation of any changes in the major ion composition of seawater is linked to the ocean's alkalinity and the global C-cycle (Zeebe, 2012).

During the past 120 Myrs, studies suggest that the Mg^{2+} and SO_4^{2-} concentration of seawater has increased from ~36 to 53 mM and ~8 to 28 mM (Horita et al., 2002; Lowenstein et al., 2003; Figure 1.1), respectively, while the Ca^{2+} concentration of seawater has decreased from ~30 to 10 mM (Horita et al., 2002; Lowenstein et al., 2003;

Figure 1.1). There is a general consensus that there has been little change in concentration of K^+ and Cl^-, with these elements remaining close to the present seawater concentrations, 10 mM and ~546 mM, respectively (e.g., Horita et al., 2002; Demicco et al., 2005; Lowenstein et al., 2014). Constant K^+ concentrations over time is inferred from K^+/Br^- concentrations of fluid inclusions and the assumption that the Br^- concentration of seawater does not change due to its long residence time in seawater (Horita et al., 2002; Lowenstein et al., 2003, 2014). The constant seawater Cl^- concentration is also assumed to be due to its long residence time (≥100 Myr; Horita et al., 2002; Lowenstein et al., 2003, 2014). Therefore, assuming the total alkalinity of seawater is constant, the Na^+ concentration of seawater is determined through charge balance (Eq. 1.1) showing that it was lower in the Cretaceous compared with modern era (Horita et al., 2002; Lowenstein et al., 2001; Turchyn and DePaolo, 2019). In addition to change in the major element composition of seawater over the past 120 Myrs, studies have shown that the $^{87}Sr/^{86}Sr$ ratio of seawater has also increased from the Cretaceous to the modern era (Veizer et al., 1999).

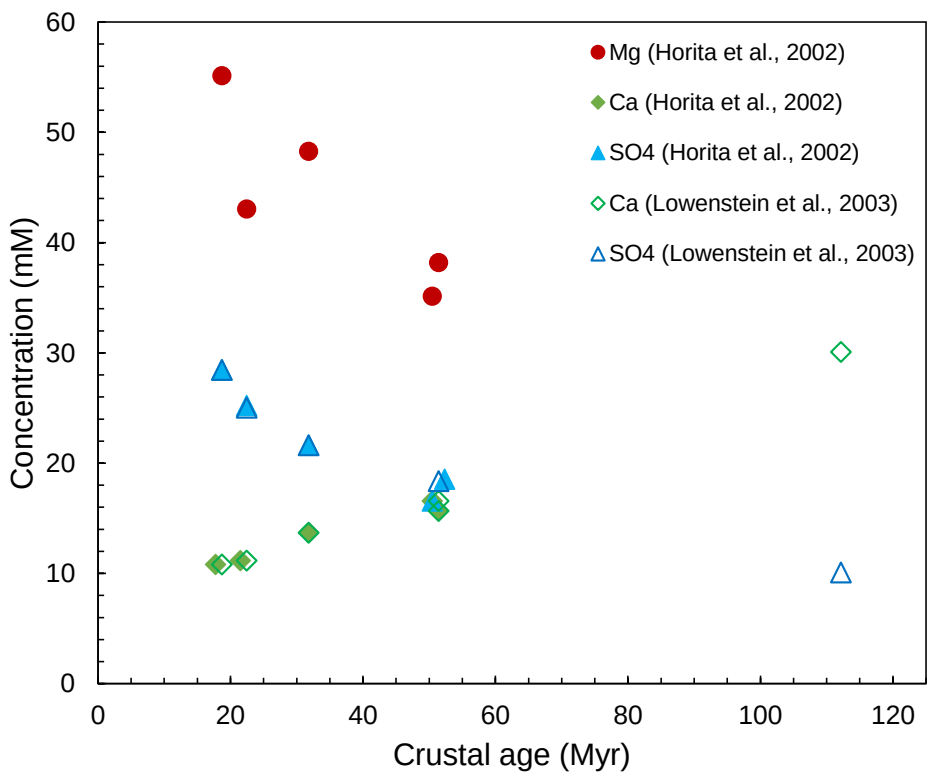

Figure 1.1. Mg^{2+}, Ca^{2+} and SO_4^{2-} concentrations of seawater reported by Horita et al. (2002) and Lowenstein et al. (2003) versus crustal age. Data show increasing trends of Mg^{2+} and SO_4^{2-} and decreasing trend of Ca^{2+} concentrations of seawater over the past 120 Myrs.

To explain the observed variation in the composition of seawater over the past 120 Myrs, different controlling processes have been proposed, including change in the seafloor spreading rate at mid-ocean ridges (MORs; e.g., Spencer and Hardie, 1990; Ivany et al., 2004; Coggon et al., 2010), the global dolomitization rate (Holland and Zimmermann, 2000; Holland, 2005), the rate of continental weathering and

sedimentation (Berner et al., 1983; Raymo and Ruddiman, 1992; Turchyn and Schrag, 2004, 2006; Fantle, 2010), and conditions within the low-temperature hydrothermal system hosted in the upper basaltic section of off-axis ocean crust (Demicco et al., 2005; Higgins and Schrag., 2015). The proposed hypotheses to reconstruct the composition of paleo-seawater are reviewed in the following sections.

1.2. Proposed controls of seawater chemistry

The observed variation in the composition of seawater from the Cretaceous to modern era is consistent with the estimated variation in global sea level over this time (e.g., Turchyn and DePaolo, 2019). Using seismic stratigraphy data, it was estimated that sea level was higher during the Cretaceous than today (Vail et al., 1977; Haq et al., 1987). The global sea level depends on topography of both continental and oceanic crust (Vail et al., 1977; Bradley, 2011). For example, continental collisions lead to mountain building events and cause thickening of the continental crust. Continental collisions compact the continents laterally, expanding the area of ocean basins (e.g., Turchyn and DePaolo, 2019). As the oceanic crust expands, it gets older and its depth increases which leads to lowering of the sea level (e.g., Bradly et al., 2011). The opposite of continental collision happens when continents are rifting and ocean basins are opening. During continental rifting, oceanic crust is young, and its depth is shallow, which leads to increased sea level (e.g., Bradly et al., 2011). Low Mg^{2+} and SO_4^{2-}, and high Ca^{2+} concentration of seawater during the Cretaceous are associated with high sea level, which is thought to be due to the breakup of Pangea, formation of the Mid-Atlantic Ridge during the Mesozoic and formation of Large Igneous Provinces in the Cretaceous (Seton et al., 2009). The observed increase in Mg^{2+}, SO_4^{2-} and decrease in Ca^{2+} concentrations of seawater during the late Cenozoic is associated with a decrease in sea level which is attributed to India-Asia collision and formation of Alpine-Himalayan mountains (e.g., Bradly et al., 2011). Therefore, a combination of changes in both continental and oceanic crustal processes are expected to control the variation in seawater chemistry.

A hypothesis to explain higher Mg^{2+} and SO_4^{2-}, and lower Ca^{2+}, concentrations of modern seawater compared to the Cretaceous is that the change in rate of continental erosion and chemical weathering, leads to a change in river chemistry. Continental uplift and formation of mountains during the Cenozoic is proposed to increase the weathering rate of continental rocks and hence increase delivery of Mg^{2+}, SO_4^{2-} and alkalinity from rivers into the ocean (Livingstone, 1963; Torres et al., 2014; Sun et al., 2016). If alkalinity increases, it would enhance precipitation of $CaCO_3$, resulting in a decrease in Ca^{2+} concentration of seawater. Moreover, Rb-rich continental crust has high $^{87}Sr/^{86}Sr$ due to decay of ^{87}Rb to ^{87}Sr (Faure and Mensing, 2005), while basaltic oceanic crust has lower $^{87}Sr/^{86}Sr$ compared to that of continental rocks (Palmer and Edmond, 1989; Butterfield et al., 2001). Hence, an increase in the flux of Sr from high Rb/Sr continental sources and increased riverine radiogenic Sr flux is also suggested as an explanation for the observed increase in $^{87}Sr/^{86}Sr$ of seawater (Veizer et al., 1999) from the Cretaceous to the modern era (Raymo and Ruddiman, 1992). However, it has been proposed that the magnitude of increase in weatherability of continental silicates is unlikely to be large enough to explain the Cenozoic rise in seawater Mg^{2+} (Higgins and Schrag, 2015).

Another hypothesis to explain the observed increase in Mg^{2+}/Ca^{2+} ratio of seawater is a decrease in volume of dolomite that formed during the Cretaceous to modern era (Holland and Zimmermann, 2000). Dolomite, which is the main sedimentary sink for Mg^{2+}, forms when the Mg^{2+} ions partially substitute for Ca^{2+} ions in the structure of $CaCO_3$. This can be driven by equilibration of calcite with, or direct growth of dolomite from, a high Mg^{2+}/Ca^{2+} solution. Holland and Zimmermann (2000) proposed that a decrease in the rate of formation of dolomite led to less substitution of Mg^{2+} for Ca^{2+} in carbonate minerals, explaining an increase in the Mg^{2+} concentration of seawater. However, a model of change in the rate of dolomitization alone cannot directly explain the observed variation in other components of seawater (for example, SO_4^{2-} concentration). Studies suggest that formation of dolomite is enhanced when there are many shallow, inland seas, which occurs when global sea level is high (Holland and Zimmermann, 2000). In addition to the formation of anhydrite, sulfate can be removed from seawater by reduction to sulfide and formation of pyrite (FeS_2) in the presence of ferrous iron. It has been hypothesized that when sea level is high (e.g., during the Cretaceous), due to an increase in flooded continental shelf area, the flux of Fe to seawater increased, enhancing the removal of SO_4^{2-} as pyrite (e.g., Rennie et al., 2018).

Several previous studies have attributed the lower Mg^{2+} and SO_4^{2-}, and higher Ca^{2+} concentration of seawater from the Cretaceous compared to the late Cenozoic to a decrease in seafloor production rate over this period of time (assuming a constant river flux with constant composition; Spencer and Hardie, 1990; Hardie, 1996; Ivany et al., 2004; Coggon et al., 2010). The proposed explanation is that when seafloor spreading is faster, it enhances uptake of Mg^{2+} and release of Ca^{2+} during high temperature hydrothermal alteration of oceanic crust at the ridge axis and formation of Mg-bearing hydroxylated silicates. Also, SO_4^{2-} would be removed from hydrothermal fluids via formation of anhydrite ($CaSO_4$) which is highly insoluble at temperatures >150°C (Edmond et al., 1979; Alt, 1995; Elderfield and Schultz, 1996). However, it is argued that anhydrite dissolves as the oceanic crust cools (i.e., solubility of anhydrite increases at temperatures <150°C; McDuff and Edmond, 1982; Elderfield and Schultz, 1996). Ligi et al. (2013) has suggested that reactions between seawater and mid ocean ridge peridotites result in release of Mg^{2+} into the seawater. At slow-spreading ridges, mantle-derived peridotites can be emplace close to seafloor, so they can interact with seawater. Ligi et al. (2013) has attributed the increase in the Mg^{2+}/Ca^{2+} of seawater from the Cretaceous to the late Cenozoic to an increase in seawater-peridotite interaction due to a decrease in seafloor production rate over this period of time. Even though a change in seafloor production rate may explain the variation in Mg^{2+} and Ca^{2+} of seawater from the Cretaceous to modern era, there are several studies arguing that the change in seafloor spreading rate was very small over this time period (e.g., Lithgow Bertelloni et al., 1993; Rowley, 2002; Gaina and Mueller, 2004; Müller et al., 2008). Hence, there is no general agreement on the change of ocean crust production rate. For example, Holland (2005) proposed that even if the ocean crust production rate in the Cretaceous was twice as large in the Cenozoic era, this is not enough to account for the observed changes in the Mg^{2+}, Ca^{2+} and SO_4^{2-} concentrations of seawater during the Cenozoic. Moreover, this hypothesis cannot explain a near constant K^+ concentration of seawater (Horita et al., 2002; Lowenstein et al., 2003, 2014). Therefore, there must be other explanations for the observed variation in seawater composition of this era.

Studies of the chemical composition of sediment pore-fluid, crustal fluids, and lavas altered at low-temperatures, reveal chemical exchange between seawater and off-axis oceanic crust. These show that during low-temperature hydrothermal alteration of the upper oceanic crust K^+ is removed from seawater and added to the upper oceanic crust while Ca^{2+} is removed from the oceanic crust and added to hydrothermal fluids (e.g., Elderfield et al., 1999; Wheat and Mottl, 2000; Staudigel, 2014). The low temperature hydrothermal alteration of basalts appears to add sulfur to hydrothermal fluid, however the net flux of S is not well understood and estimations of the net flux of sulfur is associated with large errors (Alt, 1995; Staudigel et al., 2014). The estimation of exchange flux of Mg^{2+} between the lava section and seawater during low-temperature hydrothermal alteration is associated with large uncertainties (e.g., the Mg concentration of fresh basalt can be very variable depending on the abundance of phenocrysts; Staudigel et al., 2014; Higgins and Schrag, 2015). However, previous studies suggest that there might be a small gain in Mg^{2+} from seawater to the oceanic crust, although the uncertainty is rather large (Staudigel et al., 1996). It has been suggested that the Mg^{2+} exchange flux between low-temperature, off-axis upper oceanic crust and seawater is small compared with large Mg^{2+} inventory of seawater such that it is unlikely that this exchange provides significant control on the Mg^{2+} content of seawater (Staudigel, 2014). To reconstruct the variation in paleo-seawater chemistry, Demicco et al. (2005) extended the model of Spencer and Hardie (1990), in particular including off-axis hydrothermal fluxes with variable rate of seawater circulation through the cold (< 60°C), off-axis upper basaltic section of ocean crust. Models by Demicco et al. (2005) found that the best fit to the pattern of major ions composition of seawater over the past 36 Myrs requires that low-temperature hydrothermal alteration of off-axis ocean crust removes large amounts of K^+ and HCO_3^- from seawater, small amount of SO_4^{2-}, no Mg^{2+} and adds small amounts of Ca^{2+} to hydrothermal fluid (while variable river water flux is assumed). Moreover, an increase in the $^{87}Sr/^{86}Sr$ of seawater (Veizer et al., 1999) can also be explained by a decrease in the flux of Sr from low Rb/Sr "basaltic" sources during low-temperature, off-axis hydrothermal dissolution of basaltic rocks (Coogan and Dosso, 2015).This hypothesis is supported by bulk rock Sr isotopic composition of the Troodos ophiolite (~90 Myr old ocean crust) showing large amounts of leached basaltic Sr into the seawater (Gillis and Robinson, 1990). Previous studies show that bottom seawater temperature responds to the global climate cooling, decreasing by 15°C to 20°C from the Cretaceous to modern era (Lear et al., 2000; Cramer et al., 2011). Also, studies suggest that dissolution of basaltic rocks in seawater-like solutions is sensitive to temperature due to high activation energy for initial basalt alteration in seawater, which is estimated between 41-92 KJ/mol (Brady and Gislason, 1997; Coogan and Dosso, 2015). Variation in bottom seawater temperature has been proposed to explain most of the rise in the seawater $^{87}Sr/^{86}Sr$ from the Cretaceous to modern era suggesting an important role of the low temperature, off-axis hydrothermal system on controlling the chemistry of seawater (Coogan and Dosso, 2015).

1.3. Characteristics of low-temperature, off-axis hydrothermal systems

1.3.1. Controls and magnitude of off-axis hydrothermal circulation

Oceanic crust is formed at divergent plate boundaries and dissipates the Earth's internal heat into the ocean (e.g., Stein and Stein, 1994; Sclater et al., 1980). Studies have shown that ~70 % of Earth's total internal heat loss (~45 TW) occurs through cooling of the oceanic lithosphere (e.g., Stein and Stein, 1994; Davies and Davies, 2010; Hasterok, 2013). The newly formed basaltic crust cools by two mechanisms: conduction and convection (Stein and Stein, 1994; Sclater et al., 1980). The convective transport of heat occurs via circulation of hydrothermal fluid. Hydrothermal fluid circulation occurs both at the ridge axis and on the ridge flanks (Figure 1.2) with most convective heat transport occurring within ~65 Myr of crustal formation before the crust is covered by impermeable sediments (Stein and Stein, 1994). The total hydrothermal heat loss is estimated at ~11±4 TW (Stein and Stein, 1994). The amount of convective heat loss above the ridge axis is estimated at ~1.8±0.3 TW (e.g., Wheat et al., 2003). Hence, the magnitude of high-temperature hydrothermal fluid circulation at oceanic spreading centers (younger than 0.1 Myr) is at most about one fourth of the total hydrothermal convective heat loss. Therefore, the majority of the heat loss occurs on the ridge flanks and powers the low-temperature, off-axis hydrothermal system (~9.2±4 TW). As a comparison, the off-axis hydrothermal fluid flux is within a range of the river flux (15 % to 50 % of river flux) and is ~1000 times larger than the on-axis hydrothermal fluid flux. In other words, a mass of fluid equivalent to the entire ocean circulates through the crust every 70-250 kyr (Coogan and Gillis, 2018).

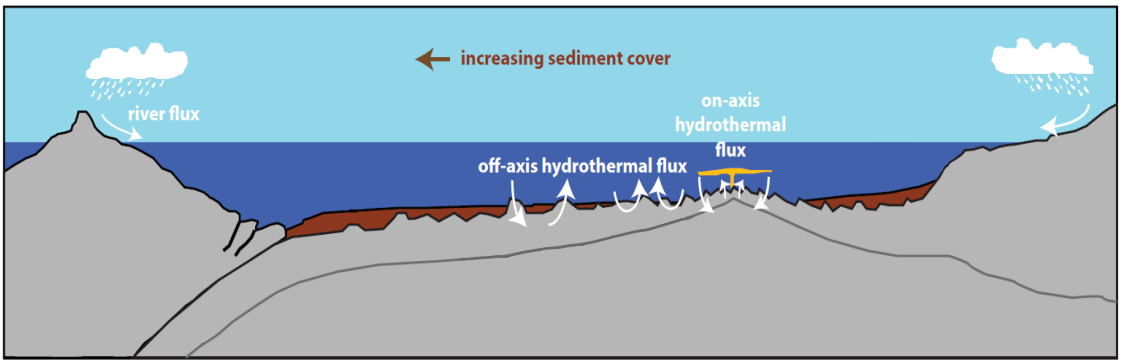

Figure 1.2. Cartoon of the global scale of hydrothermal fluid circulation through the upper oceanic crust. High-temperature hydrothermal fluid circulation is focused on the ridge axis, and low-temperature hydrothermal fluid circulation occurs away from the ridge axis, on the ridge flanks. The magnitude of fluid circulation decreases as the distance from the ridge axis increases and sediment thickness increases (from Coogan and Gillis, 2018).

Over 75 % of oceanic crust is currently being produced at intermediate to fast spreading ridges (>35 mm/yr for half rate; Bird, 2003). At these ridges the crust generally has a layered structure including permeable lavas that overlie much lower permeability sheeted dikes and plutonic rocks. As sediments accumulate on top of the lavas, open circulation of seawater through the lava section is restricted and inflow of seawater is thought to enter and exit the crust through topographic highs that remain sediment free in

an “outcrop-to-outcrop” model (e.g., Langseth and Herman, 1981; Baker et al., 1991; Langseth et al., 1992, 1984; Fisher et al., 2003; Hutnak et al., 2008; Anderson et al., 2012). Between outcrops fluid flows through the permeable lavas beneath the sediment layer (meters to 100’s of meters thick). The permeable lava section which is called the “aquifer”, typically has a thickness of ~600 m (e.g., Coogan and Gillis, 2018). Within this layer the permeability is variable and is controlled by lithology. For example, massive flows are less permeable than pillow lavas and their presence can decrease fluid flow across the aquifer. The outcrop-to-outcrop model assumes seawater enters the crust from recharging conduits and returns to the ocean via discharging conduits. The recharging and discharging conduits are bathymetric highs, where accumulation of sediment is much slower than elsewhere. When seawater enters the crust (with bottom seawater temperature), it circulates through the rocks moving laterally within the aquifer. As the cold seawater interacts with oceanic crust, its temperature increases and composition changes. Warmer fluid is more buoyant and as it reaches the next outcrop, it moves upward and exits from the oceanic crust through the discharge conduits. The gradient of temperature and hence pressure between recharge and discharge conduits is thought to be the main driving force of hydrothermal fluid circulation through the upper permeable oceanic crust (e.g., Fisher and Becker, 2000).

1.3.2. Mineralogical and chemical changes of upper oceanic crust during low-temperature hydrothermal alteration

Massive low-temperature hydrothermal fluid circulation through off-axis upper oceanic crust modifies the mineralogical and geochemical composition of the crust and ocean (e.g., Coogan and Gillis, 2018; Davis et al., 2003). Basaltic rocks are mainly made up of volcanic glass, plagioclase and clinopyroxene and there is a large disequilibrium between these and seawater. Volcanic glass and silicate minerals react with seawater and secondary minerals precipitate. Secondary minerals start to develop between 0.02 and 0.1 Myrs after crustal accretion (Schramm et al., 2005). Smectite group minerals (clay minerals) and celadonite (a mica) are the most abundant type of secondary minerals and fill voids (e.g., veins and amygdales) and replace igneous phases (e.g., Staudigel, 2014). During low-temperature hydrothermal alteration of basalts, the conditions of alteration can transition from more oxidative to more reducing (e.g., due to progressive thickening of sediment blanket). Hence, reduced minerals (e.g., pyrite and Fe-saponite) can form in close proximity with oxidized minerals (celadonite and Mg-saponite; Alt and Honnorez, 1984; Donnelly et al., 1979a, b; Bednarz and Schmincke, 1989; Gillis and Robinson, 1990; Schramm et al., 2005; Staudigel, 2014). Other secondary minerals include zeolite group minerals, carbonates, orthoclase (K-feldspar), Fe- and Mg-oxides and hydroxides, sulphides and silicate minerals (e.g., Coogan and Gillis, 2018). Low-temperature hydrothermal alteration of lavas (to 600 m below sediments) is not pervasive and primary igneous phases (glass, phenocrysts and groundmass) may coexist with secondary minerals (e.g., Staudigel, 2014). During low-temperature hydrothermal alteration of the upper crust, chemical exchange includes addition of H, Li, B, C, K, Rb and Cs from seawater to the crust and removal of Ca from the crust to seawater (Staudigel et al., 1996). The leached Ca can also precipitate again (in variable amounts) as carbonates (e.g., Alt and Honnorez, 1984; Staudigel et al., 1996; Johnson and Semyan, 1994; Staudigel, 2014). However, the extent of chemical exchange depends on local parameters

such as basement topography and the lithological make-up of the aquifer, and generally decreases with depth in the lava pile (e.g., Schramm et al., 2005).

1.4. Li concentration and Li-isotopic composition of seawater as a tracer for the evolution of the Earth system

Lithium and its isotopes (^{6}Li and ^{7}Li) are sensitive indicators of hydrothermal alteration processes and one of the tracers used to study the impact of silicate weathering on changes in seawater chemistry. Lithium is the lightest alkali metal with an ionic radius of 78 pm. In solution, Li ion can form complexes with 3 to 8 surrounding water molecules; however, it is thought to be most stable when it is complexed with four water molecules in a tetrahedral geometry (Wenger and Armbruster, 1991). Within the crust, Li is mainly hosted in silicate minerals with only minor amounts in carbonates. During alteration of silicate minerals and formation of clay minerals, Li^{+} can substitute for Al^{3+} and Fe^{2+} (77 pm) and especially for Mg^{2+} (72 pm) in structural octahedral sites of clay minerals (Huh et al., 1998). It has also been suggested that Li^{+} may be incorporated in interlayer positions as an exchangeable cation (e.g., Berger et al., 1988; Huh et al., 1998; Vigier et al., 2008; Hindshaw et al., 2019).

Lithium has two stable isotopes of atomic mass 6 and 7 amu which, due to their large relative mass difference, are subjected to both large kinetic and equilibrium isotopic fractionations. Equilibrium isotopic fractionation depends on bond energies (e.g., Hoefs, 2015) and, due to the different atomic environments that Li is found in (e.g., tetrahedral versus octahedral coordination), it is prone to equilibrium isotopic fractionation (O'Neil, 1986). Of importance for Li-isotope fractionation during low-temperature fluid-mineral interaction, during Li incorporation in clay minerals, ^{6}Li is preferentially incorporated to the higher coordinated number (octahedral coordination) in alteration products than in the fluid phase (tetrahedral coordination; Schauble, 2004; Hoefs, 2015).

1.4.1. Record of Li concentration and Li-isotopic composition of paleo-seawater

The evolution of Li concentration of seawater over time is not well understood. Based on the measured Li/Ca ratio of biogenic carbonates, the Li concentration of seawater is thought to remain nearly constant from the Cretaceous to modern era (~26 μM; Delaney and Boyle, 1986). However, more recent studies have demonstrated that the Li/Ca ratio of biogenic carbonates depends on environmental parameters such as temperature of precipitation (e.g., Marriott et al., 2004a, 2004b; Dellinger et al., 2018). Moreover, the Li/Ca data from Misra and Froelich (2012) show considerable scatter, suggesting that the Li/Ca concentration of biogenic calcites may be highly species dependent. Hence, with the current data on Li/Ca of seawater it seems difficult to draw robust conclusions about the evolution of Li concentration of paleo-seawater.

The lithium isotopic composition (δ^{7}Li) of seawater has been suggested to have become heavier over the past 120 Myr, from ~22 to ~31 ‰ (Figure 1.3; Hathorne and James, 2006; Misra and Froelich, 2012; Pogge Von Strandmann et al., 2013; Lechler et al., 2015). A large scatter is observed in the measured δ^{7}Li of bulk foraminifera at ~65 Myrs (Misra and Froelich, 2012) and it is thought that this may be due to mixture of

multi-species foraminifera. Studies have shown that calcite shells of different species can have a wide range of Li-isotopic composition (e.g., Dellinger et al., 2018). Records of Li-isotopic composition of Cretaceous seawater are very limited (Figure 1.3). There are two studies available that are focused on δ^7Li of seawater before, during and after Ocean Anoxic Events 1 and 2 (OAE 1 and 2) which occurred 120.3 and 93.7 Myrs ago, respectively (Pogge Von Strandmann et al., 2013; Lechler et al., 2015). Both studies suggest a decrease in δ^7Li of biogenic carbonates during OAEs which, alongside the scattered carbonate δ^7Li data before and after these intervals, adds large uncertainty on δ^7Li of seawater at these ages (Figure 1.3). Comparing the δ^7Li of foraminifera with inorganic calcite shows a similar range of δ^7Li, suggesting that Li is not subject to vital effects for foraminifera (Hathorne and James, 2006; Marriott et al., 2004a, 2004b; Misra and Froelich, 2009). Hence, studies on the δ^7Li of paleo-seawater have assumed that carbonates have the same δ^7Li as seawater (Hathorne and James, 2006; Misra and Freolich, 2012; Pogge Von Strandmann et al., 2013; Lechler et al., 2015), however, this may not be correct. Even though the physiological processes responsible for calcification in foraminifera are poorly understood, the composition of fluid which foraminifera's shell is growing from, is thought to be different than composition of seawater (e.g., Toyofuku et al., 2017; Dellinger et al., 2018). For example, seawater passes through membranes of living organisms to reach to the site of calcification which can affect the δ^7Li of seawater (e.g., Fritz, 1992).

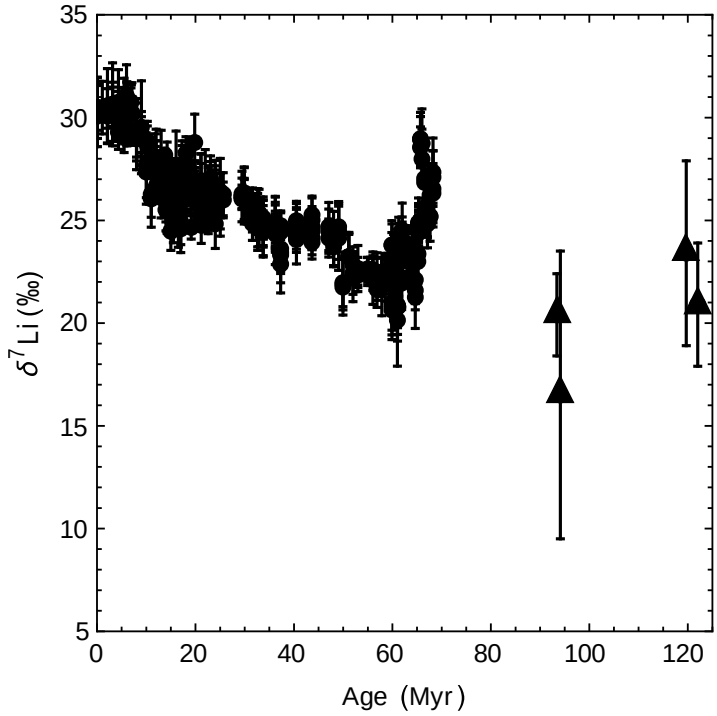

Figure 1.3. Lithium isotopic composition of seawater over the past 120 Myrs. Circle symbols show the Li isotopic composition of seawater based on the Li isotopic composition of bulk foraminifera (Misra and Froelich, 2012) and triangles show the Li isotopic composition of seawater based on leaching of bulk sediments to extract the carbonate fraction (Pogge Von Strandmann et al., 2013; Lechler et al., 2015). In both cases the carbonate is assumed to have the same δ^7Li as the seawater it grew from. This data suggests an ~9 ‰ increase in the Li isotopic composition of seawater over the past 90 Myrs.

1.4.2. Controls on sources and sinks of Li in seawater

Despite years of research on the global Li-cycle, the flux and Li-isotopic composition of the main input and output fluxes of Li into and out of the ocean remain incompletely understood (Figure 1.4). Rivers and high temperature hydrothermal fluids are the main Li inputs to the ocean and the main sinks are through the low-temperature, off-axis, hydrothermal alteration of the upper ocean crust and sediment diagenesis (Figure 1.4).

Upper continental crust has an average Li concentration of ~35 ppm and a δ^7Li ~0 ‰ (e.g., Teng et al., 2004). Dissolution of continental rocks into river waters increases the Li concentration of riverine input, but does not influence the δ^7Li of riverine inputs because the process of dissolution is not associated with isotopic fractionation. On the other hand, if continental rocks partially dissolve and clay minerals precipitate during the chemical weathering of rocks, clays would act as a sink of Li, while preferentially taking up more ^{6}Li. Hence, formation of clay minerals during weathering of continental crust is thought to be associated with lowering of the Li concentration and increasing the δ^7Li of riverine inputs into the seawater.

Based on studies on major world rivers, the Li concentration and δ^7Li of riverine input into the ocean span a wide range (0.1-0.4 μM and 1-44 ‰) with a mean value of 0.2 μM and 23 ‰, respectively (e.g., Stoffyn-Egli and Mackenzie, 1984; Huh et al., 1998; Dellinger et al., 2013). Therefore, with a modern riverine fluid flux of 3.74×10^{16} kg/yr (Palmer and Edmond, 1989), the riverine flux of Li would be between $4\text{-}15 \times 10^9$ mol/yr (Figure 1.4).

The other source of Li for seawater is high temperature hydrothermal fluids that discharge at the ridge axis into the ocean. Studies have shown that during high temperature hydrothermal alteration of basalts, Li is leached from the rocks into the fluid by both dissolution and diffusion processes, and significant isotopic fractionation can occur during diffusion of Li at high temperatures, which can lead to an increase in Li concentration and decrease the Li isotopic composition of hydrothermal fluid (i.e., ^{6}Li diffuses faster than ^{7}Li due to its lower atomic mass; Verney et al., 2011). The Li concentration of high temperature hydrothermal fluids in mafic hosted hydrothermal systems-is between 700-1275 μM (e.g., Edmond et al., 1979; Chan et al., 1994) and the δ^7Li is between 2-10 ‰ (Chan et al., 1994). Hence, a hydrothermal fluid flux of $\sim 1 \times 10^{13}$ kg/yr (Chan et al., 1992) yields a Li flux between $7\text{-}13 \times 10^9$ mol/yr (Figure 1.4).

Lithium is a moderately incompatible element, hence, formation of phenocrysts does not significantly compromise using volcanic glasses to obtain fresh crystalline Mid Ocean Ridge Basalts (MORBs) compositions (Coogan et al., 2017). Studies have shown that fresh MORB glasses have Li concentration mainly between 2-10 ppm (Chan et al., 1992; Gale et al., 2013; Brandl et al., 2016; Coogan et al., 2017) with an average of ~6.2±2.8 ppm (2SD) and the δ^7Li of fresh MORBs is measured between 1.6-5.6 ‰ with a mean of ~3.7±0.4 ‰ (2SD; Chan et al., 1992; Tomascak et al., 2008).

The main sinks of Li from seawater are thought to be via incorporation of Li in marine authigenic aluminosilicate clays which form during low-temperature, hydrothermal

alteration of off-axis, upper oceanic crust and sediment diagenesis (Mackenzie and Garrels, 1966; Seyfried et al., 1998), however, the output fluxes of Li are poorly understood. Interpretation of the Li concentration and isotopic composition of sediments and sediment pore-fluid samples can be complicated due to the existence of various exchange processes between sediments and water such as decomposition of organic matter and dissolution of sediments (Zhang et al., 1998). The bulk δ^7Li of global sediments varies widely (-4.3 to 14.5 ‰), reflecting the effect of sediment types, origin of sediments and diagenetic processes (Chan et al., 2000; 2006; Scholz et al., 2010). It has been suggested that the Li input flux during sediment diagenesis can account for ~5-10 % of the total Li inputs from rivers and high temperature hydrothermal fluids (Zhang et al., 1998).

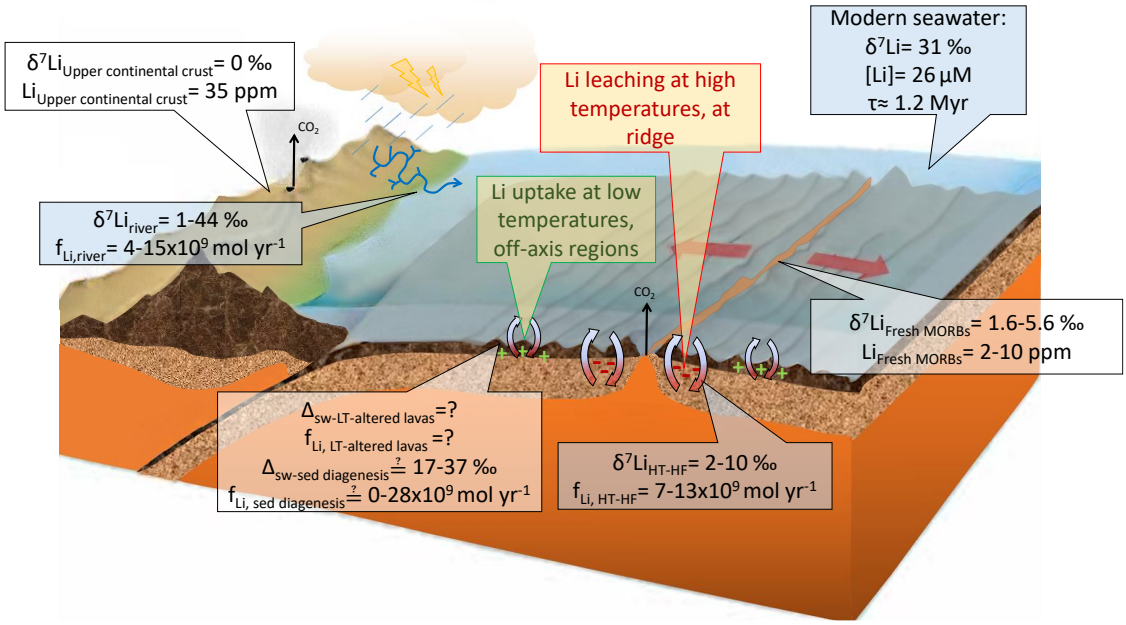

Figure 1.4. Cartoon of the global Li cycle showing the large uncertainty on the Li fluxes and isotopic composition of sources and sinks of Li to the seawater based on previously published data. f: flux; LT: low temperature; HT: high temperature; HF: hydrothermal fluid; sed: sediments; τ: residence time of Li in seawater. Sources of data: Stoffyn-Egli and Mackenzie (1984); Seyfried et al. (1984); Huh et al. (1998); Teng et al. (2004); Chan et al. (2006); Tomascak et al. (2008); Misra and Froelich (2012) and Gale et al. (2013).

1.4.3. Models to explain the increase in δ^7Li of seawater over the last 120

A number of studies attribute the increase in the δ^7Li of seawater over the last 120 Myr to an increase in lithium flux and/or lithium-isotopic composition of riverine inputs into the ocean (e.g., Misra and Froelich, 2012; Vigier and Godderis, 2015). Misra and Froelich (2012) modeled the lithium isotopic composition of seawater by only changing the lithium isotopic composition of riverine inputs into the ocean over 65 Myrs from 3 ‰ to 23 ‰. The 20 ‰ increase in the riverine lithium isotopic composition is attributed to a change in the continental weathering regime from a congruent weathering regime with limited clay mineral formation to an incongruent dominated regime with a high rate of clay formation due to intensified tectonic activity (increase in continental denudation, e.g., Himalayan orogeny) later in the Cenozoic. Vigier and Godderis (2015) proposed a

model in which an increase in the riverine Li flux from 2 to $13x10^9$ mol/yr, while high temperature hydrothermal Li flux is assumed to be constant, can explain the variation of lithium isotopic composition of Cenozoic seawater.

An alternative model which was proposed to explain the increase in δ^7Li of seawater over Cenozoic is an increase in removal of Li into sedimentary authigenic clays due to an increase in the flux of degraded continental aluminosilicates over the Cenozoic (Li and West, 2014). Li and West (2014) assumed constant Li uptake into the low-temperature altered upper oceanic crust. They also assumed that Li-isotopic fractionation factor between the removed Li into the sediments is larger compared to the fractionation factor into altered oceanic crust. This latter assumption was justified by the difference between the temperature of diagenetic reactions (i.e., which occurs at ambient seawater temperature), and oceanic crust hydrothermal alteration (i.e., which in their model occurs in more elevated and more variable range of temperatures; Li and West, 2014).

All of the models discussed above assume a constant Li isotopic fractionation factor (~16 ‰) between the bulk altered upper oceanic crust and seawater over time (Misra and Froelich, 2012; Li and West, 2014; Vigier and Godderis, 2015). However, the global climate cooling which is associated with cooling of bottom seawater over the past 120 Myrs (Lear et al., 2008; Cramer et al., 2011) is a potential factor to influence the Li isotopic fractionation factor between the altered off-axis, upper oceanic crust and seawater over this period of time.

This thesis is focused on better understanding of behaviour of Li and Li isotopes during low-temperature hydrothermal alteration of off-axis upper oceanic crust and investigating the role of low-temperature hydrothermal systems on Li concentration and isotopic composition of seawater over the past 120 Myrs. In this thesis three main questions are addressed: (i) How does solution chemistry affect elemental and isotopic fractionation of Li during precipitation of calcite? This question is important because if we are to interpret the Li isotopic composition of seawater recorded on carbonates, first we have to know about the fundamental parameters which may influence the recorded data; (ii) How do Li and Li-isotopes behave during low-temperature hydrothermal alteration of upper oceanic crust?, and (iii) What was the role of low-temperature hydrothermal alteration of the upper oceanic crust in controlling the Li isotopic composition of seawater over the past 120 Myrs?

1.4.4. Previous work on Li elemental and isotopic exchange in off-axis hydrothermal systems

Some studies of the Li content and isotopic composition of old oceanic crust were published before and during the development of this thesis. An early study by Chan et al. (1992) showed that the Li isotopic composition of dredged samples from oceanic crust (1 to 46 Myr oceanic crust), that were weathered at ambient bottom seawater temperatures, become increasingly heavier (up to ~14 ‰) due to addition of seawater Li to the lavas. This observation was attributed to two-component mixing of basaltic Li and seawater-derived Li that was incorporated in alteration products (e.g., clay minerals). An apparent Li-isotopic fractionation factor between altered end-member, off-axis oceanic crust and

seawater was proposed to be ~19 ‰ (Chan et al., 1992). The Li isotopic composition of lava samples from DSDP drill Holes 504B and 896A (5.9 and 8.6 Myr oceanic crust) also show a positive correlation with Li concentration (Chan et al., 2002), however a smaller apparent Li-isotopic fractionation factor was inferred from these holes compared to the dredged samples (~16 ‰). This difference was attributed to significantly higher alteration temperatures at Holes 504B/896A than the dredged samples. The Li flux associated with low-temperature alteration of the upper lava section of the oceanic crust was calculated to be ~$2x10^9$ mol/yr (Chan et al., 2002). This Li uptake flux is significantly lower than the $14x10^9$ mol/yr uptake flux of Li into altered lavas calculated for the Troodos ophiolite (91 Myrs oceanic crust; Coogan et al., 2017). In contrast to the studied lava samples from the Holes 504B/896A and the dredged lavas, samples from the Troodos ophiolite do not show a clear positive correlation between Li concentration and isotopic composition. Instead, a variation in both Li concentration and isotopic composition of lava samples with depth in the crust is observed (Coogan et al., 2017). This correlation is consistent with results of a study on altered lava samples from DSDP Holes 417A/417D/418A (119 Myr oceanic crust; Bouman et al., 2004). Lava samples from Holes 417A/417D/418A and the Troodos ophiolite suggest higher Li concentration and lighter δ^7Li in uppermost parts of oceanic crust compared to the deeper sections (Bouman et al., 2004; Coogan et al., 2017). However, the origin of these observed variations in Li concentration and isotopic composition of lavas with depth is not well understood. Gao et al. (2012) studied the Li concentration and δ^7Li of altered lava samples from Holes 1256C/1256D (15 Myr oceanic crust), showing mainly leaching of Li from lava samples and a wide range of δ^7Li (-3 to 14 ‰) throughout the upper ~600 m below sediments. The removal of Li from lava samples at Site 1256 is thought to be due to unusually high alteration temperatures (~60°C; Gao et al., 2012).

1.5. Thesis outline

1.5.1. Chapter 2: An assessment of the parameters controlling the accuracy and precision of Li-isotope measurements using single collector Inductively Coupled Plasma Mass Spectrometry (ICP-MS)

This chapter investigates some approaches to optimise the precision and accuracy of Li-isotopic analyses of silicate rocks using a single collector ICP-MS as was used in this study. The effect of variability in the concentration of the acid in the matrix of samples and standards and the effect of instrumental conditions for Li-isotope analysis are discussed in this chapter. Additionally, the impact of the matrix effects, associated with the imperfect separation of Li from the other ions in the sample, on the precision and accuracy of Li-isotopic measurements are tested. Finally, a previously published method (NaCl-wash method) for improving the precision of Li-isotope measurements is discussed. This chapter provides the background on the analytical approaches used in this thesis and details of methodologies are given in Appendix C.

1.5.2. Chapter 3: The effect of solution chemistry on elemental and isotopic fractionation of lithium during precipitation of inorganic calcite

The motivation for studying the controls on the Li cycle in seawater is to understand the various processes that drive changes in the Li-isotopic composition of seawater. Our record of this comes from the Li-isotopic composition of carbonate minerals, including both "pristine" foraminifera (Hathorne and James, 2006; Misra and Froelich, 2012) and bulk carbonate sediments (Pogge Von Strandmann et al., 2013; Lechler et al., 2015). These studies generally assume the Li-isotopic composition of seawater is similar, or identical, to the Li-isotopic composition of calcite based on sparse experimental data that suggest this. However, both primary recrystallization and diagenetic processes may lead to carbonate minerals growing under a range of conditions that may differ from those of the experimental studies. In this chapter, the effect of solution chemistry on elemental and isotopic fractionation of lithium during inorganic precipitation of calcite is investigated experimentally and I show that solution chemistry can lead to a large change in the Li-isotope fractionation factor between calcite and solution.

1.5.3. Chapter 4: Lithium and lithium isotopic exchange between seawater and off-axis oceanic crust: A case study from DSDP Holes 417A, 417D and 418A

This chapter is focused on better understanding the behaviour of Li and its isotopes during low-temperature hydrothermal alteration of upper oceanic crust using detailed studies of three closely spaced drill cores in ~120 Myr old upper oceanic crust. Several models to explain the variability in the Li-isotopic composition of rocks altered in off-axis hydrothermal systems are tested using the observed variation in Li concentration and isotopic composition with depth for Holes 417A, 417D and 418A. I conclude that changes in Li concentration and isotopic composition of hydrothermal fluids provide the most plausible explanation for the observed variations. A simple one-dimensional fluid flow model (lateral or vertical) cannot explain the data, and instead a conceptual model of free-circulation of fluid within the upper tens of meters of the ocean crust and leakage of seawater with slightly modified composition, best explains the data.

1.5.4. Chapter 5: The role of low-temperature hydrothermal alteration of off-axis oceanic crust in controlling the Li concentration and isotopic composition of seawater over the past 120 Myrs

In this chapter I consider the way that Li uptake by the upper oceanic crust may have been affected by changing environmental conditions over the last 120 Myrs. Studies have shown that conditions within off-axis hydrothermal systems in the oceanic crust responded to the global climate cooling over the past 120 Myrs with fluid temperatures decreasing over this time. I present Li-isotope data for lavas from five drill cores from this time interval, substantially increasing the number of drill cores that have been studied for the Li-isotopic composition. I conclude that the Li-uptake flux into the off-axis upper oceanic crust has decreased while the Li-isotopic composition of bulk altered crust has increased over the past 120 Myrs. No evidence of systematic variations in the Li-isotopic fractionation factor between altered off-axis oceanic crust and seawater with crustal age and alteration temperature is found in this chapter. I suggest that the change in Li uptake

flux and isotopic composition of off-axis, upper oceanic crust could be a result of a change in the Li concentration and isotopic composition of seawater over the past 120 Myrs.

1.5.5. Chapter 6: Conclusions and future work

This chapter summarizes the significant findings from each chapter in this thesis and describes future studies/experiments to extend the studies that are presented in this thesis.

2. An assessment of the parameters controlling the accuracy and precision of Li-isotope measurements using single collector Inductively Coupled Plasma Mass Spectrometry (ICP-MS)

2.1. Introduction

Lithium isotopes of mass 6 and 7 have nearly 15 % mass difference which causes large isotopic fractionations during alteration of silicate rocks. Although the large mass difference between Li isotopes makes them a valuable geological proxy, it also leads to large fractionations associated with analysis. Lithium isotopes are susceptible to fractionation in any mass-dependent process from the sample preparation process such as column chromatography to the isotopic measurements using ICP-MS instrument.

The Multi Collector ICP-MS (MC-ICP-MS) instrument was built to improve precision of isotope measurements while the precision obtained with the "conventional" ICP-MS is limited by the single collector ion detection systems (e.g., Jeffcoate et al., 2004). The MC-ICP-MS is equipped with a magnetic sector mass spectrometer with multiple Faraday cups. The multiple Faraday cups permit simultaneous measurement of multiple isotopes and improves the precision of isotope measurements (e.g., Millot et al., 2004). This improvement is because in the MC-ICP-MS, precision of the isotopes measurements is not affected by short-term intensity fluctuation of ion beams which are produced in the ICP (e.g., Rehkämper et al., 2001). Even though a MC-ICP-MS is a more precise instrument for measuring Li-isotopes, in this Chapter I demonstrate that using a single collector ICP-MS one can achieve high precision measurements of Li isotopes ratio. However, this requires a good understanding of possible sources of imprecision and inaccuracy when using a single collector instrument.

Over the past two decades several studies focused on identifying and eliminating the sources of uncertainties during Li isotopic measurements using ICP-MS (e.g., Bryant et al., 2003; Jeffcoate et al., 2004; Lin et al., 2016). Lithium is a trace element in silicate rocks, hence complete separation of it from the major components of silicate rocks is near-impossible. The most abundant element accompanying Li after column separation is Na. Existence of variable ions with variable masses in the ICP-MS instrument leads to space charge effects which is a consequence of the mutual repulsion of the same sign charges (Tanner, 1992; Burgoyne et al., 1997; Busch, 2004). Space charge, before and after mass separation (before and after the ion beam enters the mass spectrometer), can cause perturbation in Li ion trajectories and decreases the quality of Li isotopic measurements. Several studies have focused on improving the precision and accuracy of Li isotope measurements through reducing the negative effect of matrix on Li isotopic measurements, and also working on methods of sample preparation; for example, matching the acid concentration of samples and standard solutions (Stewart and Olesik, 1998a), and tuning the instrument in such a way as to improve precision and accuracy of Li isotope measurements (Bryant et al., 2003; Andren et al., 2004).

This chapter describes experiments performed to test several of the most important parameters that have the potential to induce imprecision in Li isotope analysis by ICP-MS. In this study, the Li-isotopic compositions of samples are calculated relative to the Li-isotopic ratio ($^7Li/^6Li$) of Li_2CO_3 standard IRMM-016. The precision of measurements is calculated based on the stability of the $^7Li/^6Li$ ratio of IRMM-016 over the course of each analysis, and the accuracy of measurements are estimated based on the analysis of international reference rocks including BHVO-2, BCR-2, JB-2, JR-2, BIR-1 and UB-N-1. To increase the precision and accuracy of Li-isotopic measurements, the impact of acid concentration, the effect of the concentration of ions accompanying Li in the analyte and the optimum instrument tuning parameters are investigated in the following sections.

2.2. Sample preparation

2.2.1. Sample digestion

Approximately 100 mg of each sample powder was digested in four steps. First, the powder was dissolved in a 10:1 mixture of concentrated HF-HNO_3 (5 ml of HF and 0.5 ml of HNO_3) in a Teflon vial at ~125°C for at least 48 hours. Second, the sample was dried and re-digested in 1 ml DI, 1 ml of concentrated HNO_3 and 1 ml of concentrated HCl on a hotplate at ~125°C overnight followed by two steps of drying and re-digesting in 4 ml of 8 M HNO_3 for at least one day and finally in 4 ml of 1 M HNO_3. If the solution was not perfectly clear at this stage, it was dried down and digested in 0.5 ml of concentrated HCl and refluxed over night at ~125°C. The HCl was then evaporated and the sample taken up again in 4 ml of 1 M HNO_3. A 0.5 ml split of the solution was removed and diluted in 12.5 ml 2% HNO_3 to produce a solution with a dilution factor of 1000 for trace element analysis. All reagents were environmental grade, HPLC grade and 18.2 MΩ.cm Millipore deionized water (DI).

2.2.2. Column chromatography

Lithium was separated from the remaining 3.5 ml of solution broadly following the method of Teng et al. (2004). Teflon columns (30 cm long and 0.95 cm inner diameter) containing 7.5 g (dry weight) of BIORAD AG 50W-x8 (200-400 mesh) were cleaned using 40 ml of 7 M HNO_3 followed by 15 ml of DI, 40 ml of 4 M HCl and a further 50 ml DI. The resin was then conditioned with 25 ml of 0.1/80 solution (a mixture of 0.1 M HNO_3 in 80 % methanol; by volume-see Appendix C, section C.1.4 for more details) based on the method of Reiman and Walton (1970). The 3.5 ml sample in 1 M HNO_3 was mixed with 0.5 ml of concentrated HNO_3 and 3.43 ml of methanol giving a mixture of 54 % 1.55 M HNO_3 and 46 % methanol. Approximately 5.9 ml of this was loaded into the columns.

Columns were calibrated several times over the course of this PhD. For the most recent calibration, a solution which was a mixture of different basalt samples was used at a dilution factor of 1000. This solution was dried down and re-diluted in a 5.9 ml mixture of 54 % 1.55 M HNO_3 and 46 % methanol. Column calibrations show that the Li and Na peaks are well separated by elution using 85 g of 1 M HNO_3 in 80 % methanol and collecting the aliquot released between 25 and 75 g (Figure 2.1).

Recovery of Li and separation of Li from Na and other major elements were tested after loading each sample into the columns. Trace element measurements were made on 10 g aliquots collected immediately before and after the peak (hereafter the pre- and post-aliquots) of samples, and showed that >99 % of Li was recovered in the peak. The amount of Li in the pre- and post- aliquots for different international reference rocks with different composition from rhyolite (JR-2) to basalt (BHVO-2) are presented in Table 2.1 showing that it never exceeds 12 ng.

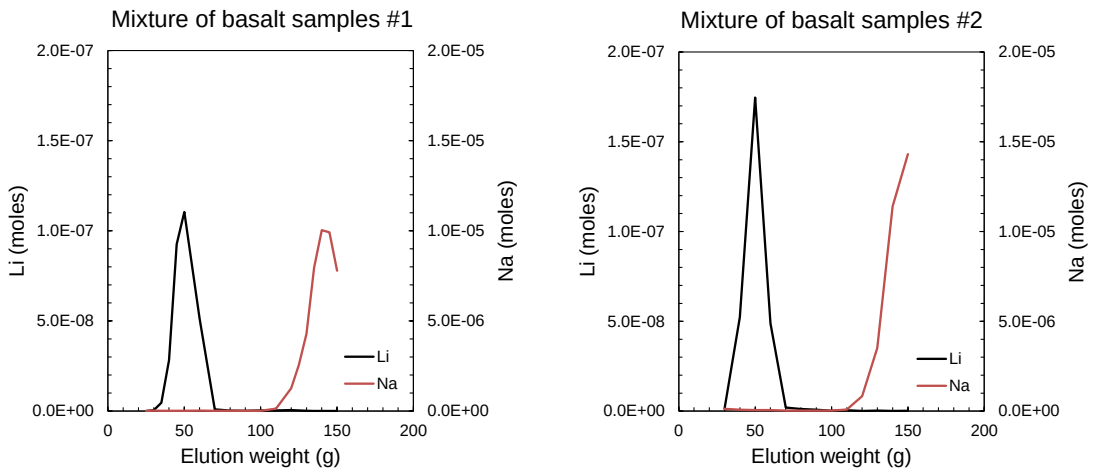

Figure 2.1. The fraction of Li (molar) and Na (molar) in aliquots collected for column calibrations using a mixture of basalt samples. The Li peak is collected between 25 g and 75 g of eluant released. The Li recovery is higher than 99 %, and the amount of Na in the Li peak is nearly zero.

Table 2.1. The amount of Li collected in the pre- and post- aliquots collected for reference rock standards used in this study.

Sample ID	Li in pre aliquots (ng)	Li in post aliquots (ng)	Sample ID	Li in pre aliquots (ng)	Li in post aliquots (ng)
BCR-2-15-8	0.2	2.9	JB-2-15-6	0.2	9.3
BCR-2-15-9	0.3	1.9	JB-2-15-7	0.4	5.1
BCR-2-15-12	0.2	0.04	JB-2-15-8	0.4	4.1
BCR-2-15-13	0.7	0.05	JB-2-16-10	7.4	0.09
BHVO-2-15-7	0.006	11.2	JB-2-16-11	0.01	0.02
BHVO-2-15-8	0.1	12.0	JB-2-17-14	0.4	0.08
BHVO-2-15-9	0.3	4.3	JB-2-17-15	0.2	0.02
BHVO-2-15-10	1.8	0.03	JR-2-15-4	0.3	0.6
BHVO-2-15-11	0.7	0.06	JR-2-15-5	0.05	3.5
BHVO-2-16-12	0.5	0.07	JR-2-15-6	0.3	0.7
BHVO-2-16-13	0.03	0.02	JR-2-15-7	0.2	1.9
BHVO-2-16-14	1.0	0.003	JR-2-15-8	0.06	1.9
BHVO-2-17-18	0.2	0.02	JR-2-15-10	2.9	0.2
BHVO-2-17-19	0.001	0.2	JR-2-16-11	1.8	0.3

BIR-1-15-6	0.1	4.5	JR-2-16-12	0.7	0.5
BIR-1-15-7	0.1	2.2	JR-2-17-15	0.3	0.07
BIR-1-15-8	0.2	1.7	JR-2-17-16	0.8	0.07
UB-N-15-1	1.8	0.3			
UB-N-15-2	1.6	0.1			

Recovered Li (peak aliquots; Figure 2.1) were dried down and dissolved in 2% HNO_3 to make solutions with the same Li concentration for isotopic analysis (10 ppb). Lithium isotopic analysis was conducted at the University of Victoria using a Thermo X series II (during the early part of this study) and an Agilent 8800 Triple Quadrupole ICP-MS (during the latter stages of this project). Analytical sessions were started with a block of ~10 IRMM-016 standard solutions to ensure stability of the instrument and define the instrumental drift. The detector's dead-time was determined by analyzing solutions of variable lithium concentrations (3 to 18 ppb) a day prior to each Li-isotope analytical session. Samples and 10 ppb IRMM-016 were then run using a standard-sample bracketing approach with another block of 10 IRMM-016 at the end of the analytical session to allow the instrumental drift to be accurately quantified.

A polynomial curve, not higher than 3rd order, was fit through the 10 ppb IRMM-016 $^7Li/^6Li$ ratios and the value given by this curve at the time of each sample was used as the standard value in calculating the δ^7Li of that sample using the normal nomenclature:

$$\delta^7\mathrm{Li} = \left(\frac{\left(\frac{^7\mathrm{Li}}{^6\mathrm{Li}}\right)_{\mathrm{sample}}}{\left(\frac{^7\mathrm{Li}}{^6\mathrm{Li}}\right)_{\mathrm{IRMM\text{-}016}}} - 1\right)*1000 \qquad \text{Eq. 2.1}$$

2.3. Parameters controlling the accuracy and precision of Li-isotopes measurements

2.3.1. Mismatching effect of acid concentration on precision and accuracy of Li isotopes measurements

Previous studies have shown that the concentration of the acid matrix can affect the signal intensity and affect the stability of the measured $^7Li/^6Li$ (e.g., Stewart and Olesik, 1998a and 1998b; Chen et al., 2016). The signal intensity of the analyte decreases as the acid concentration increases (e.g., Marichy et al., 1993; Stewart and Olesik, 1998a and 1998b) due to changes in the aerosol generation and transport processes. Also, acid concentration can change in the plasma's local condition for example, the plasma temperature, which can change the ions kinetic energy and the transmission efficiency of ions from the plasma to the mass spectrometer (Stewart and Olesik, 1998a and 1998b; Agatemor and Beauchemin, 2011; Chen et al., 2016). For instance, an increase in the acid concentration results in cooler plasma condition which can reduce the analyte ionization efficiency (Tanner, 1995; Stewart and Olesik, 1998a and 1998b). Moreover, a higher acid concentration means less water in the solvent, and less efficient evaporation during aerosol formation. Hence, the aerosol will contain more liquid which decreases its

transport rate to the plasma, leading to a drop in the signal intensity (Stewart and Olesik, 1998a and 1998b). However, the magnitude of drop in signal intensity of ^{7}Li and ^{6}Li may not be the same and the measured $^{7}Li/^{6}Li$ ratio changes if the acid concentration changes (Bryant et al., 2006; Lin et al., 2016).

The impact of changing of the acid concentration on Li signal intensity and stability of $^{7}Li/^{6}Li$ ratio was tested by running a 5 ppb IRMM-016 solution in different matrices including 1 %, 2 % (made separately from the standard 5 ppb IRMM-016), 3 % and 10 % HNO_3, bracketing with 5 ppb IRMM-016 in 2 % HNO_3. The result shows ~14 % decrease in the signal intensity of ^{7}Li from using 1 % HNO_3 as solvent to 10 % HNO_3 (Figure 2.2) consistent with previous studies (Stewart and Olesik, 1998a and 1998b; Chen et al., 2016). The measured $^{7}Li/^{6}Li$ of samples increases with increasing acid concentration (Figure 2.2) which is opposite of previous studies by Lin et al. (2016) and Bryant et al. (2006); however, the concentration of acid in these previous studies never went beyond 3 %. This latter observation might be due to a greater suppression of ^{6}Li over ^{7}Li. Regardless of the reason for the drop in signal intensity, and increase in $^{7}Li/^{6}Li$ ratio, this study shows that the acid concentration in the samples and bracketing solutions need to be kept constant during any single analytical session.

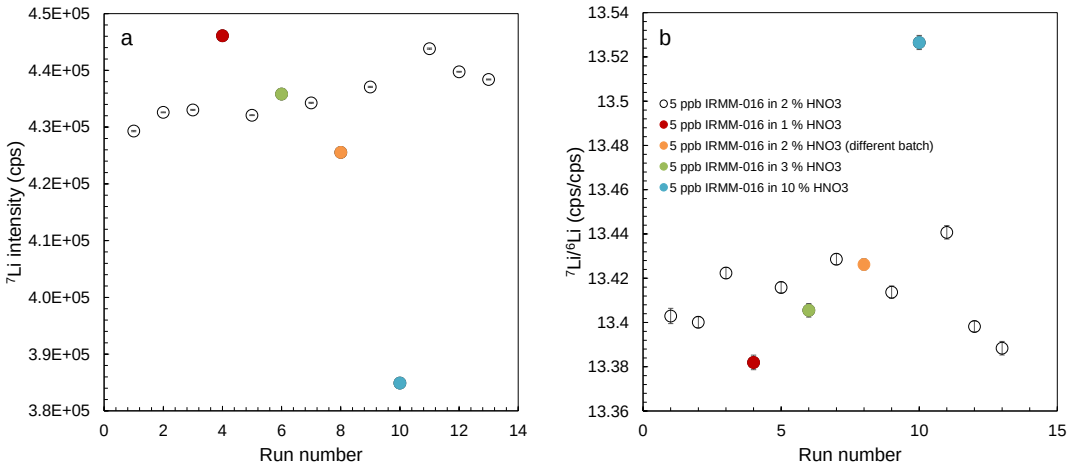

Figure 2.2. (a) The effect of acid concentration of matrix of solutions on ^{7}Li signal intensity and (b) measured $^{7}Li/^{6}Li$ of IRMM-016. The ^{7}Li signal intensity decreases with increasing concentration of nitric acid. The green circle is a 5 ppb IRMM-016 in 2% HNO_3, however, the 2% HNO_3 used to dilute this sample was made from a different batch of 2 % HNO_3 than the standard solution (open circles). Error bars showing the Relative Standard Deviation (RSD) of Li isotope measurements which accounts for minimum uncertainty of the measurements.

2.3.2. Instrument condition and set up for Li-isotopic analysis

2.3.2.1. Lab temperature

Having a steady temperature in the ICP-MS room is important for many aspects of ICP-MS analysis. For example, the spray chamber works efficiently at temperatures ~2°C and minimizes formation of oxide-based interferences and prevents overloading the plasma with solvent (Wilschefski and Baxter, 2019). Hence, a change in room

temperature can decrease the aerosol transport efficiency to the ICP and reduces the signal intensity. Measuring the room temperature during the course of analysis showed that the room temperature increases by ~1°C over ~80 minutes after the instrument is turned on (Figure 2.3). Hence, sample analysis only began >80 minutes after turning the instrument on.

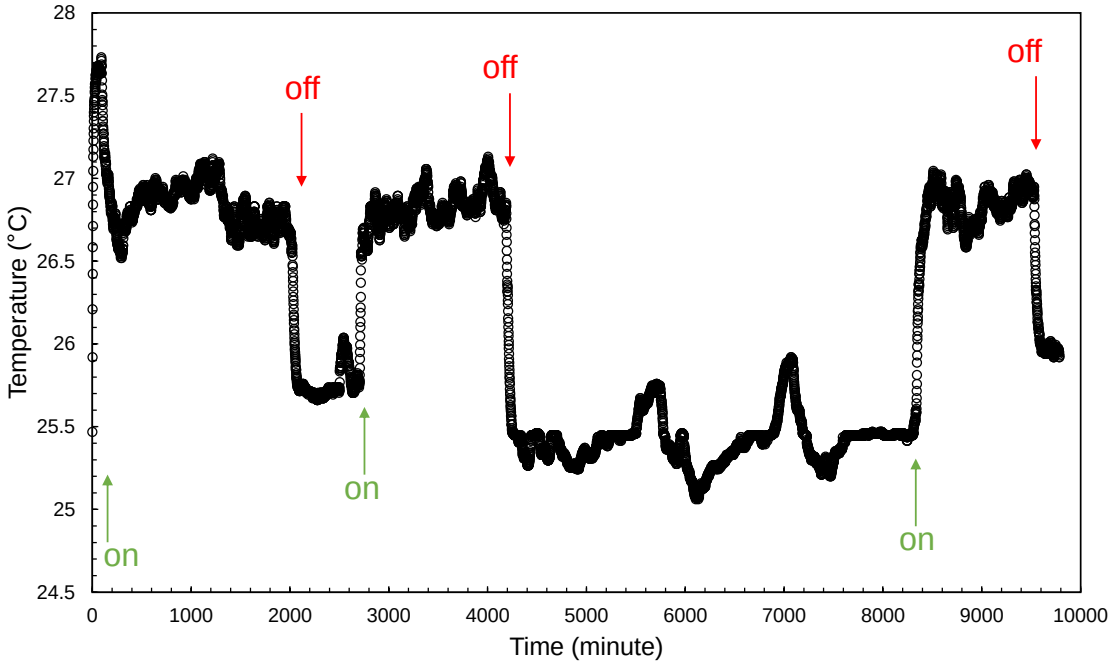

Figure 2.3. Plot of the room temperature in the ICP-MS lab over the course of three ICP-MS sessions. The green and red arrows show the time when the instrument was turned on and off respectively. About 1°C increase and decrease in the room temperature occurs during 80 minutes after turning the instrument on and off, respectively.

2.3.2.2. Cold vs. hot plasma

ICP-MS analysis can be performed under different RF forward power conditions. At a condition of low RF power (600-800 W) and high nebulisation gas flow rate (>1 L/min), the energy of the plasma can be substantially reduced, generating a so-called "cold" (or cool) plasma (e.g., Becker, 2007; Wilschefski and Baxter, 2019). Performing ICP-MS under high RF power (800-1500 W) is referred to as a "hot plasma" condition. In this study, both cold and hot plasma techniques have been used for Li isotopic analysis. Cold plasma conditions increase the sensitivity of measurements for Li by decreasing the count rates on the background (e.g., decreasing the chance of formation of the doubly charged ions $^{14}N^{2+}$ and $^{12}C^{2+}$ which can cause spectroscopic interference during the Li-isotope measurements; Tanner, 1995; Bryant et al., 2003). Previous studies have shown that cold plasma conditions are much more susceptible to major element (mainly Na) induced matrix effects, especially for Na/Li > 0.3 M/M (Bryant et al., 2003). Therefore, if the matrix of the solution has high concentration of ions other than Li, cold plasma conditions can be problematic.

In this study, the effect of the plasma temperature was tested by analysing the international rock standards BHVO-2, BCR-2, JR-2 and JB-2 at 10 ppb Li concentration under hot (RF power of 1400 W) and cold (RF power of 700 W) plasma conditions. The results did not show any systematic difference in the accuracy and precision of the Li isotopic measurements of silicate rocks under these different conditions. Based on this, analyses were done under hot plasma conditions in this study (Table 2.2).

2.3.2.3. Plasma positioning

Tuning the axial position of the torch box (X and Y positions) is an important parameter which needs optimization to minimize isotope discrimination before running any isotopic measurements. Setting one of the positions, for example the Y-position of the torch perfectly on the center of plasma gives the maximum density of the heavier isotope and high dispersal for lighter isotopes (Andren et al., 2004), therefore, it needs optimizing at the beginning of each analytical session.

Sampling depth (Z position of the torch) and sample gas flow rate both affect the mass bias variation in the same way. Sampling from the end of the torch results in more efficient uptake of lighter isotopes which are more discriminated on top of the torch. Studies suggest low sampling depth (large distance between the sampler cone and torch) and high sample gas flow rate (Andren et al., 2004) can minimize the mass bias. Hence, both torch Z position and sample gas flow rate need optimizing at the beginning of each session.

To achieve a stable $^{7}Li/^{6}Li$, each of these parameters was manually adjusted to obtain the maximum intensity of each isotope, then the parameters were moved away from the peak intensities to keep the $^{7}Li/^{6}Li$ ratio as stable as possible. The two lithium isotopes were measured sequentially. Since ^{7}Li is more abundant than ^{6}Li in nature (92.48 % ^{7}Li and 7.52 % ^{6}Li), the measurement time for ^{7}Li was much smaller than for ^{6}Li. Dwell times of 50 ms and 250 ms were used for ^{7}Li and ^{6}Li, respectively with 5 ms settling time (Brant et al., 2012; Table 2.2).

Table 2.2. Instrumental conditions for Li-isotopic analyses

Instrument	Agilent 8800 Triple Quadrupole
Forward power	1400 W
Sample depth	~8 mm
Carrier gas flow rate	1.1 L/min
Nebulizer pump	0.1 rps
Extraction voltage	-190 V
Dwell time mass 6	250 ms
Dwell time mass 7	50 ms

2.4. Impact of the matrix effect on precision and accuracy of the Li-isotopic measurements

Previous studies suggest that parameters such as plasma power and sampling depth do not appear to have a strong effect on matrix effects and these mainly depend on the absolute concentration of the matrix elements (Tan and Horlick, 1987). To test the effect

of matrix Na on Li-isotope analyses, a 10 ppb IRMM-016 solution in 2 % HNO_3 was doped with different amounts of Na, with Na/Li ratios ranging from 1 to 25 ppb/ppb (equal to 0.3 to 7.5 M/M). These samples were analysed bracketed with a 10 ppb IRMM-016 solution in 2% HNO_3. The results show that the $^7Li/^6Li$ ratio of IRMM-016 remains insensitive to the amount of Na in the solution across this range of Na contents (Figure 2.4).

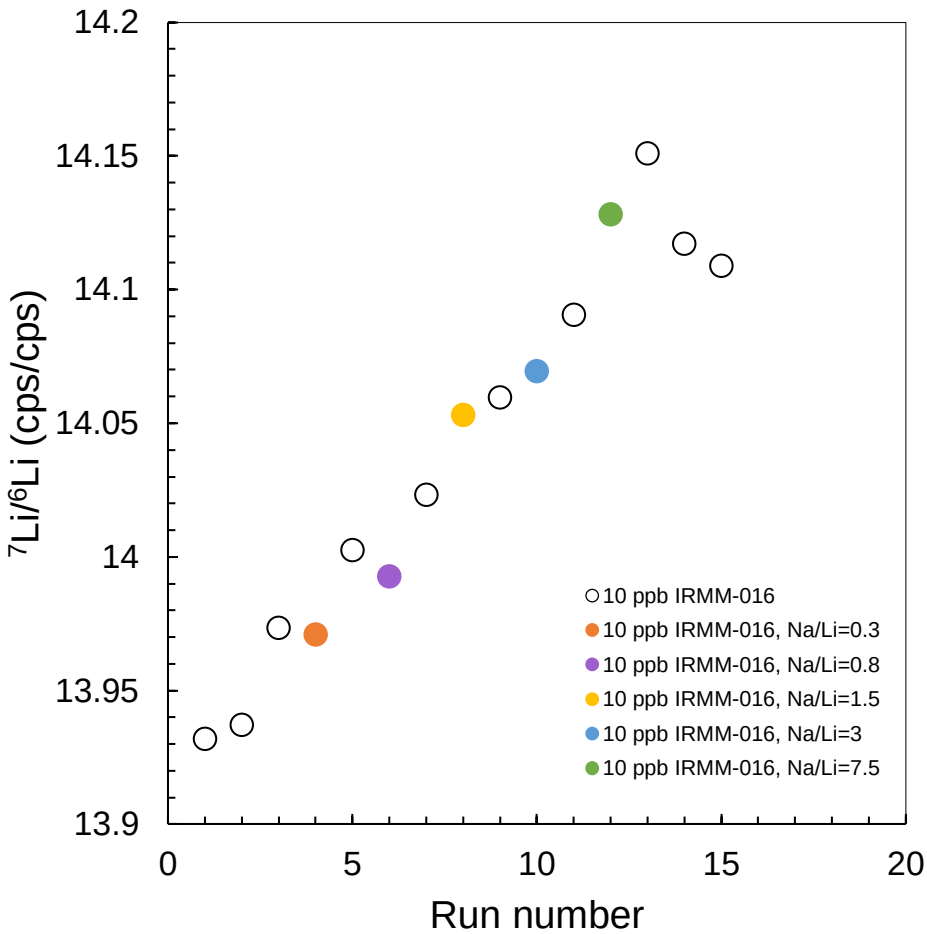

Figure 2.4. The $^7Li/^6Li$ of 10 ppb IRMM-016 with Li/Na ratio between 0.3 to 7.5 M/M versus run number. The Na/Li ratio ≤ 7.5 M/M in samples do not influence the precision and accuracy of the measurements and do not lead to significant matrix effect.

Measurement of the major element concentrations of several international standard rock solutions which had been through the columns in preparation for isotopic analysis showed Na/Li < 2 M/M (Figure 2.5), suggesting that the Na/Li ratio of samples are likely in a range that does not result in significant matrix effect. The higher concentration of ions in BHVO-2 and JB-2 compared with JR-2 is due to the higher initial Li concentration in JR-2 (~80 ppm) compared with BHVO-2 (~4.5 ppm) and JB-2 (~8 ppm).

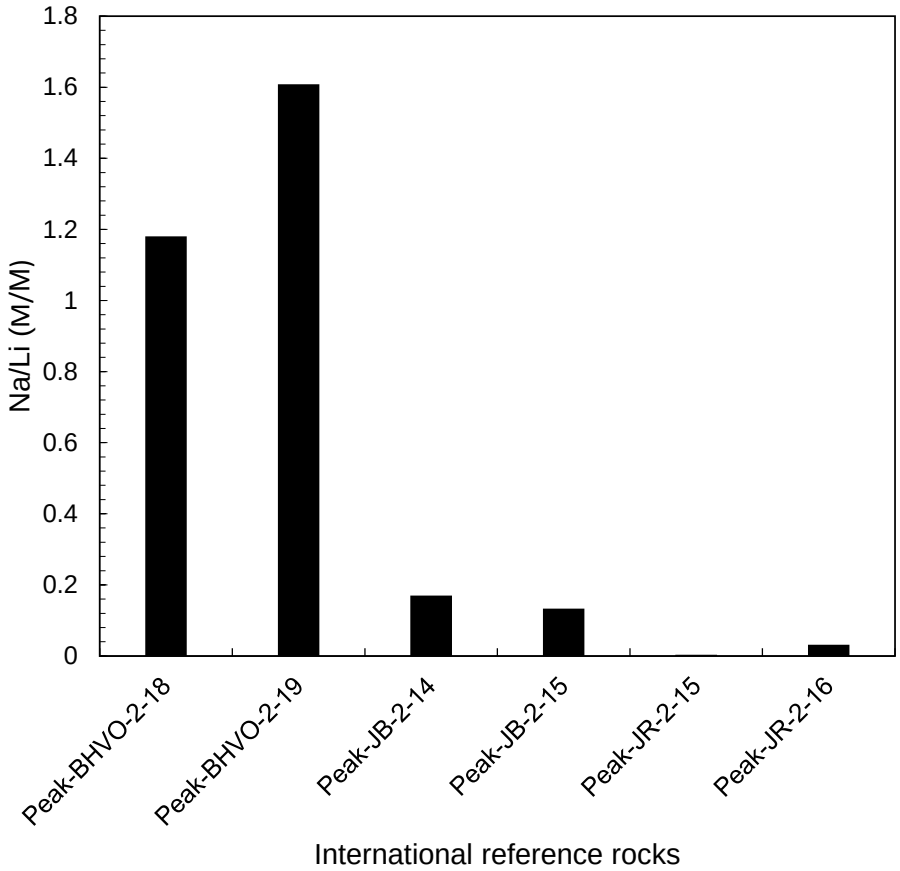

Figure 2.5. The Na/Li ratio of international reference rock solutions which were prepared for Li isotope analysis with 10 ppb Li concentration. The Na/Li ratio is less than 2 M/M for all international reference rock solutions.

2.5. NaCl wash method

2.5.1. Effect of NaCl wash on stability of $^{7}Li/^{6}Li$ ratio

Previous studies have shown that the instrumental background and memory effect of Li in the mass spectrometer can be a significant source of uncertainty during Li isotope measurements (Jeffcoate et al., 2004; Rosner et al., 2007; Lin et al., 2016). Lin et al. (2016) proposed a method to reduce the instrumental Li background and memory effect by running a highly concentrated 5 wt% NaCl solution at the beginning of the run. Their results show that this leads to a low Li background if the same solution is run through the ICP for 1 minute every 3 hours. Lin et al. (2016) hypothesized that a thin Na film coats the inlet system, and reduces lithium deposition, reducing the Li background.

I tested the effect of the NaCl wash method on the Li memory effect and stability of $^{7}Li/^{6}Li$ ratio of 10 ppb IRMM-016 to determine if this method improves the precision of Li isotope measurements. A spec-pure NaCl powder (99.999 % purity) was dissolved in 2 % HNO_3 to make a 5 wt% solution. Before analysing the NaCl solution, a 2 % HNO_3 blank solution was run several times. The background count rate was at most ~175 cps (Figure 2.6). To build up the Li background, a 10 ppb IRMM-016 solution was run 15

times. A 2 % HNO_3 blank was run after each block of 5 IRMM-016 solutions to determine the Li background. When the Li background count rate reached ~500 cps, the 5 wt% NaCl solution was introduced to the ICP for 1 minute (at run number 27 in Figure 2.6). A 2 % HNO_3 run immediately after the NaCl wash, showed a large drop in the background ^{7}Li signal intensity to 130 cps (Fig. 2.6). This procedure was then repeated but the count rate of ^{7}Li in the 2 % HNO_3 blank after running the NaCl solution stayed relatively constant rather than increasing over time (~300 cps; Figure 2.6). These results support the general finding of Lin et al. (2016) that running a concentrated NaCl solution can reduce the Li background. The count rate of ^{7}Li in the 10 ppb IRMM-016 remained constant before running the NaCl and increased ~20 % immediately after running the NaCl solution and remained nearly constant to the end of run (Figure 2.6).

The stability of $^{7}Li/^{6}Li$ in 10 ppb IRMM-016 was tested before and after running the NaCl solution (Figure 2.6). The $^{7}Li/^{6}Li$ ratio was stable before running the NaCl solution but running the NaCl solution appears to induce a large drift in $^{7}Li/^{6}Li$ (Figure 2.6). The stability of $^{7}Li/^{6}Li$ ratio was tested by calculation of $\delta^{7}Li$ of the IRMM-016 samples using the average of $^{7}Li/^{6}Li$ ratios of 10 ppb IRMM-016 before and after each sample as a reference standard value. The stability of the $\delta^{7}Li$ measurements improved by ~0.5 ‰ after running the NaCl solution (Figure 2.6). This test shows that the NaCl washing method has the capability of improving the precision of $\delta^{7}Li$ of simple matrix solutions like IRMM-016. However, whether this method improves the stability of $^{7}Li/^{6}Li$ of standard solutions while running actual samples with more complex matrix needs more investigation.

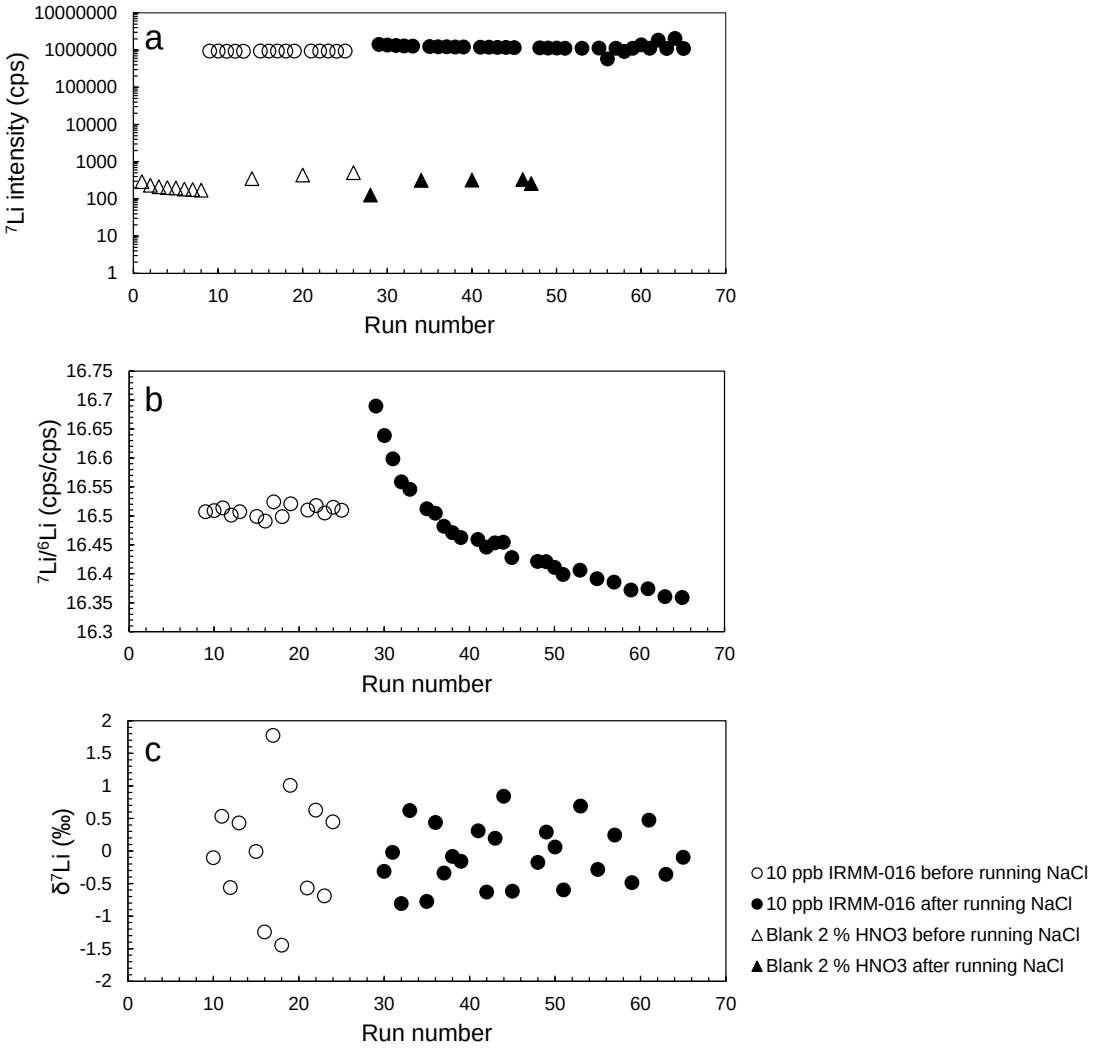

Figure 2.6. (a) The ^{7}Li signal intensity of blank 2 % HNO_3, 10 ppb IRMM-016 before and after running the 5 wt% NaCl solution at run number 27. The NaCl washing method reduces the Li count rate of the background. (b) The ^{7}Li/^{6}Li ratio of IRMM-016 versus the run number before and after introducing the 5 wt% NaCl solution to the ICP. A large drift introduces after running the NaCl solution in ^{7}Li/^{6}Li ratio. (c) The δ^{7}Li of 10 ppb IRMM-016 solutions versus the run number showing that the precision of measurements is improved by ~0.5 ‰.

2.5.2. Effect of NaCl wash on the matrix effect from Na and other trace metals

The effect of the NaCl washing method on matrix effects was tested by running a series of 6 ppb IRMM-016 which were doped with a range of single element solutions (Na, Ca, Zn, Ti, V and Cr) with different concentrations (Table 2.3). The analytical session was started with a 5 % HNO_3 blank solution, followed by a minute of the 5 wt% NaCl solution and a blank solution after the NaCl solution. A block of 17, 6 ppb IRMM-016 was analyzed to achieve a stable ^{7}Li/^{6}Li ratio, followed by samples which were bracketed with 6 ppb IRMM-016 (Figure 2.7).

Results show that the ^{7}Li count rates of blank solutions before (~600 cps) and after running the NaCl solution (~250 cps) is consistent with the previous results, confirming the effectiveness of running a NaCl solution in decreasing the Li background. The ratio of $^{7}Li/^{6}Li$ of 6 ppb IRMM-016 during running of the samples was stable before running samples which were doped with over 2.2 μM Na. When the Na content of the solution was increased to ≥ 2.2 μM (Na/Li >2.4 M/M), the stability of the $^{7}Li/^{6}Li$ decreased, reducing the precision of the measurements (Figure 2.7). A Na/Li ratio of 2.4 M/M at the transition to an analytically resolvable matrix effect from Na is less than that of 7.5 M/M found without pre-treatment with a NaCl solution at the beginning of the run (section 2.4). Based on this, and the increased drift induced by running such a solution I did not use the NaCl wash during sample analysis in this study.

Table 2.3. The composition of IRMM-016 solutions used to test the NaCl washing method on the matrix effect.

Sample ID	Li (μM)	Na (μM)	Zn (μM)	Ti (μM)	Ca (μM)	V (μM)	Cr (μM)	Total ions other than Li (μM)	Na/Li (M/M)
6 ppb IRMM-016, Na doped-1	0.9	0.4						0.4	0.5
6 ppb IRMM-016, Na doped-2	0.9	0.9						0.9	0.9
6 ppb IRMM-016, Na doped-3	0.9	2.2						2.2	2.4
6 ppb IRMM-016, Na doped-4	0.9	4.5						4.5	4.8
6 ppb IRMM-016, Zn doped-1	0.9		0.2					0.2	
6 ppb IRMM-016, Zn doped-2	0.9		0.3					0.3	
6 ppb IRMM-016, Zn doped-3	0.9		0.8					0.8	
6 ppb IRMM-016, Zn doped-4	0.9		1.5					1.5	
6 ppb IRMM-016, Ti doped-1	0.9			0.2				0.2	
6 ppb IRMM-016, Ti doped-2	0.9			0.4				0.4	
6 ppb IRMM-016, Ti doped-3	0.9			1.1				1.1	
6 ppb IRMM-016, Ti doped-4	0.9			2.1				2.1	
6 ppb IRMM-016, Ca doped-1	0.9				0.3			0.3	
6 ppb IRMM-016, Ca doped-2	0.9				0.5			0.5	
6 ppb IRMM-016, Ca doped-3	0.9				1.3			1.3	
6 ppb IRMM-016, Ca doped-4	0.9				2.5			2.5	
6 ppb IRMM-016, Mix-1	0.9	0.4	0.2	0.2	0.2	0.2	0.2	1.4	0.5
6 ppb IRMM-016, Mix-2	0.9	0.9	0.3	0.4	0.5	0.4	0.4	2.9	1.0
6 ppb IRMM-016, Mix-3	0.9	2.2	0.8	1.1	1.3	1.0	1.0	7.2	2.4

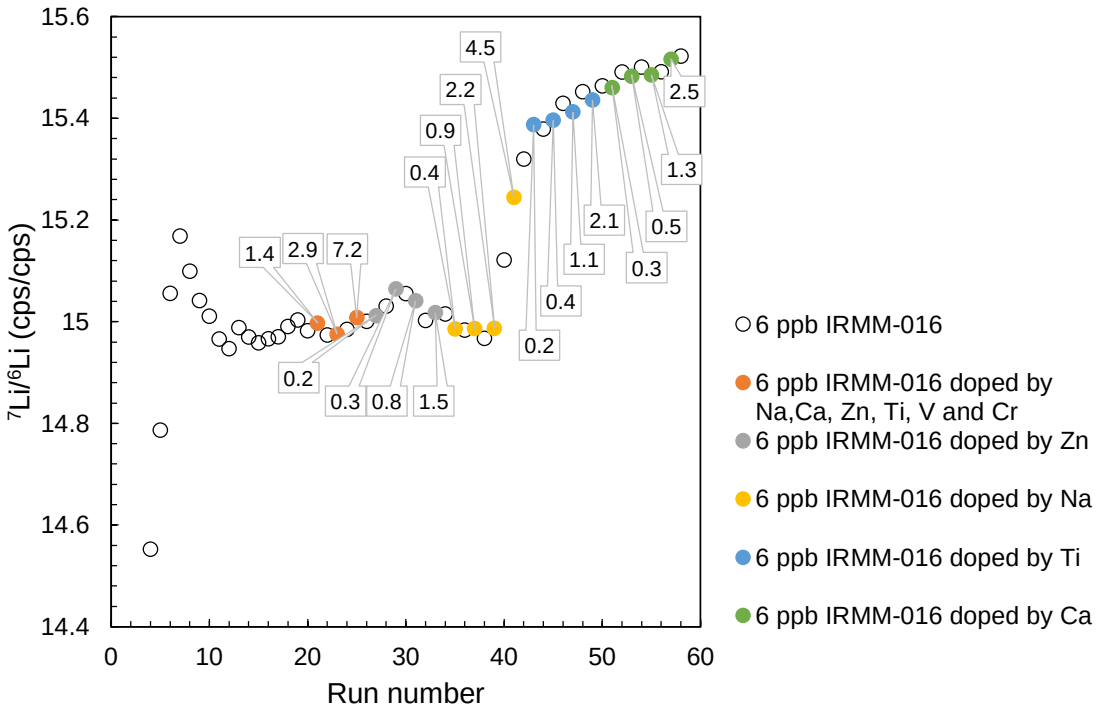

Figure 2.7. The $^{7}Li/^{6}Li$ ratio of 6 ppb IRMM-016 solutions with variable compositions versus the run number. The labeled numbers are showing the total molar concentrations of solutions (excluding Li). The 5 wt% NaCl solution was run at the beginning of the run (run number 1). The precision of measurements is disturbed after running the samples with Na ≥ 2.2 µM (Na/Li ≥ 2.4 M/M), showing the significant effect of Na in inducing matrix effects and inefficiency of the NaCl washing method in eliminating the induced matrix effect by increasing the Na content of matrix.

Without using the NaCl washing method, the Li isotopic compositions of six different international reference rocks, BCR-2, BHVO-2, BIR-1, JB-2, IR-1 and U-BN were measured multiple times with a precision of measurements better than 1 ‰ ($2S_{\bar{x}}$; two standard error). The measured Li isotopic composition of reference rocks has an average absolute difference with published values better than 1.7 ‰ (Figure 2.8).

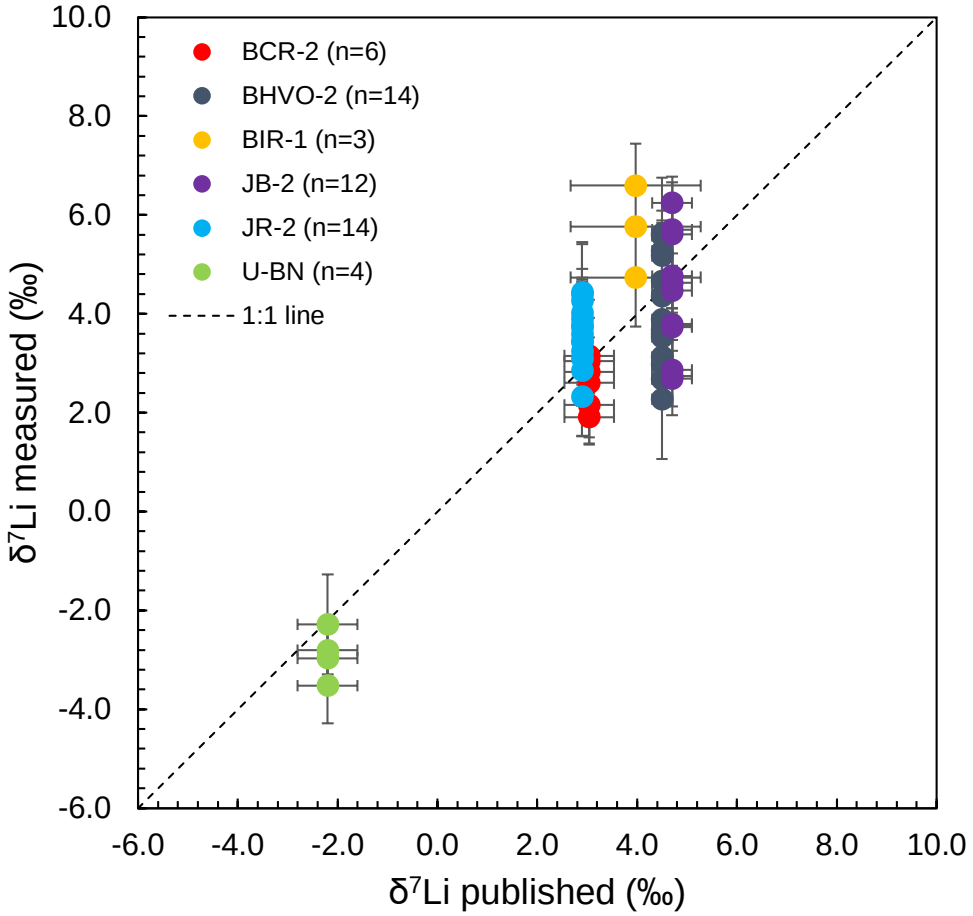

Figure 2.8. The Li isotopic composition of international reference rocks is plotted against their published values. Error bars showing 2 standard error of measurements. For an updated list of published values see http://georem.mpch-mainz.gwdg.de).

2.6. Summary

This chapter discusses several of the important sources of uncertainty during Li isotopic measurements using an ICP-MS which need to be taken into account when running Li isotopic analysis. The mismatch between the concentration of acid used to dilute the samples and standards has a significant effect on the accuracy of the measurements. Hence, using the same batch of acid to dilute the samples and standard solutions is essential. The proposed NaCl washing method by Lin et al. (2016) has potential to decrease the Li background and results in a stable $^{7}Li/^{6}Li$ ratio of a standard solution, but both the increased drift induced by this approach, and the increased sensitivity to Na based matrix effects, led me not to use this approach. Further work is required before using this method for measurement of Li isotopes of silicate samples. Among the tuning parameters of ICP-MS instrument, tuning to ensure the signal intensity is not highly sensitive to tuning parameters, which requires being offset from the peak sensitivity, is important for precise isotope measurement.

3. The effect of solution chemistry on elemental and isotopic fractionation of lithium during inorganic precipitation of calcite

3.1. Introduction

The Li content and isotopic composition of seawater are potentially powerful proxies with which to study global chemical weathering and the long-term carbon cycle. This is because the behaviour of Li is largely controlled by the dissolution and precipitation of silicate minerals. Carbonate micro- and macro-fossils, and bulk carbonate sediments, have been used to try to reconstruct the Li-content and Li-isotopic composition of ancient oceans (e.g., Delaney and Boyle, 1986; Lear and Rosenthal, 2006; Hathorne and James, 2006; Misra and Froelich, 2012; Pogge von Strandmann et al., 2013; Lechler et al., 2015). In combination with studies of the sources and sinks of Li, these data have been used to interpret the global Li-cycle and link this with the long-term C-cycle (e.g., Chan et al., 1992; Huh et al., 1998; Millot et al., 2010; Misra and Froelich, 2012; Pogge von Strandmann et al., 2013; Vigier and Godderis, 2014; Li and West, 2014; Coogan et al., 2017; Dellinger et al., 2018; Murphy et al., 2019). The efficacy of this approach is entirely dependent on the interpretation of the paleo-records in terms of the composition of paleo-seawater. Calibrations against modern samples and laboratory cultures have been used to test this approach with somewhat variable results (e.g., Delaney et al., 1985; Delaney et al., 1989; Hathorne and James, 2006; Misra and Froelich, 2012; Vigier et al., 2015; Roberts et al., 2017; Dellinger et al., 2018). While biologically induced carbonate precipitation is more complex than inorganic carbonate precipitation, the latter provides a critical starting point for a mechanistic understanding of the fractionation of elements between solution and mineral. Furthermore, many ancient carbonates have undergone some extent of diagenetic recrystallization where inorganic precipitation controls the growth of diagenetic calcite. Thus, if we are to understand the evolution of the Li-cycle over extended periods of Earth history we need to understand the partitioning of Li between inorganic calcite and aqueous solutions and the associated isotopic fractionation. This project, while not directly applicable to pristine biogenic calcite, have important implications for interpreting the Li content of calcite that has undergone any diagenetic modification (e.g., all bulk carbonate Li-isotope data). Diagenesis under variable conditions provides a viable alternative explanation for Li-isotope excursions in carbonate sediment sequences that have been interpreted as indicating changing seawater δ^7Li.

Laboratory experiments have previously been performed to investigate the controls on the Li content and isotopic composition of both biogenic (Delaney et al., 1985; Langer et al., 2015; Vigier et al., 2015; Roberts et al., 2017) and inorganic (Okumura and Kitano, 1986; Marriott et al. 2004a, 2004b; Füger et al., 2019) calcite. I focus on the latter here because the fluid biogenic calcite precipitates from is not the same as the fluid the organism lives in and so the fundamental chemical constraints on the partitioning of Li between calcite and fluid cannot be directly determined from comparison of the composition of biogenic calcite and the bulk solution. Okumura and Kitano (1986) grew

calcite by degassing CO_2 from a calcium bicarbonate solution spiked with high concentrations of Li (up to 1000 ppm Li). This approach means the calcite grew from solutions with variable pH (increasing from 6 to 8 over the experiment) and Ca content (decreasing by a factor of ~7 over the experiments) and unnaturally high Li contents (up to 200 ppm Li). Marriott et al. (2004a) grew calcite from a mixed $CaCl_2$-$NaHCO_3$ solution, with near constant composition (including Li content) and constant PCO_2 (with bubbling air into the solutions), between 5 and 30°C. The Li content of the calcite increased with decreasing experimental temperature but the isotopic fractionation factor was constant at about -8.5 ‰. Using an "identical" method, Marriott et al. (2004b) investigated the role of salinity in controlling the partitioning of Li between calcite and seawater. They used a single artificial seawater starting solution and diluted it to change the salinity; hence the Li and Ca contents, but not Li/Ca of the growth solution, was varied. The Li/Ca of the calcite grown in their variable salinity experiments increased linearly with solution Li content (and salinity) from 15 to 63 µmol mol^{-1} with an increase in salinity from 10 to 50 psu. The Li exchange coefficient ($Kd(Li/Ca)=[Li_{calcite}/ Ca_{calcite}]/[Li^{+}_{solution}/ Ca^{2+}_{solution}]$) in these experiments increased from $0.8x10^{-3}$ to $3.1x10^{-3}$ across the same range of salinity, slightly lower than reported in Marriott et al. (2004a) were Kd(Li/Ca) increased from $3x10^{-3}$ to $10x10^{-3}$ with decreasing temperature.

Marriott et al. (2004a, 2004b) also measured the isotopic fractionation factor in both sets of experiments they performed. This was independent of temperature (Marriott et al., 2004a) and of salinity (Marriott et al., 2004b). However, in their variable temperature experiments the calcite had a Li-isotopic composition around 8.5‰ lower than that of the solution (Marriott et al., 2004a) and in their variable salinity experiments the calcite had a Li-isotopic composition about 3‰ lower than the solution it grew from (Marriott et al., 2004b). This ~5‰ difference in isotopic fractionation between these experiments remains unexplained. The one difference in the reported experimental conditions, that seems most plausible to explain the difference in partition coefficient and isotopic fractionation, is a ~1 unit difference in pH between the solution in these two sets of experiments. Those experiments that resulted in a -3‰ fractionation were performed at a pH of ~8 (Marriott et al. 2004a) and the experiments resulting in -8‰ fractionation were performed at a pH of ~7 (Marriott et al., 2004b). The potential for pH to play an important role in Li isotope fractionation between calcite and aqueous solutions was suggested by computational simulations of Li speciation (Bogatko et al., 2013), however the results of this study have large uncertainties. More recently both inorganic calcite-solution Li fractionation (Füger et al., 2019) and biogenic calcite-solution Li-isotope fraction (Roberts et al., 2018) have been shown to correlate with changing solution pH in lab experiments. These previous studies motivated us to experimentally investigate whether the chemistry of the growth solution affects Li-isotope fractionation between calcite and solution.

The elemental and isotopic partitioning of Li between calcite and solution obviously depends on both phases. The speciation of Li in aqueous solutions is uncertain with studies suggesting hydrated Li-ion coordination by 3 to 9 water molecules although most studies suggest 4 to 5 (e.g., Newsome et al., 1980; Mähler and Persson, 2011; Wenger and Armbruster, 1991; Rudolph et al., 1995; Yamaji et al., 2001; Bogatko et al., 2013). Other potential aqueous Li species include hydrated Li-hydroxide, and hydrated Li-(bi-) carbonate species (e.g., Moskovits and Michaelian, 1980; Bogatko et al., 2013).

Quantifying the speciation of Li in aqueous fluids has proved challenging for both experimental and modelling studies leaving substantial uncertainty in how the speciation of Li may change with solution chemistry and what effect this could have on isotope fractionation (Yamaji et al., 2001; Bogatko et al., 2013). Changes in the speciation of aqueous Li ions with changing pH, and isotopic fractionation between different aqueous species, has been suggested (Bogatko et al., 2013) based on computational simulations but these have large uncertainties. The incorporation mechanism of Li in calcite is also rather unclear. While several studies have suggested Li is incorporated as an interstitial ion rather than replacing Ca (e.g., Okumura and Kitano, 1986), the charge balance associated with this heterovalent incorporation mechanism has not been described.

Here I present the results of a series of experiments designed to better constrain the role of solution chemistry in the elemental and isotopic fractionation of Li during inorganic calcite growth. Experiments were performed in which vaterite (a metastable polymorph of $CaCO_3$) recrystallized to calcite in solutions of variable pH, Ca^{2+} and Na^{+}. These demonstrate a strong correlation of both the partition coefficient and isotopic fractionation factor with solution chemistry. I also investigated whether solution pH affects the relative diffusivity of ^{6}Li and ^{7}Li (through changing the distribution of Li species in the solution) and show that, at least across the range of conditions I considered, the relative diffusivity of the isotopes varies little with pH. The simplest interpretation of the data is that Li is incorporated in inorganic calcite as $LiHCO_3$ leading to a partitioning dependence on the solution H^{+}/Ca^{2+}. The explanation of the dependence of the isotopic fractionation factor on solution chemistry is uncertain. Most likely this either reflects a kinetic isotopic effect, for example, due to changes in calcite growth rate and/or an equilibrium effect due to changes in Li speciation in the aqueous fluid.

3.2. Experimental methods

In order to grow calcite across a range of solution pH and Li concentration, I designed a series of experiments in which metastable vaterite recrystallizes to calcite in contact with calcite saturated solutions of different compositions (e.g., Hobbs and Reardon, 1999) as described below. In order to test whether changes in solution pH could affect the isotopic fractionation factor through changing the relative diffusivity of Li-isotopes in the solution I also performed a series of diffusion experiments following the approach of Richter et al. (2006).

3.2.1. Calcite growth experiments

3.2.1.1. Vaterite preparation

Pure vaterite was grown following the method of Kralj and Brečević (1990). Solutions of $CaCl_2$ and Na_2CO_3 (both 1.1 M) were prepared using 99.5% purity (ACS grade) powders and 18.2 MΩ.cm deionized water. To precipitate vaterite, 50 ml of each of these solutions were mixed together rapidly at room temperature and shaken vigorously for 3 to 4 minutes, filtered through a 0.2 μm membrane filter, and washed with DI. The precipitates were dried on a hotplate at ~50° C for a few hours. X-Ray powder Diffraction (XRD) analysis showed only vaterite peaks suggesting this was the sole phase

present (Appendix A, Section A.6). However, the detection limit of XRD for percent crystallinity range from 0.2 to 5% (Newman et al., 2015) and if phases with quantities within or smaller than this range were present in my samples, they probably would not be detectable. The $CaCl_2$ and Na_2CO_3 powders contained ~30 ppb Li and the resulting vaterite ~55 ppb Li as background contamination.

3.2.1.2. Calcite growth experiments

Solutions containing variable concentrations of $CaCl_2$ and $NaHCO_3$ were prepared for the calcite growth experiments using 99.5% purity (ACS grade) powders (containing ~30 and 6 ppb Li, respectively) and 18.2 MΩ.cm deionized water. Air was bubbled through the $CaCl_2$ solution for 24 hours to equilibrate them with the atmosphere then $NaHCO_3$ was slowly added until the solution began to turn milky due to precipitation of $CaCO_3$. The solutions were left with air bubbling through them for 24 hours and then filtered using a 0.2 µm membrane filter. This approach ensured that the solutions were very close to calcite saturation at the start of the experiment. The filtered solutions were doped with ~850 ppb Li (IRMM-016) and the pH (7 to 9.4) of the starting solution was measured on a subsample (Supplementary Table D.1.1). Two experiments were designed separately to test the effect of the Li concentration of the solution on the Li partition coefficient and isotopic fractionation factor. At a constant pH of ~9, two splits of filtered solutions were doped with ~650 and ~4000 ppb Li (IRMM-016).

Approximately 100 mg of vaterite was placed in Teflon vials with ~10 ml of solution, the vials were then wrapped in parafilm and placed in a water bath at 20.7±1.5 °C (2SD). Multiple experiments were performed with each starting solution in a time series with experiments ranging from 5 to 400 days. At the end of each experiment the solution was separated carefully from the precipitated $CaCO_3$ using a pipette with a thin layer of solution left on top of the calcite at the base of the vial. The calcite was then recovered by filtering using a 0.2 µm membrane filter and washed with DI several times. The pH of the solution was measured on a split of the sample. Alkalinity of both the initial and final solutions were measured using an automated titrator (HI84531-Hanna instruments). To prepare solutions for alkalinity measurements, ~2 ml of solution was diluted in DI by a dilution factor of 25. Only the alkalinity of solutions with pH > 8.5 were within the detection range of the technique (0.6 to 8.0 meq/l). The rest of the solution was used for geochemical analysis (Supplementary Table D.1.1). The calcite was dried and analysed by XRD, confirming calcite was the sole phase present (except in two short duration experiments, see below). In some cases, the calcite was examined by SEM, and in all cases analysed for Li content and isotopic composition. Calcite saturation state and carbonate chemistry parameters of experiments with available alkalinity was calculated using PHREEQC program (Parkhurst and Appelo, 2013; Supplementary Table D.1.1).

Even though the calcite was rinsed several times with DI, two experiments were also designed to quantify the amount of solution-derived Li which may remain on the surfaces of calcite crystals after drying. The maximum possible amount of Li which may have been added to the surface of calcite crystals from solution was tested by doping two splits of starting solutions at pH ~9 with ~500 ppb Rb and ~650 and ~4000 ppb Li. Rubidium was assumed to have close to zero partition coefficient between calcite and solution. The

results of these experiments were compared with two experiments without Rb and with ~650 and ~4000 ppb Li also at pH ~9.

3.2.2. Diffusion experiments

To examine the effect of solution chemistry on the relative diffusivity of ^{7}Li and ^{6}Li (D_{7Li}/D_{6Li}) diffusion experiments were performed using the method of Richter et al. (2006). In this approach Li diffuses from a small (~1.25 ml) aqueous source solution into a larger (~ 500 ml), initially Li-free, sink solution through a narrow ~5 mm long and 1.2 mm diameter cylindrical tube. The source solution contained ~100 ppm Li (IRMM-016) but in all other ways was identical to the sink solution. Four solutions were used in the experiments: (i) ~8.7 M $(NH_4)_2CO_3$; (ii) ~1.5 M $(NH_4)_2CO_3$; (iii) ~0.000025 M CH_3COOH; and (iv) ~0.0015 M CH_3COOH. Experiments were designed such that the tube connecting the source and sink solutions pointed upwards at 45° to try to ensure diffusion was the only mechanism of mass transfer. Experiments were run at room temperature for 80 to 211 days. At the end of the experiments the Li content of both source and sink solutions were measured to determine the fraction of Li that had diffused out of the source (and to ensure mass balance), along with the isotopic composition of the source solution that is modified due to faster diffusive loss of ^{6}Li than ^{7}Li.

3.3. Analytical methods

The major, trace and Li-isotopic compositions of the experimental products were analysed at the University of Victoria using an Agilent 8800 Triple Quadrupole ICP-MS. A complete description of the analytical methodology is given in the Appendix A. Briefly, Li was separated from the sample matrix for isotopic analysis, using 15 ml micro-columns filled with BIORAD AG 50W-x8 (200-400 mesh) using the method of Misra and Froelich (2009). Analyses consisted of a block of 10 IRMM-016 standard analyses at the beginning and then alternating sample and standard analyses followed by another block of 10 IRMM-016 analyses at the end of the run. The Li-isotopic composition of samples was calculated relative to the value of IRMM-016 given by a polynomial drift curve fit through the standard analyses. Isotopic analysis of the dissolved calcite samples was performed using solutions containing ~1.4 ppb Li and the isotopic composition of the solutions that the calcite grew in, and the source solutions from the diffusion experiments, were analysed using 10 ppb solutions. An Alfa Aesar (99.999% purity) $CaCO_3$ powder was crushed in agate to try to produce a homogeneous in-house standard to monitor precision. Analysis of small amounts (5 mg) showed that the Li is not evenly distributed in this material but on average the Li content of this material is similar to, or less than, that of the calcite grown in the experiments. Larger aliquots of this powder (50 mg) were analysed for their isotopic composition with all analytical sessions (a total of 16 over the duration of this work) to test precision of the isotope method giving a standard deviation of 1.1 ‰.

3.4. Results

3.4.1. Mineralogy and fluid chemistry in calcite growth experiments

In all but two experiments XRD analysis showed only calcite in the final solid (Appendix A, section A.6). The exceptions were the two shortest duration experiments (5 days) performed at the highest pH (9.4 and 7.8). In these experiments both vaterite and calcite were present at the end of the experiment, consistent with results of Hobbs and Reardon (1998) who showed that the rate of recrystallization of vaterite to calcite decreases with increasing pH. These two experiments are not discussed further here. Crystals from a few experiments were examined using a SEM revealing that the calcite is generally blocky and ~10 µm wide, with no obvious difference with experiment duration or solution chemistry (Appendix A, section A.5).

The composition of the solution changed somewhat during the experiments (Supplementary Table D.1.1), reflecting dissolution of the vaterite and equilibration with the calcite grown during the experiment. Changes in the total mass of carbonate minerals present will change both the pH and Ca content of the solution and these are observed in some experiments. However, all such changes are small relative to the range of solution compositions used in the experiments. The Li content and isotopic compositions of the solutions remained similar throughout the experiments with variable pH and Ca content of solution. I caution that the absolute concentration of Ca in the low Ca experiments may be subject to significant uncertainty due to the extreme sensitivity of these data to contamination by minute amounts of calcite. One experiment in which this clearly occurred is noted in the figures and discussion below.

3.4.2. Lithium partitioning between calcite and solution

The ratio of the Li content of the calcite to that of the solution (Li partition coefficient) is higher in experiments in which the calcite grew from higher pH solutions than from lower pH solutions (Figure 3.1b). Solution pH covaries with solution Na and Ca contents and hence the partition coefficient also correlates with the concentration of these elements. The larger relative change in solution Ca content than in Li partition coefficient across the range of experiments means that the Li exchange coefficient ($Kd(Li/Ca)=[Li_{calcite}/Ca_{calcite}]/[Li^{+}_{solution}/Ca^{2+}_{solution}]$) decreases with increasing solution pH; i.e. at constant solution Li content and calcite Ca content, the Li content of the calcite grown at high pH is somewhat higher than that grown at low pH but the Ca content of the solution is much lower than in the experiments at low pH (Figure 3.1a). There is no systematic variation in exchange coefficient with the duration of the experiment or Li content of solution (Figure 3.2). The results of the experiments reported here are broadly consistent with those reported by Marriott et al. (2004a, 2004b) both in terms of the absolute values of the exchange coefficients and the relative change in exchange coefficient with changing solution pH (Figure 3.1). However, the data reported by Füger et al. (2019), while having similar partition coefficients, do not show the same correlation with experiment pH (Fig. 1b); in contrast, they do have similar exchange coefficients (Figure 3.1a). As discussed below, I interpret this difference to reflect the difference in experimental method that led to Ca and pH not being strongly correlated in their

experiments as they were in mine. Because the pH and $Ca_{(aq)}$ of the solution changed dramatically during the calcite growth experiments of Okumura and Kitano (1985) it is not meaningful to compare their data directly with those presented here. Overall, the data suggest a strong control of solution chemistry on the partitioning of Li between calcite and an aqueous solution.

Two experiments were doped with ~500 ppb Rb in the starting solution to test whether any experimental solution was not washed off when the calcite was separated at the end of the experiment. These show (Supplementary Table D.1.1) that even if Rb is assumed to be entirely derived from the experimental solution attached to the surface of the calcite, with none incorporated into the calcite, the average amount of Li derived from this is <4 % of the Li in the calcite (with a maximum of 15 % for the experiment in which calcite has the lowest Li content).

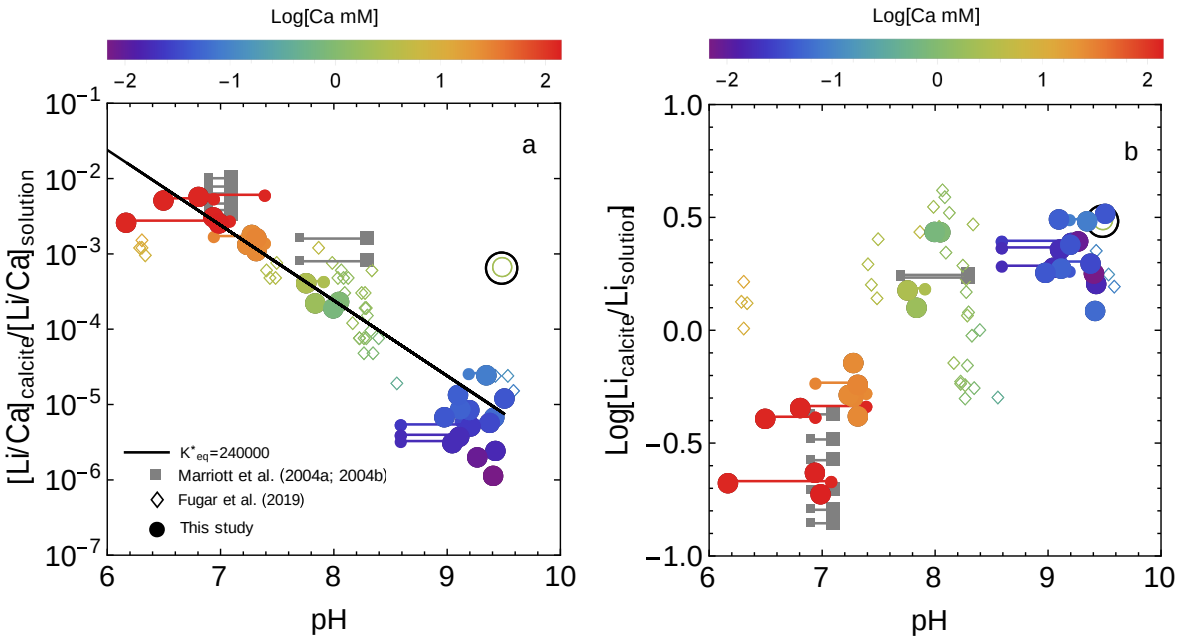

Figure 3.1. The (a) Li/Ca exchange coefficient, and (b) Li partition coefficient plotted against the pH of the final solution in the experiments. Symbol colour (this study and Fügar et al., 2019) reflects the solution Ca content. Large and small symbols, connected by a line, show the final and initial solution pH respectively; the pH variation was less than 0.1 unit for samples shown as a single symbol. Because of the experimental design the solution pH and Ca content inversely correlate. Uncertainties in the y-axis are smaller than the symbols. The data point surrounded by an open black circle has a much higher Ca concentration in its final solution compared to the other high-pH (≥ 9) experiments, which I interpret as due to contamination by calcite during separation of the solution from the calcite. The solid line shows a model for incorporation of Li in calcite as $LiHCO_3$ (see text for details).

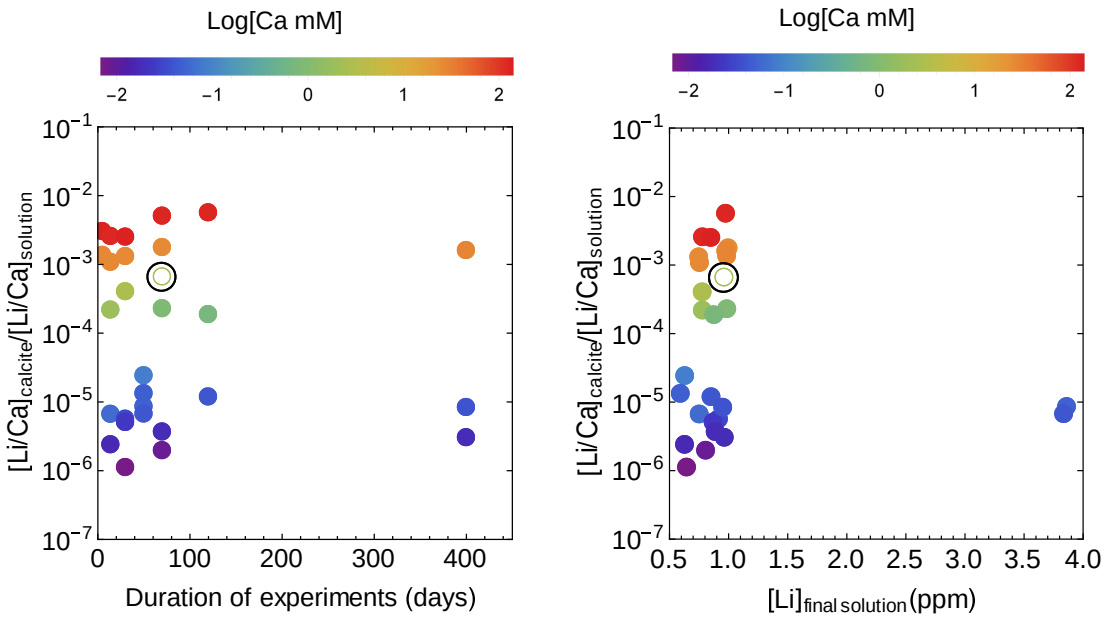

Figure 3.2. The Li/Ca exchange coefficient plotted against the duration of experiments (left) and Li content of solution at the end of experiments (right). Symbol colour reflects the Ca content of solutions at the end of experiments. Both plots show that variation of the Li/Ca exchange coefficient is independent of the duration of experiments and Li content of solution. The data point surrounded by an open black circle has a much higher Ca concentration in its final solution compared to the other high-pH (≥ 9) experiments, which I interpret as due to contamination by calcite during separation of the solution from the calcite.

3.4.3. Lithium isotopic fractionation between calcite and solution

The Li-isotope fractionation between calcite and solution increases by ~8‰ as the solution pH increases from ~6.5 to ~9.5, and $Ca_{(aq)}$ decreases (Figure 3.3; Supplementary Table D.1.1). There is no systematic variation in the fractionation factor with the duration of the experiment or the Li content of solution (Figure 3.4). The results of Marriott et al. (2004b) are consistent with the results presented here. In contrast, the isotopic fractionation measured by Marriott et al. (2004a) at a pH of ~7 is ~3‰ larger than that determined here. A substantial difference between those studies and the experiments reported here is the much more rapid calcite precipitation rate in their studies in which 0.5 to 1 g of calcite was precipitated in 5 hours compared to 0.1 g of calcite growing in 5 to 400 days in my experiments. When I attempted to replicate their methodology I commonly (but not always) produced a mixture of vaterite and calcite. However, Marriott et al. (2004a, 2004b) report that they confirmed the mineralogy as calcite by XRD suggesting some aspect of the experimental design was not identical.

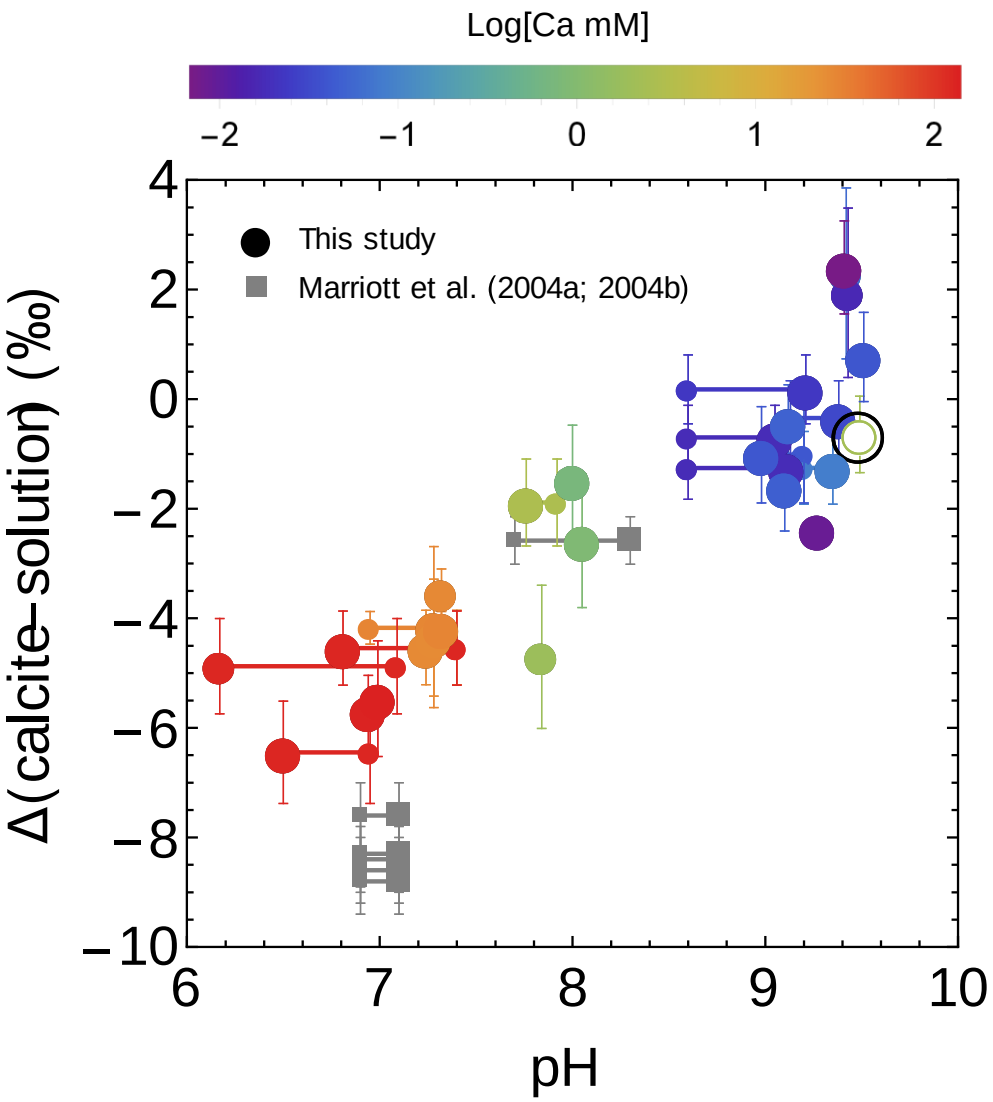

Figure 3.3. Variation in measured difference in Li isotopic composition of calcite and the solution it grew in (Δ) with solution pH. Symbol colour reflects the solution Ca content (this study only). Large and small symbols connected by a line show the final and initial solution pH respectively; the pH variation was less than 0.1 unit for samples shown as a single symbol. The data point surrounded by an open black circle has a much higher Ca concentration in its final solution compared to the other high-pH (≥ 9) experiments, which I interpret as due to contamination by calcite during separation of the solution from the calcite.

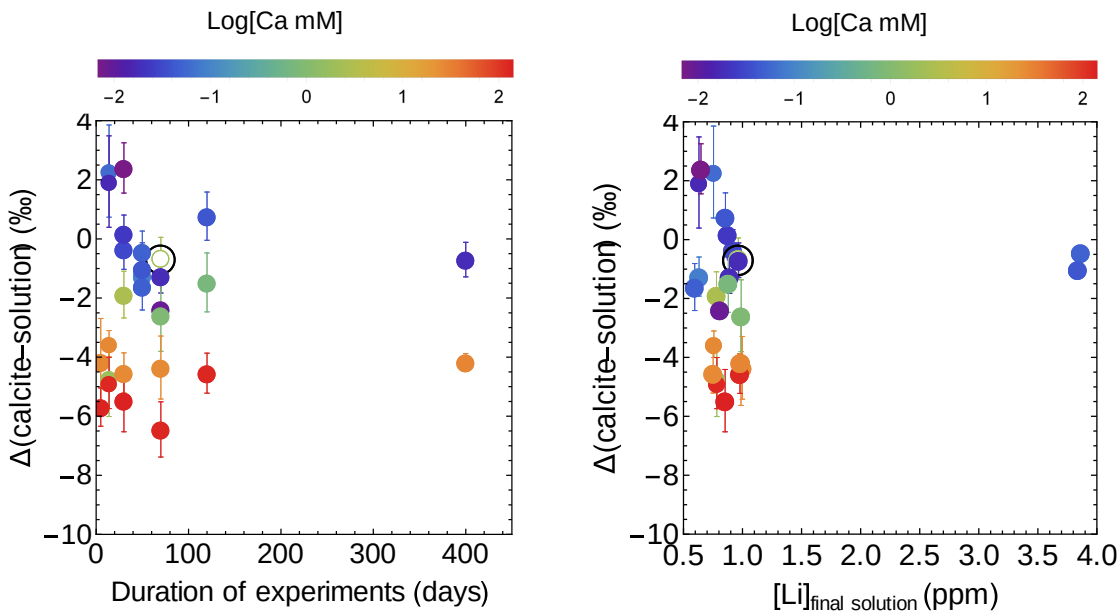

Figure 3.4. The measured Li isotopic fractionation factor (Δ) between calcite and the final solution plotted against the duration of experiments (left) and Li content of solution at the end of experiments (right). Symbol colour reflects the Ca content of solutions at the end of experiments. Both plots show that the Li isotope fractionation factor is independent of duration of experiments and Li content of solution. The data point surrounded by an open black circle has a much higher Ca concentration in its final solution compared to the other high-pH (≥ 9) experiments, which I interpret as due to contamination by calcite during separation of the solution from the calcite.

3.4.4. Relative diffusivity of ^{6}Li and ^{7}Li in different aqueous solutions

Over the duration of the diffusion experiments the pH of the high pH solutions decreased somewhat probably due to equilibration with the head-space in the containers (Supplementary Table D.1.2). This change was completed before the first experiment was taken off, hence I assume that the pH was that of the final solution for most of the duration of the experiment. The fraction of the initial Li remaining in the source solution decreased systematically with time in the diffusion experiments as expected (e.g., Richter et al., 2006). In parallel with this drop in Li content, the source solution δ^{7}Li increased indicating that ^{6}Li diffused out of the source vial faster than ^{7}Li (Figure 3.5). In the longest duration experiments (211 days), irrespective of the solution matrix, the source retained 2-3 % of its initial Li content, and had a δ^{7}Li 6-7 ‰ higher than its starting composition. While there may be slight differences in the relative diffusivity of the two isotopes with solution matrix, the data are consistent with there being no control of solution matrix of the relative diffusivity. In contrast, Richter et al. (2006) using a DI matrix, and LiCl source solution, found a slightly larger difference in the relative diffusivity of the two isotopes (Figure 3.5). The other difference between their experiments and those reported here is that they were performed at 75°C rather than room temperature (under these conditions the pH is expected to have been ~6.35 (Light, 1984) although this was not reported).

To obtain the ratio of diffusivity coefficients of ^{7}Li and ^{6}Li (D_7/D_6), the equation for evolution of the concentration of the source solution was solved for a condition of finite source to sink volumes ratio, using the following equations (Richter et al., 2006):

$$J_i = \frac{D_i A(C_{i,1} - C_{i,2})}{L} \qquad \text{Eq. 3.1}$$

$$\frac{\partial C_{i,N}}{\partial t} = -\frac{J_i}{M_N} \qquad \text{Eq. 3.2}$$

where, J_i is the diffusion flux of the isotope i, A and L are the inner cross-section area and length of the tube connecting the source and sink, and $C_{i,N}$ is the concentrations of isotope i in container N (N = 1 for source and N = 2 for sink container) and M is the container mass. Solving the above differential equation results in the following:

$$\frac{R}{R_0} = \frac{f_j^{(\frac{M_1}{M_2}+1)\frac{D_{7_{Li}}}{D_{6_{Li}}}} + (\frac{M_1}{M_2})}{f_j^{(\frac{M_1}{M_2}+1)} + (\frac{M_1}{M_2})} \qquad \text{Eq. 3.3}$$

where, R is the ratio of ^{7}Li/^{6}Li in the source solution at any given time and R_0 is the initial value of R, and f is the molar fraction of the initial Li still remaining in the source container. See Richter et al. (2006) for further discussion. Eq. 3.3 was used to determine the value of D_{7Li}/D_{6Li} that best fits the results of each series of experiments (Figure 3.5) using a weighted least square fitting procedure. All four experimental time series fit well with ^{6}Li diffusing ~0.2 % faster than ^{7}Li (D_{7Li}/D_{6Li} from 0.9979 to 0.9982; Supplementary Table D.1.2) whereas the experiments reported by Richter et al. (2006) suggest ^{6}Li diffused ~0.24 % faster than ^{7}Li (D_{7Li}/D_{6Li} of 0.9976 from refitting the data reported by Richter et al. (2006) using Eq. 3.3 rather than a linear fit as they report).

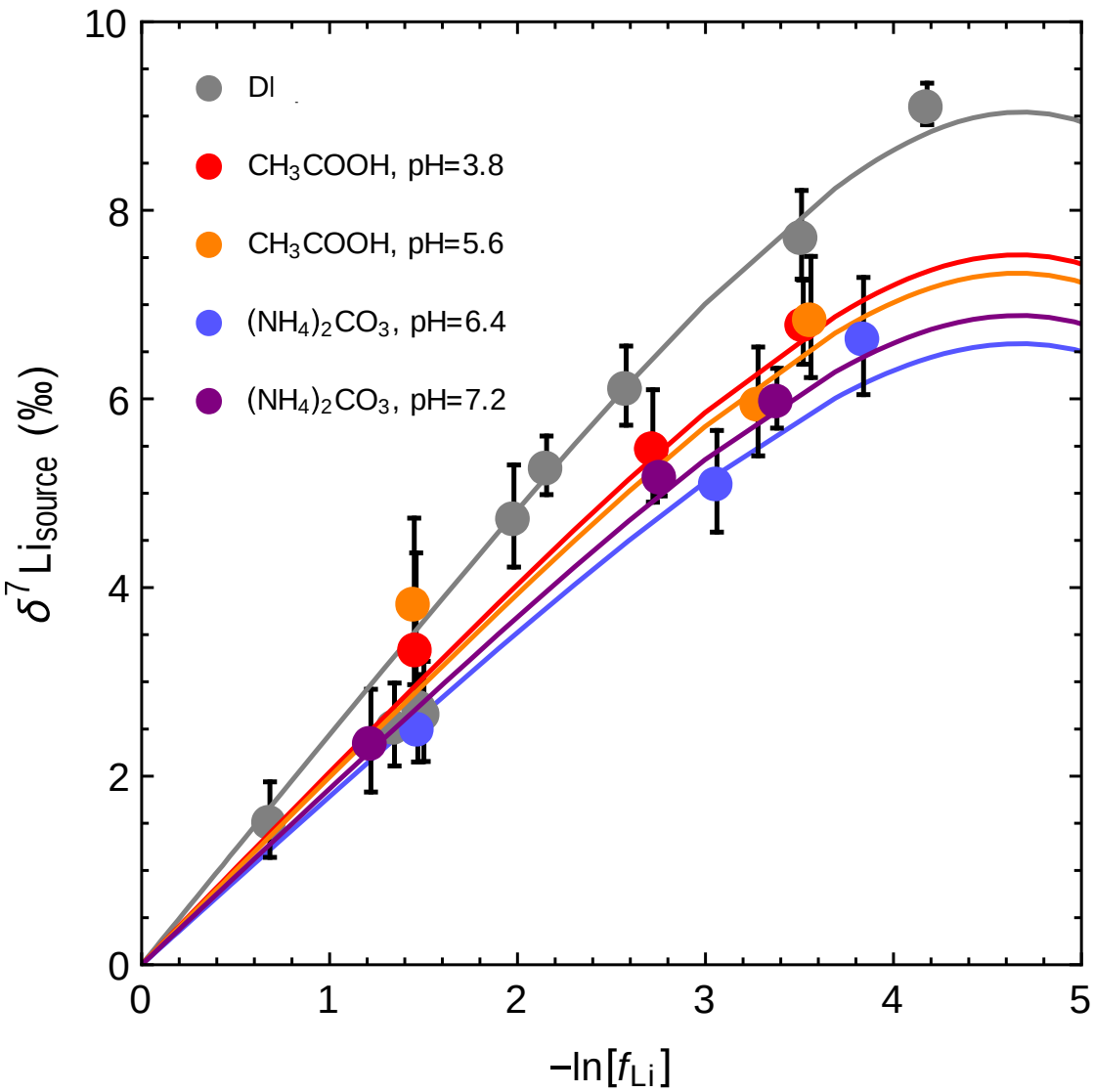

Figure 3.5. Li-isotopic composition of the source solution in the diffusion experiments as a function of the fraction of Li remaining in the source (f_{Li}). The curves are fit through data from each experimental time series performed at a different pH using a non-linear model (Eq. 3.3) weighted according to the uncertainty on the Li-isotope data (Supplementary Table D.1.2). Data for experiments in a DI matrix are from Richter et al. (2006) performed at 75°C (versus ~21°C in this study).

As discussed elsewhere (Moller et al., 2005; Richter et al., 2006), the small difference in diffusivity of the two Li-isotopes, despite their large mass difference, suggests that they diffuse as much heavier aqueous species where the mass difference is much smaller. This small difference in relative diffusivity suggests that diffusion will generally lead to only small Li-isotope fractionations. The lack of a large change in the relative diffusivity of the isotopes with changing solution chemistry suggests that, for the solutions considered here, the diffusing species do not change dramatically with changing solution chemistry. For example, if the diffusing species are hydrated Li ions, $Li(H_2O)_x^+$, and if the number of hydrating water molecules (x) changed substantially across the range of

solutions considered, then the relative mass difference between the ^{6}Li and ^{7}Li species would change substantially; in this case I should see a change in the relative diffusivity of the isotopes with changing solution chemistry. The lack of such a signal constrains the magnitude of any change in mass of the diffusing species.

3.5. Discussion

3.5.1. Lithium incorporation into calcite

The systematic change in the partitioning of Li between inorganic calcite and aqueous solution with solution chemistry (Fig. 1) provides insight into the incorporation of Li into calcite. Because of the experimental design the pH, $Ca_{(aq)}$, $Na_{(aq)}$ and carbonate chemistry (e.g., DIC, HCO_3^-, CO_3^{2-}) of the solutions changed systematically with one another and have to be considered together. Charge balance allows three simple substitution mechanisms for Li into calcite grown in these solutions in which Li, Na and Ca were the only cations:

Model A:

$$2Li^+(aq)+CaCO_3(s) \rightleftharpoons Li_2CO_3(s)+Ca^{2+}(aq) \qquad \text{Eq. 3.4a}$$

$$K^*_{eq} \propto \frac{C_{Li_{calcite}}}{C_{Li^+}} \times \frac{C_{Ca^{2+}}}{C_{Li^+}} \qquad \text{Eq. 3.4b}$$

Model B:

$$Li^+(aq)+Na^+(aq)+CaCO_3(s) \rightleftharpoons LiNaCO_3(s)+Ca^{2+}(aq) \qquad \text{Eq. 3.5a}$$

$$K^*_{eq} \propto \frac{C_{Li_{calcite}}}{C_{Li^+}} \times \frac{C_{Ca^{2+}}}{C_{Na^+}} \qquad \text{Eq. 3.5b}$$

Model C:

$$Li^+(aq)+H^+(aq)+CaCO_3(s) \rightleftharpoons LiHCO_3(s)+Ca^{2+}(aq) \qquad \text{Eq. 3.6a}$$

$$K^*_{eq} \propto \frac{C_{Li_{calcite}}}{C_{Li^+}} \times \frac{C_{Ca^{2+}}}{C_{H^+}} \qquad \text{Eq. 3.6b}$$

where, K^*_{eq} is an approximation of the respective equilibrium constants. Only for model C do the values of K^*_{eq} remain similar across the range of solution chemistry (Figure 3.6). Based on this I suggest that Li incorporation in calcite, at least under the conditions of these experiments, is most likely as a $LiHCO_3$ component. If Li is incorporated as a $LiHCO_3$ component (Eq. 3.6), the partition coefficient of Li into calcite increases as the solution H^+/Ca^{2+} increases. This means that a decrease in the pH of a solution, at constant Ca and Li concentration, will lead to an increase in the Li content of the calcite. The apparent "inverse" effect in my experiments (Figure 3.1b) reflects the larger decrease in Ca^{2+} than decrease in H^+ as the solution pH increases, leading to an increase in H^+/Ca^{2+}, and hence in Kd_{Li} ($Li_{calcite}/Li^+_{solution}$), with increasing pH. This model

can also explain the lack of a correlation of Li partition coefficient and pH in the experiments of Füger et al. (2019), unlike in this study (Figure 3.1b), because the Ca content of the solution in their experimental design was not tied to the solution pH. If instead of considering the partitioning of Li between calcite and solution I consider the exchange coefficient $(Li/Ca)_{calcite}/(Li^{+}/Ca^{2+})_{solution}$, as is commonly the case (e.g., Marriott et al., 2004a, 2004b; Füger et al., 2019), then the role of solution Ca content is directly accounted for and the exchange coefficient should simply depend on pH with a slope of -1; this is the case for both my data and that reported by Füger et al. (2019; Figure 3.1a). Incorporation of Li^{+} in calcite as $LiHCO_3$ may also be testable using Fourier-Transform Infrared spectroscopy (FTIR), by measuring H contents of calcite. Moreover, previous studies have suggested that incorporation of monovalent cations in calcite can be accompanied by a CO_3^{2-} vacancy or through an ion-coupled mechanism (e.g., Li^{+}-HCO_3^{-}; Yoshimura et al., 2017; Füger et al., 2019). Further studies are required to test these models.

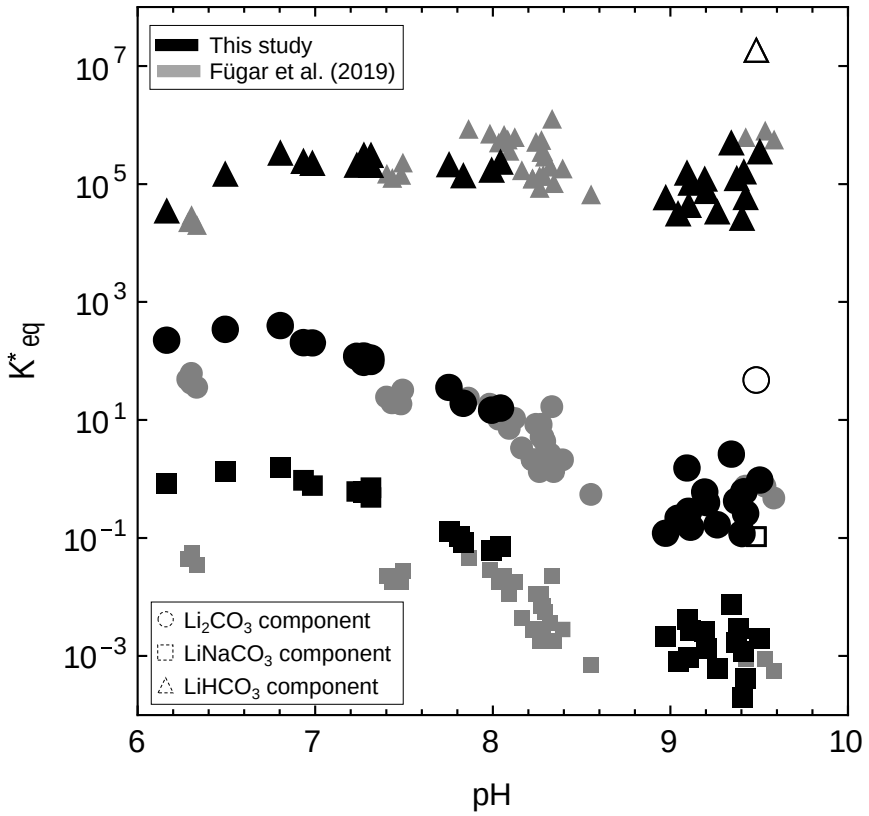

Figure 3.6. Calculated approximate equilibrium constant (K^{*}_{eq}) based on measured concentrations for Li incorporation into calcite as the Li_2CO_3, $LiNaCO_3$ and $LiHCO_3$ components (models A, B and C discussed in the text) plotted against the pH of the final solution in the experiment for both my study and that of Füger et al. (2019) which agree reasonably well with one another despite different experimental designs. Only for Li incorporation as $LiHCO_3$ is the calculated equilibrium constant similar for all experiments meaning that this is a plausible substitution mechanism and the others are not. The open symbols show a sample that has a higher Ca concentration in its final solution compared to the other high-pH (≥ 9) experiments, almost certainly due to calcite contamination during the separation of the solution from the precipitated calcite.

An alternative explanation for the change in exchange coefficient with changing solution chemistry is that it may reflect different calcite growth rates under different conditions (e.g., Füger et al., 2019). Both previous work (Hobbs and Reardon, 1999) and my study shows that the recrystallization of vaterite to calcite occurs faster under lower pH conditions. If faster recrystallization is accompanied by faster calcite growth the calcite grown at lower pH should have a higher Li content (Füger et al., 2019) which is the inverse of what I observe. While I do not have direct measurements of calcite growth rates I consider this a less parsimonious model to explain the data and favour the model outlined above (incorporation Model C) to explain the control of solution chemistry on Li partitioning. Füger et al. (2019) have shown that nearly an order of magnitude increase in growth rate is correlated with an order of magnitude increase in the Li exchange coefficient. If such a large change in growth rate occurred in this study, an obvious change in calcite crystal size/morphology would be expected to be observed in SEM images, but the SEM images (Appendix A, Section A.5) show no obvious difference with experiment duration or solution chemistry. However, subtle variations in growth rate may be responsible for some of the scatter in the data and for some of the differences between the results of this study and previous work.

3.5.2. The lithium isotopic fractionation between calcite and solution

I consider three hypotheses to explain the change in Li-isotope fractionation factor with changing solution chemistry (Figure 3.3): (i) isotope fractionation during diffusion of Li in the solution towards or away from the growing calcite; (ii) kinetic isotope fractionation associated with surface attachment of Li ions; and (iii) changes in the equilibrium fractionation factor due to changes in the aqueous speciation of Li with changing solution chemistry.

It is possible for Li-isotopes to be fractionated by diffusion in an aqueous solution (Richter et al., 2006; Bourg et al., 2010; Figure 3.5). While the relative diffusivity of the isotopes does not appear to be directly dependent on pH (Figure 3.5), because the partitioning of Li between solution and calcite changes with solution chemistry, this would have led to differences in the concentration gradient of Li in the solution around the growing calcite crystals. In turn, through the dependence of the diffusive flux on the concentration gradient, this could lead to diffusive isotopic fractionation. When there is more Li in calcite than solution (high pH in my experimental set up; Supplementary Table D.1.1) there would be a Li flux towards the growing crystals and when there is less Li in calcite than solution (low pH in my experimental set up) there would be a Li flux away from the growing crystals. Faster diffusion of ^{6}Li than ^{7}Li (Figure 3.5) means that if aqueous diffusion of Li controlled the isotopic fractionation the calcite in high pH experiments would be isotopically lighter than the calcite in the low pH experiments – this is the inverse of what is observed (Figure 3.3). Thus, aqueous diffusion cannot have been the dominant control on the observed change in isotopic fractionation factor with changing solution chemistry.

A second model to explain the change in Li-isotope fractionation with changing solution chemistry is that the kinetics of Li incorporation at the growing crystal surface change with solution chemistry (Watson, 2004; DePaolo, 2011). Two possible ways for

such surface kinetic effects to explain the data are considered. First, calcite growth rate may have varied as a function of solution chemistry and surface kinetic effects depend strongly on crystal growth rate (Watson, 2004; DePaolo, 2011; Hofmann et al., 2012). In this scenario the lighter isotope is generally incorporated more strongly during faster growth. Unfortunately, I have no independent constraint on growth rates. While the vaterite to calcite transformation occurred more slowly in the high pH experiments, and the experiment duration was not correlated to the observed isotopic fractionation under any conditions, neither of these observations directly constrain crystal growth rate variations. A second mechanism by which surface kinetic effects could explain the data is if the rate of desolvation of Li ions during incorporation into calcite depends on solution chemistry. The slower desolvation of the heavier isotope has been shown to be associated with significant fractionation of a magnitude relevant to that observed (~8 ‰ for Li based on molecular dynamics simulations of pure water desolvation; Hofmann et al., 2012). How the magnitude of this kinetic isotope fractionation transfers into an isotopic fractionation between the mineral and fluid is unclear. It is plausible that the rate of desolvation depends sufficiently on solution chemistry that this leads to the observed variation in isotopic fractionation across the range of solution chemistry (e.g., Roberts et al., 2018). Further experiments that constrain both growth rate and aqueous Li speciation will be required to test whether the variation in isotopic fractionation factor observed in the experiments is due to surface kinetic effects.

A third mechanism to explain the observed dependence of the fractionation factor on solution chemistry is if this records a change in the equilibrium isotope fractionation factor. This would require that the dissolved Li species changed in such a way as to lead to the heavier isotope being more strongly retained in the solution under the conditions of my low pH experiments. While the diffusion experiments (Figure 3.5) show no evidence for a change in the aqueous Li-species with changing pH, they do not preclude one provided the change in the mass difference between the ^{6}Li- and ^{7}Li-bearing species is small. Bogatko et al. (2013) proposed the following pH dependent changes in Li speciation in aqueous solutions:

$$Li(OH)(H_2O)_x + CO_3^{2-} \rightleftharpoons Li(CO_3)(OH)(H_2O)_{x-2}^{2-} + 2H_2O \qquad \text{Eq. 3.7}$$

$$Li(H_2O)_x^{+} + H_2O \rightleftharpoons Li(OH)(H_2O)_{x-1} + H_3O^{+} \qquad \text{Eq. 3.8}$$

The fractionation of Li-isotopes between such species is difficult to determine (e.g., Bogatko et al., 2013) and at this stage I feel it is premature to speculate further about whether changes in the speciation of Li in solution could generate the observed Li-isotope fractionation through equilibrium effects. Thus, I conclude that either a kinetic isotope fractionation associated with surface attachment of Li to the calcite, or a change in the equilibrium fractionation factor, could explain the observed change in fractionation factor with changing solution chemistry. Either way, it is clear that assuming the isotopic fractionation factor is constant and small when interpreting the composition of inorganic calcite will lead to ambiguous results.

3.5.3. Li in biogenic calcite

I have avoided discussion of biogenic calcite to this point because the solution biogenic calcite grows from is not necessarily the same composition as the bulk solution. Understanding the relevance of the results presented here, and of the model for Li partitioning into calcite as a $LiHCO_3$ component, for the interpretation of the Li systematics of biogenic calcite requires an understanding of the controls on the chemistry of the calcifying fluid. A detailed discussion of this is beyond the scope of this study but I note two important differences that may be key for explaining apparent differences in the behaviour of biogenic calcite and inorganic calcite. First, if calcification is driven by elevation of pH in the calcifying fluid, and the proton pumps involved in this can transport Li (Vigier et al., 2015), the Li content, as well as carbonate chemistry, of the solution biogenic calcite precipitates from may differ from that of the bulk solution. Second, Li isotopes can be strongly fractionated by diffusion across membranes (Fritz, 1992) and thus the limited diffusive fractionation in aqueous solutions discussed above (Figure 3.5) may not be relevant to Li incorporation into biogenic calcite were ions have to be transferred across membranes to reach the site of calcite growth – instead diffusive isotope fractionation may be very important for biogenic calcite.

3.5.4. Possible geological signals of the control of solution chemistry on Li in calcite

As an example of how the results presented here could change interpretations of the Li-isotopic composition of carbonates from the geological record I briefly discuss the change in δ^7Li across Ocean Anoxic Event 2 (OAE2) reported by Pogge von Strandmann et al. (2013). They show that the Li-isotopic composition of carbonates leached from samples from OAE2 have systematically lower δ^7Li than samples from above or below this interval. They interpret this as reflecting a change in the Li isotopic composition of seawater – a reasonable interpretation. However, the results presented here suggest an alternative model may need considering. Either a significant change in ocean chemistry, or more likely, a difference in the pore fluid chemistry in this interval during diagenesis, may have led to this isotope anomaly in the sediments. For example, Du Vivier et al. (2015) suggest that the simplest explanation of the Ca-isotope anomaly associated with OAE2 is a change in the Ca-isotope fractionation factor, possibly due to ocean acidification – the same should be considered for the Li-isotope anomaly. Alternatively, enhanced organic carbon sedimentation during OAE2, followed by diagenetic degradation of the organic carbon, could lead to recrystallization of the carbonate sediments under low pH conditions leading the growth of diagenetic calcite with a low δ^7Li. A drop in pH at near constant fluid Ca content could also explain the significant increase in Li/Ca of the carbonates from the OAE reported by Pogge von Strandmann et al. (2013). Indeed, the up to an order of magnitude increase in Li/Ca associated with the drop in δ^7Li, and variation in this between sections, would be simpler to explain in a diagenetic model than in a model in which these reflect constant partitioning from an ocean with variable Li content. In reality diagenetic reactions may well also involve silicate phases which would complicate the situation. However, I caution that in general, before using such bulk carbonate analyses to interpret changes in the Li-isotopic

composition of seawater changes in the fractionation factor during both primary carbonate sedimentation, and especially during diagenesis, should be seriously considered. A similar conclusion has recently been reached from an entirely different approach by Murphy et al. (2018).

3.6. Conclusions

New experimental data show that both elemental and isotopic fractionation of Li between inorganic calcite and an aqueous solution depends on the solution chemistry. The solution chemistry control on the Li partition coefficient is most simply explained by Li substituting into calcite as a $LiHCO_3$ component and thus the Li content of calcite increasing with increasing H^+/Ca^{2+} of the solution all other things being equal. This means that for solutions where the Li and Ca contents are roughly constant (e.g., seawater) the Li content of inorganic calcite will increase with decreasing pH. The effect of solution chemistry on the Li-isotope fractionation factor may either come from a kinetic effect associated with surface attachment, or from an equilibrium effect due to changes in the speciation of Li in the solution. Irrespective of the interpretation of the mechanism involved, the experimental data presented here, alongside recent results from Füger et al. (2019), demonstrate that the partitioning and isotopic fractionation of Li between inorganic calcite and aqueous solutions is more complex than generally thought. We also caution that, while my results help towards building a framework for understanding the fundamental controls on Li incorporation into calcite, they should not be directly applied to biogenic calcite. They are, however, relevant to interpretation of any carbonates that have undergone even partial diagenetic recrystallization. Changes in the Li content and Li-isotopic composition of such sediments may reflect changes in the solution the final calcite grew from rather than changes in ocean chemistry.

4. Lithium and lithium isotope exchange between seawater and off-axis oceanic crust: A case study from DSDP Holes 417A, 417D and 418A

4.1. Introduction

Formation of oceanic crust at mid-ocean ridges (MOR) introduces Earth's interior heat into the ocean (e.g., Stein and Stein, 1994; Sclater et al., 1980). The majority of this heat loss occurs during circulation of seawater in the upper permeable oceanic crust away from the ridge axis (Stein and Stein, 1994) and causes extensive low-temperature hydrothermal alteration of the basaltic crust. During low-temperature interaction between seawater and oceanic crust, Li is generally taken up into secondary clay minerals and Li-isotopic exchange occurs between hydrothermal fluid and clay minerals. Due to the extensive circulation of seawater through the upper oceanic crust, low-temperature alteration in the off-axis setting may have an important role in the oceanic lithium cycle, but this is poorly understood.

The main sources of lithium into seawater are riverine fluxes and high temperature hydrothermal fluid fluxes at MORs, and the main sinks of Li are low-temperature hydrothermal alteration of the oceanic crust and sediment diagenesis (e.g., Chan et al., 1992; Misra and Froelich, 2012; Coogan et al., 2017; Figure 1.1). Despite decades of research on the ocean Li cycle, there are still major uncertainties in the magnitude of the Li fluxes and the isotopic composition of the input and outputs of Li to the ocean (Figure 1.3). To understand the role of low-temperature off-axis hydrothermal systems in the global lithium cycle, it is important to first understand the process of lithium and lithium-isotope exchange between seawater and ocean crust. There are several studies of the Li content and isotopic composition of off-axis oceanic crust but either the studied areas have non-typical environmental settings, or the number of studied samples are insufficient to confidently extrapolate the interpretation of the data. The first study reports the composition of dredged samples from the seafloor in the Atlantic along a timeline from 0 to 46 Myr old crust (Chan et al., 1992). This study estimated a δ^7Li of ~16 ‰ for the altered end-member of upper oceanic crust which had interacted with seawater with δ^7Li of ~31 ‰, suggesting an apparent isotopic fractionation factor of 15 ‰ ($\Delta_{sw\text{-}oc}=\delta^7Li_{sw}-\delta^7Li_{oc}$). Another study of the Li composition of altered oceanic crust was undertaken on the cores from ODP Holes 504B and 896A (5.9 and 6.8 Myr old crust, respectively) which have anomalously rapid sedimentation rates and hence warm temperatures of alteration (Chan et al., 2002). The temperature of alteration in the upper crust is also high at IODP Site 1256 (15 Myr old crust), which is another example of oceanic crust with rapid sedimentation. In addition to rapid sedimentation, Site 1256 is capped with a thick massive flow (Alt et al., 2010) which led to low water-to-rock ratios and caused fluid-rock interaction at unusually high temperatures (23 to 77°C; Coggon et al., 2006; Alt et al., 2010), and apparently caused little or no Li addition to the rocks (Gao et al., 2012). Bouman et al. (2008) presented a small dataset of the Li content and isotopic composition of altered lavas from Deep Sea Drilling Project (DSDP) Sites 417 and 418 (119 Myr old crust) which includes two individual lava samples and three composite basalt samples. This study showed higher Li contents and lighter δ^7Li of altered basaltic

rocks at shallow depths below sediments compared with deeper sections. Coogan et al. (2017) studied the Li content and isotopic composition of altered lavas from four sections of the Troodos ophiolite (~90 Myrs) with variable hydrological settings, providing considerable number of data on Li content of lavas, however, the δ^7Li data is less focused on the uppermost lavas where the majority of Li is added into the crust.

Here I present a detailed study of the behaviour of Li and Li-isotopes in Holes 417A, 417D and 418A, which were drilled into the 119 Myr Western North Atlantic ocean crust that have different hydrological histories, up to 600 m penetration into the crust and 60-70 % hard rock recovery. I use both bulk rock and mineral separate data, to better understand the processes involved in Li- and Li-isotope exchange between the ocean and upper oceanic crust that control the bulk lithium flux and bulk Li-isotope fractionation factor. I show that the Li concentration and isotopic composition of altered lavas changes with depth, and shallow samples, with the highest Li contents, have the lightest δ^7Li (lighter or similar to the δ^7Li of fresh mid-ocean ridge basalts (MORBs)). Several hypotheses are tested to explain the observed variation in Li content and isotopic composition of altered lavas with depth which are divided in two groups: (i) a change in the Li partition coefficient and isotopic fractionation factor between altered rocks and hydrothermal fluid due to a change in mineral assemblages of altered lavas with depth, and (ii) evolution of the Li concentration and isotopic composition of the hydrothermal fluid and lavas during continuous fluid-rock interaction as fluid flows through the crustal aquifer. I conclude that neither mineralogy, nor evolution of the hydrothermal fluid composition during one-dimensional fluid flow can explain the measured Li concentrations and isotopic compositions of lavas from the upper oceanic crust. Instead I propose that a conceptual model of free-circulation of seawater within the shallow crust, before accumulation of significant amount of sediments, can explain the high Li concentrations and light isotopic composition of the uppermost altered lavas. After accumulation of significant amount of sediments, fluid-rock reaction would happen under more restricted conditions, explaining the lower Li content and heavier isotopic composition of the deeper crust compared to the shallower levels.

4.2. Study area and sample suite

During Legs 51, 52 and 53 of the DSDP Holes 417A and 417D were drilled 450 m apart, and Hole 418A was drilled ~6.5 km away from these holes in 119 Myr old ocean crust at the Southern end of the Bermuda Rise (Donnelly et al., 1979a and 1979b). Hole 417A is located at a topographic high relative to the location of adjacent Holes 417D and 418A (Figure 4.1), hence the sedimentation rate was slower at Hole 417A than at Holes 417D and 418A (Donnelly et al., 1979a and 1979b). Based on the age of basal sediments, Hole 417A was open to seawater for ~20 Myr (Table 4.1). Holes 417D and 418A penetrated deeper into the basaltic rock compared with Hole 417A (Table 4.1).

The sediments directly overlying the crust differ between holes (Table 4.1). Based on the sediment major element composition and published descriptions, Hole 417A is overlain by “zeolitic clay” sediments (Donnelly et al., 1979a). Basal sediments at Hole 417D and 418A are divided into two groups: “radiolarian nannofossil” sediments with high Al_2O_3 and SiO_2, and low CaO and total C, and “nannofossil chalk and ooze” with

low SiO_2 and Al_2O_3, but very high CaO and total C (Table 4.1). More generally, the sediments can be divided in two groups, siliceous (including both zeolitic clay and radiolarian nannofossil sediments) and calcareous.

The lithostratigraphy of the drill holes is shown in Figure 4.1. The uppermost lavas in Holes 417A and 417D are pillow basalts whereas Hole 418A has ~5 m of pillow basalt underlain by a thick (~60 m) massive flow (Figure 4.1). Below this, all holes have a mix of pillow basalt, breccia and massive basalt.

The type and distribution of secondary minerals is variable among Holes 417A, 417D and 418A. For example, celadonite and saponite are abundant in all three holes but Al-rich clay minerals are only abundant in Holes 417A and 417D, and are absent in Hole 418A (Alt and Honnorez, 1984). Secondary K-feldspar replaced primary plagioclase phenocrysts and is intergrown with Al-rich clay mineral in samples from Site 417 due to extensive circulation of oxygenated seawater (Alt and Honnorez, 1984). Partial replacement of plagioclase phenocrysts by K-feldspar is also reported in the Hole 418A (Humphris et al., 1980). Calcite is one of the most common secondary minerals at both Sites 417 and 418 and fills vesicles, veins and veinlets (Alt and Honnorez, 1984; Humphris et al., 1980). Based on measured calcite O-isotope compositions, and assuming the O-isotopic composition of 119 Myr old seawater was -1 ‰ (Cramer et al., 2011), the temperature of alteration in the upper ~150 m of the crust was ~20 to 25°C (Richardson et al., 1980; Lawrence, 1979; Javoy and Fouillac, 1979; Meuhlenbach1979; Hart and Staudigel, 1979; Scarfe, 1979). The temperature of alteration is almost uniform throughout the upper 150 m below sediments of all three Holes 417A, 417D and 418A (Table 4.1). Hole 418A, which penetrated deeper into the crust compared with Holes 417A and 417D, shows higher average of temperature through the entire crust (Table 4.1).

Table 4.1. Summary of the key characteristics of DSDP Holes 417A, 417D and 418A

	417A	417D	418A
Crustal age (Myr)	119	119	119
Sediment thickness (m)	208	342	324
Sedimentation rate (m/Myr)	1.7	2.9	2.7
Penetration into the basalt (m)	200	366	548
*Average temperature of alteration through the hole (°C)	22	22	35
*Average temperature of alteration in upper 150 m below sediments (°C)	22	21	24
Basal sediment type	Zeolitic clay	Nannofossil chalk and ooze	Nannofossil chalk and ooze
Age of basal sediment (Myr)	66-100	113-119	113-119

* See text for data sources; temperatures calculated using Kim and O'Neil (1997)

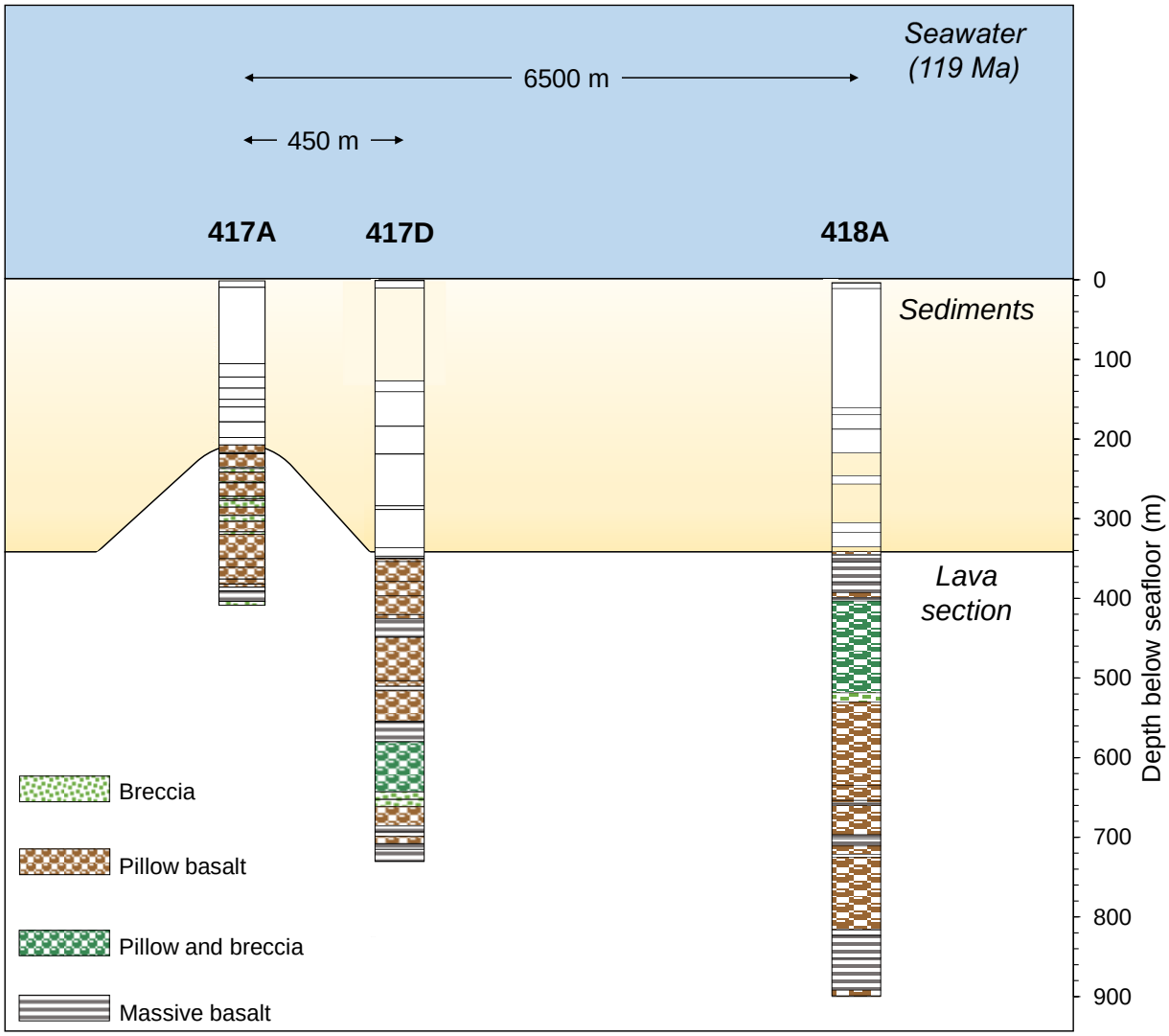

Figure 4.1. Cartoon showing the location of Holes 417A, 417D and 418A relative to each other. The stratigraphy of the drill holes and sediment types are taken from the DSDP preliminary reports (Donnelly et al., 1979a and Donnelly et al., 1979b). The gaps in the sediment sections are regions without recovery.

Sixty-nine lava samples and nine sediment samples were selected from Holes 417A (27 lava samples and 3 sediments), 417D (27 lava samples and 3 sediments) and 418A (15 lava samples and 3 sediments). The lavas were selected based on the following criteria: (i) to cover the depth range of the cores with denser sampling at the top where previous studies suggested a change in the Li content and isotopic composition of altered lavas (Coogan et al., 2017; Bouman et al., 2008); (ii) to focus on pillow margins to make inter-sample comparison more meaningful; and (iii) to sample differing lithologies (pillow interior, breccia and massive flow) to allow assessment of the role of lithology in controlling the behaviour of Li during fluid-rock reaction. The sediments were collected to sample the main lithologies immediately overlying the basement rocks and are mainly silicates.

A suite of three lava samples was also selected for major and trace element, and XRD analysis to examine the composition and mineralogy of their constituent parts. These lava samples were crushed to ~500 µm sized pieces and the constituent parts were hand picked using a binocular microscope. The sub-samples include groundmass with different levels of oxidation (based on their shades of red colour), altered phenocrysts and altered glass with different textures (Table 4.2). The picked sub-samples were pulverized in agate pestle and mortar.

4.3. Analytical methods

4.3.1. Silicate materials

Bulk rock powders were crushed using a jaw crusher and an agate planetary mill. Major elements of lava and sediment samples where determined by X-Ray Fluorescence (XRF) at Acme labs (standard package of whole rock major oxides and total C and S analysis at Acme Analytical Labs Ltd., Vancouver, Canada). Major elements of lava sub-samples were determined by ICP-MS at the University of Victoria; XRF analysis was not possible due to lack of material. Hence the silicon content of these samples was not measurable due to the digestion of the samples in HF acid. For trace element and isotopic analysis, around 100 mg of each sample powder (bulk rocks and silicate mineral separates) was digested in four steps. First, the powder was dissolved in 5.5 ml of a 10:1 mixture of concentrated HF-HNO_3 in a pre-cleaned Teflon vial at ~125°C for at least 48 hours. Second, the sample was dried and re-digested in 1 ml DI, 1 ml of concentrated HNO_3 and 1 ml of concentrated HCl on a hotplate at ~125°C over night followed by two steps of drying and re-digesting in 4 ml of 8 M HNO_3 for at least one day and finally in 4 ml of 1 M HNO_3. If the solution was not perfectly clear at this stage, it was dried down and digested in 0.5 ml of concentrated HCl and refluxed over night at ~125°C. The HCl was then evaporated and the sample taken up again in 4 ml of 1 M HNO_3. A 0.5 ml split of the solution was removed and diluted in 2% HNO_3 to produce a solution with a dilution factor of 1000 for trace element analysis.

Trace element analysis was conducted at the University of Victoria using a Thermo X series II ICP-MS and an Agilent 8800 Triple Quadrupole generally following the method of Eggins et al. (1997). The solutions were spiked online with ~3 ppb In, Rh and Re as internal standards and the primary drift was corrected by normalizing to ^{115}In. Secondary drift was corrected using a drift monitor solution run after every 5 samples. After blank correction (which was always negligible), measurements were calibrated using the rock standards of BHVO-2, BCR-2, JB-2, JR-2 and UB-N-1 (Supplementary Table D.2.7). Averages of multiple measurements of each reference rock (80 analyses in total) which were used for calibration, deviate from the published values between 15 % (at a low Li concentration of 4.5 ppm) and 1 % (at a high Li concentration of 87 ppm). Reproducibility of Li measurements, based on 87 total procedural duplicates (including reference standards of BHVO-2, BCR-2, JB-2, JR-2, BIR-1 and UB-N-1 and bulk samples), over the course of this PhD, is better than 10 % (Relative Standard Deviation (RSD); Supplementary Table D.2.7).

Lithium was separated from the matrix of the remaining 3.5 ml of the dissolved sample broadly following the method of Teng et al. (2004). Teflon columns (30 cm long and 0.95 cm inner diameter) filled with 7.5 g (dry weight) of BIORAD AG 50W-x8 (200-400 mesh) were cleaned using 40 ml of 7 M HNO_3 followed by 15 ml of deionized H_2O (DI), 40 ml of 4 M HCl and a further 50 ml DI. The resin was conditioned with 25 ml of 20 % 0.1 M HNO_3 in 80 % methanol (by volume) based on the method of Reiman and Walton (1970; for more details see Section C.1.4 of Appendix C). The 3.5 ml sample in 1 M HNO_3 was mixed with 0.5 ml of concentrated HNO_3 and 3.43 ml of methanol giving 1.55 M HNO_3 in a 46 % methanol matrix. 5.9 ml of this mixed solution was loaded into the columns. Column calibrations show that the Li and Na peaks are well separated by elution using 85 g of a solution of 1 M HNO_3 in 80 % methanol (Chapter 2) and collecting the aliquot released between 25 and 75 g. Trace element analysis of a 10 g aliquot before and after the peak showed that >99 % of the lithium was recovered in the peak aliquot in all cases. Peak aliquots were dried down and dissolved in 2 % HNO_3 to make a 10 ppb Li concentration solution for isotope analysis. All reagents used were environmental grade, HPLC grade and 18.2 MΩ.cm Millipore DI.

Lithium isotope analysis was conducted at the University of Victoria using the same ICP-MS instrument used for trace element analysis. The two lithium isotopes were measured sequentially using single collector quadrupole ICP-MS. Dwell times of 50 ms and 250 ms were used for ^{7}Li and ^{6}Li, respectively, with 5 ms settling time. Thirty blocks of 24 analyses for a total run time of ~7 minutes is used for analysis of each sample. Each sample was analysed 4 or 5 times with the reported value being the average of these analyses.

Analytical sessions started with a block of 10 ppb IRMM-016 standard solution to determine stability of the instrument and define the instrumental drift. The dead-time was then determined by analysing solutions of variable lithium concentrations (3 to 20 ppb). Samples and 10 ppb IRMM-016 were then run using a standard-sample bracketing approach with another block of IRMM-016 at the end of the analytical session. It was ensured that samples and standards were made up in exactly the same (2% HNO_3) matrix as any differences influence the ^{7}Li/^{6}Li ratios during the run (Chapter 2).

A second or third order polynomial curve was fit through the 10 ppb IRMM-016 ^{7}Li/^{6}Li ratios to define the instrumental drift and the value given by this curve at the time of each sample analysis was used in calculating the δ^7Li of that sample using the normal nomenclature:

$$\delta^7\text{Li}=\left[\frac{\left(\frac{^7\text{Li}}{^6\text{Li}}\right)_{\text{sample}}}{\left(\frac{^7\text{Li}}{^6\text{Li}}\right)_{\text{IRMM-016}}}-1\right]\times 1000 \qquad \text{Eq. 4.1}$$

The instrumental precision was assessed by four or five replicate analyses of samples during each analytical session and the average of measurements shows a precision better

than 1.5 ‰ ($2S_{\bar{x}}$; two standard error). Replicate analysis of samples and international rock standards showed a procedural precision better than 3 ‰ (2SD). Measured δ^7Li of samples compared to reported δ^7Li values of international rock standards shows a difference less than ±1.7 ‰ (Supplementary Table D.2.7).

The sediment samples from Hole 417A were digested and treated the same way as lavas for chemical analysis, but the sediments from Holes 417D and 418A did not fully dissolve using this approach. An alternative dissolution approach using 3 ml of H_2O_2 (a strong oxidizing agent) as a pre-treatment, followed by the regular acid digestion steps was tested, but still did not lead to complete digestion of the samples. Thus, incompletely digested samples, in 4 ml of 1 M HNO_3, were centrifuged for 15 minutes at 3000 rpm to separate the solid material and then prepared for trace element and isotopic analysis following the same procedures described above. No attempt was made to identify the undigested fraction but it is hypothesised to be dominated by organic material. Sediments prepared with both the regular digestion method and using a H_2O_2 pre-treatment have similar concentrations of Li (<10 % difference) and other mobile elements (e.g., Rb), even though the amount of undissolved material remaining after using a H_2O_2 pre-treatment was noticeably lower, suggesting that the main hosts of Li were dissolved using both approaches.

4.3.2. Carbonates

To prepare carbonate samples for trace element and Li isotope analysis, 50 mg of uncrushed chips of hand-picked carbonates were transferred into a 5 ml centrifuge tube and rinsed with DI multiple times. Samples were dissolved in 3 ml of 1 N HCl, shaken well to homogenize the solution, and then divided into a ~0.6 ml split for elemental analysis and a ~2 ml split for isotopic analysis.

Lithium was separated from the sample matrix for isotopic analysis, using 15 ml micro-columns filled with BIORAD AG 50W-x8 (200-400 mesh) using the method of Misra and Froelich (2009). Li-isotope analyses consisted of 5 analyses of a “conditioning solution” made from mixing small aliquots of multiple in-house $CaCO_3$ standard samples, bracketed with IRMM-016 standard solution, and then alternating sample and standard analyses followed by 3 analyses of IRMM-016 at the end of the run to quantify the instrumental drift. All solutions were analysed at a concentration of 1 ppb Li. The isotopic composition of samples was measured only once (due to the limited volume of sample). The Li-isotopic composition of samples was calculated relative to the average value of IRMM-016 before and after each sample; i.e. using a standard bracketing approach. Six analyses of two splits of an in-house $CaCO_3$ standard (Alfa Aesar 99.999% purity $CaCO_3$ powder) gave a procedural precision of ±1.3 ‰ ($2S_{\bar{x}}$). A complete description of the analytical methodology is given in Appendix C, section C.2.

4.3.3. X-Ray Diffraction (XRD)

To determine the mineralogy of silicate and carbonate minerals separated from samples XRD analysis was conducted. To prepare an oriented mount, a DI slurry was made with a small amount of the sample powder (<10 mg) on a zero-background substrate and left to

dry. To distinguish between the basal d-spacings of different clay minerals, samples were placed in a sealed chamber with ethylene glycol at ~60° C for ~5 hours. Oriented sample films were analysed before and after glycolation to monitor shifts in basal peak positions. The XRD analysis was conducted at the University of Victoria using a PANalytical X'pert instrument with Cu Kα source, 45 kV accelerating voltage and 40 mA current. To identify mineral assemblages using the XRD data, I used HighScore Plus software. To process the data, the background noise was determined and subtracted from the whole pattern and the position and intensity of each of the recorded signals were extracted. Using the database of the HighScore Plus software, those minerals which their pattern showed the best match with the extracted signals were assumed to exist in the sample.

4.4. Results

4.4.1. Lithium abundance in bulk samples

The Li content of all lavas correlate positively with their B, K and Rb concentrations and negatively with their Ca contents (Supplementary Table D.2.1), consistent with previous work that has shown uptake of Li, B, K and Rb and removal of Ca during low-temperature hydrothermal alteration of lavas (e.g., Alt et al., 1986a; Staudigel et al., 1996; Johnson and Semyan, 1994; Staudigel, 2014). The Li content of the lavas range from 10 to 70 ppm, but to understand the change in Li content of a lava due to hydrothermal alteration it is essential to consider the initial Li content of the sample. Fresh MORB Li contents range from 2 to 20 ppm (Gale et al., 2013), increasing during magmatic differentiation in the same way as other moderately incompatible elements such as Y. Thus, Li/Y is relatively constant in fresh MORB and elevated Li/Y is an indicator of Li addition to rocks (Figure 4.2). Lithium addition can be quantified using glass compositions to define a protolith Li content (Li_{proto} =0.14Y+1.79; Figure 4.3) and a change in Li content due to hydrothermal alteration can then be calculated (ΔLi) as the difference between the measured Li content and Li_{proto}. All of the bulk-rock samples from Holes 417A, 417D and 418A have higher Li/Y than fresh rocks, indicating uptake of Li during low-temperature hydrothermal alteration (Figure 4.3). Samples from Hole 417A have highly elevated Li/Y (Figure 4.2) with an average ΔLi of 24 ppm. Samples from Holes 417D and 418A have an average ΔLi of 5 and 7 ppm, respectively.

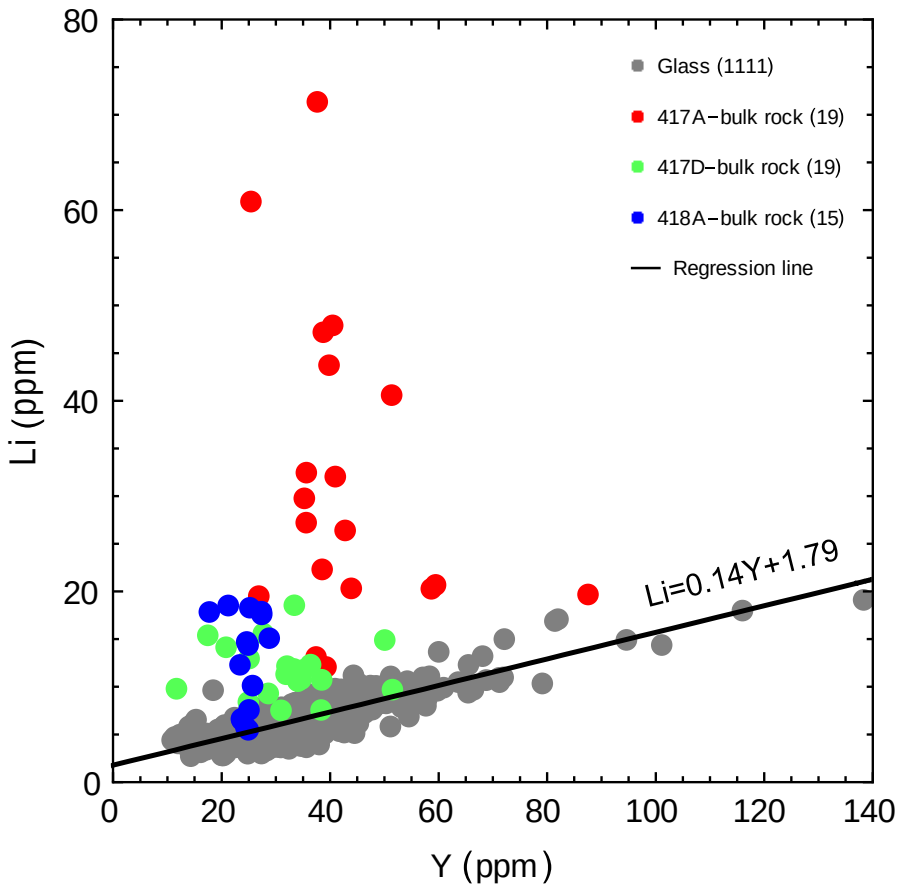

Figure 4.2. Li vs. Y concentration of lava samples. The black line shows a regression through MORB glass data interpreted as the magmatic differentiation trend (Gale et al., 2013). The altered lavas fall above the line, indicating Li uptake during low-temperature hydrothermal alteration of the upper lava section of the ocean crust. Numbers in brackets is the number of samples.

In each drill hole the highest Li contents are generally in the uppermost samples but there are significant differences between holes (Figure 4.3 and Supplementary Table D.2.1). In Hole 417A the Li content decreases smoothly with depth, with no dependence on the lithology, but even at the base of the hole the Li content is substantially elevated relative to fresh rocks. In contrast samples from Holes 417D and 418D are much less Li-rich (5-20 ppm) and thus there is less difference between the upper samples relative to deeper samples.

Sediments directly overlying the lavas from each hole were analysed to evaluate if exchange between hydrothermal fluids and sediment pore-fluids, or contamination of the lava samples by sediment, influenced lava compositions. The siliceous sediment samples from immediately above basement in Holes 417A and 417D contain 55 to 67 ppm Li (Figure 4.3), 7-20 wt% Al_2O_3, 50-65 wt% SiO_2, and < 1 wt% CaO and < 2 wt% total C (Supplementary Table D.2.2). In contrast, the siliceous sediment samples from immediately above basement in Hole 418A, which have similar major element compositions to those from Site 417, have Li concentrations roughly half of those in the Site 417 samples. Calcareous samples from Holes 417D and 418A have lower Li contents

broadly consistent with mixing between a silicate sediment and an almost Li-free carbonate component.

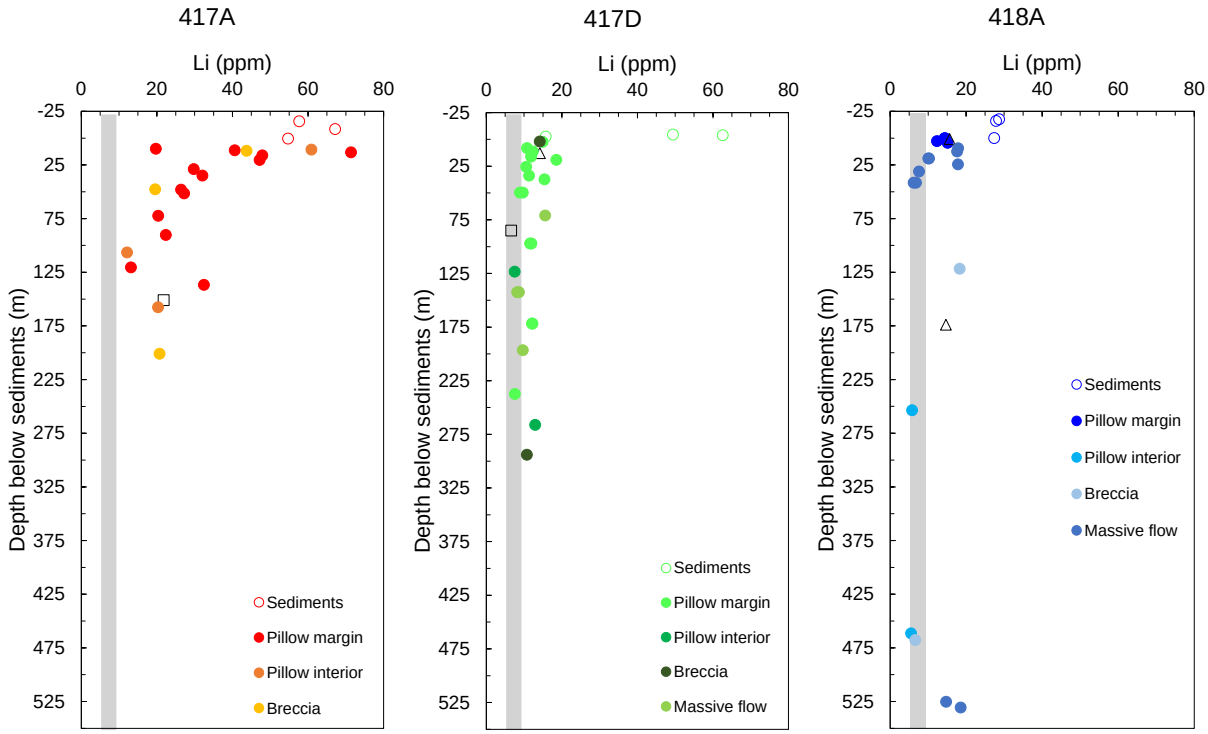

Figure 4.3. Lithium concentration versus depth below sediments in Holes 417A, 417D and 418A. The solid symbols represent basalt samples. Basalt sample lithologies are shown with different colours and open circles show sediments. Open symbols with black rims identify previously published data (triangles are composite samples and squares are basalt samples; Bouman et al., 2008). The gray band shows the range of Li concentrations of fresh MORBs at these sites. In general, Li concentration decreases from the top of crust to deeper levels. An elevated Li concentration of massive flow samples at the deepest levels of the Hole 418A might be due to longer residence time of hydrothermal fluid and hence longer fluid-rock interaction in low-permeable massive basalts with small input/output hydrothermal fluid flux.

4.4.2. Lithium isotopic composition of bulk samples

During low-temperature hydrothermal alteration of silicate rocks the isotopic composition of the rocks can become isotopically lighter or heavier than the fresh rock depending on the initial isotopic composition of the rock and fluid and the isotopic fractionation factor. The lithium isotopic composition of fresh MORBs has a mean δ^7Li of 3.7 ‰ (with a range from 1.6 ‰ to 5.6 ‰, n=31; Tomascak et al., 2008) whereas altered lavas measured in this study range from -1 ‰ to 13 ‰ (Figure 4.5). Lava samples from all three holes are significantly isotopically lighter at the top of the lava section than deeper in the crust with data from the study of Bouman et al. (2008) consistent with the data reported here (Figure 4.4). This isotopically light upper-section of lavas, that coincides with the most Li-rich portion of the lavas, is 30 to 40 m thick. Beneath this isotopically light upper region, almost all basalts are isotopically heavier than the

protoliths and show no systematic change in Li-isotopic composition with depth or lithology (Figure 4.4). Notably, samples from Hole 417A, the most Li enriched core, do not extend to as light an isotopic composition as samples from the less Li-rich cores from Holes 417D and 418A (Figure 4.5).

The sediments overlying the basement have systematically different δ^7Li between the three holes. Siliceous sediments from Hole 417A have δ^7Li of 0 to 1 ‰ and both siliceous and carbonate-rich sediments from Hole 417D have δ^7Li of 2 to 4 ‰. However, carbonate-rich sediment immediately overlying the lavas in Hole 418A has similar δ^7Li (~3 ‰) as carbonate-rich sediment from Hole 417D, but the siliceous sediments from Hole 418A have δ^7Li of 8 to 10 ‰ (Figure 4.4).

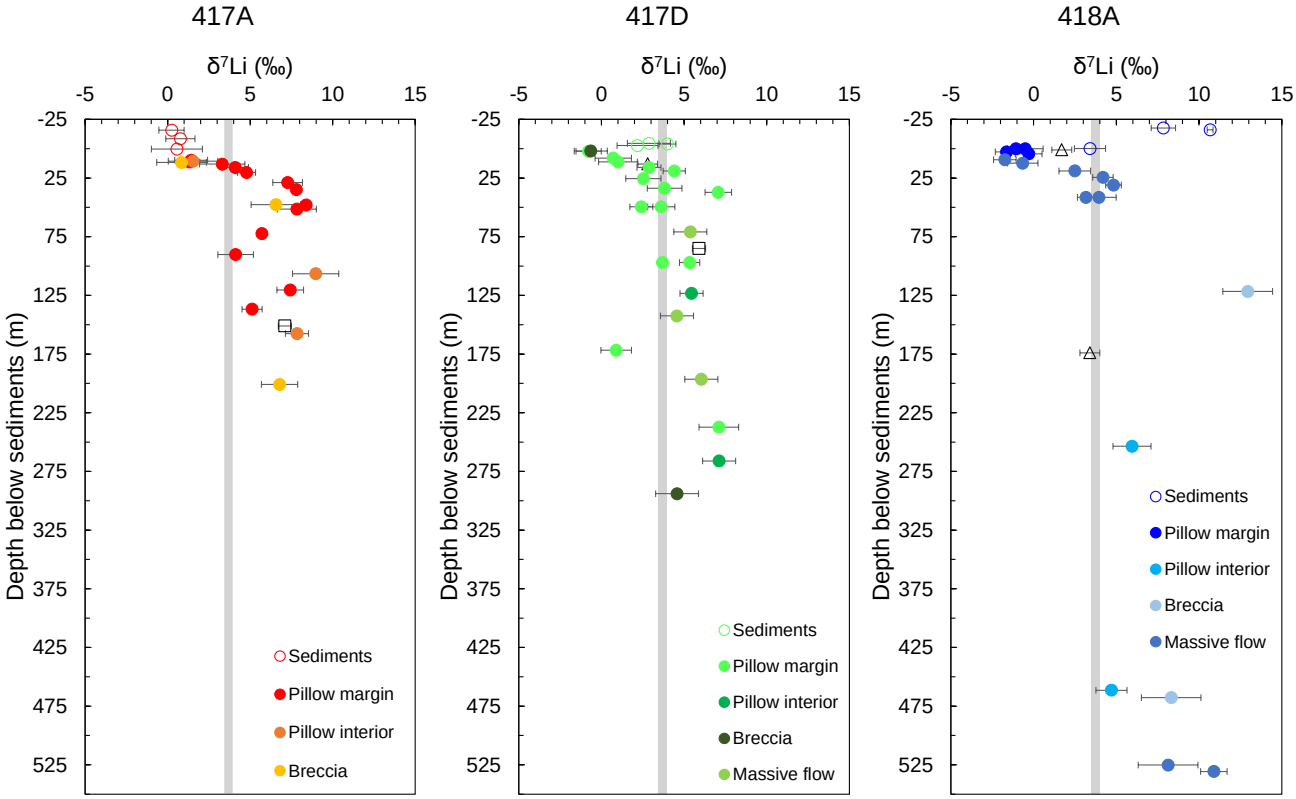

Figure 4.4. Lithium isotopic composition versus depth below sediments in Holes 417A, 417D and 418A. The solid symbols represent basalts. Basalt sample lithologies are shown with different colours and open circles show sediments. Open symbols with black rims are taken from previously published data (triangles are composite samples and squares are basalt samples; Bouman et al., 2008). The gray band shows the range of Li isotopic compositions of fresh MORBs. In general, Li-isotopic composition increases from the uppermost part of crust to ~30 m below sediments, then fluctuates in deeper levels. I suggest that a high Li-isotopic composition of samples at deep levels (deeper than 475 m blow sediments) of the Hole 418A might be due to interaction of rocks with a highly evolved hydrothermal fluid with high Li-isotopic composition. Horizontal error bars represent ±2SDE on replicate analysis of δ^7Li of samples.

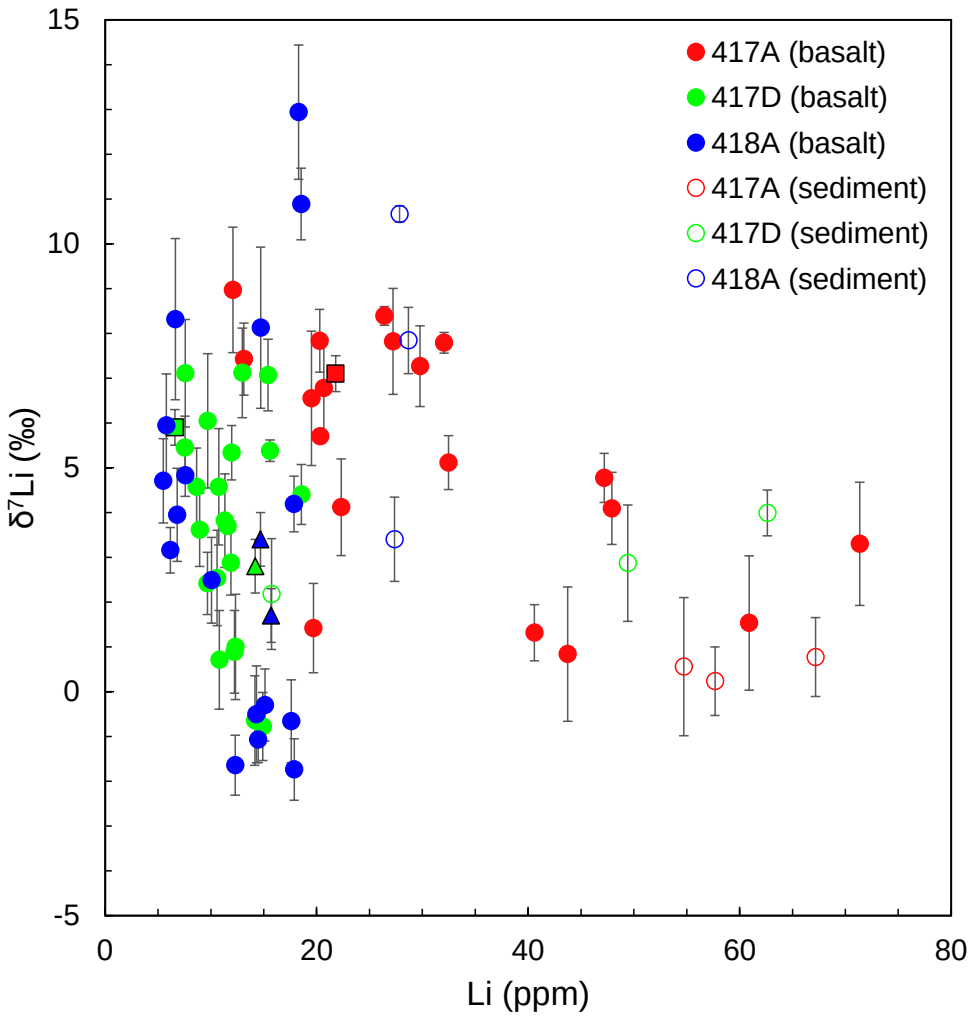

Figure 4.5. Lithium isotopic composition versus Li concentration at the Holes 417A, 417D and 418A. The solid symbols represent basalt samples and open circles show sediments. Symbols with black rims are taken from previously published data (triangles are composite samples and squares are basalt samples; Bouman et al., 2008). Vertical error bars represent ±2SDE on replicate analysis of δ^7Li of samples.

4.4.3. Sub-sample analyses

4.4.3.1. Silicate sub-samples

Different minerals have different capacity for storing Li and different isotopic fractionation factors. To investigate the role of mineralogy in controlling the Li content and isotopic composition of altered lava samples, the Li concentration and isotopic composition of the constituent parts of three lava samples with a range of Li content and isotopic composition were determined: two samples from Hole 417A (417A-24R-2-70-75, 417A-28R-1-19-24) and one from Hole 418A (418A-33R-2-14-17). The selected lavas are from ~10 m, ~50 m and ~120 m below the lava-sediment boundary. The constituent parts include the groundmass, altered phenocrysts and/or altered glass. A detailed description of each separated part is presented in Supplementary Tables D.2.4

and D.2.4.1. Major and trace element compositions are reported in Supplementary Table D.2.4.

To determine the mineral assemblages of each sub-sample, standard and ethylene glycol treated-XRD analyses were conducted on the samples. For each sub-sample, an assemblage of orthoclase (replacing plagioclase), clay minerals, Fe-hydroxides, and/or calcite was identified, consistent with previous studies of these cores (e.g., Alt and Honnorez, 1984; Humphris et al., 1980; Table 4.2). The specific clay types were identified by their basal peaks before and after glycolation. The greatest uncertainty comes from the identification of one phase, assumed to be a clay mineral based on a broad basal peak and large d-spacing (~1.54nm after glycolation; Figure 4.7). Sub-samples with this probable clay phase also contain orthoclase. The sub-samples containing this clay phase have high Al_2O_3 and low K_2O contents (Supplementary Table D.2.4). Excluding Al_2O_3 that can be assigned to orthoclase (assigning all K_2O to orthoclase), the bulk composition of these sub-samples is still Al-rich. This suggests that a plausible interpretation for this unidentified phase is an Al-rich clay (beidellite) that is found as a replacement of plagioclase in association with orthoclase in Holes 471A and 417D (e.g., Alt and Honnorez, 1984), and other older drill holes (Coogan and Gillis, 2018). Even though kaolinite and gibbsite are common Al-rich alteration products of orthoclase, but their main peak were absent in the XRD pattern of Al-rich sub-samples. Henceforth, this phase is referred to as “unknown clay”.

To estimate the proportion of each phase in the sub-samples, a simple Mathematica code was used to minimize the difference between the sum of the mineral composition (using seven major elements of SiO_2, Al_2O_3, Fe_2O_3, CaO, MgO, Na_2O and K_2O) multiplied by their mass fractions of each sample and the whole sample chemical composition given the constraints that mineral fractions have to be between 0 to 1 and the sum of their fractions has to equal 1 (Table 4.2 and Figure 4.6). SiO_2 contents were not measured and are calculated by difference, therefore these calculations only give an estimation of the proportion of each phase.

Table 4.2. Constituent parts of altered lava samples and proportion of detected minerals

Lava sample ID (Hole-core-section, upper-lower interval (cm))	Parts separated	Proportion of parts separated (%)	Texture	Mineral assemblages**/ proportion (%)								
				Aug	An-Ab	Orth	Phi	Unk-clay	Cel-sap	Sap-Fe	Hem	Calc
417A-24R-2, 70-75*	Groundmass	70	Moderately oxidized		20	30		30			20	
	Altered glass	10	Layered-fine grained			30		70				
	Altered phenocryst	15	Pseudomorph after plagioclase			70		30				
417A-28R-1, 19-24*	Groundmass	70	Highly oxidized			40				50		10
			Less oxidized			50				40		10
	Altered glass	20	Layered			15	40		45			
			Fine grained			10	50		40			
418A-33R-2, 14-17	Groundmass	80	No oxidation	20	50					30		
	Altered phenocryst	20	Pseudomorph after plagioclase		20	50		30				

* In addition to the constituent parts of each sample, there was ~5 % vein and veinlets in sample 417A-24R-2-70-75, and ~10 % pseudomorphs of plagioclase in sample 417A-28R-1-19-24 which were not separated for chemical analysis and mineralogical study.
**Aug: augite; An-Ab: anorthite-albite; Unk-clay: Unknow-clay; Orth: Orthoclase (secondary K-feldspar); Phi: phillipsite; Cel-sap: celadonite-saponite; Sap-Fe: saponite-iron oxide; Hem: hematite; Calc: calcite

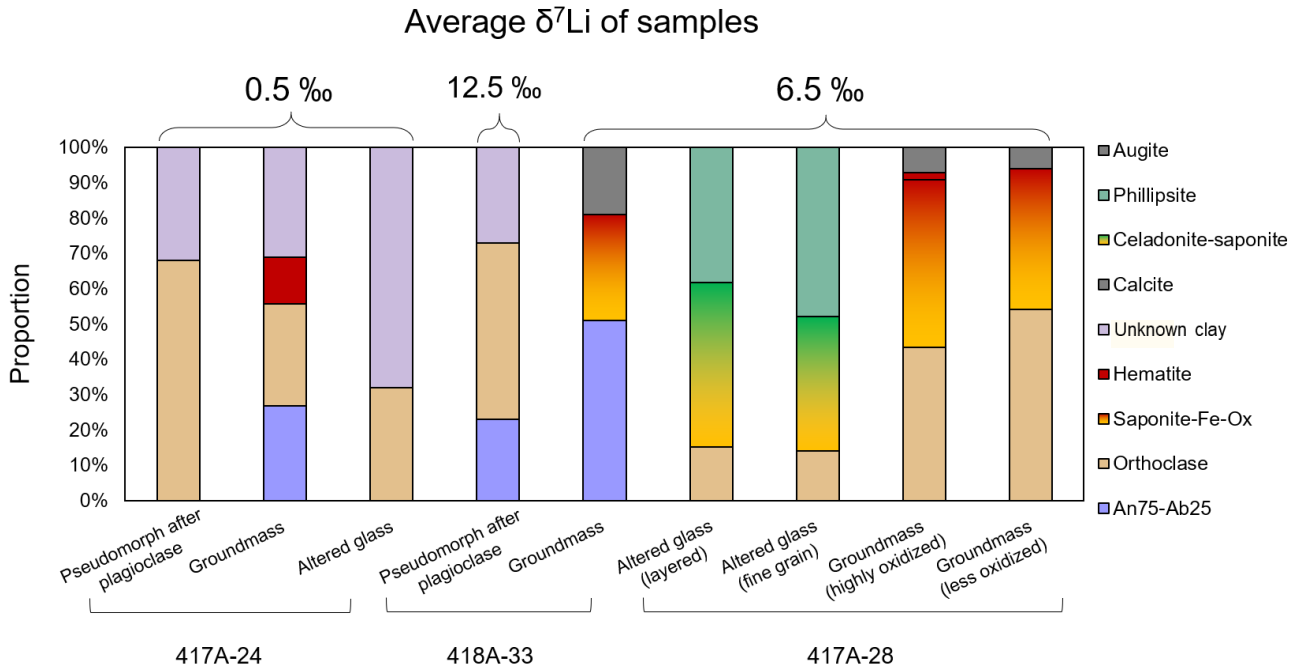

Figure 4.6. Calculated proportions of each secondary phase determined using XRD and chemical analysis data for the sub-samples.

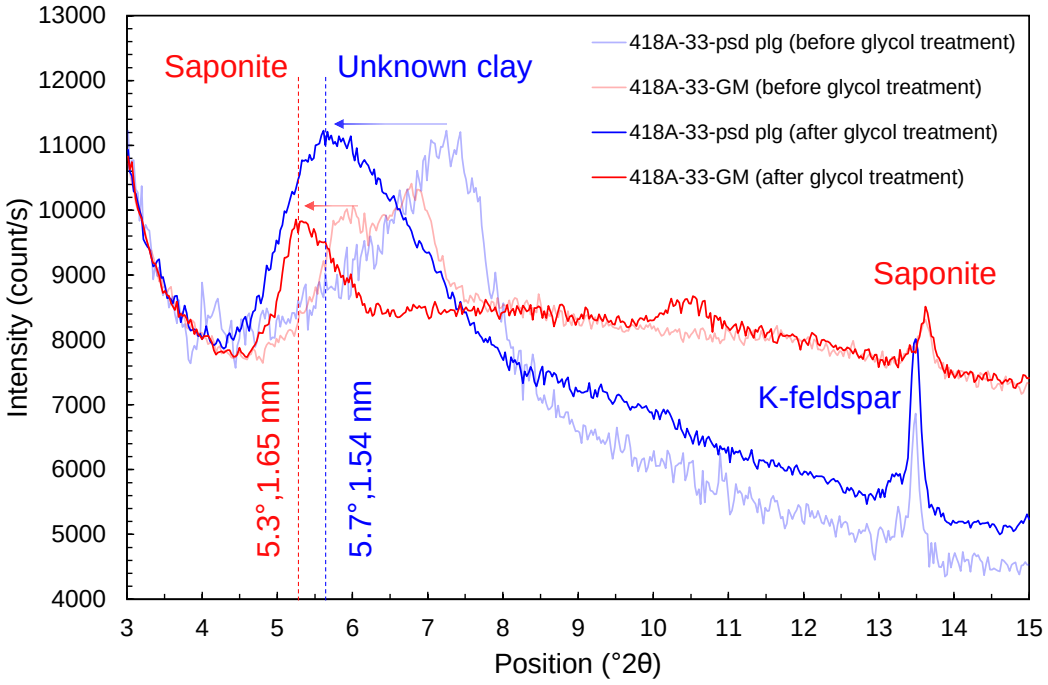

Figure 4.7. XRD patterns for lava sample 418A-33R-2-14-17. Shifts in basal peak positions of groundmass (GM) and pseudomorph after plagioclase (psd plg) sub-samples after ethylene glycol vapor treatment are shown by arrows. The two sub-samples show different basal peak positions, the 0.11 nm difference in d-spacing indicates the presence of two different clay minerals (Supplementary Table D.2.6).

The Li content and δ^7Li for the bulk rocks and their constituent parts (sub-samples) are shown in Figure 4.8. The sub-samples of groundmass, altered glass and pseudomorph after plagioclase phenocrysts from sample 417A-24R-2-70-75 (12 m below sediments) have a wide range of Li contents from 40 to 105 ppm Li, while they have similar δ^7Li of ~0 ‰ (Figure 4.8). The bulk rock composition is similar to the groundmass. The groundmass and altered glass sub-samples from deeper in this hole (sample 417A-28R-1-19-24; 47 m below sediments) have Li contents between 20 and 60 ppm and they also have similar δ^7Li of ~6.5 ‰ (Figure 4.8), with the bulk rock values overlapping the groundmass values. The groundmass of the deepest sample, from the Hole 418A (418A-33R-2-14-17) has similar δ^7Li to the constituent parts of sample 417A-28, and its Li concentration is 15 ppm. In contrast, the pseudomorph of plagioclase has a high δ^7Li of ~13 ‰ but with Li concentration of 20 ppm (Figure 4.8), overlapping the bulk rock value. The bulk rock Li concentration is slightly higher than the groundmass, but its δ^7Li is ~7 ‰ higher.

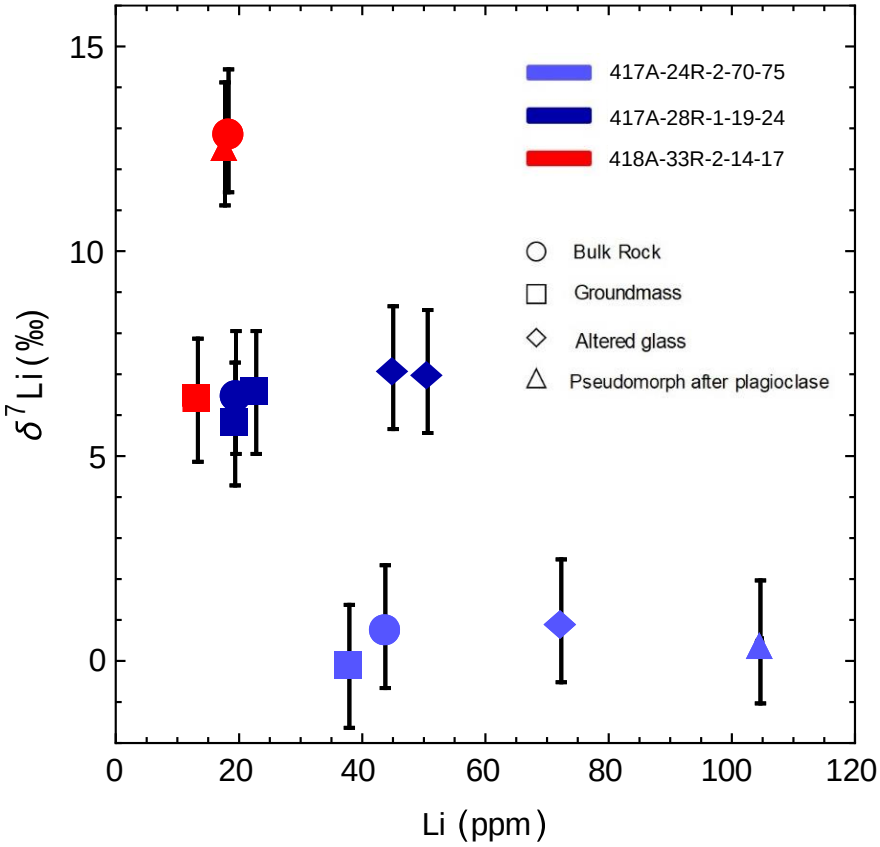

Figure 4.8. The lithium isotopic composition of three lavas with their separated parts versus their lithium concentration. It depicts that different altered parts (except the groundmass of 418A-33-2R-14-17 which is mainly identified fresh-see text for detail) of the same lava have the same lithium-isotopic composition regardless of the amount of lithium they have taken up.

Secondary minerals, in particular clay minerals, are the main hosts of Li in these samples and hence it is useful to investigate the relationship between the secondary mineral assemblages and the Li content and isotopic composition of their host sample. This is first examined by sample, followed by a brief comparison between samples.

The constituent parts of sample 417A-24R-2-70-75 have similar δ^7Li (~0 ‰), with unknown clay and orthoclase as the dominant alteration minerals. As clay minerals are the dominant sink for Li, the range in Li content may reflect an increase in the abundance of clay in the altered glass and plagioclase pseudomorph subsamples.

Sample 417A-28R-1-19-24 has two groundmass and two altered glass subsamples, with each sample type having similar Li content and δ^7Li (Figure 4.8). The groundmass subsamples are altered to orthoclase, saponite, hematite and calcite. Altered glass sub-samples are altered to an assemblage of zeolite, celadonite-saponite and orthoclase, although they are texturally different. The range in Li content suggests mineralogical differences are controlled by the alteration assemblage but the difference in alteration assemblages of the groundmass and altered glass sub-samples do not have an important role in controlling the δ^7Li of the sample.

The final sample to consider, 418A-33R-2-14-17, has a ~8 ‰ difference in δ^7Li between the groundmass and plagioclase pseudomorph subsamples. The groundmass is altered to saponite and orthoclase, whereas plagioclase pseudomorph is altered to orthoclase and unknown clay. The bulk rock Li and δ^7Li is similar to the plagioclase pseudomorph.

Comparison of the Li content and δ^7Li and mineral assemblages between samples does not identify any clear mineralogical controls on the Li content and isotopic composition of altered lava samples. The two plagioclase pseudomorph sub-samples are altered to the same assemblage and have ~12 ‰ difference δ^7Li, suggesting that their δ^7Li is not mineralogically controlled. Saponite was identified in the groundmass and altered glass sub-samples of 417A-28R-1-19-24 which all have a similar δ^7Li as the groundmass (Figure 4.7). The presence of similar type of clay mineral (saponite) may explain their similar δ^7Li, since smectitic clay minerals are a known Li host (e.g., Seyfried et al., 1984). The lack of any consistent relationships between alteration mineralogy and bulk chemistry, suggests secondary mineralogy is not the main controlling parameter of δ^7Li and that there must be another important parameter controlling it. For more intuition about Li concentration and isotopic composition of each secondary mineral (e.g., clays, zeolites and celadonite), further study can be conducted by measuring the Li concentration and isotopic composition of altered lavas using Laser Ablation-ICP-MS (LA-ICP-MS).

4.4.3.2. Carbonate minerals

Void-filling carbonate minerals in the upper oceanic crust grew from a seawater-derived fluid that had interacted with the lavas and hence their composition potentially

provides insight into the composition of the hydrothermal fluid. To study the change in the Li content and isotopic composition of hydrothermal fluid with depth, four lava samples with thick carbonate veins and vesicles were selected from ~12 m, ~63 m, ~75 m and ~175 m below sediments in Hole 417A (Supplementary Table D.2.3). The carbonate veins and vesicles were separated from the lava, crushed and hand-picked using a binocular microscope. To minimize contamination from lavas, the picked carbonates were re-picked three times. A few of less clean grains of carbonates were pulverized for carbon and oxygen isotope analysis. Chips of clean carbonates were used for Li concentration and isotope analysis. XRD analysis showed all samples are calcite.

Four calcite veins from the Hole 417A have Li concentrations between 21 ppb and 79 ppb (Figure 4.9). The $\delta^{13}C$ and $\delta^{18}O$ isotopic composition of these carbonates (relative to VPDB) are between 2.31 ‰ and 2.99 ‰, and -2.24 ‰ and -0.79 ‰, respectively, similar to previous data from this core (Supplementary Table D.2.3). The two carbonate samples with 79 ppb and 53 ppb Li also have high Al concentration (73 ppm and 43 ppm, respectively; Figure 4.9), suggesting contamination from silicate material and are excluded from further discussion. The remaining two samples, from 63 m and 175 m below sediments have negligible Al concentrations (< 5 ppm), suggesting there is no, or minimal contamination. Duplicate analyses of one of these carbonate samples showed significant variability in the Li content (21 versus 39 ppb), suggesting heterogeneity of Li concentration in uncrushed chips of samples or, perhaps, different amounts of contamination. The deepest carbonate sample has a Li content of 49 ppb (Figure 4.9). The calcite samples (with duplicate analysis) from ~63 m below sediments have similar $\delta^{7}Li$ of 9.9 ‰ and 10.9 ‰; however, the Li concentration of these two duplicates from the same lava sample are 20 ppb different (Figure 4.9). The deepest calcite sample has a $\delta^{7}Li$ of ~18 ‰.

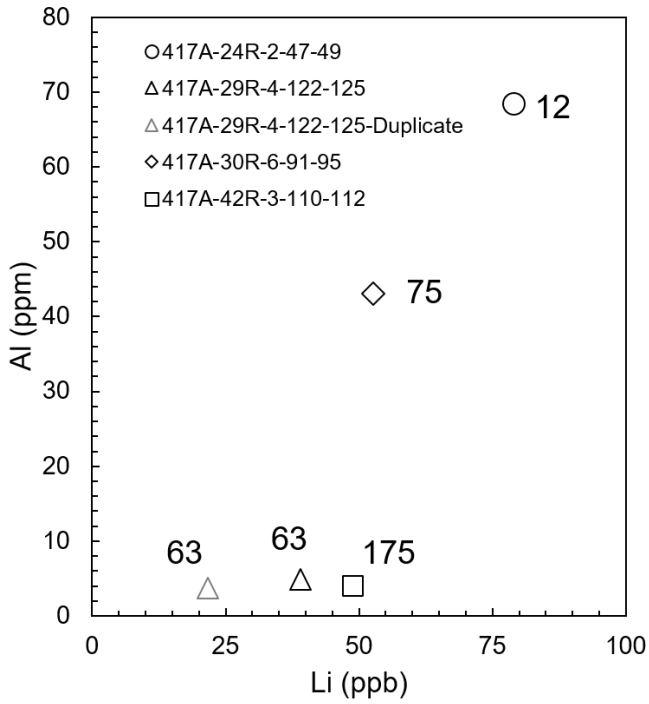

Figure 4.9. Al versus Li contents of calcite samples hosted in the lava samples from variable depths in the Hole 417A. Two samples with the highest Al contents are assumed to be contaminated with silicates. Duplicate analysis of one sample (417A-29R-4-122-125) shows heterogeneity in the Li content in the picked chips of carbonate. Numbers next to each symbol shows the depth below sediment (m) of each sample.

4.5. Discussion

Previous studies have suggested that Li uptake by the upper oceanic crust during low-temperature hydrothermal alteration occurs by simple addition of a seawater-derived component to the rocks with a constant isotopic fractionation factor (e.g. Chan et al., 1992; Chan et al., 2002; Coogan et al., 2017). This leads to linear mixing lines in plots of 1/Li versus δ^7Li. In contrast to these studies, the data presented here cannot be explained with such a model as the data do not fall on a mixing line in 1/Li versus δ^7Li (Figure 4.10). Instead, the data could be explained by a model in which the effective bulk fractionation factor between the crust and seawater varied with depth in the crust either due to: (i) alteration occurring at different temperatures, (ii) the secondary mineral assemblage being different, or (iii) a change in the Li-isotopic composition of the fluid that had evolved from that of seawater (either within the lava pile and/or due to interaction with overlying sediments). Before exploring these models, it is useful to consider the bulk Li-isotope exchange between lavas and seawater.

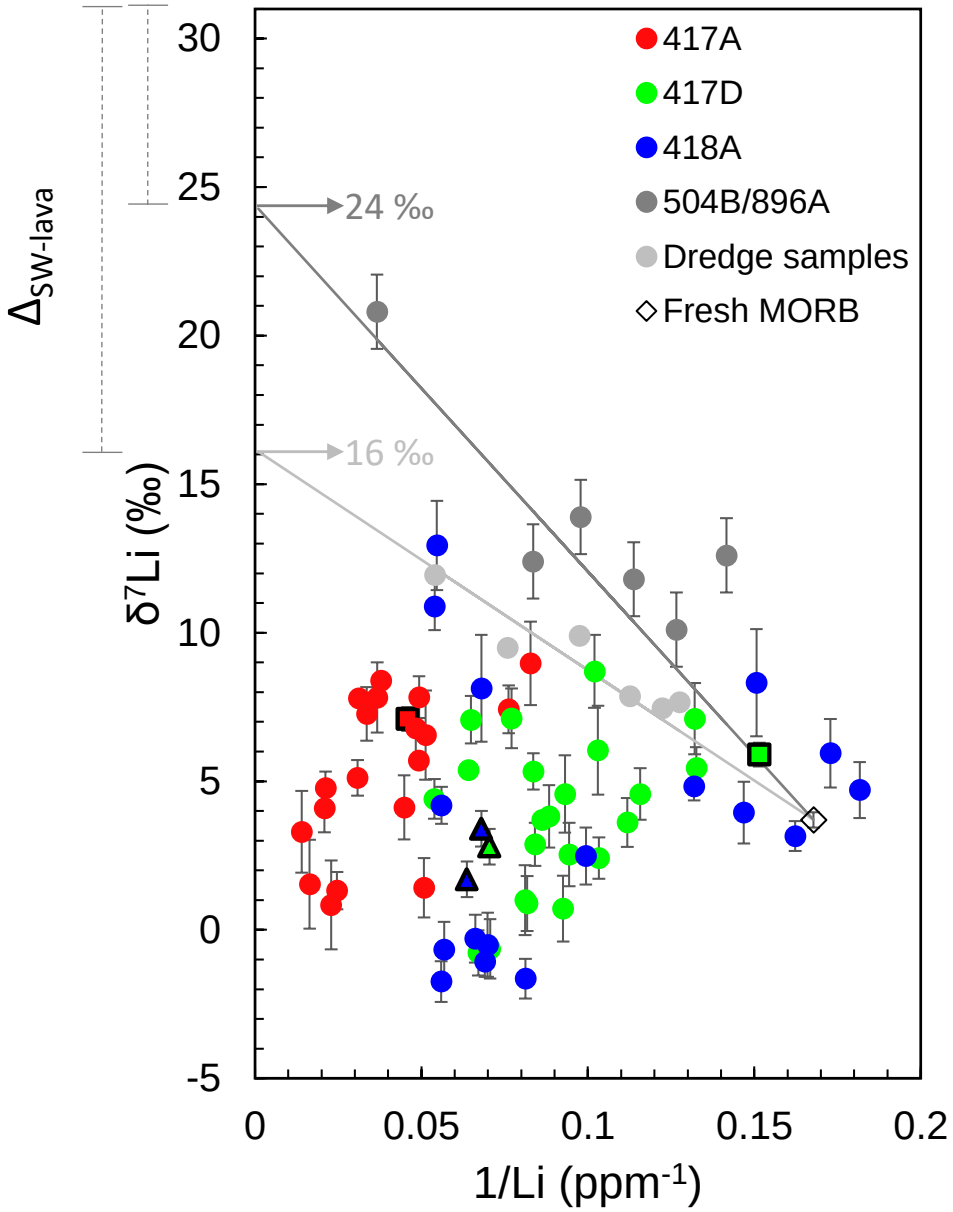

Figure 4.10. Li-isotopic composition versus reciprocal Li concentration. Dredge samples and samples from Holes 504B/896A from 5.9 to 6.8 Myr old oceanic crust (Chan et al., 1992 and Chan et al., 2002) which are assumed to have interacted with modern-like seawater (180 ppb Li and δ^7Li of 31 ‰) show that δ^7Li becomes heavier as Li is added to the rock. Fitting a line to published data starting from fresh MORB gives end-member altered rock δ^7Li of 16 ‰ and 24 ‰, for dredged samples and Holes 504B/896A samples, respectively. These suggest apparent Li isotopic fractionation factors of 15 ‰ and 7 ‰, respectively ($\Delta_{SW\text{-}lava}=\delta^7Li_{SW}-\delta^7Li_{lava}$). Observed correlation between 1/Li and δ^7Li of samples from Holes 504B/896A and dredge samples does not exist in samples from Holes 417A, 417D and 418A. Symbols with black rims are taken from published data (triangles are composite samples and squares are lava samples; Bouman et al., 2008). Open diamond symbol represents fresh MORB. Vertical error bars represent ±2SDE on replicate analysis of δ^7Li of samples.

The amount of Li added to a sample (ΔLi) and the change in the sample's δ^7Li (relative to fresh δ^7Li of 3.7 ‰; Tomascak et al., 2008) was calculated for each lava sample from Holes 417A, 417D and 418A. Average ΔLi and δ^7Li were calculated for lava samples of Holes 417A, 417D and 418A at 30 m intervals. The average δ^7Li and average of amount of seawater Li that was added to the uppermost 30 m of these cores are compared with averages of deeper 30 m intervals in Table 4.3. The depth and concentration weighted average δ^7Li of the entire core is calculated for each hole (Table 4.3). The amount of Li added to the uppermost 30 m of the crust is nearly two times greater than the deeper sections in all three holes and δ^7Li is significantly lower (Table 4.3). This indicates that there was a flux of heavy Li out of the upper oceanic crust during alteration at these sites. This is in contrast to previous suggestions that the upper oceanic crust acts as a sink for isotopically heavy Li from the ocean. If seawater had a much lower δ^7Li 120 Myr ago than today, then this could be explained with a constant bulk-isotopic fractionation factor between seawater and the oceanic crust. Alternatively, the mechanism of Li-isotope exchange may have led to a difference in the effective bulk fractionation factor between the crust and seawater in these sites as discussed below.

Table 4.3. Averages of δ^7Li and Li added to the shallow and deeper intervals of oceanic crust in Holes 417A, 417D and 418A

Holes	Avg ΔLi (ppm)	2SDE (ppm)**	Avg δ^7Li (‰)	2SDE (‰)**
417A (uppermost 30 m interval)	37	13	3	2
417A (deeper 30 m intervals)	15	6	7	1
417A (the entire ~200 m crust) *	**125**	**15**	**0.8**	**0.1**
417D (uppermost 30 m interval)	7	2	2	2
417D (deeper 30 m intervals)	4	2	5	1
417D (the entire ~300 m crust) *	**43**	**11**	**0.4**	**0.2**
418A (uppermost 30 m interval)	9	2	1	2
418A (deeper 30 m intervals)	5	6	8	3
418A (the entire ~550 m crust) *	**36**	**5**	**1.2**	**0.1**

*Averages of δ^7Li for the entire crust are calculated based on the average ΔLi and δ^7Li of uniform 30 m intervals in each hole.
** Errors are calculated following error propagation method.

4.5.1. Controls on the behaviour of Li in Holes 417A, 417D and 418A

4.5.1.1. Does variation in the temperature of alteration explain the variable behaviour of Li?

The equilibrium isotopic fractionation factor is a thermodynamic parameter, so the temperature of isotopic fractionation is a primary control on the fractionation factor, which decreases with increasing temperature. Both experimental and empirical studies (e.g., Vigier et al., 2008; Coogan et al., 2017) have suggested that change in temperature could be important for Li-isotopic fractionation in clay-dominated systems like Holes 417A, 417D and 418A. However, (i) carbonate O-isotope thermometry shows little systematic variation in temperature over the upper 100 m of these drill cores where the main variation in δ^7Li is observed (temperature variations do occur deeper in the cores; Table 4.1); and (ii) additionally, thermal models for off-axis hydrothermal systems suggest limited temperature variability is possible over <100 m depth range at any given time (e.g., Anderson et al., 2013). I have assumed that the formation temperature of secondary clay minerals (as the main host of Li) is similar to the formation temperature of carbonates. This is a valid assumption, because during fluid-rock reaction alkalinity generates and primary basalt components also release into the hydrothermal fluid at the same time. Hence, fluid becomes oversaturated with respect to both calcite and clay minerals, leading to simultaneous precipitation of these phases at the same temperature. Thus, it appears that variation in temperature cannot explain the depth variability of δ^7Li of lava samples observed in the upper 100 m of these cores.

4.5.1.2. Does variation in the secondary mineral assemblages explain the variable behaviour of Li?

Formation of different secondary minerals during low-temperature alteration of the upper oceanic crust depends on the exact alteration conditions (e.g., Gillis and Robinson 1990; Alt, 1995). Different minerals have different partition coefficients and isotopic fractionation factors. An indication that secondary minerals could explain the very light isotopic composition of altered basalts comes from a ~0.5 m section of intensely altered basalts from IODP Hole 1256D that has both a different mineralogy (beidellite, an Al-rich smectite clay mineral, celadonite, K-feldspar and Fe-oxyhydroxide; Alt et al., 2010) and a substantially lighter Li-isotopic composition than the rest of this core (-1.7 ‰ versus 5.5±5.4 ‰ (2SD) for other lavas in the core; Gao et al., 2012). Also, Coogan et al. (2017) report lighter Li isotopic compositions for altered lavas from the uppermost lavas of the Troodos ophiolite (~90 Myrs oceanic crust), which also contain beidellite and K-feldspar, compared with deeper sections where these minerals are absent. Aluminium-rich clays and K-feldspar are common secondary minerals in the uppermost lavas studied here (Alt and Honnorez, 1984) and thus the possibility that this alteration assemblage leads to the uptake of very isotopically light Li in the uppermost lavas is considered next.

As discussed in Section 4.4.3, Al-rich clay was not definitively identified in the samples studied by XRD. Compiled mineral assemblage data from Holes 417A, 417D

and 418A (Coogan and Gillis, 2018) show variation in secondary mineral assemblages in these three drill cores (Figure 4.11). For example, Al-rich clay in Hole 417A is abundant in the uppermost ~80 m, this depth interval covers the entire range of δ^7Li from light to heavy. Al-rich clay is less abundant in Hole 417D and was not identified in Hole 418A (Figure 4.11). The distribution of Li isotopic compositions with depth is similar in these three holes, but the distribution in type of all clay minerals is different (Figure 4.11). The main Li-isotopic variations occur in the upper 30 m of the lavas and there is limited mineralogical data in this interval preventing a firm conclusion being drawn, but the currently available data does not indicate a strong mineralogical control on the Li-isotopic composition of altered lavas.

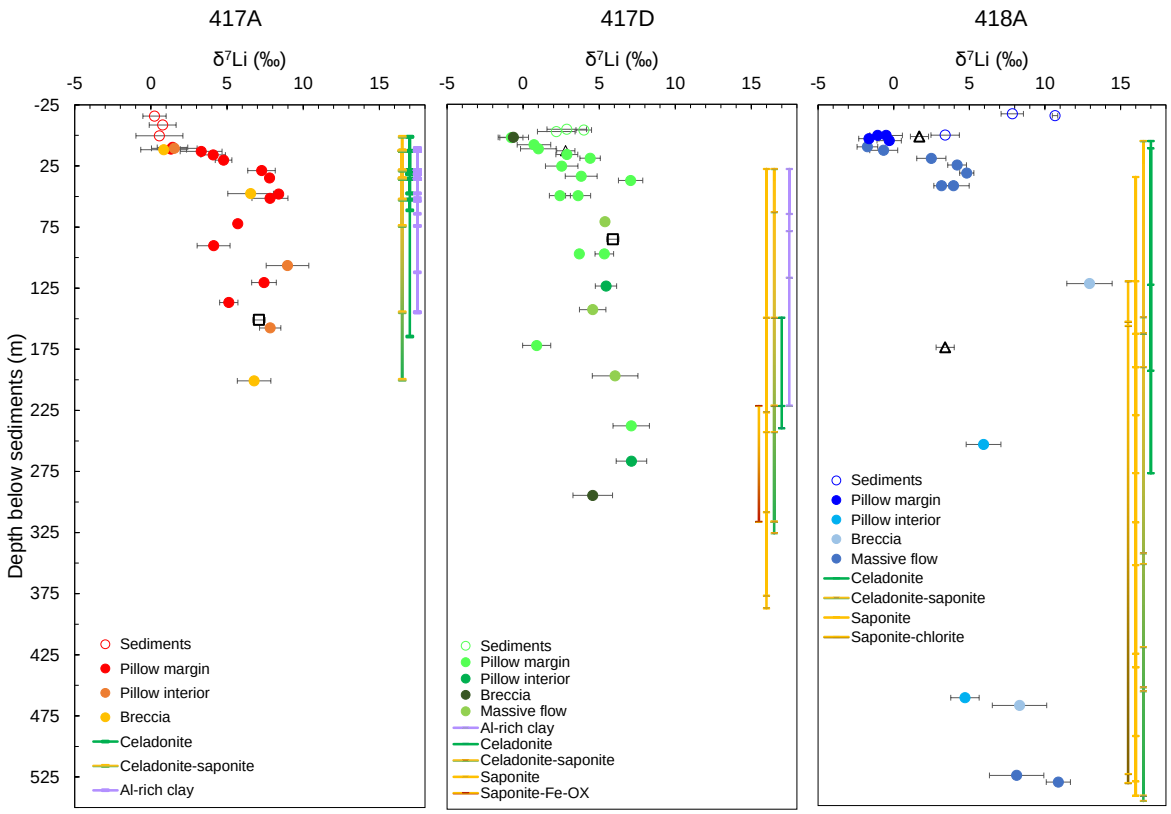

Figure 4.11. Depth distribution of clay minerals at Holes 417A, 417D and 418A is shown with different colours (right side of each panel). The vertical lines show the depth range for each clay mineral type and the horizontal lines on each vertical line identify the depths where each mineral was identified (published works; compiled mineral assemblage data from Holes 417A, 417D and 418A are reported by Coogan and Gillis, 2018). Comparison of the mineralogy with the δ^7Li of samples shows that variation of δ^7Li with depth is not obviously correlated with the type of secondary clay minerals. Open symbols with black rims are taken from previously published data (triangles are composite samples and squares are lava samples; Bouman et al., 2008).

4.5.1.3. Could Li exchange with overlying sediments affect the Li-isotopic composition of the lavas?

Bouman et al. (2004) suggested that one explanation for the lighter Li isotopic composition of the uppermost samples in Holes 417A, 417D and 418A could be interaction of basalts with seawater that had previously interacted chemically with, and leached isotopically light Li from, the overlying sediments. The basal sediments overlying the basalts from Holes 417D and 418A are isotopically heavier than those from Hole 417A while the uppermost basalts have similar δ^7Li in all three holes (Figure 4.4). This suggests that modification of hydrothermal fluid compositions due to mixing with sediment pore-fluids is an unlikely explanation for the observed variation in Li content and isotopic composition of lavas with depth. Moreover, Hole 417A is located on a topographic high, where the basal sediment age is ~20 Myrs younger than the underlying basalts, whereas sedimentation commenced shortly after crustal formation at Holes 417D and 418A (Table 4.1). Previous studies suggest that the majority of the alteration of these basalts happened within ~20 Myr of crustal formation (e.g., Richardson et al., 1980; Staudigel et al., 1986; Coogan et al., 2016). Therefore, it is expected that the majority of alteration of lavas in Hole 417A occurred before sediment accumulated. Hence, the hypothesis of sediment pore-fluids mixing with hydrothermal fluid seems an unlikely explanation for the observed variation in Li content and isotopic composition of lavas with depth.

4.5.1.4. Does the evolution of hydrothermal fluid compositions explain the variation in Li-isotopic composition observed in the crust?

In a fluid-rock system, as fluid flows along a pathway, chemical exchange occurs between the fluid and rock. During low-temperature hydrothermal alteration, Li is removed from fluid into the rocks, hence the Li concentration of the fluid is expected to decrease as it moves further along its flow path. Due to the preferential uptake of lighter Li isotopes by secondary minerals, the δ^7Li of fluid is expected to become heavier as fluid moves forward. Therefore, rocks that are further along the pathway interact with a fluid that is depleted in Li and isotopically heavier. To model the exchange of Li and its isotopes between rock and fluid a linear kinetic model is used following Lassey and Blattner (1988) and Bickle (1992). The linear kinetic process involves advective transport of Li and Li exchange between fluid and rock, which depends on the rate of recrystallization of secondary minerals (e.g., Bickle, 1992). The mathematics and details of the model are explained in Appendix B.

The Damköhler number (N_D) accounts for the relative rates of fluid-solid Li exchange to advective transport of Li (Boucher and Alvez, 1959). If fluid-rock exchange is slower than the advective transport of Li, then rock and fluid cannot achieve equilibrium (e.g., Bickle, 1992; DePaolo, 2006). In the following models, N_D is varied between 0.1 to 100, because at N_D>100 fluid and rock compositions get close to equilibrium conditions, and for N_D<0.1 variation in fluid and rock compositions becomes negligible (Bickle, 1992). The following models assume that the Li partition coefficient (Kd_{Li}), Li-isotope

fractionation factor between seawater and oceanic crust ($\Delta_{s\text{-}f}$), and temperature and pressure are constant in the fluid-rock system. Parameter values used to model the evolution of the Li and Li isotopic composition in rocks are presented in Table 4.4. Crustal porosity and fluid flux are allowed to vary in these models. In the fluid-rock system, porosity is usually in the range of 0.05-0.1 (e.g., Furnes and Staudigel, 1999; Lauer et al., 2018; however, to model extreme cases I have extended the lower range to 0.001 v/v). Assuming a residence time of 20,000 yrs for circulation of hydrothermal fluid in the off-axis oceanic crust with a fluid velocity of 10 m/yr (Baker et al., 1991), the length scale of fluid penetration in the off-axis crust is calculated as 200 km. Hence, in the following models, the fluid flux is assumed to vary between 0.02-2x10^7 kg/m^2.

4.5.1.4.1. Fluid-rock reaction during vertical fluid flow

One model to explain the variation of Li concentrations and isotopic compositions with depth is that fluid-rock reaction largely occurred during vertical fluid flow as fluid recharged the system. Assuming a constant porosity and permeability and fluid flux, the fluid velocity is constant, so the N_D is controlled solely by the Li exchange rate constant (Appendix B). Models for three time-integrated fluid fluxes of 2x10^7, 0.6x10^7 and 0.02x10^7 kg/m^2 and four different N_D of 0.1, 1, 10 and 100 are compared to the data using constant Kd_{Li} and $\Delta_{fluid\text{-}rock}$ (300 and 25 ‰ respectively; Figure 4.12). A model with a fluid flux of 0.6x10^7 kg/m^2 and N_D of 0.1 generally fits the Li and δ^7Li data for Holes 417D and 418A. However, no model could be found that fits both the Li concentration and δ^7Li of samples from Hole 417A (Figure 4.12). Therefore, it seems unlikely that a model of vertical fluid flow with constant fluid flux, fractionation factor and partition coefficient can explain the Li concentration and isotopic composition of altered crust in this area.

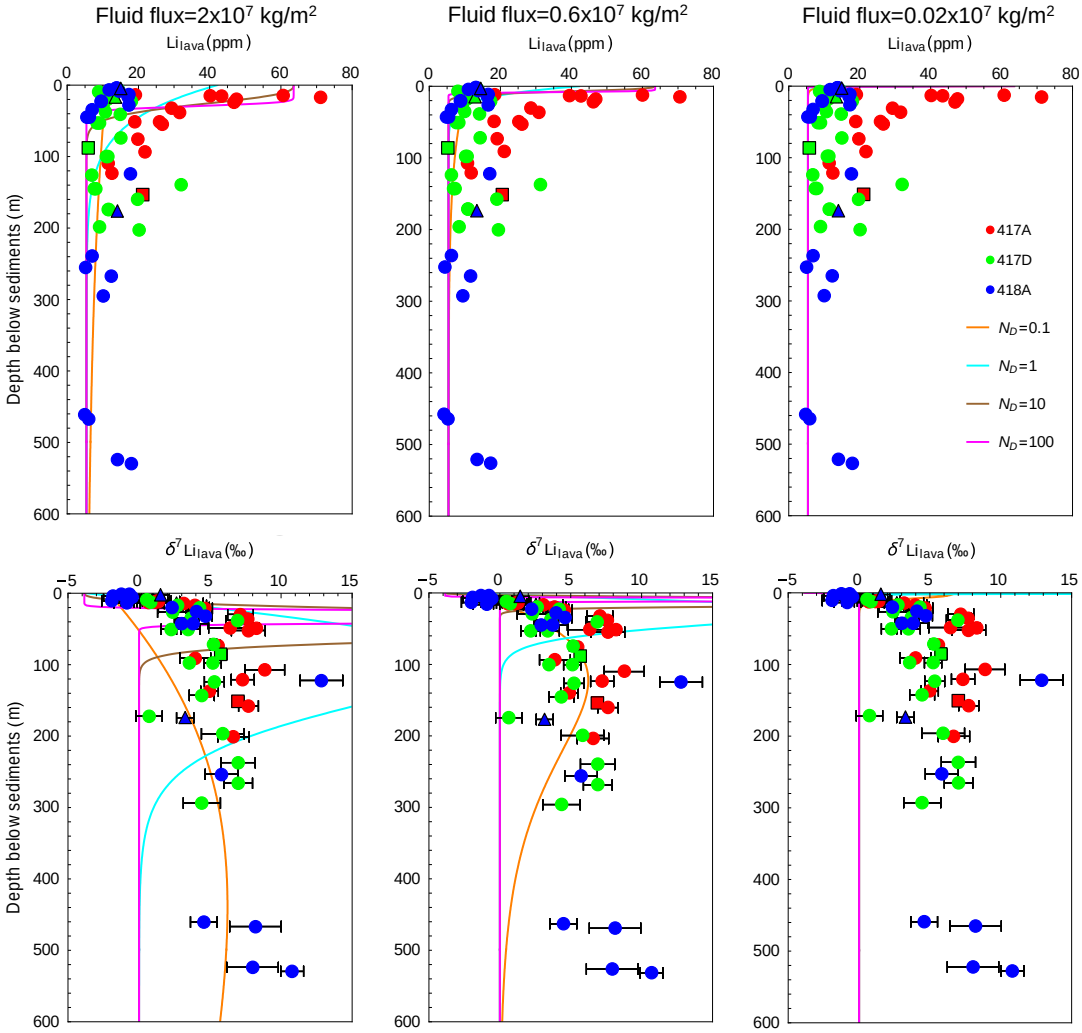

Figure 4.12. Models (solid lines) for the evolution of Li concentration (top row) and Li-isotopic composition (bottom row) for three different fluid fluxes and four different N_D during vertical fluid flow. The Kd_{Li} and $\Delta_{s\text{-}f}$ are assumed to be constant at 300 and -25 ‰, respectively. Symbols show the measured Li concentration and δ^7Li of lava samples from Holes 417A, 417D and 418A. There does not seem to be a good fit for both Li concentration and δ^7Li of all three cores. Symbols with black rims are from previously published data (triangles are composite samples and squares are lava samples; Bouman et al., 2008).

Table 4.4. Parameters used to model Li concentration and isotopic composition of lava samples

Symbol*	Definition	Values	Unit	Ref
ρ_f	Seawater density	1.02	$g.cm^3$	
ρ_s	Basalt density	2.6	$g.cm^3$	
φ	Crustal aquifer porosity	0.001-0.1	v/v	Furnes and Staudigel (1999)
C_{s0}	Li concentration in MORB	5	ppm	
C_s*	Li concentration that solid would have at equilibrium		ppm	
C_{f0}	Li concentration in seawater	0.18	ppm	
kd_{Li}	Li partition coefficient (C_s/C_f)	300	ppm/ppm	
$\delta_{s,i}$	Li isotopic composition in fresh MORB	6	‰	
$\delta_{f,i}$	Li isotopic composition of Cretaceous seawater	21	‰	Lechler et al. (2015)
t	Average residence time in oceanic crust	20000	yr	Baker et al. (1991)
ω_0	Fluid velocity in porous rock medium	10	$m.yr^{-1}$	Baker et al. (1991)
h	Length scale for kinetic exchange ($h=\omega_0 t$)	200000	m	
z	Distance in direction of fluid flow		m	
F_f	Time-integrated fluid flux ($F_f=h\varphi\rho_f$)	0.02-2	10^7 $kg.m^{-2}$	
Δ_{s-f}	Apparent Li isotopic fractionation factor	-25	‰	
α	Li isotopic fractionation factor			
κ	Exchange rate for linear kinetic exchange		s^{-1}	
ϕ'	Ratio of fraction of Li in fluid to fraction of Li in solid in volume of rock			
$K(x,y)$	Bessel K-function (Eq. B.13)			Lassey (1982)
I_0	Modified Bessel I-function order zero			Lassey (1982)

* Subscripts s and f in symbols represent solid and fluid, respectively.

The upper assume that the upper 150 m of the lavas in all three Holes, 417A, 417D and 418A, interacted with the same ~119 Myr seawater. The δ^7Li of 119 Myr seawater is not known. The closest estimation of δ^7Li of seawater is that of Lechler et al. (2015) who measured the δ^7Li of marine carbonates before, during and after Ocean Anoxic Event 1 (OAE1) which happened 120.3 Myr ago. This study suggests a δ^7Li of seawater of ~21 ‰ before and after the OAE1 and this value is used here. The Li concentration of seawater at 119 Myr is also assumed to stay constant as today (180 ppb).

A value of 300 is assigned to Kd_{Li}, which is orders of magnitude higher than experimentally obtained partition coefficients for smectites synthesized at low temperatures (25 to 50°C). For example, Berger et al. (1988) measured Kd_{Li} of 2.4 for smectite minerals at temperatures of ~50°C (using seawater-like composition) accounting for both exchangeable and structural Li, while Vigier et al. (2008) reported a Kd_{Li} of 0.01 for hectorite (Li-rich smectite), only accounting for structural Li at 25°C. However,

Vigier et al. (2008) did not use a seawater-like composition for their experiments. Based on the experimental studies, natural smectites that precipitated from seawater with 0.18 ppm Li concentration at moderate temperatures would have Li concentrations between 0.002 to 0.4 ppm. In contrast, the Li contents of smectites in the upper oceanic crust have been determined to be between 2 to 10 ppm in ODP Hole 504B (Chan et al., 2002) and 10-275 ppm in the Troodos ophiolite (Gillis et al., 2015) and in this study, clay-rich sub-samples have Li contents up to 105 ppm. These natural samples suggest a much higher Li partition coefficient than the experimental data. This difference between experimental and natural smectite Li partitioning is attributed to several differences between experimental studies and the conditions of formation of natural secondary minerals such as the effect of seawater composition on Kd_{Li} (Vigier et al., 2008) and perhaps a lack of achievement of equilibrium at low temperatures in experimental studies.

Values are assigned to Kd_{Li} and $\Delta_{s\text{-}f}$ in a way to reconstruct the Li concentration and δ^7Li of lavas at top of the cores. To explain the most Li concentrated and the lightest δ^7Li lavas at uppermost parts of Holes 417A, 417D and 418A (with a range of N_D between 0.1 to 100), Kd_{Li} values between 250 to 350 and a $\Delta_{s\text{-}f}$ between 20 ‰ to 26 ‰ are required.

4.5.1.4.2. Fluid-rock reaction during lateral fluid flow

An alternative hypothesis to explain the distribution of Li and δ^7Li in the lavas at Sites 417 and 418 is a change in the fluid flux with depth in the crust. Anderson et al. (2013) showed that carbonate precipitation temperatures cannot be explained in these cores with a “well mixed aquifer” model and are better explained by a model in which fluid flux decreases with depth during lateral flow. The simplest way to explain this would be a decrease in permeability with depth. Previous studies have shown that fracture width in lavas decreases with depth in the upper oceanic crust (e.g., Newmark et al., 1985b; Morin et al., 1989). Based on this, it is assumed that the fluid flux decreases with depth. As fluid flows laterally and interacts with rocks, the Li concentration and δ^7Li of the fluid and rocks evolve and these vary as a function of depth due to varying fluid fluxes.

Model parameters and their values are the same as for vertical flow models (Table 4.4). Models developed for five crustal porosities of 0.1, 0.05, 0.03 and 0.01 and with a penetration length scale of 200 km; corresponding time-integrated fluid fluxes at each crustal porosity were calculated (2, 1, 0.6 and 0.2 x10^7 kg/m^2, respectively; Figure 4.13). Since Hole 417A is located at a topographic high (Figure 4.1), it is assumed that this hole is close to a recharging conduit. To explain the Li concentration of lava samples from Hole 417A, it is assumed that this hole is 20 m away from the recharging conduit. In this hole, if fluid flux decreases from the top of the basement to 60 m below the sediments and remain constant in deeper sections, a model with N_D of 10 generally fits the Li concentration data (Figure 4.13), but it cannot explain the δ^7Li of the rocks (Figure 4.14). Holes 417D and 418A are 450 m and 6500 m away from Hole 417A, respectively. Models show that at fluid penetration distances over ~500 m, with the range of fluid flux and N_D used here, there is almost no change in the Li concentration of the lavas, regardless of fluid flux and N_D (Figure 4.13). For Holes 417D and 418A, no model can be found to explain the δ^7Li of lavas (Figure 4.14).

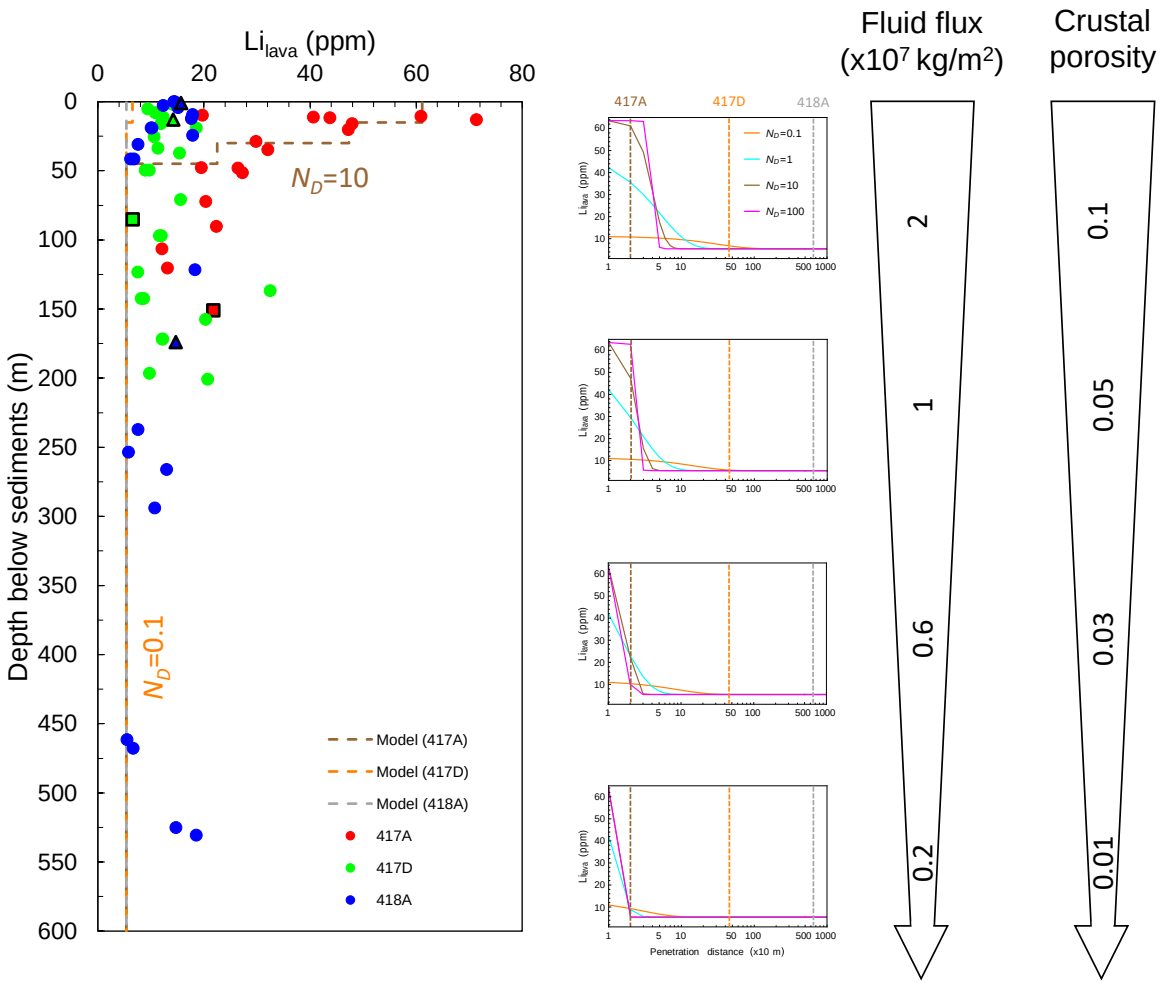

Figure 4.13. Models of the evolution of Li concentration of lava samples during interaction with hydrothermal fluid flowing laterally at four different porosities and corresponding fluid fluxes with variable N_D of 0.1, 1, 10 and 100 (central panel; for model parameters and values see Table 4.4). The models assume a decrease in fluid flux and crustal porosity with depth (right panel). The general variation in Li concentration of lava samples with depth for Hole 417A can be explained with a model at a lateral distance of 20 m, if fluid fluxes decreases from 2 to 0.2 x10^7 kg/m^2 from top to ~60 m below sediments and a N_D of 10 (brown dashed line; left panel). Hole 417D and 418A are 450 and 6500 away from Hole 417A, respectively (lateral distances of the three holes relative to each other are marked on the plots of the central panel). At lateral location of 417D (~470 m), only a model with N_D of 0.1 (orange dashed line) shows slight variation in Li concentration at different fluid fluxes which does not fit the data from this hole. Gray dashed line shows predicted Li concentration for any N_D between 0.1 to 100 at Hole 418A. No model can explain the data from Holes 417D and 418A regardless of N_D and fluid flux (left panel). Symbols with black rims are from previously published data (triangles are composite samples and squares are lava samples; Bouman et al., 2008).

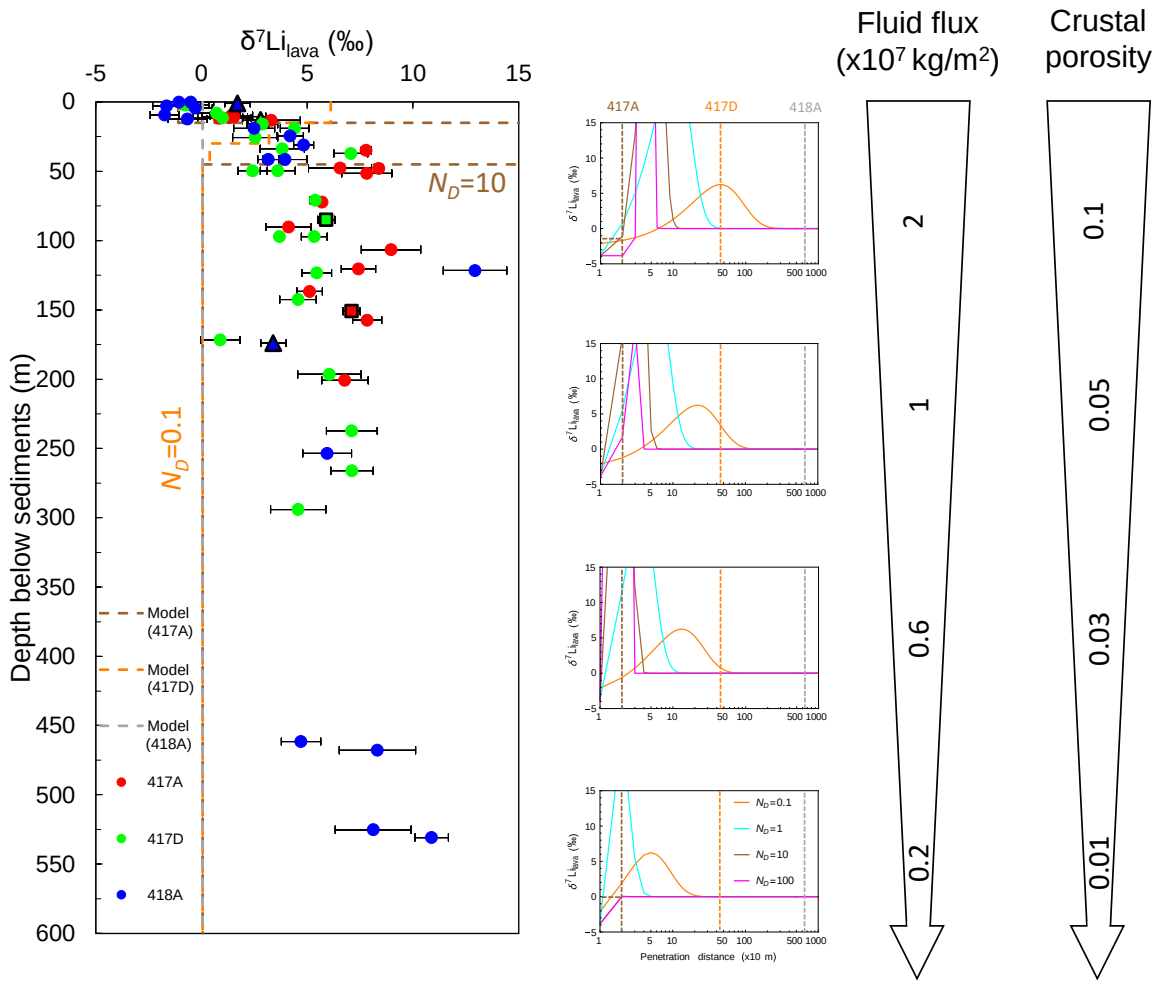

Figure 4.14. Models of the evolution of δ^7Li of lava samples during interaction with hydrothermal fluid flowing laterally at four different porosities and corresponding fluid fluxes with variable N_D of 0.1, 1, 10 and 100 (Central panel; for model parameters and values see Table 4.4). The models assume a decrease in fluid flux and crustal porosity with depth (right panel). The model which explains Li concentration from Hole 417A (with N_D of 10 at lateral distance of 20 m) cannot explain δ^7Li of lava samples from this hole. Hole 417D and 418A are 450 and 6500 away from Hole 417A, respectively (lateral distances of the three holes relative to each other are marked on the plots of the central panel). At lateral location of 417D (~470 m), only a model with N_D of 0.1 (orange dashed line) shows variation in δ^7Li at different fluid fluxes which does not fit the data from this hole. Gray dashed line shows predicted δ^7Li for any N_D between 0.1 and 100 at Hole 418A. No model can explain the δ^7Li data from Holes 417A, 417D and 418A, regardless of N_D and fluid flux (left panel). Symbols with black rims are from previously published data (triangles are composite samples and squares are lava samples; Bouman et al., 2008). Horizontal error bars represent ±2SDE on replicate analysis of δ^7Li of samples.

Neither end-member model of 1D lateral or vertical fluid flow, with fluid-rock reaction governed by linear kinetics and with constant fractionation factor and partition coefficient, can explain the data (Figure 4.12, Figure 4.13 and Figure 4.14). These results can be understood by considering the Rayleigh distillation that is expected to occur as

fluid-rock reaction removes Li from the hydrothermal fluid and preferentially incorporates ^{6}Li into the rock. This process means that further along the flow path the fluid is depleted in Li but has an elevated ^{7}Li/^{6}Li. This means that rocks that react with the fluid further along the flow path should be less enriched in Li than those that react closer to the seawater source but should be relatively enriched in ^{7}Li over ^{6}Li. If fluid flows vertically reacting with the crust then the large Li enrichment in the shallowest rocks in Hole 417A should have led to a very large enrichment in the ^{7}Li/^{6}Li of the fluid reacting with the rocks slightly deeper in the crust and hence high ^{7}Li/^{6}Li of these altered rocks but this is not observed (Figure 4.12). If instead, fluid flow was lateral with Hole 417A, as a topographic high, being closer to a recharge site, then the uppermost lavas here could have elevated Li concentrations as observed but the residual fluid that reached further points along the flow path, like those samples at Holes 417D and 418A, should again have been enriched in ^{7}Li/^{6}Li. Such an enrichment is the inverse of what is observed (Figure 4.14).

Given that both the quantitative models (Figure 4.12, Figure 4.13 and Figure 4.14) and the conceptual model just discussed indicate that 1D fluid flow with constant reaction parameters cannot explain the data, an alternative model is considered based on a more complex, but realistic, hydrological regime. Fluid flow within the upper oceanic crust is not expected to be simply lateral or vertical and it seems likely, at least at the shallowest levels in the crust, that fluid flows into and out of the crust freely until some thickness of sediment has accumulated. For example, at seamounts within-seamount circulation has been suggested to be a key heat loss mechanism under some circumstances (e.g. Kawada et al., 2011). Likewise, open exchange between the crust and an almost infinite reservoir of seawater has been suggested to be responsible for Mg loss from the uppermost lavas (e.g., Coogan and Gillis, 2018). Thus, it is possible that soon after crustal accretion, and before sufficient sediment was deposited to impede seawater entering and leaving the crust at any site, alteration happened under open conditions. At this time, fluid-rock reactions at the seafloor would have occurred at an almost infinite water-rock ratio and the shallowest samples would have become isotopically equilibrated with seawater. A small fraction of the fluid would have leaked deeper into the crust, evolving to a lower Li content and higher δ^{7}Li relative to seawater, due to fluid-rock reactions that added low δ^{7}Li to the overlying lavas. Reaction of this fluid with the rocks would have led to the rocks deeper in the lavas taking up less Li than those at shallower levels but with a higher δ^{7}Li. After some time, a sufficient thickness of sediment would have been deposited at Holes 417D and 418A inhibiting fluid penetration directly into the crust through the sediment. Instead, fluid reacting with the crust in these locations would have entered the crust through a topographic high, such as that drilled at Hole 417A, and flowed laterally beneath the sediments to reach the crust at these sites. During transport to these sites fluid-rock reactions would have depleted the fluid in Li and increased its δ^{7}Li. Reaction of the crust with such a fluid would lead to minimal Li-enrichment, and the Li-isotopic composition of the crust becoming somewhat higher as observed at deeper levels in the 417D and 418A cores. In contrast, at Hole 417A the lack of sediment cover would have allowed the crust to continue to be altered in an open system leading to much more Li uptake at this site.

Based on this conceptual model, if Cretaceous seawater has δ^7Li of 21 ‰ (Lechler et al., 2015), and if the Li-isotopic fractionation factor is constant throughout the upper oceanic crust at Holes 417A, 417D and 418A, then the uppermost, Li-rich lava samples are representative of altered end-member crust. Since the uppermost lava samples in Holes 417A and 417D/418A have δ^7Li of ~-1±0.5 ‰ and ~-1±1.5 ‰, respectively, then the Li-isotopic fractionation factor between altered end-member crust and seawater for Holes 417A and 417D/418A would be -22±0.5 ‰ and -22±1.5 ‰, respectively. Based on this latter $\Delta_{s\text{-}f}$ for the Hole 417A and δ^7Li of lava samples in deeper sections (2 ‰ to 8 ‰ at depths deeper than 30 m below sediments), and assuming equilibrium fractionation conditions, the δ^7Li of hydrothermal fluid in Hole 417A is expected to be between 24 ‰ to 30 ‰ ($\delta^7 Li_f = \delta^7 Li_s - \Delta_{s\text{-}f}$). Two calcite veins from Hole 417A were measured for their Li-isotopic compositions (Section 4.4.3.2) and the shallower one has a lighter δ^7Li than the deeper one (Figure 4.15). As discussed in Chapter 3, there are different parameters which can influence the Li isotopic fractionation factor for calcite including pH of the calcite saturated solution. If samples were precipitated at a pH~7 with $\Delta_{fluid\text{-}calcite}$~-7 ‰ (Chapter 3), then the δ^7Li of hydrothermal fluid would be closer to the predicted range of δ^7Li by the above conceptual model (Figure 4.15). However, data from only two samples is insufficient to test this model.

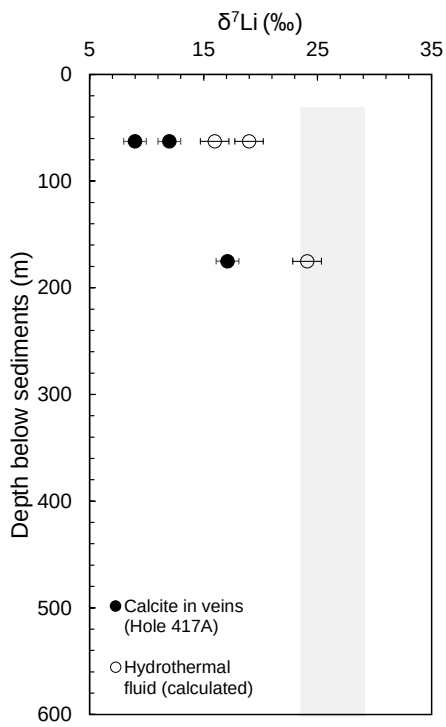

Figure 4.15. Calculated range of δ^7Li of hydrothermal fluid based on δ^7Li of lava samples from deeper than 30 m below sediments in Hole 417A, and assuming a constant Li-isotopic fractionation factor between altered crust and seawater of -22 ‰ throughout the entire core (gray shaded area). Black symbols show the measured δ^7Li of calcite samples from veins in Hole 417A. If samples were precipitated at pH~7, the δ^7Li of hydrothermal fluid would be ~7 ‰ heavier than the calcite (open symbols). Two symbols shown at the same depth are duplicates from the same sample, possibly suggesting heterogeneity of δ^7Li of calcite samples.

4.6. Conclusions

This study demonstrates that the Li content and isotopic composition of altered oceanic crust from Holes 417A, 417D and 418A change through the upper 600 m below sediments such that the Li concentration and δ^7Li decrease continuously through the upper ~30 m below sediments and remain nearly constant in deeper sections. There is no evidence that variations in the type of secondary mineral assemblages are the primary control on the Li concentration and δ^7Li of the lavas in these cores although this hypothesis cannot be disproved with the current data. Modification of the Li content of the hydrothermal fluid due to mixing with sediment pore-fluid also does not appear to be able to explain the observed variations in Li content and isotopic composition in these cores.

Models of the evolution of the Li composition of lavas during one dimensional fluid flow with fluid-rock reaction controlled by linear kinetics were developed. These models show neither vertical nor lateral fluid flow can explain both the variation of the Li concentration and δ^7Li of lava samples from all three studied cores. Instead, a conceptual model of free circulation of seawater through the uppermost lava section of the oceanic crust can explain the observed high Li content of lavas. Assuming the Li-isotopic composition of the uppermost lavas are offset from seawater by equilibrium isotopic fractionation factor, this model can explain the light Li-isotopic composition of the shallowest lava samples. The hydrothermal fluid which has been reacted with the uppermost rocks, would have lower Li content and heavier Li isotopic composition. Leakage of small fraction of this fluid deeper into the crust would lead to less Li with heavier isotopic composition being added to the deeper rocks. Thickening of the sediment layer over time would lead to more restricted fluid flow into the crust, so fluid can enter and exit the crust only through the topographic highs. Fluid-rock reactions during the lateral transport of the fluid between two topographic highs would have depleted the fluid in Li and increased its δ^7Li. Reaction of the crust with such a fluid would lead to slight Li-enrichment, and the Li-isotopic composition of the crust becoming somewhat heavier, explaining the low Li concentration and somewhat heavier Li isotopic composition of the lavas at deeper levels in the crust. If this model is correct, and δ^7Li of Cretaceous seawater was 21 ‰, then the apparent Li-isotopic fractionation factor between altered end-member crust in Holes 417A 417D and 418A was ~-22 ‰ which is larger than what suggested in previous studies (-16 ‰).

5. The role of low-temperature hydrothermal alteration of the upper oceanic crust in controlling the Li concentration in, and isotopic composition of seawater over the past 120 Myrs

5.1. Introduction

The Earth's climate became cooler over the past 120 Myr and transitioned from a "greenhouse Earth" to an "icehouse Earth" from the Cretaceous to the modern era probably due to a decline in the CO_2 content of the atmosphere (e.g., Berner, 1994). The role of global denudation and changes in the continental weathering regime on the evolution of Earth's C-cycle and climate cooling over the Cenozoic era has been investigated for decades (e.g., France-Lanord and Derry, 1997; Godderis and Francois, 1995; Raymo et al., 1988). It has been suggested that an increase in CO_2 drawdown was driven by tectonic activity (e.g., the Himalayan orogeny; Gaillardet et al., 1999; Raymo et al., 1988; Riebe et al., 2004; West et al., 2005) although this model is controversial (e.g., Berner and Caldeira, 1997). Changes in the conditions of low-temperature, off-axis hydrothermal alteration of oceanic crust has also been suggested as another feedback in long-term climate regulation (Brady and Gislason, 1997). However, the question still remains as to whether changes in the continental or oceanic environment provide a larger feedback on the long-term CO_2 cycle as the planetary thermostat and which is a greater controller of the composition of seawater.

The Mg^{2+}/Ca^{2+} ratio and $\delta^{18}O$ of benthic foraminifera provide robust proxies of bottom seawater temperature (e.g., Lear, 2000; Cramer at el., 2011). Estimation of bottom seawater temperature suggest a 15 to 20°C decrease from the Cretaceous to the modern era (Cramer et al., 2011; Figure 5.1). The temperature of seawater that circulates through the off-axis oceanic crust controls the hydrothermal alteration reactions that occur between the fluid and rocks in terms of the thermodynamics of reactions and rates of mineral dissolution. Oxygen isotope thermometry of carbonates precipitated during hydrothermal alteration of basalts shows that the temperature of alteration decreased from the early Cretaceous to modern era by ~20°C (e.g., Gillis and Coogan, 2011), consistent with the estimated 15 to 20°C decrease in bottom seawater temperature over the past ~120 Myr (Cramer et al., 2011). The average alteration temperature is controlled by several factors including sedimentation rate, the permeability of the crust and bottom seawater temperature. The average temperature of alteration is generally ≤10°C higher than bottom seawater temperature (Figure 5.1) except in areas with anomalously high sedimentation rates (Figure 5.1).

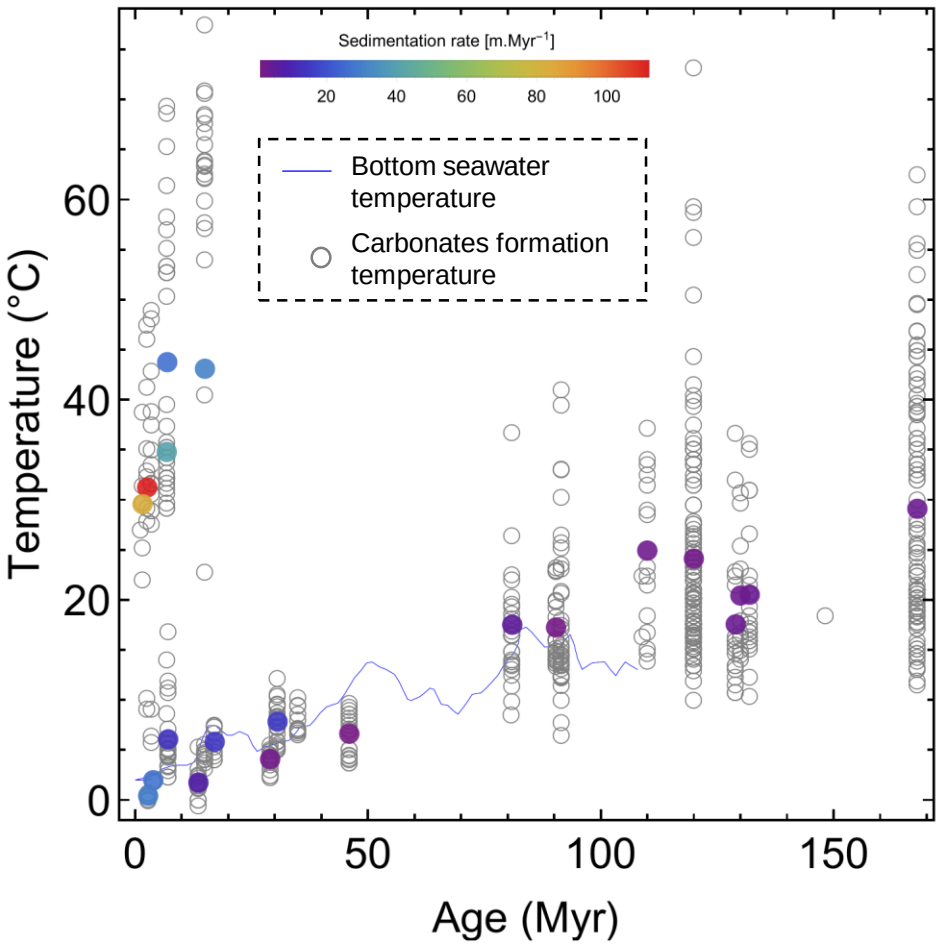

Figure 5.1. Carbonate formation temperature (circles) and estimated bottom seawater temperature (blue line) versus age of oceanic crust. Carbonate formation temperatures were obtained using the oxygen isotopic composition of precipitated carbonates (using the Kim and O'Neil (1997) thermometer). The average of carbonate temperatures at each age is colour coded based on the sedimentation rate. The estimate of bottom seawater temperature is from Cramer et al. (2011).

While the Li concentration of seawater is thought to stay constant (Delaney and Boyle, 1986), the Li-isotopic composition of seawater has become heavier over the past 120 Myr, from ~21 to ~31 ‰ (Hathorne and James, 2006; Misra and Freolich, 2012; Pogge von Strandmann et al., 2013; Lechler et al., 2015). A number of studies attribute this change to an increase in the Li flux from, and/or the Li-isotopic composition of, riverine inputs due to changes in continental weathering conditions linked to changing tectonic conditions (Misra and Freolich, 2012; Vigier and Godderis, 2015). An alternative model attributes the change in δ^7Li of seawater to a change in both the δ^7Li and Li flux of riverine input into the ocean, and change in the magnitude and isotopic composition of the flux of Li into marine authigenic clay minerals during sediment diagenesis (Li and West, 2014). These studies assume a constant Li-isotopic fractionation factor between seawater and oceanic crust over time. Coogan et al. (2017) proposed that a major portion of the increase in the lithium isotopic composition of seawater over the past 120 Myr can be explained by an increase in the bulk fractionation factor between seawater and Li

added to the upper oceanic crust during low-temperature, off-axis, hydrothermal alteration mainly as a result of a decrease in bottom seawater temperature.

Here, I test this latter hypothesis by investigating the significance of low-temperature alteration of the lava section of ocean crust on the lithium isotopic composition of seawater. If the Li isotopic composition of bulk altered crust remained constant over the past 120 Myrs, this would suggest that the apparent Li-isotopic fractionation factor increased over this period of time. If the Li isotopic fractionation factor between the ocean and the sinks of Li from the ocean (low temperature hydrothermal alteration of oceanic crust and diagenetic minerals on the seafloor) increased by 9 ‰, this could explain all of the increase in the Li isotopic composition of seawater over the Cenozoic. To investigate this possibility, I measured the Li content and δ^7Li of altered lava samples from five ODP/DSDP drill cores. These new data are interpreted in combination with the new data reported in Chapter 4 and previously published data (Chan et al., 1992; Chan et al., 2002; Bouman et al., 2004; Gao et al., 2012; Coogan et al., 2017). To evaluate the variation in the Li isotopic fractionation factor between altered upper oceanic crust and seawater, the Li isotopic composition of bulk altered crust is evaluated using a weighted average of the measured Li-isotopic composition of lava samples at each study area (weighting by the amount of Li added from seawater to lava samples). Additionally, where possible, a binary mixing model is used to extract the Li-isotopic composition of altered end-member crust. This was done by assuming that the measured Li-isotopic composition of lavas are a binary mixture between Li-rich altered material and a Li-poor protolith; in this scenario the altered end-member δ^7Li can be extracted by fitting a mixing line in δ^7Li vs. Li^{-1} plots (e.g., Chan et al., 1992; 2001). An empirical Li-isotope fractionation factor for each site is calculated from the difference between the Li-isotopic composition of contemporaneous seawater and the altered end-member. Since the mixing model does not account for the possible changes in composition of hydrothermal fluid and hence the altered rocks (for example in Sites 417/418; Chapter 4), a linear kinetic model of evolution of fluid-rock composition during vertical fluid flow (developed in Chapter 4) is also tested to evaluate what range of parameters is required to obtain an approximate fit on the Li concentration and isotopic composition data at each study area.

5.2. Study areas and sample suite

Thirty-six lava samples from DSDP and ODP cores from the Atlantic (Holes 543A and 396B; Figure 5.2) and Pacific (Holes 597C, 1224F/D and 595B; Figure 5.2) ocean basins that formed 13.6 to 95 Myr ago were analysed for major and trace element and lithium isotopic compositions (Supplementary Tables D.3.2). These new samples come from the upper 140 m of the crust and were altered at low temperature conditions based on previous studies (e.g., Gillis and Coogan, 2011; Alt and Honnorez, 1984; Böhlke et al., 1980). The alteration temperature in each core is estimated from the oxygen isotopic composition of hydrothermally precipitated calcium carbonates (Kim and O'Neil, 1997; Table 5.1). Crustal sections formed in the Cretaceous (595B and 543A) were altered under warmer bottom seawater conditions, with carbonate formation temperatures of 16-17°C, than the Cenozoic Sites 1224, 597 and 396 with carbonate formation temperatures between 1.5 to 6°C (Table 5.1). Samples were selected using the following criteria: (i) to

cover the depth range of the cores and (ii) to sample highly altered lavas based on published alkali elements concentrations. Sample preparation for chemical analysis and analytical procedures for the trace element and Li isotopic analyses are described in Chapter 4 (Section 4.3.1).

Most lava samples had a coherent structure with a range of colour from light to dark gray. Veins and veinlets were abundant in many of the studied samples and were filled with secondary minerals (e.g., carbonate) and surrounded with yellow to orange alteration halos. Around 60 % of the studied lava samples have <10 % phenocrysts (plagioclase ± pyroxene ± olivine) and the remaining samples have 10 % to 35 % phenocrysts. In most of the samples, phenocrysts were partially altered to secondary green to brown minerals (e.g., clay minerals ± Fe-oxyhydroxide; see Supplementary Tables D.3.2 for detailed visual description of samples).

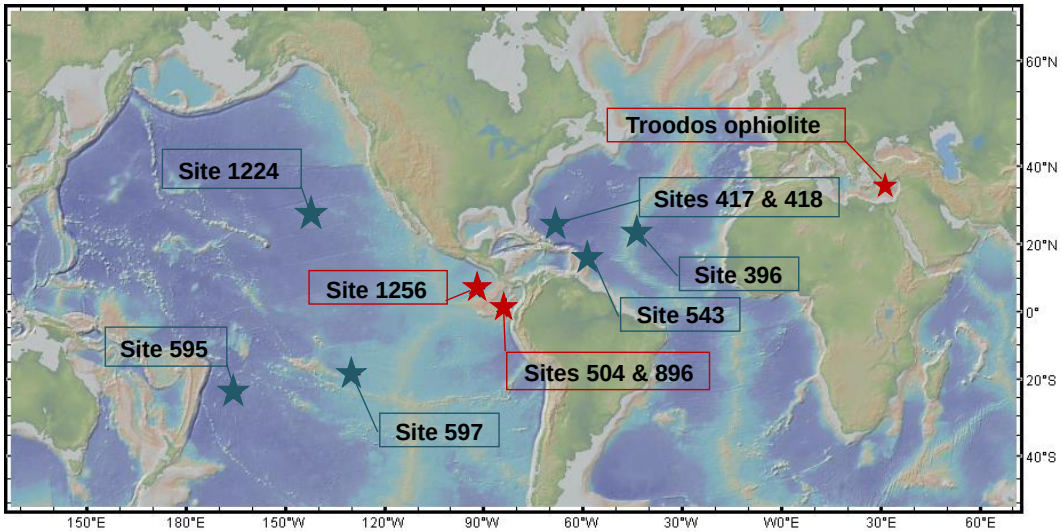

Figure 5.2. Approximate location of each studied site is shown on the map. Green stars show sites included in this study and red stars show those sites for which there is published data.

In addition to comparing the new data collected as part of this study with all previously published analyses of seafloor lavas with Li-isotope data, I compiled a database of the Li concentrations of lava samples from 48 different DSDP/ODP sites. These 48 sites are from published studies with available Li and Y data over the past ~120 Myrs ago. The data was downloaded from the PETDB website (http://www.petdb.org) using following criteria: (i) selecting all DSDP and ODP expeditions, (ii) choosing igneous, veins and altered material, and (iii) filtering the downloaded data on the basis of tectonic setting of "off-axis" and "old oceanic crust".

Table 5.1. Key characteristics of DSDP/ODP sites for which Li-isotopic data for lavas exist.

Hole	Crustal age (Myr)	Basement depth penetration (m)	Sediment thickness (m)	Sedimentation rate (m/Myr)	Average alteration temperature (°C)*	Age of basal sediment (Myr)	Seafloor topography	Reference
417A[1]	119	209	208	1.7	22	66-100	High	Donnelly et al. (1979a)
417D[1]	119	365	342	2.9	22	113-119	Flat-lying	Donnelly et al. (1979a)
418A[1]	119	544	320	2.7	35	113-119	Flat-lying	Donnelly et al. (1979b)
595B	95	55	70	0.8	17		Flat-lying	Jordan et al (1987)
Troodos ophiolite[2]	91			1	14	Regional variation	Regional variation	Bear (1960); Mukasa and Ludden (1987); Gillis et al. (2015)
543A	81	44	411	5	17	72-81		Biju-Duval et al. (1984)
1224F	46	175	28	0.6	6	41-46		Stephen et al. (2003)
597C	28	91	52	2	2	23-28	Flat-lying	Leinen et al. (1986)
1256D[3]	15	751	251	16.7	61	11-15		Wilson et al. (2003)
396B	13.6	255	150	11.1	2	11-13.6		Dimitriev et al. (1978)
504B[4]	5.9	571	274	40.4	34	5.8-6.4	Flat-lying	Cann et al. (1983)
896A[4]	6.8	290	179	26.3	43	5.8-6.4	High	Alt et al. (1993)
Dredged[5]	0-10				4			Chan et al. (1992)

* Based on calcite O-isotope thermometry (Kim and O'Neil, 1997). Temperature data from compilation in Gillis and Coogan (2011) and Gillis et al. (2015).

Li-isotopic data are from:

[1] Bouman et al. (2008); Chapter 4.

[2] Brant et al. (2012); Coogan et al. (2017)

[3] Gao et al. (2012)

[4] Chan et al. (2002)

[5] Chan et al. (1992)

5.3. Results

5.3.1. Lithium abundances in lava samples

Most of lava samples from the studied sites (both this study and published data) were highly altered, however, the range of Li concentration is widely variable between different sites (Figure 5.3). To evaluate the amount of Li added to or leached from lava samples during low-temperature hydrothermal alteration, protolith Li concentrations are quantified using the approach described in Chapter 4 (Li_{proto} =0.14Y+1.79; Section 4.4.1, Figure 4.2). Most of the lava samples from the different sites, except Site 1256, have higher Li/Y than fresh MORB glass, indicating Li uptake during low-temperature hydrothermal alteration (Figure 5.3). Samples from Hole 417A and the Troodos ophiolite have highly elevated Li/Y (Figure 5.3), with an average ΔLi ($\Delta Li = Li_{lava} - Li_{proto}$) of ~18 ppm. Most of the samples from Site 1256 have Li/Y < MORB, thus appear to have lost Li. This is not surprising given the higher temperature of alteration at this site (~22-77°C in the lava pile; Alt et al., 2010). Of the other sites, Holes 595B and 1224D&F have taken up the least lithium, with average ΔLi values of 3 ppm and 0.5 ppm, respectively, whereas Holes 417D, 418A, 543A, 597C and 396B have average ΔLi values of 4 to 10 ppm.

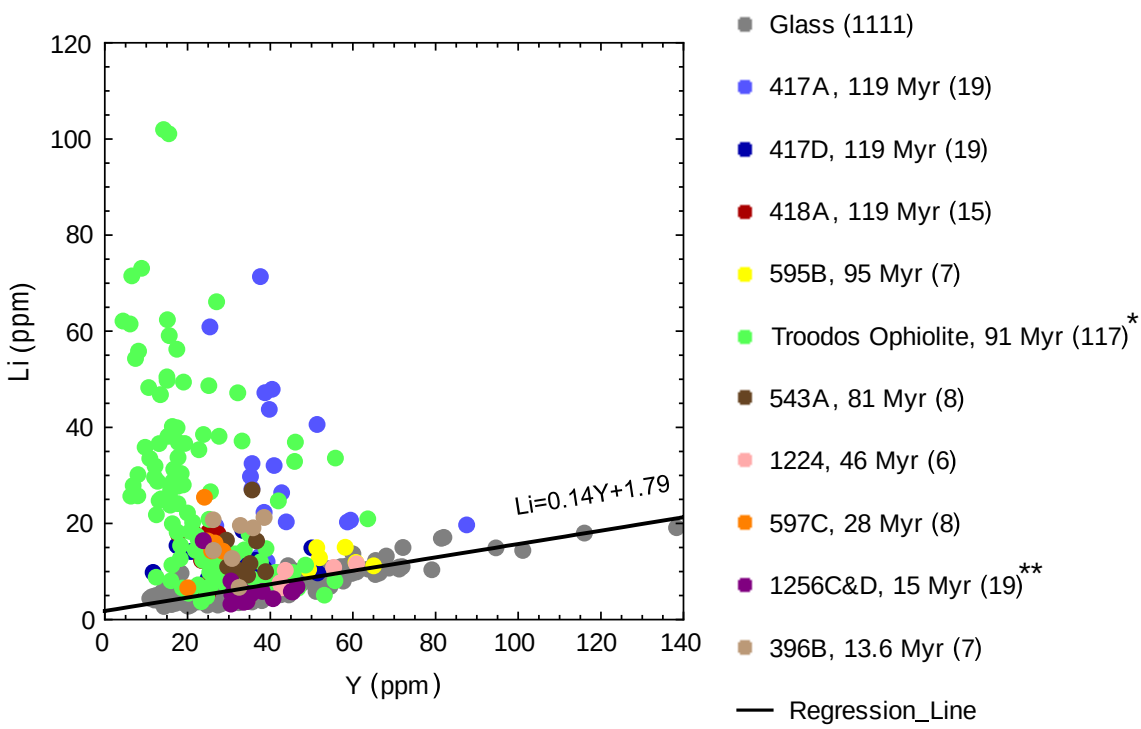

Figure 5.3. Li vs. Y concentration of lava samples. The black line shows a regression through MORB glass data interpreted as the magmatic trend for fresh glass (Gale et al., 2013). The altered lavas from most of the holes fall above the line, indicating Li uptake during low-temperature hydrothermal alteration. The number in brackets is the number of data. * Coogan et al. (2017); ** Gao et al. (2012). Published data for Holes 417A, 417D, 418A (Bouman et al., 2008), 504B/896A (Chan et al., 2002) and dredged samples (Chan et al., 1992) are not included in this plot due to lack of Y data.

The ΔLi is also calculated for compiled data (Figure 5.4; Supplementary Tables D.3.3). The majority of the downloaded data are classified as "igneous rocks", hence, it is possible that many of these downloaded data are from studies which avoided using the most altered lava samples. For example, the average Li concentration of lava samples which I studied (with the aim of selecting the most altered samples) from Sites 417/418 is ~18±3 ppm (2SDE) which is over two times the average of published data from these sites (~7.5±0.5 ppm; Staudigel et al., 1980).

There is a wide variability in the Li uptake between sites, however, at all sites ΔLi decreases with depth below sediments such that there is more Li added to the crust at shallower levels (Figure 5.4). To evaluate the approximate depth where the ΔLi starts to decrease, averages ΔLi are calculated in depth intervals. Both the upper 50 m, and the 50 to 100 m, below sediments interval have an average ΔLi of ~8 ppm. Deeper than 100 m, the averages of ΔLi are calculated for intervals of 100 m. Average ΔLi gradually decreases with depth to ~0 ppm at 600 m below sediments; in sections deeper than 600 m below sediments it appears that Li was leached from the rocks (ΔLi<0; Figure 5.4).

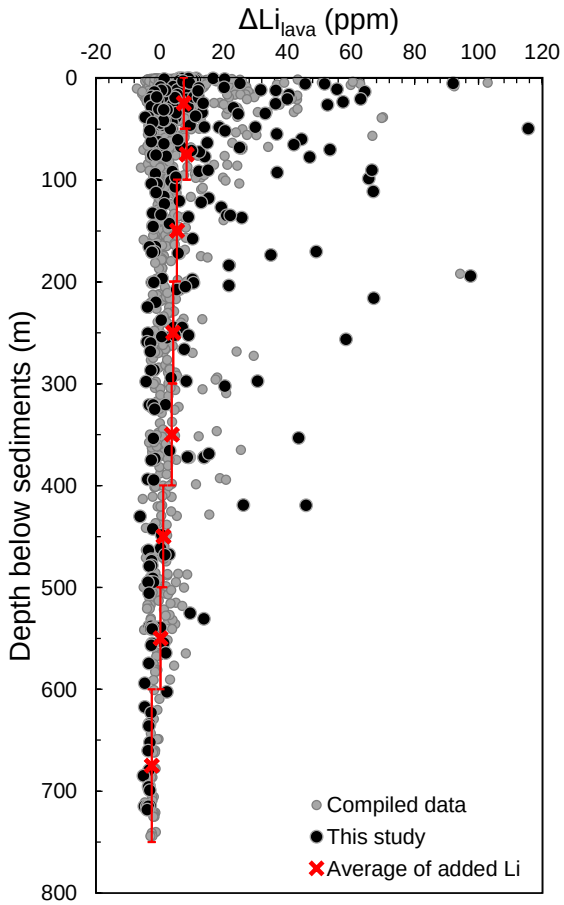

Figure 5.4. Lithium added (ΔLi) to the lava samples versus depth below sediments for compiled data (with available Li and Y data; gray symbols) and sites studied here (Table 5.1; black symbols). Red crosses represent the average of ΔLi and the red solid lines indicate the depth interval that the average was calculated for.

Correlation between Li and other common geochemical proxies for the extent of low-temperature alteration has been tested here. This analysis shows that Mesozoic oceanic crust has a broader range of Li, Rb and K_2O content than Cenozoic crust, however, there is no correlation between the Li content of lava samples and their K_2O and Rb contents (Figure 5.5).

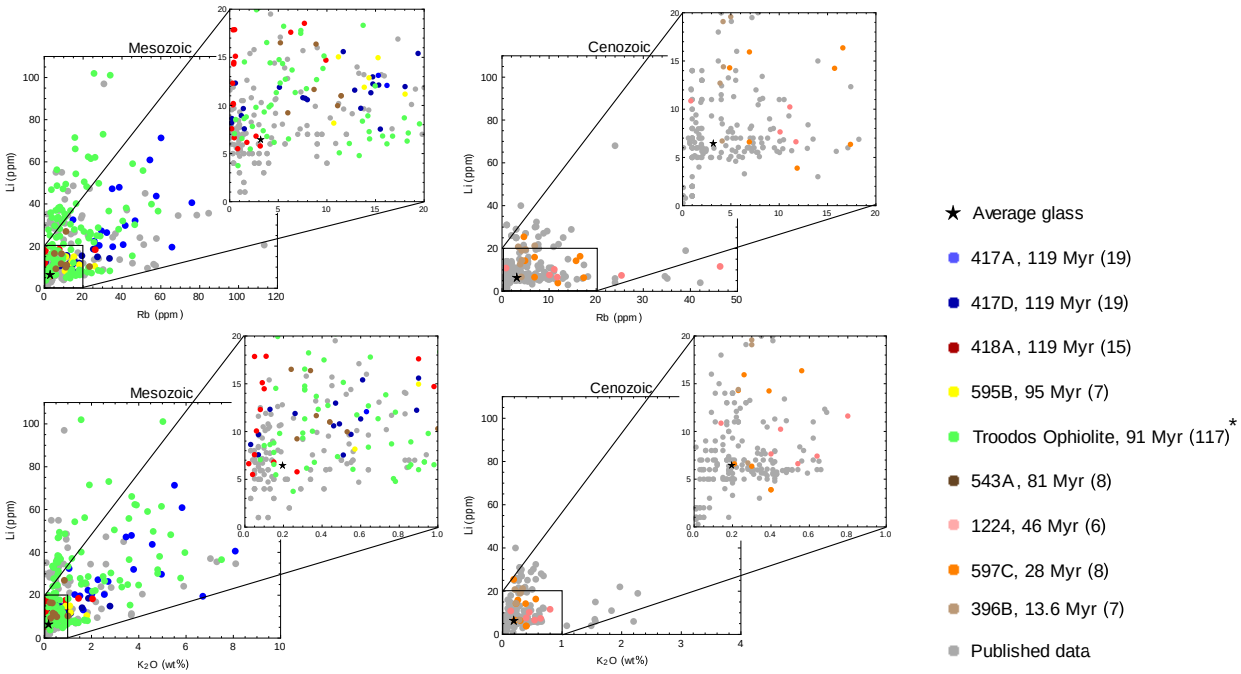

Figure 5.5. Lava Li vs. K_2O (bottom) and Li vs. Rb (top) for Mesozoic (left) and Cenozoic (right) drill sites. There is no obvious correlation between Li and Rb or K_2O although some individual areas (e.g., Holes 417A, 417D and 418A; Chapter 4) do show strong correlations between different proxies for extent of low-temperature hydrothermal alteration. The average MORB glass composition is from Gale et al. (2013). Number in brackets is the number of data.* Coogan et al. (2017).

5.3.2. Lithium isotopic composition of lava samples

Fresh MORB has a mean δ^7Li of 3.7 ‰ (1.6 ‰ to 5.6 ‰, n=31; Tomascak et al., 2008) whereas altered lavas measured in this and previous studies range from -2.3 ‰ and 20.8 ‰ (Figure 5.6). Mesozoic samples are assumed to have interacted with seawater with higher δ^7Li than the Cenozoic samples, which here are from ≤46 Myr. Hence the δ^7Li data is divided into two age groups: Cenozoic and Mesozoic. Variation of δ^7Li of studied samples is investigated based on their depth below sediments (Figure 5.6). There is no systematic variation in lithium isotopic composition of altered lavas with depth in the crust for Cenozoic crust and the δ^7Li for those lava samples which have taken up Li (ΔLi>0) fluctuates between ~3 ‰ and ~21 ‰ (Figure 5.6). In contrast, the Li isotopic composition of the Cretaceous lava samples from Holes 417A, 417D, 418A and the Troodos ophiolite generally have lower δ^7Li in the top ~30 m of the crust, and are generally isotopically heavier than fresh MORB deeper in the crust. All lava samples from the other two Cretaceous drill cores studied (Holes 595B and 543A), which come

from the upper 50 m of the lava pile, have δ^7Li of 4±1.5 ‰ with no systematic variation with depth or Li content; i.e., while they have taken up Li during hydrothermal alteration their Li-isotopic composition has not changed significantly from that of the fresh rock. Most samples from Site 1256 have lost lithium and they have variable δ^7Li between -2 ‰ to 14 ‰. Most lava samples from Site 1256 with high δ^7Li are from the deep sections where temperature of alteration increases from 60 °C to 80 °C (Alt et al., 2010). Faster diffusion of ^{6}Li than ^{7}Li during leaching of Li from lavas at high temperatures is one possible explanation for heavy isotopic composition of lava samples from Site 1256.

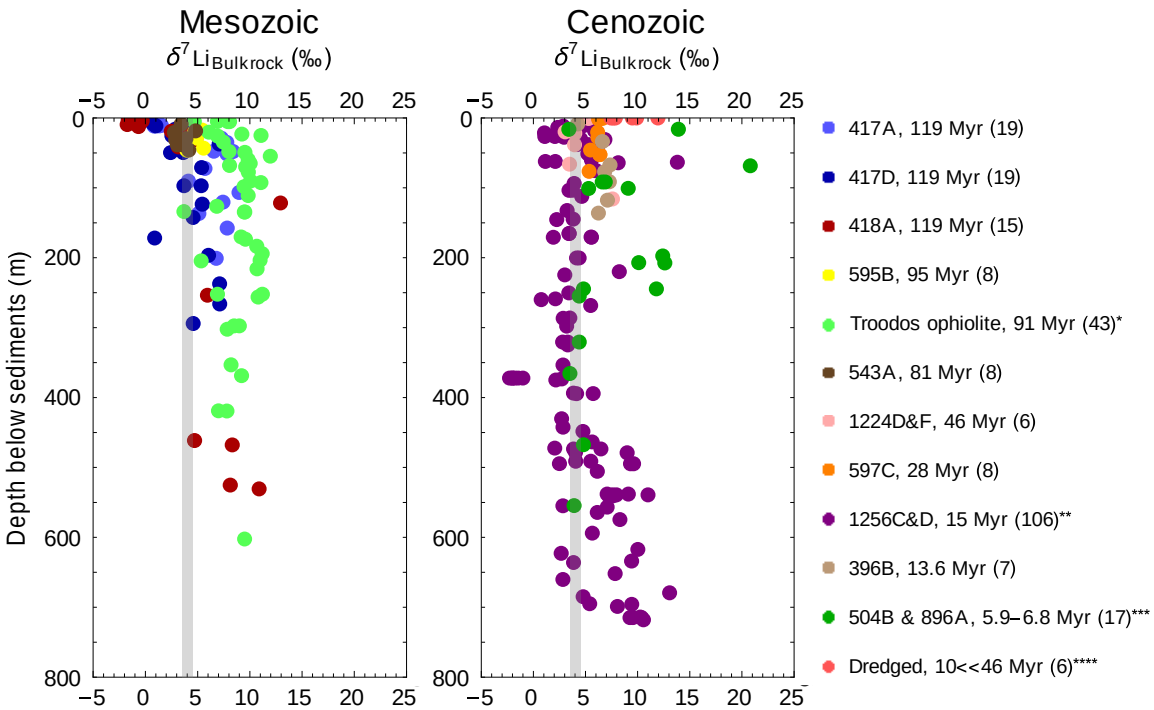

Figure 5.6. Lava lithium isotopic compositions versus depth below the sediment-lava contact for Mesozoic (left) and Cenozoic (right) cores. The light gray shaded area shows the average lithium isotopic composition of fresh MORBs (3.7±0.4 ‰; Tomascak et al., 2008). *Coogan et al. (2017). **Gao et al. (2012). * Chan et al. (2002). **** Chan et al. (1992).**

5.4. Discussion

5.4.1. Effect of crustal age, alteration temperature and sedimentation rate on Li uptake in off-axis oceanic crust

Variation of ΔLi of lava samples (from the upper 100 m below sediments) is tested against the crustal age, sedimentation rate and alteration temperature. To ensure that the correlation of ΔLi with depth does not cover any possible correlation of ΔLi with other parameters, lava samples from only the upper the 100 m below sediments are used. The sedimentation rate is calculated using sediment thickness at each study area divided by the crustal age. The temperature of alteration in the lava section of ocean crust is determined for each study area using the O-isotopic composition of carbonates (Figure 5.7). Fluid-rock reaction which results in formation of secondary minerals also

accompanies generation of alkalinity which is required for precipitation of carbonates. Moreover, age of formation of carbonates and other low-temperature alteration phases suggests that they form over the same time interval (e.g., Coogan et al., 2016). Hence, I assume that the temperature of carbonate formation is representative of the alteration temperature. Average temperature of alteration in Hole 418A is higher than at Holes 417A and 417D because these samples suite include samples from deeper in the lavas than the other holes (≥350 m below sediments; Figure 5.7). Temperature of alteration is uniform in the upper ~30 m below sediments in Troodos ophiolite (8±1C°) and increases with depth (Figure 5.7). Available temperature data from the Holes 595B and 543A is within the upper ~50 m below sediments which is consistent with the depth range of Li concentration and δ^7Li data. Average temperature of alteration in all studied Cretaceous sites is between 14°C to 35°C while it is between 2°C to 6°C in Mesozoic holes with normal sedimentation rate (Holes 1224F, 597C and 396B; Figure 5.7) showing the effect of decrease in bottom seawater temperature over the past 120 Myr (Figure 5.7). The young ocean crust at Sites 504 and 896 (5.9 and 6.8 Myr, respectively) have anomalously high carbonate formation temperatures of ~34 and ~43°C, respectively, due to very high sedimentation rates (Table 5.1, Figure 5.7). At Site 1256, the lava section is capped with a 75 m thick sheet flow which probably restricted fluid circulation within the crust, leading to a high temperature of alteration (~60 °C; Table 5.1, Figure 5.7). For the compiled data, due to a lack of carbonate O-isotopes data for most sites, the temperature of alteration is obtained using the estimated variation in alteration temperature of off-axis ocean crust with crustal age (Gillis and Coogan, 2011).

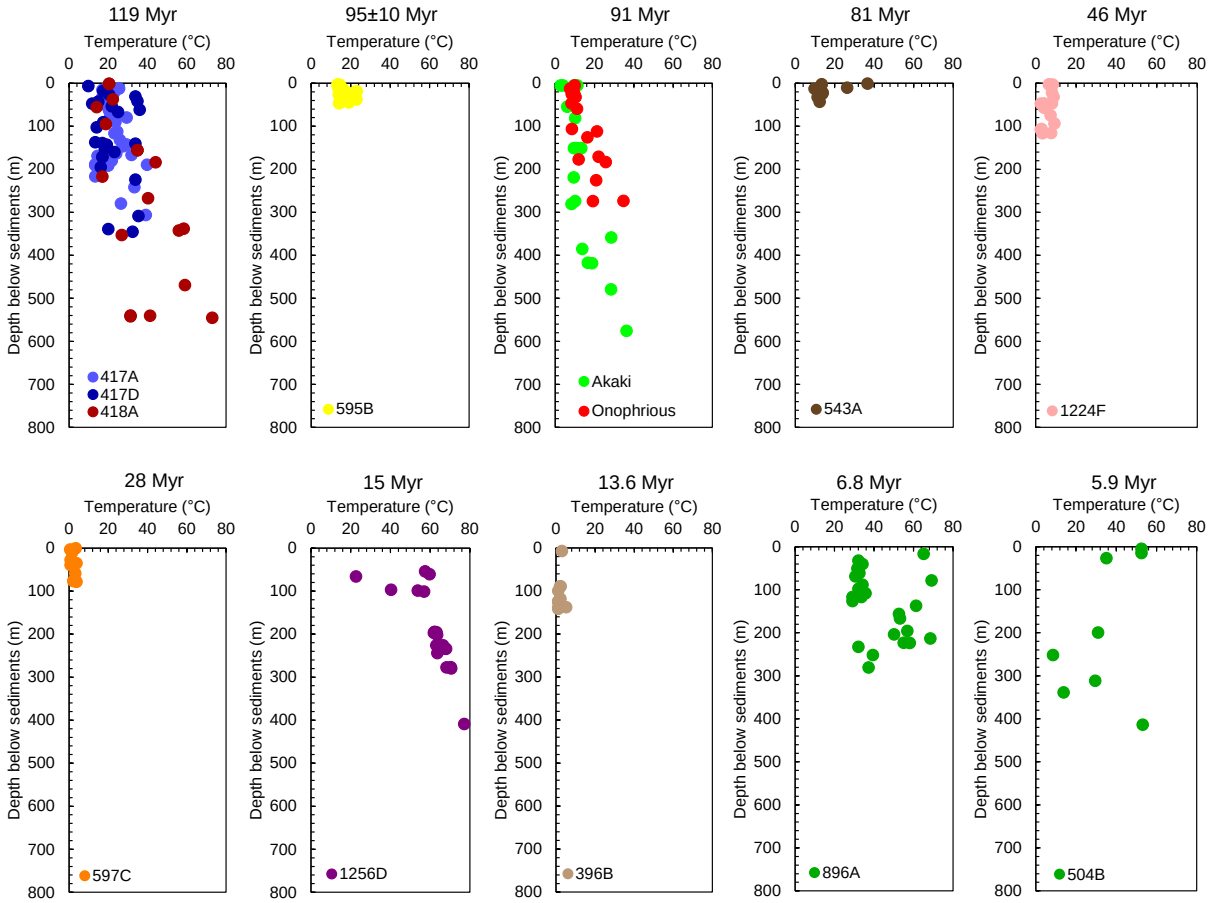

Figure 5.7. Carbonate formation temperature versus depth below sediments at study areas with available Li-isotopic composition. Oxygen-isotopic composition of precipitated carbonates is used to calculate the carbonate formation temperature (using the Kim and O'Neil (1997) thermometer), which is assumed as temperature of alteration of lava samples (e.g., Gillis and Coogan, 2011; Gillis et al., 2015). Cretaceous study areas have 15°C to 20°C higher alteration temperatures compared with Cenozoic sites (except young oceanic crust from Holes 1256D, 504B and 896A which have experienced anomalously high temperatures of alteration due to restriction of fluid penetration into the crust as a result of rapid sedimentation rate (504B/896A)).

There is a very weak correlation (r^2= 0.1) between the amount of Li take up by the upper oceanic crust from seawater and the crustal age (Figure 5.8a and Figure 5.8d). The correlation is stronger (r^2=0.2) between the averages of ΔLi (at each crustal age) and the crustal age (Figure 5.8b and Figure 5.8e). To ensure that the observed correlation is not due to a sampling bias, averages of ΔLi to the upper 100 m oceanic crust in 5 Myr intervals was calculated, suggesting an even stronger positive correlation (r^2=0.3) between Li uptake into the oceanic crust and crustal age (Figure 5.8c and Figure 5.8f). The averages of ΔLi in the upper 100 m of the oceanic crust decreases from ~18±6 ppm (SDE) at the Cretaceous to ~3±1 ppm (SDE) at Late Cenozoic. However, low recovery of the most altered parts of the ocean crust during drilling means that these are probably underestimated. Most sites with high ΔLi (>~10 ppm) are also associated with high alteration temperature and slow sedimentation rate (Figure 5.8c and Figure 5.8f).

However, at the sites with low ΔLi (< ~10 ppm) alteration temperature has much wider range than the sedimentation rate (Figure 5.8c and Figure 5.8f).

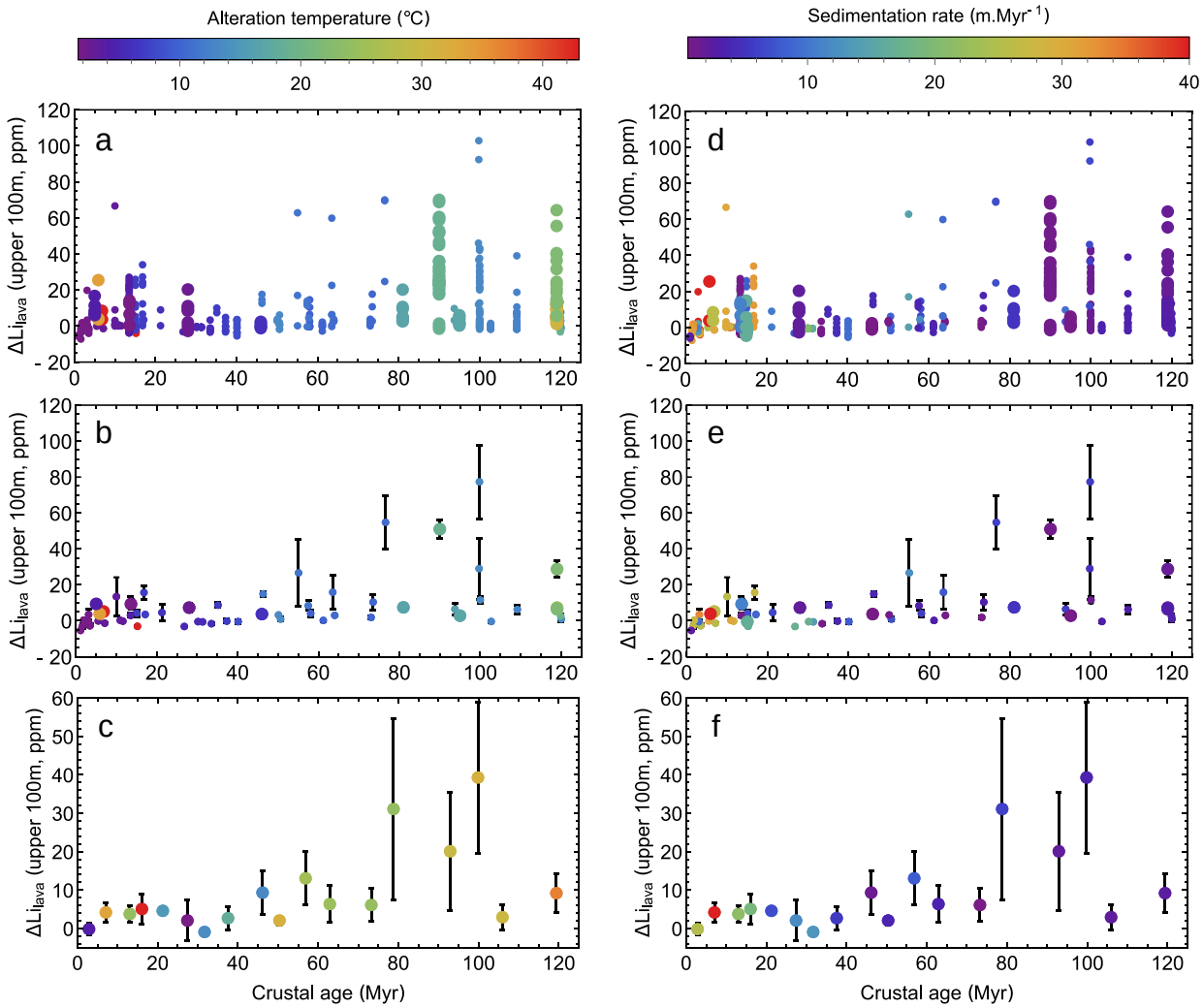

Figure 5.8. Calculated amount of Li added to the upper 100 m of the oceanic crust versus crustal age colour coded by alteration temperature (left) and sedimentation rate (right) for the compiled dataset (smaller symbols) and this study (larger symbols). The data are from: (a and d) upper 100 m below sediments, (b and e) averages at each study area, (c and f) averages of added Li (both compiled and this study) in 5 Myr crustal age intervals, showing positive correlation (r^2=0.3) between Li uptake into the oceanic crust and crustal age. Error bars on the Y-axis represents the SDE of the data.

The Li/Ca of benthic foraminifera shows relatively little change over the past 60 Myr (Delaney and Boyle, 1986). However, the Li/Ca of planktic foraminifera shows considerable variation (Misra and Froelich, 2012). Several studies have shown that the Li/Ca ratio of both organic and inorganic carbonates are sensitive to changes in temperature such that increasing of temperature results in a decrease in Li/Ca of carbonates (e.g., Delaney and Boyle, 1986; Delaney et al., 1989; Marriott et al., 2004a, 2004b). Since currently, there is little data on Li/Ca of seawater during the past 120 Myrs, it is difficult to find conclusive empirical evidence for changes in Li concentration of

seawater during this timescale. However, considering the lower partitioning of Li/Ca in carbonates at higher temperatures (e.g., Delaney and Boyle, 1986; Delaney et al., 1989; Marriott et al., 2004a, 2004b), the constant Li/Ca of foraminifera during the period where the bottom seawater temperature was warmer than today, may have been due to the higher Li concentration of seawater than today. Observed higher ΔLi in the upper 100 m of the lava section of the upper oceanic crust (Figure 5.8) during the Cretaceous than in the late Cenozoic supports the suggestion that there may have been a higher Li concentrations of seawater during this time. However, this higher Li uptake during the Cretaceous compared with late Cenozoic also coincides higher bottom water (and alteration) temperatures and the Cretaceous drill cores studies were generally more slowly sedimented than the Cenozoic ones (Figure 5.8). When sedimentation rate is slow, large amount of seawater can ingress into the off-axis, upper oceanic crust which can lead to higher Li uptake of lava samples.

Alteration temperature largely correlates with crustal age, consistent with cooling of bottom seawater temperature during the past 120 Myr. Only beneath areas with high productivity such as the equatorial Pacific, or close to continental margins where terrigenous sediments supply leads to very high sedimentation rates, does sediment thickness impact alteration temperatures (e.g., ODP Sites 504, 896 and 1256; Coogan and Gillis, 2018). Higher Li uptake into the upper oceanic crust during the Cretaceous compared with late Cenozoic (Figure 5.8) can also be attributed to the higher bottom seawater temperature during the Cretaceous, which can leads to more rapid fluid-rock reaction and hence Li uptake.

5.4.2. Lithium isotopic composition of bulk altered oceanic crust

To estimate the δ^7Li of bulk altered upper oceanic crust, weighted averages of the δ^7Li are calculated at each study area; the averages ΔLi are used to weight the isotope data (Table 5.2; Figure 5.9). The calculated δ^7Li of bulk altered upper oceanic crust increases with decreasing crustal age such that it is ~4 ‰ in the Cretaceous and increases to ~6 ‰ during ~45 to 15 Myrs ago and then increases to ~10 ‰ at the modern era (Table 5.2; Figure 5.9). This increase appears to be consistent with ~9 ‰ increase in the δ^7Li of seawater during this time (Figure 5.9). However, the δ^7Li of seawater from the Cretaceous is poorly known. The only available δ^7Li data for Cretaceous seawater come from two studies that investigated the variation of δ^7Li of seawater before, during and after Ocean Anoxic Events 1 and 2 (OAE1 and OAE2), which occurred 120.3 and 93.7 Myrs ago (Pogge Von Strandmann et al., 2013; Lechler et al., 2015). Both studies suggest a drop in δ^7Li of biogenic carbonates during these OAEs (Chapter 3), which adds to the uncertainty of the δ^7Li of Cretaceous seawater (Figure 5.9).

Equilibrium Li isotopic fractionation between solid and fluid phases depends on differences in bond energies between the two phases for the light and heavy isotopes (e.g., Wenger and Armbruster, 1991). This correlates with the inverse of temperature (e.g., Hoefs, 2015). The anomalously large δ^7Li of young altered crust (Holes 504B/896A; Table 5.2, Figure 5.9) could be explained by the effect of high alteration temperatures on the Li-isotopic fractionation factor (Coogan et al., 2017). Apart from Holes 504B/896A, the δ^7Li of bulk altered crusts correlates with alteration temperature,

such that when the temperature of alteration is higher the δ^7Li of bulk altered crusts is lower (Figure 5.9a). This correlation is probably only due to the correlation between the crustal age and alteration temperature (Figure 5.1) and it is probably not the main control on the δ^7Li of bulk altered crust. If there was a strong control from the alteration temperature on the δ^7Li of the bulk altered crust, those crustal sections altered at higher temperatures should show a δ^7Li close to δ^7Li of seawater. This does not observe here and the calculated apparent Li isotopic fractionation factor ($\Delta_{sw\text{-}crust}=\delta^7Li_{sw}-\delta^7Li_{crust}$) does not correlate with the alteration temperatures (Figure 5.9b), unless the current understating of the δ^7Li of seawater is not correct and the δ^7Li of Cretaceous seawater was smaller than that of the average Cretaceous carbonates (~21 ‰). To estimate the Li-isotopic fractionation factor between the altered upper oceanic crust and seawater, other approaches are discussed in the following sections.

Table 5.2. Lithium isotopic composition of altered crust in all studied areas.

Hole	Age (Myr)	Avg alteration temperature (°C)*	Weighted average composition of bulk altered crust		
			Avg ΔLi (ppm)	Avg δ^7Li_{crust} (‰)	2SDE (‰)
417A	119	22	24	4.4	1.2
417D	119	22	5	3.5	1.2
418A	119	35	7	3.7	2.6
595B	95	17	3	4.5	1
Troodos ophiolite	91	14	40	9.1	0.5
543A	81	17	7.5	3.7	0.9
1224	46	6	1	5.3	1.5
597C	28	2	7.5	6.3	0.8
396B	13.6	2	10	6.9	1
504B/896A	5.9	39	2.5	16.7	2.4
Dredged	≤10	4	5	10.2	1.5

* Average temperature of alteration based on calcite O-isotope thermometry (Kim and O'Neil, 1997) at each study area.

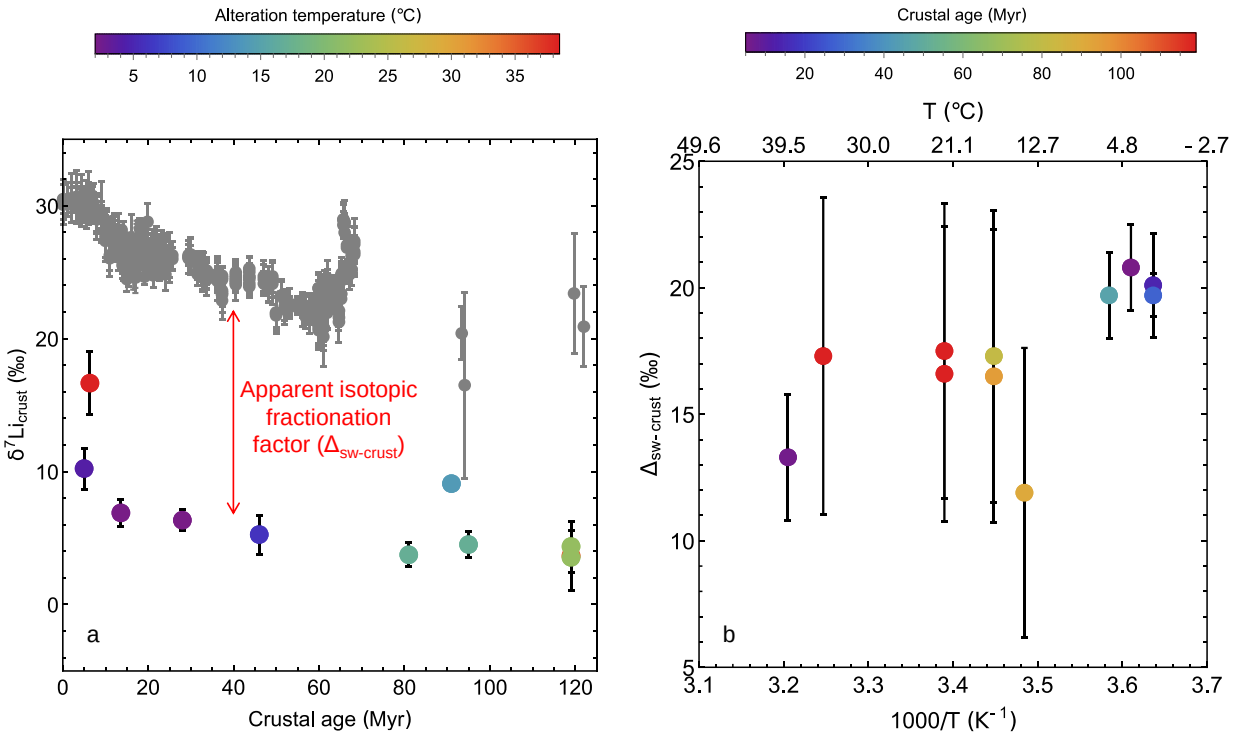

Figure 5.9. (a) Weighted average Li-isotopic composition of bulk altered upper lava section of oceanic crust (δ^7Li_{crust}; temperature colour coded circles) and δ^7Li of seawater for the last 120 Myr (gray symbols; Hathorne and James, 2006; Misra and Froelich, 2012; Pogge Von Strandmann et al., 2013; Lechler et al., 2015) versus the crustal age. The δ^7Li of bulk altered crust is obtained based on weighted averages of δ^7Li of lava samples at each study area, and the averages ΔLi are used to weight the isotope data. (b) The apparent Li-isotopic fractionation factors ($\Delta_{sw\text{-}crust}$) versus the inverse of alteration temperature (crustal age colour coded). The calculated $\Delta_{sw\text{-}crust}$ are the difference between the δ^7Li of seawater and bulk altered upper ocean crust. The δ^7Li of Cretaceous seawater is assumed 21 ‰. Vertical error bars are 2SDE and they are calculated following the error propagation method.

5.4.3. Lithium-isotopic fractionation factors between altered crust and seawater over the past 120 Myrs

Two approaches, other than the above estimations, are tested to quantify the Li-isotopic fractionation factor between altered oceanic crust and seawater: (i) extraction of δ^7Li of altered end-member oceanic crust and calculation of the difference between this and δ^7Li of seawater, and (ii) using the linear kinetic model described in Chapter 4 and adjusting the Li-isotopic fractionation factor to fit the observed variation of δ^7Li and Li concentration of lava samples at each study area.

5.4.3.1. Lithium isotopic composition of altered end-member oceanic crust

An apparent lithium isotope fractionation factor between seawater and altered end-member oceanic crust can be estimated as the difference between the lithium isotopic composition of seawater and completely altered lavas ($\Delta_{SW\text{-}lava}$ =1000ln(α)); where SW stands for seawater, and α is the equilibrium Li-isotopic fractionation factor between

seawater and altered lava (e.g., Chan et al., 1992). To estimate the lithium isotopic composition of an altered end-member, it is assumed that lavas are binary mixtures of fresh MORB and low-temperature alteration products which have a fixed composition for each study area. In this model it is assumed that progressive hydrothermal alteration of rocks drives samples from the fresh to altered composition, adding Li and changing the rock δ^7Li towards a value of $\delta^7Li_{SW} - \Delta_{SW\text{-}lava}$. For each study area, lava samples which did not take up lithium during low-temperature hydrothermal alteration (i.e., Li/Y less than or equal to that of fresh glass; Figure 5.3) are excluded from the mixing modelling. The fresh end-member Li is calculated at each new study area based on Y concentration of lava samples, and if Y data is not available, the average Li concentration of fresh glass samples from previous studies have been used (Chan et al., 1992; Brandl et al., 2016). The δ^7Li of the protolith is assumed to be constant at 3.7±0.4 ‰ (2SD, n=31; Tomascak et al., 2008) for all sites. Assuming a fixed δ^7Li for fresh MORB is a reasonable assumption because lithium isotopes do not fractionate significantly during partial melting or fractional crystallization at magmatic temperatures (Tomascak et al., 1999).

A correlation between δ^7Li vs. Li^{-1} was observed for a subset of the study areas (Holes 595B, 543A, 1224, 597C, 396B, 504B/896A and dredged samples < 10 Myr).To extract the Li-isotopic composition of the altered end-member for these study areas, a line was fitted through δ^7Li vs. Li^{-1} of fresh MORB and altered rocks.

The regression line is weighted by the uncertainty on the Li-isotopic composition of the samples. The uncertainties on the lithium isotopic composition of the altered end-member for each study area (where a mixing model fits the data; Figure 5.10) was estimated by generating 10,000 synthetic datasets with the statistical properties of the data and determining the intercept at infinite lithium content; i.e., random data were draw from probability distributions using the measured δ^7Li as the average and its uncertainty as the standard deviation. Number of δ^7Li values the same as the number of samples are randomly selected with replacement among the 10,000 δ^7Li generated for each sample and then a regression line was fitted through the synthetic data set. This process is iterated 1000 times and the average and two standard deviation of the 1000 intercepts generated were then used as the estimate of the Li-isotopic composition of the altered end-member (Figure 5.10; Table 5.4). The altered end-member Li-isotopic composition calculated this way for sites with normal sedimentation rates from the Cenozoic (1224, 597C, 396B and dredged samples) appears to be higher (12±4 ‰; 2SDE) than those from the Mesozoic (595B and 543A; 4.5±2.5 ‰; 2SDE). This result is consistent with the observed correlation between the average δ^7Li of bulk altered crust with crustal age discussed in the previous section.

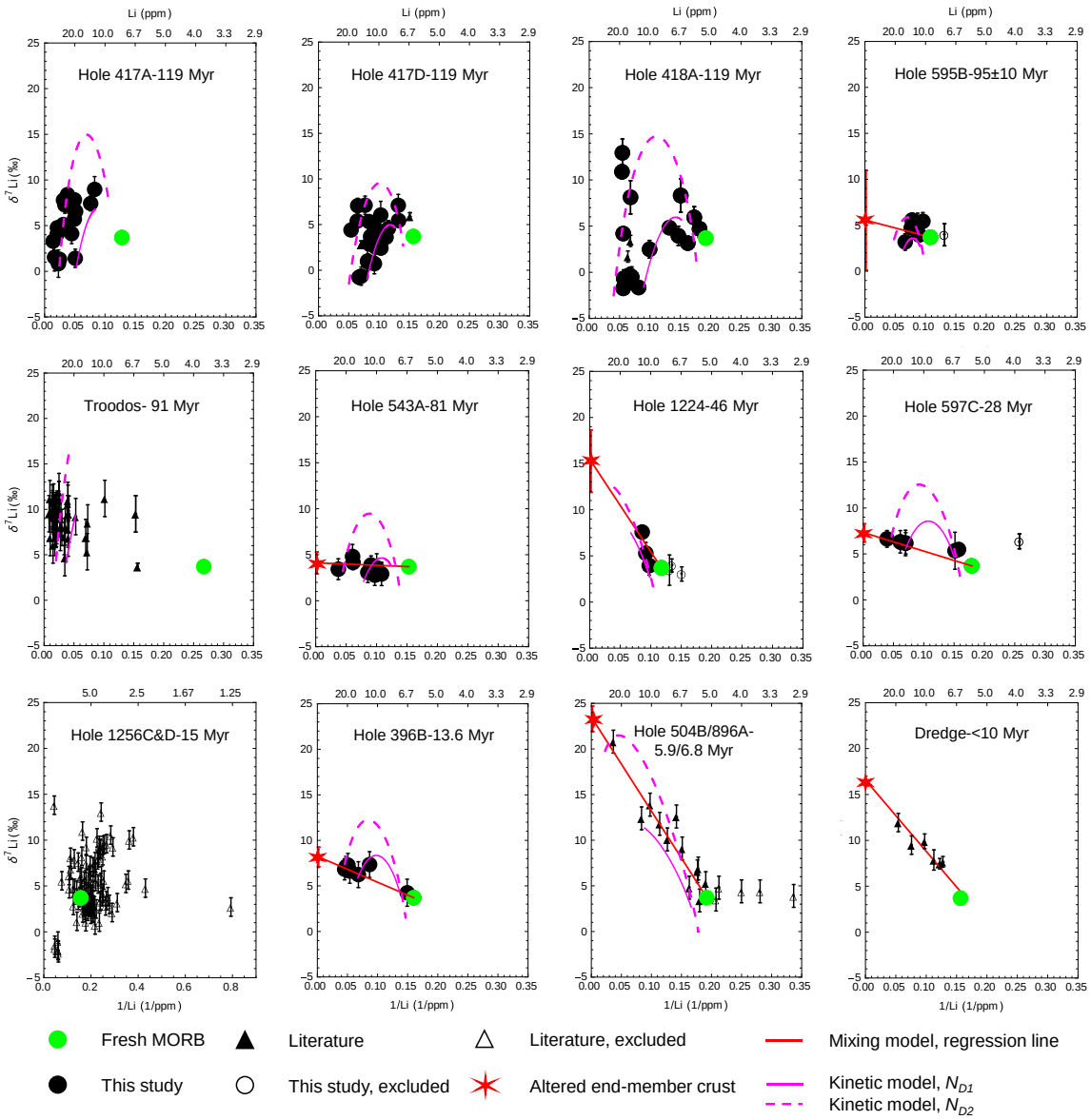

Figure 5.10. Lava δ^7Li versus Li^{-1} for each study area. A mixing model (regression line) is shown based on the assumption that lavas compositions are binary mixtures of fresh rock (green circle) and secondary minerals. This model is used to extract the lithium-isotopic composition of altered crust end-member (red star). Only samples with lithium contents higher than fresh MORB are used to define the mixing line (black symbols). Linear kinetic models (pink curves) for two different N_D values are tested against the data at studied sites where variation in reacting fluid composition is possible (see Table 5.3 for model parameters and Chapter 4 for mathematics of the model). Published data is from: Chan et al. (1992), Chan et al. (2002), Bouman et al. (2008), Gao et al. (2012) and Coogan et al. (2017). For the Dredged samples (Chan et al., 1992) only the transact basalts from the Mid-Atlantic Ridge older than 10 Myr (10 to 46 Myr) are included. These samples are old enough that their δ^7Li is overprinted by modern seawater composition.

A simple mixing model does not fit the data for samples from Holes 417A, 417D, and 418A (Chapter 4) and the Troodos ophiolite because there is no correlation between Li^{-1} and δ^7Li, and samples with high Li concentrations have a wide range of δ^7Li (Figure 5.10). The Li content and isotopic composition of lavas from these sites change with depth. The origin of this variation in Li content and isotopic composition of lavas from Holes 417A, 417D and 418A is discussed in Chapter 4, where it is proposed that the Li-rich, low δ^7Li samples at the top of these cores were probably altered when the uppermost part of the oceanic crust was exposed to seawater and the deeper samples probably interacted with a fluid with modified composition. In this scenario, Li is taken into the upper few meters of the crust at near infinite water/rock ratio. If the Li-isotopic fractionation factor is constant throughout the depth where most of the δ^7Li variations occur (Chapter 4), then the uppermost samples from Holes 417A, 417D and 418A are representative of altered end-member oceanic crust. If Cretaceous seawater has δ^7Li of 21 ‰, then the $\Delta_{SW\text{-}lava}$ was 22 ‰ at Holes 417A, 417D and 418A (Chapter 4, section 4.5.1.4.2).

The Li content of lavas from the Troodos ophiolite also shows similar variation with depth as of that in Sites 417 and 418, but the uppermost lavas have not been studied in as much detail in this ophiolite. Four regions in the Troodos ophiolite were studied that have different sedimentation history, dominant lithology and seafloor topography (Table 5.3; Coogan et al., 2017). Regardless of the differences between lithology and sedimentation history (Coogan et al., 2017), the Li concentration and isotopic composition of the lavas from these four studied regions have similar variations with depth (Figure 5.11). The δ^7Li of the uppermost lavas in the Troodos ophiolite varies between ~4 ‰ and ~8 ‰ and the deeper lavas generally range between 8 ‰ and 12 ‰. If the origin of the high Li concentrations and relatively light Li-isotopic compositions of the uppermost lavas in the Troodos ophiolite was similar to that at Sites 417 and 418, and if the δ^7Li of seawater 91 Myrs ago was ~21 ‰ (Pogge Von Strandmann et al., 2013), then the Li-isotopic fractionation factor in uppermost parts of this ophiolite would have been ~15±2 ‰. Alternatively, if the fractionation factor was the same during alteration of the Troodos ophiolite as during alteration at Sites 417 and 418, 91 Myr old seawater would be predicted to have a δ^7Li of ~25 ‰. Differentiating between these models will require, among other things, more detailed sampling of the uppermost lavas in the Troodos ophiolite.

Table 5.3. Properties of different study areas in the Troodos ophiolite.

	Mitsero seamount	Akaki canyon CY1/1A	Politico	Onophrious graben
Age of basal sediment (Myr)	≤23	≤70	≤70	~90
Seafloor topography	High	Normal	Normal	Low
Dominant lithology	Pillows and sheets	Pillows and sheets	Pillows and sheets	Sheet flows

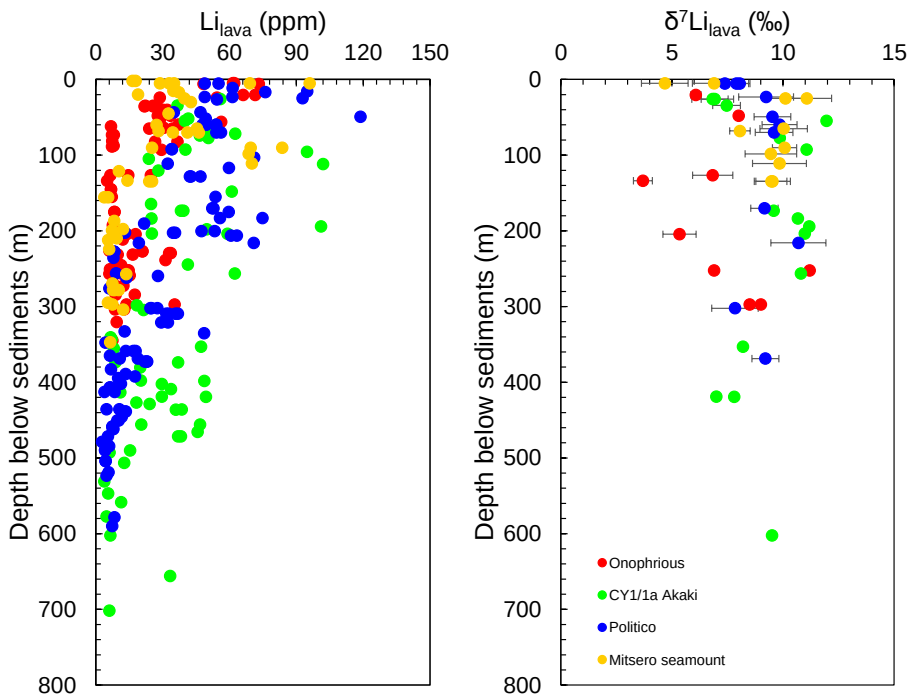

Figure 5.11. Li concentration (left) and δ^{7}Li (right) of lava samples from four regions of the Troodos ophiolite versus depth below sediment. The Li and δ^{7}Li profiles are similar in all four studied regions despite their having different lithologies and sedimentation histories. Data is from Coogan et al. (2017).

5.4.3.2. Vertical fluid flow model

Lava samples from most studied areas, apart from DSDP Sites 417 and 418 and the Troodos ophiolite, are from upper ~100 m below sediment, where the majority of variation in Li concentration and isotopic composition of lavas from Sites 417 and 418 and the Troodos ophiolite were observed. However, due to the small number of data, the origin of variation in the δ^{7}Li of lava samples as function of Li^{-1} in studied areas other than Sites 417 and 418 and the Troodos ophiolite is not clear. This variation may have originated from a variation in the Li concentration and isotopic composition of hydrothermal fluid, similar to the model proposed for Sites 417 and 418. Alternatively, it may be a result of simple mixing of fresh MORB and completely altered lavas, without any significant change in Li concentration and isotopic composition of hydrothermal

fluid. Therefore, a binary mixing model that does not account for variation in hydrothermal fluid composition is one possible model to explain variation of δ^7Li of lava samples as function of Li^{-1} in studied areas other than Sites 417 and 418 and the Troodos ophiolite. However, if the δ^7Li of the hydrothermal fluid changed during interaction with lavas in all studied areas (except the dredged samples), the δ^7Li of the altered end-member oceanic crust obtained using a mixing model (Figure 5.10) would not be representative of the δ^7Li of bulk altered upper oceanic crust. The only study area where a binary mixing model can be confidently used to predict the δ^7Li of the entire sink of Li into the altered crust, is the dredged samples from the Mid-Atlantic Ridge where lavas were altered at near infinite water/rock ratio. Hence, a vertical fluid flow model which was developed in the Chapter 4 is applied on all studied areas except the dredged samples.

As fluid travels along a flow pathway and interacts with the surrounding rocks, its composition evolves and hence, rocks which are further along the fluid pathway interact with a compositionally modified fluid. Therefore, the Li content and isotopic compositions of secondary materials precipitated further along a flow path are expected to be different than those precipitated from unmodified seawater. A model of the evolution of the Li concentration and isotopic composition of lava samples during vertical fluid flow, with constant porosity, fluid flux, Li partition coefficient and isotopic fractionation factor within the upper oceanic crust, was developed in Chapter 4. This model is compared with the measured Li concentration and δ^7Li of lava samples from study areas where the hydrothermal fluid could have varied in composition. To explain variation of δ^7Li of lava samples as a function of Li^{-1} at each study area, some of the model's parameters were adjusted. Adjusted parameters, for each study area, are the fluid flux (by changing fluid penetration distance), Li-isotopic fractionation factor ($\Delta_{sw\text{-}crust}$) and the Damköhler number (N_D; Boucher and Alvez, 1959). Models are developed for a constant basaltic crust porosity (0.075 v/v) and Li partition coefficient (300 ppm/ppm) in all studied areas. Two models with two different N_D values were developed for each study area to provide upper and lower limits of the N_D which broadly cover the variation of δ^7Li of the lava samples as a function of Li^{-1} (Figure 5.10; Table 5.4). For a given N_D, changing $\Delta_{sw\text{-}crust}$ has a strong effect on the model rock δ^7Li at the beginning of a fluid flow pathway (i.e., in altered lavas with higher Li contents, where chemical exchange between rock and fluid is large). Hence, the $\Delta_{sw\text{-}crust}$ was adjusted so as to fit the δ^7Li and Li concentrations of Li-rich lava samples (Figure 5.10; Table 5.4). For a given N_D and $\Delta_{sw\text{-}crust}$, lower fluid fluxes lead to a smaller change in the composition of altered rocks from initial fresh MORB values (Chapter 4, Section 4.5.1.4.1). The fluid flux was adjusted at each study area to cover the range of Li concentrations and δ^7Li of the studied lava samples (Figure 5.10; Table 5.4).

Table 5.4. Model results and parameters used to extract the Li-isotopic fractionation factor between seawater and altered oceanic crust.

Hole	Age (Myr)	δ^7Li_{sw} (‰)[a]	2SD (‰)	Avg $Li_{protolith}$ (ppm)[b]	2SDE (ppm)	Avg T (°C)[c]	Mixing model				Kinetic model[e]				
							$\delta^7Li_{end\text{-}member}$ (‰)	2SDE (‰)	$\Delta_{sw\text{-}crust}$ (‰)	2SDE (‰)	Fluid flux ($x10^7$ kg/m^2)	$\Delta_{sw\text{-}crust}$ (‰)	2SDE (‰)	N_{D1}	N_{D2}
417A	119	21	5.7	7.8	0.9	22	-[d]	-	-	-	18	20	2	0.2	0.8
417D	119	21	5.7	6.4	0.5	22	-[d]	-	-	-	6	23	1	0.1	0.3
418A	119	21	5.7	5.2	0.2	35	-[d]	-	-	-	6	24	1	0.1	0.4
595B	95	21	5.7	9.3	0.9	17	5	5.5	16	7.9	6	14	1	0.1	0.2
Troodos ophiolite	91	21	5.7	3.7	0.2	14	-[d]	-	-	-	98	16	1	0.5	1.5
543A	81	21	5.7	6.6	0.3	17	4	1.2	17	5.8	6	16	1	0.1	0.3
1224	46	25	0.8	8.5	0.9	6	15	3.4	10	3.4	6	5	5	0.1	0.3
597C	28	26	0.3	5.6	0.5	2	7	1	19	1	6	16	1	0.2	0.3
396B	13.6	27	1.8	6.2	0.5	2	8	1.1	19	2.1	6	16	2	0.1	0.3
504B/896A	5.9-6.8	30	0.7	5.2	0.3	41	23	1.4	7	1.6	4	7	4	0.1	1
Dredged	≤10	31	0.8	6.4	1.1	4	17	1.3	14	1.5					

[a] The δ^7Li of seawater is from Hathorne and James (2006), Misra and Froelich (2012), Pogge Von Strandmann et al. (2013) and Lechler et al. (2015). There is no available δ^7Li of seawater from ~81 Myrs ago; it is assumed that Cretaceous seawater has similar δ^7Li of ~21 ‰.
[b] Protolith Li concentration is calculated either using the Y concentration of lava samples or in case of lack of Y data, average of fresh glass composition is used from Brandl et al. (2016) and Chan et al. (1992).
[c] Average temperature of alteration based on calcite O-isotope thermometry (Kim and O'Neil, 1997) at each study area.
[d] Mixing model is not applicable for these studied areas (see text for more discussion).
[e] Linear kinetic model is based on vertical fluid flow model (with constant porosity and Li partition coefficient at all study area; 0.075 v/v and 300 ppm/ppm, respectively) which is developed in Chapter 4. Model parameters which are not listed in the table, are the same as Chapter 4 (Table 4.4). Parameters are adjusted to explain general variation of δ^7Li versus Li^{-1} of lava samples.

To broadly explain the variation in the Li concentration and isotopic composition of the lava samples using a vertical fluid flow model, three parameters were be adjusted simultaneously (i.e., fluid flux, Li-isotopic fractionation factor and N_D; Table 5.4). However, this can result in over fitting the data (for example at Holes 543A, 597C) and decrease the model's generalization capability compared to a simpler model (e.g., binary mixing model). On the other hand, the obtained range of parameters appears to be viable. For example, the high fluid flux calculated for Hole 417A and the Troodos ophiolite is consistent with their conditions of alteration. Hole 417A is located in a topographic high and the ~20 Myr difference between the basal sediments and basaltic basement suggests its top was altered in exchange with a near infinite reservoir of seawater (Table 5.1). Very high Li uptake into the lava samples of the Troodos ophiolite are also consistent with the suggestion of a high fluid flux in this study area (e.g., Coogan et al., 2017).

The estimated Li-isotope fractionation factor derived from fluid-rock reaction modelling using a linear kinetic model is not significantly different than that of using a mixing model and it appears that there is no correlation between these $\Delta_{sw\text{-}crust}$ values and crustal age (Figure 5.12). Averages of the $\Delta_{sw\text{-}crust}$ calculated using the mixing and linear kinetic models for the entire range of crustal age (excluding Sites 504 and 896, with anomalously high sedimentation rates) is 15.8±5.4 ‰ and 16.7±5.7 ‰ (2SDE), respectively. Effect of alteration temperature on the Li-isotopic fractionation factor are not clear in any studied area except at Sites 504/896. If these estimated isotopic fractionation factors are representative of bulk Li isotope fractionation between altered crust and seawater, it seems that a ~20°C decrease in bottom seawater temperature and hence alteration temperature over the past 120 Myrs does not provide a significant control on the Li isotopic composition of altered crust, and cannot explain the observed ~9 ‰ increase in seawater δ^7Li during this period of time. However, uncertainties on estimated Li-isotopic fractionation factors are very large. Collecting more Li-isotopic composition data for altered lava samples from sites where the number of samples studied is small (e.g., Holes 505B, 543A and 1224F) would be useful to better constrain model parameters and decrease uncertainties.

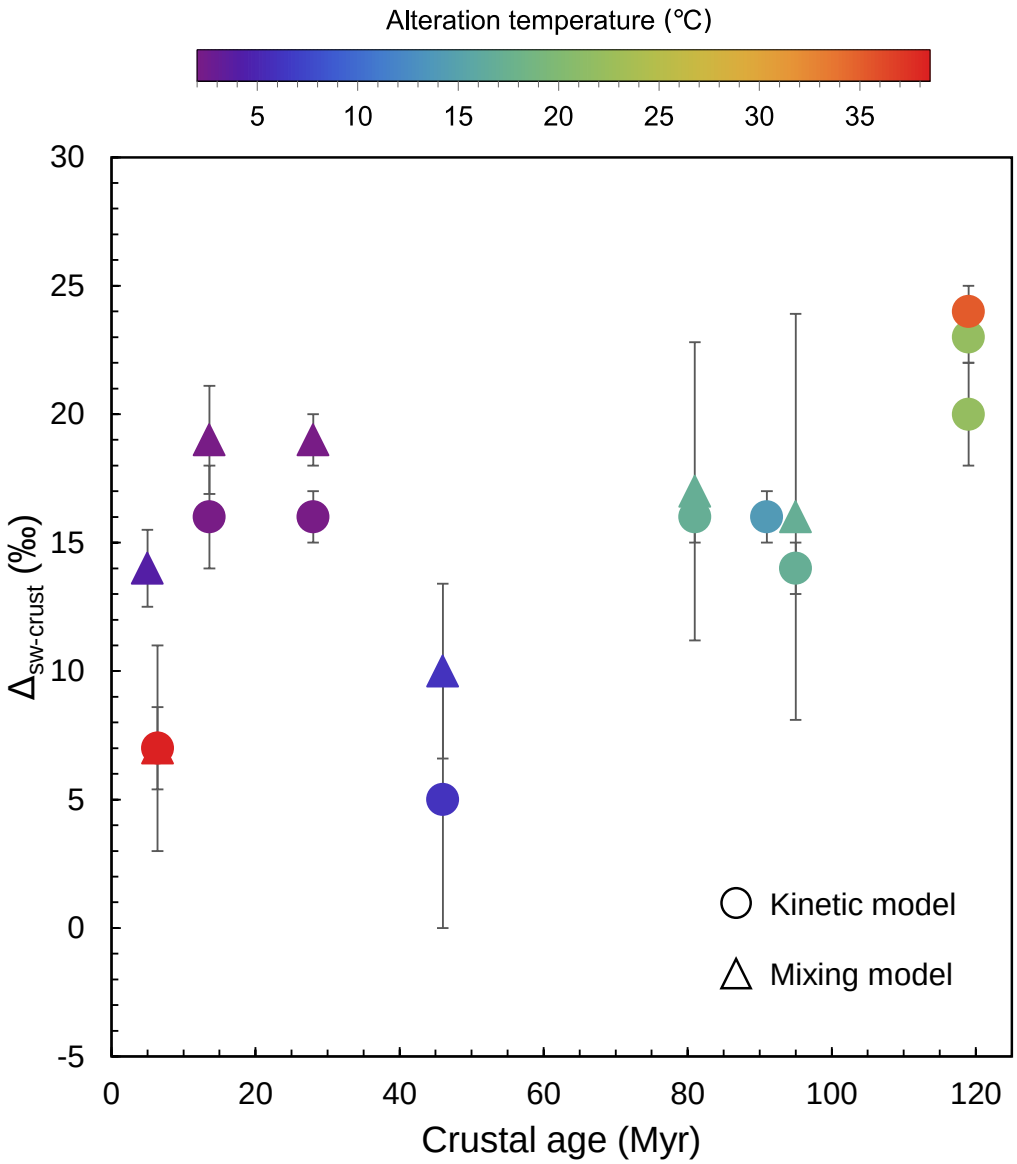

Figure 5.12. The estimated Li-isotopic fractionation factor ($\Delta_{sw\text{-}crust}$) between the off-axis lava section of the oceanic crust and seawater using a binary mixing (triangles) and a linear kinetic model (i.e., vertical fluid flow; circles) versus the crustal age. The data is colour coded with alteration temperatures. There is no correlation between either crustal age or alteration temperature. Vertical error bars at each study area is representative of 2SDE.

5.5. Conclusions

The upper lava section of the ocean crust at five DSDP/ODP drill cores was studied to better understand Li and Li-isotope exchange between seawater and the upper ocean crust on ridge flanks. Results of this study, in combination with previous studies, show that the amount of Li taken up during low temperature hydrothermal alteration of the upper oceanic crust correlates with depth below sediments such that the averages amount of Li added to the upper 100 m crust is ~8 ppm and this gradually decreases to nearly zero at ~600 m below sediments. Higher amounts of Li appear to have been added to the upper

100 m lava section of Cretaceous oceanic crust compared to the late Cenozoic. This increase could be attributed to higher Li concentration of seawater in Cretaceous. However, other controlling parameters such as alteration temperature and sedimentation rate may also play a role in controlling the larger amount of Li added to the crust during the Cretaceous. To determine which of these parameters, had the largest impact on Li uptake into the upper lavas of oceanic crust during the Cretaceous, a more thorough statistical analysis may be useful. Moreover, this study suggests that the average Li-isotopic composition of the bulk altered crust increases from the Cretaceous to the modern era by ~6 ‰. This increase may be attributed to an increase in seawater δ^7Li over this time. Moreover, there is no evidence of a systematic change in the estimated apparent Li-isotopic fractionation factor between seawater and off-axis, lava section of ocean crust (with normal sedimentation history) with either alteration temperature or crustal age.

Finally, it appears that the observed decrease in alteration temperature of the off-axis upper oceanic crust, as a result of global climate cooling, over the past 120 Myr does not significantly impact the Li-isotopic fractionation factor between bulk altered off-axis, upper oceanic crust and seawater. Hence, this observed variation in alteration temperature of the off-axis upper oceanic crust appears unlikely to explain the suggested ~9 ‰ increase in δ^7Li of seawater over the past 120 Myr. However, scarcity of information and large uncertainty of the δ^7Li of Cretaceous seawater is a source of uncertainty for the estimated Li-isotopic fractionation factors from studied areas older than 65 Myr. This uncertainty, in combination with uncertainties that come from small number of samples analysed from some of the studied areas, have potential to change the interpretation of the role of changes in alteration temperature of off-axis, upper oceanic crust on δ^7Li of seawater over the past 120 Myr.

6. Conclusions

6.1. Summary and significance of findings

The research goals addressed in this thesis were to: (i) evaluate and minimize the sources of uncertainty during Li isotopic measurement using an ICP-MS, (ii) identify effects of solution chemistry on elemental and isotopic fractionation of lithium during precipitation of inorganic calcite, (iii) characterize the controls on the lithium concentration and isotopic composition of the lava section of the oceanic crust which is altered at low-temperatures in the off-axis, and (iv) investigate the role of low-temperature hydrothermal alteration of the upper oceanic crust in controlling the lithium concentration and isotopic composition of seawater.

6.1.1. Sources of uncertainty during measurement of Li-isotopes using ICP-MS

Lithium isotopes are subjected to fractionation in any mass-dependent process from sample preparation to the isotopic measurements using an ICP-MS. It was demonstrated that a mismatch between the concentration of the acid which is used to dilute a sample and standard solutions has a significant effect on the accuracy of the measurements (Chapter 2). The operating conditions of the ICP-MS and its tuning parameters were investigated with the aim of improving the precision of Li-isotopic measurements. Tuning the axial position of the torch box was found to be an important parameter which needs optimization to reduce isotope discrimination before running any isotope ratio measurements. A previously proposed method using a “NaCl wash” by Lin et al. (2016) was tested to investigate its effect on the precision of Li-isotope measurements. This method has potential to decrease the Li background, and result in a stable $^{7}Li/^{6}Li$ ratio of standard solution, but it was found that this method causes significant drift and increases the sensitivity to Na based matrix effects.

6.1.2. The effect of solution chemistry on Li partitioning and isotopic fractionation between inorganic calcite and aqueous solution

Carbonate rocks provide a potential record of paleo-seawater Li-chemistry if we understand the elemental and isotopic fractionation associated with calcite growth, and especially diagenesis, under varying conditions. Experiments were performed under varying solution chemistry, using mixed $CaCl_2$-$NaHCO_3$ solutions spanning a range of pH (and H^+/Ca^{2+}) from ~6 to ~9.5. Experimental results (Chapter 3) show that the Li partition coefficient, and Li-isotope fractionation factor, increase from ~0.2 to ~3 and -6 ‰ to +2 ‰ respectively, with increasing pH (increasing H^+/Ca^{2+}). The change in the kd_{Li} between calcite and solution ($(Li/Ca)_{calcite}/(Li/Ca)_{solution}$) is consistent with Li incorporation into calcite as $LiHCO_3$ and hence a dependence on solution H^+/Ca^{2+}. If this interpretation is correct, then the Li content of inorganic calcite precipitated from seawater at a fixed calcite saturation state, and fixed Ca and Li concentrations, will increase with decreasing pH.

To better understand the role of diffusive Li-isotope fractionation during growth of calcite from an aqueous solution, a series of experiments were performed to determine the relative diffusivity of ^{6}Li and ^{7}Li in aqueous solutions with different pH. The results suggest little or no difference in the relative diffusivity of the two isotopes ($D^{6}Li \sim 0.998\ D^{7}Li$) across the range of solution chemistry considered (pH 4 to ~7.5). This implies that diffusive fractionation is not likely to be the main source of the observed variation in Li-isotopic fractionation between inorganic calcite and solution with changing solution pH. In general, aqueous diffusion will lead to only small isotopic fractionations in nature.

6.1.3. Lithium concentration and isotopic composition of the upper lava section of the oceanic crust

Detailed study of lava samples from the upper 600 m of DSDP Holes 417A, 417D and 418A from 119 Myr oceanic crust in the Western Atlantic shows that the Li concentration and isotopic composition of lava samples change with depth. Results show that the Li concentration decreases, and $\delta^{7}Li$ increases continuously through the upper ~30 m below sediments and remain nearly constant in deeper sections (Chapter 4). In contrast to most previous studies, this research shows that low-temperature hydrothermal alteration of the upper oceanic crust does not always lead to an increase in the Li-isotopic composition of the lavas and the uppermost lavas can be significantly isotopically lighter than fresh MORBs (down to -2 ‰). There is no evidence that variation in the secondary mineral assemblage is the primary control on the Li concentration and $\delta^{7}Li$ of the lavas in these cores. Modification of the Li content of the hydrothermal fluid due to mixing with sediment pore-fluid also does not appear to be able to explain the observed variation in Li content and isotopic composition in these cores. Fluid-rock reaction during fluid flow, with Li-exchange modelled using linear kinetics (Bickle, 1992), also cannot explain both the variation in the Li concentration and isotopic composition of lava samples with depth. Instead, a conceptual model of free-circulation of seawater through the upper few meters of the oceanic crust and leakage of water with a slightly modified composition to deeper sections best matches the observed Li concentrations and $\delta^{7}Li$ of these crustal sections.

6.1.4. The effect of low-temperature off-axis hydrothermal alteration within the oceanic crust in controlling the Li concentration and isotopic composition of seawater

Study of altered lava samples from DSDP/ODP drill cores with a range of crustal age shows that the bulk $\delta^{7}Li$, and the average uptake of Li from seawater, vary (Chapter 5). Lithium uptake during low-temperature hydrothermal alteration of the upper oceanic crust appears to be higher during the Cretaceous compared with the late Cenozoic. This could be due to a higher Li concentration of seawater during the Cretaceous era. Higher alteration temperatures during this period could also play a role in the higher Li uptake into the crust by increasing fluid-rock reaction rates. Similar to crustal age, the average amount of Li added to the crust also correlates with the sedimentation rate. This correlation could be due to the strong correlation that exists between crustal age and sedimentation rate (i.e., an artifact of technology), or it could also control averages of added Li to the crust by impacting the amount of seawater that ingresses into the crust.

The δ^7Li of bulk altered oceanic crust also appears to be higher during the Cretaceous compared with the Cenozoic, consistent with an increase in the Li-isotopic composition of seawater during this time scale. The Li-isotopic fractionation factor between altered oceanic crust and seawater appears to have stayed nearly constant during this period of time. Estimated Li-isotopic fractionation factors, determined using two different models (binary mixing and linear kinetic models), are associated with large uncertainties. However, they do not indicate any systematic variation in fractionation factor with either the crustal age or alteration temperature, suggesting that there is not a strong control from alteration of off-axis oceanic crust on the Li-isotopic composition of seawater over the past 120 Myrs.

6.2. Future work

6.2.1. Decoupling the effect of Ca^{2+} concentration and pH of solution on Li partitioning between inorganic calcite and solution

The experiments I conducted to investigate the effect of solution chemistry on Li partitioning and Li-isotopic fractionation between solution and inorganic calcite, involved simultaneously changing the pH and Ca^{2+} concentrations of the solution. If Li is incorporated into the calcite structure in the form of $LiHCO_3$, then a change in the Ca^{2+} concentration of solution while Li^+ concentration, pH and saturation state with respect to calcite are held constant, would lead to a change in the Li concentration of precipitated calcite such that the D(Li/Ca) remains constant. In order to change the Ca^{2+} concentration of a solution without changing its pH and saturation state with respect to calcite, the concentration of dissolved inorganic carbon (DIC) must change. For example, to keep two solutions equally saturated with respect to calcite, but adding less Ca^{2+} to one of them, would require a higher CO_3^{2-} concentration. To avoid increasing of the pH as a result of increasing CO_3^{2-} concentrations, the concentration of DIC would need to increase. Basically, the effect of Ca^{2+} concentration of solution can be decoupled from the pH of solution by supplying adequate amount DIC. Dietzel et al. (2004; 2009) developed a technique for co-precipitation of trace elements during formation of single-phase carbonates at constant pH, while supplying the required amount of DIC by diffusion of CO_2 through a polyethylene membranes from a container with higher dissolved CO_2 (i.e., saturating a solution with CO_2 gas) to another one with lower fugacity of CO_2. To adjust the amount of DIC, membranes with different thicknesses could be used. Following this method could be a starting point to decouple the effect of pH and Ca concentration during precipitation of inorganic calcite, however, its capability in keeping the pH of growing solution constant and precipitation of pure calcite needs further exploration.

6.2.2. Effect of temperature on Li partitioning and isotopic fractionation between inorganic calcite and solution

Marriott et al. (2004a; 2004b) tested the effect of temperature on Li partitioning and the Li isotope fractionation between inorganic calcite and solutions and proposed that the Li/Ca partition coefficient negatively correlates with temperature, while Li-isotopic

fractionation does not show significant correlation with temperature. The experimental setup used by Marriott et al. (2004a; 2004b) for Li incorporation during calcite formation was adopted from Tesoriero and Pankow (1996). I made several attempts to produce pure calcite following the experimental design of Marriott et al. (2004a; 2004b), but was not successful, vaterite impurities were often found in the precipitated carbonates. However, both Tesoriero and Pankow (1996) and Marriott et al. (2004a; 2004b) claim that their XRD results for the precipitated material confirm pure calcite, but they do not provide evidence for it (e.g., did not publish XRD patterns). Even if small amounts of vaterite co-precipitate with calcite, it may significantly influence the Li partitioning and isotopic fractionation between precipitated carbonate and solution. Structural Ca in calcite has a coordination number of 6, while in vaterite it bonds with 8 oxygens. The Li isotopic fractionation between fluid and solid becomes larger when the coordination number of incorporated Li in solid phase increases. The Li-isotopic composition of inorganic calcite which was precipitated at a range of temperature between 5°C to 30°C and at constant pH ~7 is between -8 ‰ and -9 ‰ (Marriott et al., 2004a). This latter range of Li-isotopic composition is lower than I measured at pH ~7 at ~21°C (between -6 ‰ and -4 ‰; Chapter 3, Fig. 3.3). This difference could be due to mixture of small amounts of vaterite with calcite in the Marriott et al. (2004a) experiments. Bottom seawater temperature is a potential parameter in controlling the fluid-rock reactions and eventually influencing the seawater chemistry and it changed during the period of time when the Li-isotopic composition of seawater is reported to be variable (Cretaceous to the modern era). Hence, I think it is worth testing the effect of temperature on Li partitioning and isotopic composition of inorganic calcites while ensuring that pure calcite precipitates from the experiments. I propose that a study with the same experimental setup as described in Chapter 3, while the only variable is the experimental temperature could be used to test the effect of temperature during incorporation of Li during pure calcite precipitation.

6.2.3. Mechanism of Li-isotope fractionation between inorganic calcite and solution

The mechanism by which the observed Li-isotopic fractionation between inorganic calcite and solution occurs with changing solution chemistry is not understood. I have suggested that a kinetically controlled process involving surface attachment of Li ions to calcite crystals may have resulted in the observed Li-isotopic fractionation. However, an equilibrium isotopic fractionation due to the existence of different Li-complexes in the aqueous solution could also be responsible for the observed Li-isotopic fractionation. To investigate whether the dominant mechanism of Li-isotopic fractionation is a kinetically controlled process, or if it is due to an equilibrium fractionation, I propose the following test.

Calcium carbonate has three polymorphs of calcite, aragonite and vaterite. Calcium in the calcite has a coordination number of 6, while in aragonite Ca has a coordination number of 9. Hence, if the equilibrium fractionation is the dominant Li-isotopic fractionation process, a considerable difference is expected between the Li-isotopic composition of calcite and aragonite precipitated from a similar solution chemistry. Based on previous studies, during precipitation of inorganic aragonite from solution, Li

isotopes are fractionated more than during calcite precipitation (i.e., $\Delta_{solution\text{-}aragonite}$=7 to 12 ‰ and $\Delta_{solution\text{-}calcite}$=2 to 5 ‰; Marriott et al., 2004a, 2004b; Gabitov et al., 2011). Alternatively, if kinetic processes are the main control of the Li-isotopic fractionation, in a condition where every aspect of the solution chemistry (i.e., temperature, pH and salinity) is the same, then the Li-isotopic composition of calcite and aragonite is expected to be the same. Hence, I suggest setting up two experiments following the same method as described in the Chapter 3 but setting up one of the experiments to precipitate aragonite instead of calcite. Two experiments can be set up at pH ~8 and room temperature. To inhibit precipitation of calcite in one of the experiments, I suggest adding Li-free $MgSO_4$ to the solution of the aragonite growth experiment. The Mg^{2+} and SO_4^{2-} concentrations can be the same as modern seawater, and to keep salinity of both experiments the same, NaCl can be added to the calcite growth experiments.

6.2.4. Identifying the main controls on changes in Li uptake into the upper lava section of the oceanic crust

I observed that the average amount of Li added to the upper 100 m of the lava section in the oceanic crust correlates with crustal age, sedimentation rate and less strongly with alteration temperature. The effect of each of these three parameters was interpreted independently (Chapter 5). (i) If the Li concentration of seawater was higher during the Cretaceous era than during the late Cenozoic, it could explain the higher added Li to the oceanic crust during the Cretaceous. Higher Li contents could also be due to: (ii) higher alteration temperatures during the Cretaceous, leading to faster fluid-rock reactions, and (iii) slower sedimentation rates, leading to higher amounts of fluid entering the crust. The three parameters of crustal age, sedimentation rate and alteration temperature are also interconnected with one another, hence it is difficult to identify which is the dominant control. I propose that multivariate modelling could be useful to identify which of these three parameters provides the strongest control on the variation of the amount of added Li to the oceanic crust.

Bibliography

Agatemor, C. and Beauchemin, D., 2011. Matrix effects in inductively coupled plasma mass spectrometry: a review. Analytica Chimica Acta, 706(1), pp.66-83.

Alt, J.C. and Honnorez, J., 1984. Alteration of the upper oceanic crust, DSDP site 417: mineralogy and chemistry. Contributions to Mineralogy and Petrology, 87(2), pp.149-169.

Alt, J.C., 1995. Subseafloor Processes in Mid-Ocean Ridge Hydrothermal Systems (American Geophysical Union (AGU), Washington, 2013), pp.85-114.

Alt, J.C., 1995. Sulfur isotopic profile through the oceanic crust: Sulfur mobility and seawater-crustal sulfur exchange during hydrothermal alteration. Geology, 23(7), pp.585-588.

Alt, J.C., Honnorez, J., Laverne, C. and Emmermann, R., 1986. Hydrothermal alteration of a 1 km section through the upper oceanic crust, Deep Sea Drilling Project Hole 504B: Mineralogy, chemistry and evolution of seawater-basalt interactions. Journal of Geophysical Research: Solid Earth, 91(B10), pp.10309-10335.

Alt, J.C., Kinoshita, H., Stokking, L.B. and Leg, O.D.P., 148 Shipboard Scientific Party (1993), Site 896. In Proc ODP, Init. Rep Vol. 148, pp.123-192.

Alt, J.C., Laverne, C., Coggon, R.M., Teagle, D.A., Banerjee, N.R., Morgan, S., Smith-Duque, C.E., Harris, M. and Galli, L., 2010. Subsurface structure of a submarine hydrothermal system in ocean crust formed at the East Pacific Rise, ODP/IODP Site 1256. Geochemistry, Geophysics, Geosystems, 11(10), pp.28.

Anderson, B.W., Coogan, L.A. and Gillis, K.M., 2012. The role of outcrop-to-outcrop fluid flow in off-axis oceanic hydrothermal systems under abyssal sedimentation conditions. Journal of Geophysical Research: Solid Earth, 117(B5).

Anderson, B.W., Gillis, K.M. and Coogan, L.A., 2013. A hydrologic model for the uppermost oceanic crust constrained by temperature estimates from carbonate minerals. Journal of Geophysical Research: Solid Earth, 118(8), pp.3917-3930.

Andrén, H., Rodushkin, I., Stenberg, A., Malinovsky, D. and Baxter, D.C., 2004. Sources of mass bias and isotope ratio variation in multi-collector ICP-MS: optimization of instrumental parameters based on experimental observations. Journal of Analytical Atomic Spectrometry, 19(9), pp.1217-1224.

Baker, P.A., Stout, P.M., Kastner, M. and Elderfield, H., 1991. Large-scale lateral advection of seawater through oceanic crust in the central equatorial Pacific. Earth and Planetary Science Letters, 105(4), pp.522-533.

Bear, J., 1992. Modeling flow and contaminant transport in fractured rocks. In: Bear, J., Tsang, C.-F., de Marsily, G. (Eds.), Flow and Contaminant Transport in Fractured Rock. Academic Press, pp.1-37.

Bear, L.M., 1960. The geology and mineral resources of the Akaki-Lythrodondha area (No. 3). Geological Survey Department, Cyprus.

Becker, J.S., 2007. Inorganic mass spectrometry: principles and applications. Chichester, UK: John Wiley & Sons, p.496.

Bednarz, U. and Schmincke, H.U., 1989. Mass transfer during sub-seafloor alteration of the upper Troodos crust (Cyprus). Contributions to Mineralogy and Petrology, 102(1), pp.93-101.

Berger, G., Schott, J. and Guy, C., 1988. Behavior of Li, Rb and Cs during basalt glass and olivine dissolution and chlorite, smectite and zeolite precipitation from seawater: experimental investigations and modelization between 50 and 300 C. Chemical Geology, 71(4), pp.297-312.

Berner, R. A.,1994. GEOCARB II: A revised model of atmospheric CO2 over Phanerozoic time, American Journal of Science, 294(1), pp.56–91.

Berner, R.A. and Caldeira, K., 1997. The need for mass balance and feedback in the geochemical carbon cycle. Geology, 25(10), pp.955-956.

Berner, R.A., Lasaga, A.C. and Garrels, R.M., 1983. The carbonate-silicate geochemical cycle and its effect on atmospheric carbon dioxide levels for the last 100 million years.American Journal of Science , 289, pp.333-361.

Bickle, M.J., 1992. Transport mechanisms by fluid-flow in metamorphic rocks; oxygen and strontium decoupling in the Trois Seigneurs Massif; a consequence of kinetic dispersion?. American Journal of Science, 292(5), pp.289-316.

Biju-Duval, B., and Moore, JC, et al., Init. Repts. DSDP A, 78, pp.227-298.

Bird, P., 2003. An updated digital model of plate boundaries. Geochemistry, Geophysics, Geosystems, 4(3).

Bogatko, S., Claeys, P., De Proft, F. and Geerlings, P., 2013. Li^+ speciation and the use of $^7Li/^6Li$ isotope ratios for ancient climate monitoring. Chemical Geology, 357, pp.1-7.

Böhlke, J.K., Honnorez, J. and Honnorez-Guerstein, B.M., 1980. Alteration of basalts from site 396 B, DSDP: Petrographic and mineralogic studies. Contributions to Mineralogy and Petrology, 73(4), pp.341-364.

Boucher, D.F. and Alves, G.E., 1959. Dimensionless analysis. Chemical Engineering Progress, 59(9), pp.55-64.

Bouman, C., Elliott, T. and Vroon, P.Z., 2004. Lithium inputs to subduction zones. Chemical Geology, 212(1), pp.59-79.

Bourg, I.C., Richter, F.M., Christensen, J.N. and Sposito, G., 2010. Isotopic mass dependence of metal cation diffusion coefficients in liquid water. Geochimica et Cosmochimica Acta, 74(8), pp.2249-2256.

Bradley, D.C., 2011. Secular trends in the geologic record and the supercontinent cycle. Earth-Science Reviews, 108(1-2), pp.16-33.

Brady, P.V. and Gíslason, S.R., 1997. Seafloor weathering controls on atmospheric CO2 and global climate. Geochimica et Cosmochimica Acta, 61(5), pp.965-973.

Brandl, P.A., Regelous, M., Beier, C., O'Neill, H.S.C., Nebel, O. and Haase, K.M., 2016. The timescales of magma evolution at mid-ocean ridges. Lithos, 240, pp.49-68.

Brant, C., Coogan, L.A., Gillis, K.M., Seyfried, W.E., Pester, N.J. and Spence, J., 2012. Lithium and Li-isotopes in young altered upper oceanic crust from the East Pacific Rise. Geochimica et Cosmochimica Acta, 96, pp.272-293.

Brennan, S.T., Lowenstein, T.K. and Cendón, D.I., 2013. The major-ion composition of Cenozoic seawater: The past 36 million years from fluid inclusions in marine halite. American Journal of Science, 313(8), pp.713-775.

Bryant, C.J., McCulloch, M.T. and Bennett, V.C., 2003. Impact of matrix effects on the accurate measurement of Li isotope ratios by inductively coupled plasma mass spectrometry (MC-ICP-MS) under “cold” plasma conditions. Journal of Analytical Atomic Spectrometry, 18(7), pp.734-737.

Burgoyne, T.W., Hieftje, G.M. and Hites, R.A., 1997. Space charge evaluation in a plasma-source mass spectrograph. Analytical Chemistry, 69(3), pp.485-489.

Busch, K., 2004. Space charge in mass spectrometry. Spectroscopy, 19(6), pp.35-38.

Butterfield, D.A., Nelson, B.K., Wheat, C.G., Mottl, M.J. and Roe, K.K., 2001. Evidence for basaltic Sr in midocean ridge-flank hydrothermal systems and implications for the global oceanic Sr isotope balance. Geochimica et Cosmochimica Acta, 65(22), pp.4141-4153.

Cann, J.R., Langseth, M.G., Honnorez, J., Von Herzen, R.P. and White, S.M., 1983. Initial Repts. Deep Sea Drill. Proj, p.69.

Chan, L.H. and Kastner, M., 2000. Lithium isotopic compositions of pore fluids and sediments in the Costa Rica subduction zone: implications for fluid processes and sediment contribution to the arc volcanoes. Earth and Planetary Science Letters, 183(1-2), pp.275-290.

Chan, L.H., Alt, J.C. and Teagle, D.A., 2002. Lithium and lithium isotope profiles through the upper oceanic crust: a study of seawater-basalt exchange at ODP Sites 504B and 896A. Earth and Planetary Science Letters, 201(1), pp.187-201.

Chan, L.H., Edmond, J.M., Thompson, G. and Gillis, K., 1992. Lithium isotopic composition of submarine basalts: implications for the lithium cycle in the oceans. Earth and Planetary Science Letters, 108(1-3), pp.151-160.

Chan, L.H., Gieskes, J.M., Chen-Feng, Y. and Edmond, J.M., 1994. Lithium isotope geochemistry of sediments and hydrothermal fluids of the Guaymas Basin, Gulf of California. Geochimica et Cosmochimica Acta, 58(20), pp.4443-4454.

Chan, L.H., Leeman, W.P. and Plank, T., 2006. Lithium isotopic composition of marine sediments. Geochemistry, Geophysics, Geosystems, 7(6).

Chen, X., Zhang, L., Wei, G. and Ma, J., 2016. Matrix effects and mass bias caused by inorganic acids on boron isotope determination by multi-collector ICP-MS. Journal of Analytical Atomic Spectrometry, 31(12), pp.2410-2417.

Coggon, R.M., Teagle, D.A., Cooper, M.J., Hayes, T.E. and Green, D.R., 2006. Data report: compositions of calcium carbonate veins from superfast spreading rate crust, ODP Leg 206. In Proc ODP Sci Results (Vol. 206, pp. 1-6).

Coggon, R.M., Teagle, D.A., Smith-Duque, C.E., Alt, J.C. and Cooper, M.J., 2010. Reconstructing past seawater Mg/Ca and Sr/Ca from mid-ocean ridge flank calcium carbonate veins. Science, 327(5969), pp.1114-1117.

Coogan, L.A. and Dosso, S., 2012. An internally consistent, probabilistic, determination of ridge-axis hydrothermal fluxes from basalt-hosted systems. Earth and Planetary Science Letters, 323, pp.92-101.

Coogan, L.A. and Gillis, K.M., 2018. Low-temperature alteration of the seafloor: Impacts on ocean chemistry. Annual Review of Earth and Planetary Sciences, 46, pp.21-45.

Coogan, L.A., Gillis, K.M., Pope, M. and Spence, J., 2017. The role of low-temperature (off-axis) alteration of the oceanic crust in the global Li-cycle: insights from the Troodos ophiolite. Geochimica et Cosmochimica Acta, 203, pp.201-215.

Coogan, L.A., Parrish, R.R. and Roberts, N.M., 2016. Early hydrothermal carbon uptake by the upper oceanic crust: Insight from in situ U-Pb dating. Geology, 44(2), pp.147-150.

Cramer, B.S., Miller, K.G., Barrett, P.J. and Wright, J.D., 2011. Late Cretaceous–Neogene trends in deep ocean temperature and continental ice volume: Reconciling records of benthic foraminiferal geochemistry (δ18O and Mg/Ca) with sea level history. Journal of Geophysical Research: Oceans, 116(C12).

Davies, J.H. and Davies, D.R., 2010. Earth's surface heat flux. Solid Earth, 1(1), pp.5-24.

Davis, A.C., Bickle, M.J. and Teagle, D.A., 2003. Imbalance in the oceanic strontium budget. Earth and Planetary Science Letters, 211(1-2), pp.173-187.

Delaney, M.L. and Boyle, E.A., 1986. Lithium in foraminiferal shells: implications for high-temperature hydrothermal circulation fluxes and oceanic crustal generation rates. Earth and Planetary Science Letters, 80(1-2), pp.91-105.

Delaney, M.L., Bé, A.W. and Boyle, E.A., 1985. Li, Sr, Mg, and Na in foraminiferal calcite shells from laboratory culture, sediment traps, and sediment cores. Geochimica et Cosmochimica Acta, 49(6), pp.1327-1341.

Delaney, M.L., Popp, B.N., Lepzelter, C.G. and Anderson, T.F., 1989. Lithium-to-calcium ratios in Modern, Cenozoic, and Paleozoic articulate brachiopod shells. Paleoceanography, 4(6), pp.681-691.

Dellinger, M., Gaillardet, J., Bouchez, J., Calmels, D., Louvat, P., Gorge, C. and Maurice, L., 2013. Lithium isotopic composition of the dissolved load in the Amazon River Basin. Mineral. Mag., 77(5), p.967.

Dellinger, M., West, A.J., Paris, G., Adkins, J.F., von Strandmann, P.A.P., Ullmann, C.V., Eagle, R.A., Freitas, P., Bagard, M.L., Ries, J.B. and Corsetti, F.A., 2018. The Li isotope composition of marine biogenic carbonates: Patterns and Mechanisms. Geochimica et Cosmochimica Acta, 236, pp.315-335.

Demicco, R.V., Lowenstein, T.K., Hardie, L.A. and Spencer, R.J., 2005. Model of seawater composition for the Phanerozoic. Geology, 33(11), pp.877-880.

DePaolo, D.J., 2006. Isotopic effects in fracture-dominated reactive fluid–rock systems. Geochimica et Cosmochimica Acta, 70(5), pp.1077-1096.

DePaolo, D.J., 2011. Surface kinetic model for isotopic and trace element fractionation during precipitation of calcite from aqueous solutions. Geochimica et Cosmochimica Acta, 75(4), pp.1039-1056.

Dickson, A.G., 1981. An exact definition of total alkalinity and a procedure for the estimation of alkalinity and total inorganic carbon from titration data. Deep Sea Research Part A. Oceanographic Research Papers, 28(6), pp.609-623.

Dmitriev L, Hertzler JR, et al., 1978. Initial Reports of the Deep-Sea Drilling Project, Vol. 46. Washington, pp.15-49.

Donnelly, T. W., G. Thompson, and M. H. Salisbury (1979b), The chemistry of altered basalts at site 417, Deep Sea Drilling Project Leg 51, in Initial Reports of the Deep Sea Drilling Project, U.S. Government Printing Office, Washington, D.C., vol. 51/52/53, pp. 1319–1330.

Donnelly, T. W., J. Francheteau, W. Bryan, P. Robinson, M. Flower, and M. Salisbury (1979a), Initial Reports of the Deep Sea Drilling Project, vol. LI, LII, LIII, Part 2, edited by T. W. US Government Printing Office, Washington, DC.

Du Vivier, A.D., Jacobson, A.D., Lehn, G.O., Selby, D., Hurtgen, M.T. and Sageman, B.B., 2015. Ca isotope stratigraphy across the Cenomanian–Turonian OAE 2: links between volcanism, seawater geochemistry, and the carbonate fractionation factor. Earth and Planetary Science Letters, 416, pp.121-131.

Dullien, F.A.L., 1979. Porous media-fluid transport and pore structure. Academic press. New York, 98.

Edmond, J.M., Measures, C., McDuff, R.E., Chan, L.H., Collier, R., Grant, B., Gordon, L.I. and Corliss, J.B., 1979. Ridge crest hydrothermal activity and the balances of the major and minor elements in the ocean: The Galapagos data. Earth and Planetary Science Letters, 46(1), pp.1-18.

Eggins, S.M., Woodhead, J.D., Kinsley, L.P.J., Mortimer, G.E., Sylvester, P., McCulloch, M.T., Hergt, J.M. and Handler, M.R., 1997. A simple method for the precise determination of≥ 40 trace elements in geological samples by ICPMS using enriched isotope internal standardisation. Chemical Geology, 134(4), pp.311-326.

Elderfield, H. and Schultz, A., 1996. Mid-ocean ridge hydrothermal fluxes and the chemical composition of the ocean. Annual Review of Earth and Planetary Sciences, 24(1), pp.191-224.

Elderfield, H., Wheat, C.G., Mottl, M.J., Monnin, C. and Spiro, B., 1999. Fluid and geochemical transport through oceanic crust: a transect across the eastern flank of the Juan de Fuca Ridge. Earth and Planetary Science Letters, 172(1-2), pp.151-165.

Fantle, M.S., 2010. Evaluating the Ca isotope proxy. American Journal of Science, 310(3), pp.194-230.

Faure, G. and Mensing, T.M., 2005. Isotopes: principles and applications.

Fernández-Díaz, L., Astilleros, J.M. and Pina, C.M., 2006. The morphology of calcite crystals grown in a porous medium doped with divalent cations. Chemical Geology, 225(3-4), pp.314-321.

Fisher, A.T. and Becker, K., 2000. Channelized fluid flow in oceanic crust reconciles heat-flow and permeability data. Nature, 403(6765), pp.71-74.

Fisher, A.T., Davis, E.E., Hutnak, M., Spiess, V., Zühlsdorff, L., Cherkaoui, A., Christiansen, L., Edwards, K., Macdonald, R., Villinger, H. and Mottl, M.J., 2003. Hydrothermal recharge and discharge across 50 km guided by seamounts on a young ridge flank. Nature, 421(6923), pp.618-621.

France-Lanord, C., Derry, L.A., 1997. Organic carbon burial forcing of the carbon cycle from Himalayan erosion. Nature 390 (6655), pp.65-67.

Fritz, S.J., 1992. Measuring the ratio of aqueous diffusion coefficients between 6Li+ Cl− and 7Li+ Cr− by osmometry. Geochimica et Cosmochimica Acta, 56(10), pp.3781-3789.

Fritz, S.J., 1992. Measuring the ratio of aqueous diffusion coefficients between $^{6}Li^{+}$ Cl^{-} and $^{7}Li^{+}$ Cl^{-} by osmometry. Geochimica et Cosmochimica Acta, 56(10), pp.3781-3789.

Füger, A., Konrad, F., Leis, A., Dietzel, M., Mavromatis, V., 2019. Effect of growth rate and pH on lithium incorporation in calcite. Geochimica et Cosmochimica Acta 248, pp.14-24.

Furnes, H. and Staudigel, H., 1999. Biological mediation in ocean crust alteration: how deep is the deep biosphere?. Earth and Planetary Science Letters, 166(3-4), pp.97-103.

Gabitov, R.I., Schmitt, A.K., Rosner, M., McKeegan, K.D., Gaetani, G.A., Cohen, A.L., Watson, E.B. and Harrison, T.M., 2011. In situ δ7Li, Li/Ca, and Mg/Ca analyses of synthetic aragonites. Geochemistry, Geophysics, Geosystems, 12(3).

Gaillardet, J., Dupré, B., Louvat, P. and Allegre, C.J., 1999. Global silicate weathering and CO2 consumption rates deduced from the chemistry of large rivers. Chemical Geology, 159(1-4), pp.3-30.

Gaina, C. and Mueller, R.D., 2004, November. Global oceanic crust production since mid-Cretaceous based on paleo-seafloor age grids. In Geological Society of America Abstracts with Programs (Vol. 36).

Gale, A., Dalton, C.A., Langmuir, C.H., Su, Y. and Schilling, J.G., 2013. The mean composition of ocean ridge basalts. Geochemistry, Geophysics, Geosystems, 14(3), pp.489-518.

Gao, Y., Vils, F., Cooper, K.M., Banerjee, N., Harris, M., Hoefs, J., Teagle, D.A.H., Casey, J.F., Elliott, T., Laverne, C. and Alt, J.C., 2012. Downhole variation of lithium and oxygen isotopic compositions of oceanic crust at East Pacific Rise, ODP Site 1256. Geochemistry, Geophysics, Geosystems, 13(10), p.24.

Gillis, K.M. and Coogan, L.A., 2011. Secular variation in carbon uptake into the ocean crust. Earth and Planetary Science Letters, 302(3-4), pp.385-392.

Gillis, K.M. and Robinson, P.T., 1990. Patterns and processes of alteration in the lavas and dykes of the Troodos ophiolite, Cyprus. Journal of Geophysical Research: Solid Earth, 95(B13), pp.21523-21548.

Gillis, K.M., Coogan, L.A. and Brant, C., 2015. The role of sedimentation history and lithology on fluid flow and reactions in off-axis hydrothermal systems: A perspective from the Troodos ophiolite. Chemical Geology, 414, pp.84-94.

Goddéris, Y. and François, L.M., 1995. The Cenozoic evolution of the strontium and carbon cycles: relative importance of continental erosion and mantle exchanges. Chemical Geology, 126(2), pp.169-190.

Haq, B.U., Hardenbol, J.A.N. and Vail, P.R., 1987. Chronology of fluctuating sea levels since the Triassic. Science, 235(4793), pp.1156-1167.

Hardie, L.A., 1996. Secular variation in seawater chemistry: An explanation for the coupled secular variation in the mineralogies of marine limestones and potash evaporites over the past 600 Myr. Geology, 24(3), pp.279-283.

Hart, S.R. and Staudigel, H., 1979. Ocean crust-sea water interaction: Sites 417 and 418. In: T. Donnelly et al. (Editors), Init. Rept. DSDP. U.S. Govt. Printing Office, Washington, DC, pp.1169-1176.

Hasterok, D., 2013. A heat flow based cooling model for tectonic plates. Earth and Planetary Science Letters, 361, pp.34-43.

Hathorne, E.C. and James, R.H., 2006. Temporal record of lithium in seawater: A tracer for silicate weathering? Earth and Planetary Science Letters, 246(3-4), pp.393-406.

Higgins, J.A. and Schrag, D.P., 2015. The Mg isotopic composition of Cenozoic seawater-evidence for a link between Mg-clays, seawater Mg/Ca, and climate. Earth and Planetary Science Letters, 416, pp.73-81.

Hindshaw, R.S., Tosca, R., Goût, T.L., Farnan, I., Tosca, N.J. and Tipper, E.T., 2019. Experimental constraints on Li isotope fractionation during clay formation. Geochimica et Cosmochimica Acta, 250, pp.219-237.

Hobbs, M.Y. and Reardon, E.J., 1999. Effect of pH on boron coprecipitation by calcite: further evidence for nonequilibrium partitioning of trace elements. Geochimica et Cosmochimica Acta, 63(7-8), pp.1013-1021.

Hoefs, J., 2015. Theoretical and experimental principles. In stable isotope geochemistry (pp.1-46). Springer, Cham.

Hofmann, A.E., Bourg, I.C. and DePaolo, D.J., 2012. Ion desolvation as a mechanism for kinetic isotope fractionation in aqueous systems. Proceedings of the National Academy of Sciences, 109(46), pp.18689-18694.

Holland, H.D. and Zimmermann, H., 2000. The dolomite problem Revisited1. International Geology Review, 42(6), pp.481-490.

Holland, H.D., 2005. Sea level, sediments and the composition of seawater. American Journal of Science, 305(3), pp.220-239.

Horita, J., Zimmermann, H. and Holland, H.D., 2002. Chemical evolution of seawater during the Phanerozoic: Implications from the record of marine evaporites. Geochimica et Cosmochimica Acta, 66(21), pp.3733-3756.

Huh, Y., Chan, L.H., Zhang, L. and Edmond, J.M., 1998. Lithium and its isotopes in major world rivers: implications for weathering and the oceanic budget. Geochimica et Cosmochimica Acta, 62(12), pp.2039-2051.

Humphris, S.E. and Thompson, R.N., 1980. 47. The mineralogy and geochemistry of basalt weathering, holes 417A and 418A. Initial Reports of the Deep Sea Drilling Project: A Project Planned by and Carried Out with the Advice of the Joint Oceanographic Institutions for Deep Earth Sampling, 51, p.1201.

Hutnak, M., Fisher, A.T., Harris, R., Stein, C., Wang, K., Spinelli, G., Schindler, M., Villinger, H. and Silver, E., 2008. Large heat and fluid fluxes driven through mid-plate outcrops on ocean crust. Nature Geoscience, 1(9), pp.611-614.

Ishikawa, M. and Ichikuni, M., 1984. Uptake of sodium and potassium by calcite. Chemical Geology, 42(1-4), pp.137-146.

Ivany, L.C., Peters, S.C., Wilkinson, B.H., Lohmann, K.C. and Reimer, B.A., 2004. Composition of the early Oligocene ocean from coral stable isotope and elemental chemistry. Geobiology, 2(2), pp.97-106.

Javoy, M. and Fouillac, A.M., 1979. Stable isotope ratios in Deep Sea Drilling Project Leg 51 basalts. In: T. Donnelly et al. (Editors), Proc. ODP, Sci. Results. U.S. Govt. Printing Office, Washington, DC, pp.1153-1157.

Jeffcoate, A.B., Elliott, T., Thomas, A. and Bouman, C., 2004. Precise/small sample size determinations of lithium isotopic compositions of geological reference materials and

modern seawater by MC-ICP-MS. Geostandards and Geoanalytical Research, 28(1), pp.161-172.

Johnson, H.P. and Semyan, S.W., 1994. Age variation in the physical properties of oceanic basalts: Implications for crustal formation and evolution. Journal of Geophysical Research: Solid Earth, 99(B2), pp.3123-3134.

Jordan, T., Menard, H., Natland, J. and Orcutt, J., 1987. Objectives and results of deep-sea drilling project leg-91 and the NGENDEI seismic experiment, and explanatory notes for volume-91-introduction.

Kawada, Y., Seama, N. and Urabe, T., 2011. The role of seamounts in the transport of heat and fluids: Relations among seamount size, circulation patterns, and crustal heat flow. Earth and Planetary Science Letters, 306(1-2), pp.55-65.

Kim, S.T. and O'Neil, J.R., 1997. Equilibrium and nonequilibrium oxygen isotope effects in synthetic carbonates. Geochimica et Cosmochimica Acta, 61(16), pp.3461-3475.

Kralj, D., Brečević, L. and Nielsen, A.E., 1990. Vaterite growth and dissolution in aqueous solution I. Kinetics of crystal growth. Journal of Crystal Growth, 104(4), pp.793-800.

Langer, G., Sadekov, A., Thoms, S., Mewes, A., Nehrke, G., Greaves, M., Misra, S., Bijma, J. and Elderfield, H., 2015. Li partitioning in the benthic foraminifera Amphistegina lessonii. Geochemistry, Geophysics, Geosystems, 16(12), pp.4275 4279.

Langseth, M.G. and Herman, B.M., 1981. Heat transfer in the oceanic crust of the Brazil Basin. Journal of Geophysical Research: Solid Earth, 86(B11), pp.10805-10819.

Langseth, M.G., Becker, K., Von Herzen, R.P. and Schultheiss, P., 1992. Heat and fluid flux through sediment on the western flank of the Mid-Atlantic Ridge: A hydrogeological study of North Pond. Geophysical Research Letters, 19(5), pp.517-520.

Langseth, M.G., Hyndman, R.D., Becker, K., Hickman, S.H. and Salisbury, M.H., 1984. The hydrogeological regime of isolated sediment ponds in mid-oceanic ridges. In Initial reports DSDP, Leg 78B, San Juan to Las Palmas (pp.825-837). US Govt. Printing Office; UK distributors, IPOD Committee, NERC, Swindon.

Lassey, K.R. and Blattner, P., 1988. Kinetically controlled oxygen isotope exchange between fluid and rock in one-dimensional advective flow. Geochimica et Cosmochimica Acta, 52(8), pp.2169-2175.

Lauer, R.M., Fisher, A.T. and Winslow, D.M., 2018. Three-dimensional models of hydrothermal circulation through a seamount network on fast-spreading crust. Earth and Planetary Science Letters, 501, pp.138-151.

Lawrence, J.R., 1979. Temperatures of formation of calcite veins in the basalts from Deep Sea Drilling Project Holes 417A and 417D. In: T. Donnelly et al. (Editors), Init. Rept. DSDP. US Gov. Printing Office, Washington, DC, pp.1183-1184.

Lear, C.H., Elderfield, H. and Wilson, P.A., 2000. Cenozoic deep-sea temperatures and global ice volumes from Mg/Ca in benthic foraminiferal calcite. Science, 287(5451), pp.269-272.

Lechler, M., von Strandmann, P.A.P., Jenkyns, H.C., Prosser, G. and Parente, M., 2015. Lithium-isotope evidence for enhanced silicate weathering during OAE 1a (Early Aptian Selli event). Earth and Planetary Science Letters, 432, pp.210-222.

Leinen, M., Rea, D.K. and Becker, K., 1986. Deep-sea drilling project leg-92, southeast pacific-ocean-introduction, cruise narrative, principal results, and explanatory notes. Initial reports of the Deep Sea Drilling Project, 92, pp.5-24.

Li, G. and West, A.J., 2014. Evolution of Cenozoic seawater lithium isotopes: Coupling of global denudation regime and shifting seawater sinks. Earth and Planetary Science Letters, 401, pp.284-293.

Light, T.S., 1984. Temperature dependence and measurement of resistivity of pure water. Analytical Chemistry, 56(7), pp.1138-1142.

Ligi, M., Bonatti, E., Cuffaro, M. and Brunelli, D., 2013. Post-Mesozoic rapid increase of seawater Mg/Ca due to enhanced mantle-seawater interaction. Scientific reports, 3, p.2752.

Lin, J., Liu, Y., Hu, Z., Yang, L., Chen, K., Chen, H., Zong, K. and Gao, S., 2016. Accurate determination of lithium isotope ratios by MC-ICP-MS without strict matrix-matching by using a novel washing method. Journal of Analytical Atomic Spectrometry, 31(2), pp.390-397.

Lithgow-Bertelloni, C., Richards, M.A., Ricard, Y., O'Connell, R.J. and Engebretson, D.C., 1993. Toroidal-poloidal partitioning of plate motions since 120 Ma. Geophysical Research Letters, 20(5), pp.375-378.

Livingstone, D.A., 1963. The sodium cycle and the age of the ocean. Geochimica et Cosmochimica Acta, 27(10), pp.1055-1069.

Lowenstein, T.K., Hardie, L.A., Timofeeff, M.N. and Demicco, R.V., 2003. Secular variation in seawater chemistry and the origin of calcium chloride basinal brines. Geology, 31(10), pp.857-860.

Lowenstein, T.K., Kendall, B., Anbar, A.D., 2014. The geologic history of seawater. In Treatise on Geochemistry, ed. KD Turekian, HD Holland, pp.569-621.

Lowenstein, T.K., Timofeeff, M.N., Brennan, S.T., Hardie, L.A. and Demicco, R.V., 2001. Oscillations in Phanerozoic seawater chemistry: Evidence from fluid inclusions. Science, 294(5544), pp.1086-1088.

Lyman, J. and Fleming, R.H., 1940. Composition of sea water. J Mar Res, 3(2), pp.134-146.

Mackenzie, F.T. and Garrels, R.M., 1966. Chemical mass balance between rivers and oceans. American Journal of Science, 264(7), pp.507-525.

Mähler, J. and Persson, I., 2011. A study of the hydration of the alkali metal ions in aqueous solution. Inorganic Chemistry, 51(1), pp.425-438.

Marichy, M., Mermet, M. and Mermet, J.M., 1990. Some effects of low acid concentrations in inductively coupled plasma atomic emission spectrometry. Spectrochimica Acta Part B: Atomic Spectroscopy, 45(11), pp.1195-1201.

Marriott, C.S., Henderson, G.M., Belshaw, N.S. and Tudhope, A.W., 2004a. Temperature dependence of δ7Li, δ44Ca and Li/Ca during growth of calcium carbonate. Earth and Planetary Science Letters, 222(2), pp.615-624.

Marriott, C.S., Henderson, G.M., Crompton, R., Staubwasser, M. and Shaw, S., 2004b. Effect of mineralogy, salinity, and temperature on Li/Ca and Li isotope composition of calcium carbonate. Chemical Geology, 212(1-2), pp.5-15.

McDuff, R.E. and Edmond, J.M., 1982. On the fate of sulfate during hydrothermal circulation at mid-ocean ridges. Earth and Planetary Science Letters, 57(1), pp.117-132.

Millot, R., Guerrot, C. and Vigier, N., 2004. Accurate and high-precision measurement of lithium isotopes in two reference materials by MC-ICP-MS. Geostandards and Geoanalytical Research, 28(1), pp.153-159.

Misra, S. and Froelich, P.N., 2009. Measurement of lithium isotope ratios by quadrupole-ICP-MS: application to seawater and natural carbonates. Journal of Analytical Atomic Spectrometry, 24(11), pp.1524-1533.

Misra, S. and Froelich, P.N., 2012. Lithium isotope history of Cenozoic seawater: changes in silicate weathering and reverse weathering. Science, 335(6070), pp.818-823.

Møller, K.B., Rey, R., Masia, M. and Hynes, J.T., 2005. On the coupling between molecular diffusion and solvation shell exchange. The Journal of Chemical Physics, 122, p.114508.

Morin, R.H., Anderson, R.N. and Barton, C.A., 1989. Analysis and interpretation of the borehole televiewer log: information on the state of stress and the lithostratigraphy at Hole 504B. In Becker, K., Sakai, H., et al., Proc. ODP, Sci. Results (Vol. 111, pp.109-118).

Moskovits, M. and Michaelian, K.H., 1980. Alkali hydroxide ion pairs. A Raman study. Journal of the American Chemical Society, 102(7), pp.2209-2215.

Muehlenbachs, K., 1979. The alteration and aging of the basaltic layer of the sea floor: Oxygen isotope evidence from DSDP/IPOD Legs 51. 52 and 53. In: T. Donnelly et al. (Editors), Proc. ODP, Sci. Results. U.S. Govt. Printing Office, Washington, DC, pp.1159-1166.

Mukasa, S.B. and Ludden, J.N., 1987. Uranium-lead isotopic ages of plagiogranites from the Troodos ophiolite, Cyprus, and their tectonic significance. Geology, 15(9), pp.825-828.

Müller, R.D., Sdrolias, M., Gaina, C. and Roest, W.R., 2008. Age, spreading rates, and spreading asymmetry of the world's ocean crust. Geochemistry, Geophysics, Geosystems, 9(4).

Murphy, J.G., Higgins, J.A. and Swart, P.K., 2018, December. Assessing the Effects of Early Marine Diagenesis on the Lithium Isotopic Composition of Shallow Marine Carbonates. In AGU Fall Meeting Abstracts.

Murphy, M.J., Porcelli, D., von Strandmann, P.A.P., Hirst, C.A., Kutscher, L., Katchinoff, J.A., Mörth, C.M., Maximov, T. and Andersson, P.S., 2019. Tracing silicate weathering processes in the permafrost-dominated Lena River watershed using lithium isotopes. Geochimica et Cosmochimica Acta, 245, pp.154-171.

Nelms, S.M., Quétel, C.R., Prohaska, T., Vogl, J. and Taylor, P.D., 2001. Evaluation of detector dead time calculation models for ICP-MS. Journal of Analytical Atomic Spectrometry, 16(4), pp.333-338.

Newman, J.A., Schmitt, P.D., Toth, S.J., Deng, F., Zhang, S. and Simpson, G.J., 2015. Parts per million powder X-ray diffraction. Analytical chemistry, 87(21), pp.10950-10955.

Newmark, R.L., Anderson, R.N., Moos, D. and Zoback, M.D., 1985. Structure, porosity and stress regime of the upper oceanic crust: Sonic and ultrasonic logging of DSDP hole 504B. Tectonophysics, 118(1-2), pp.1-42.

Newsome, J.R., Neilson, G.W. and Enderby, J.E., 1980. Lithium ions in aqueous solution. Journal of Physics C: Solid State Physics, 13(32), L923.

O'Neil, J.R., 1986. Theoretical and experimental aspects of isotopic fractionation. Reviews in Mineralogy, 16, pp.1-40.

Okumura, M. and Kitano, Y., 1986. Coprecipitation of alkali metal ions with calcium carbonate. Geochimica et Cosmochimica Acta, 50, pp.49-58.

Olesik, J.W., 2000. Inductively coupled plasma mass spectrometry. Practical Spectroscopy Series, 23, pp.67-158.

Palmer, M.R. and Edmond, J.M., 1989. The strontium isotope budget of the modern ocean. Earth and Planetary Science Letters, 92(1), pp.11-26.

Parkhurst D. L. and Appelo C. A. J. (2013) Description of input and examples for PHREEQC version 3—A computer program for speciation, batch-reaction, one-dimensional transport, and inverse geochemical calculations. U.S. Geological Survey Techniques and Methods, book 6, chap. A43, 497 p., available only at: <https://pubs.usgs.gov/tm/06/a43/>.

Pilson, M.E.Q., 1998. An Introduction to the Chemistry of the Sea Prentice-Hall. Upper Saddle River, New Jersey, 431.

Rajam, S. and Mann, S., 1990. Selective stabilization of the (001) face of calcite in the presence of lithium. Journal of the Chemical Society, Chemical Communications, (24), pp.1789-1791.

Raymo, M.E. and Ruddiman, W.F., 1992. Tectonic forcing of late Cenozoic climate. Nature, 359 (6391), pp.117-122.

Raymo, M.E., Ruddiman, W.F. and Froelich, P.N., 1988. Influence of late Cenozoic mountain building on ocean geochemical cycles. Geology, 16(7), pp.649-653.

Rehkämper, M., Schönbächler, M. and Stirling, C.H., 2001. Multiple collector ICP-MS: Introduction to instrumentation, measurement techniques and analytical capabilities. Geostandards Newsletter, 25(1), pp.23-40.

Reiman, W. and Walton, H., 1970. Ion-exchange in Analytical Chemistry, International Services of Mongraphs in Analytical Chemistry. Pergamon Press, Oxford, 295.

Rennie, V.C., Paris, G., Sessions, A.L., Abramovich, S., Turchyn, A.V. and Adkins, J.F., 2018. Cenozoic record of δ 34 S in foraminiferal calcite implies an early Eocene shift to deep-ocean sulfide burial. Nature Geoscience, 11(10), pp.761-765.

Richardson, S.H., Hart, S.R. and Staudigel, H., 1980. Vein mineral ages of old oceanic crust.Journal of Geophysical Research, 85, pp.7195-7200.

Richter, F.M., Davis, A.M., DePaolo, D.J. and Watson, E.B., 2003. Isotope fractionation by chemical diffusion between molten basalt and rhyolite. Geochimica et Cosmochimica Acta, 67(20), pp.3905-3923.

Richter, F.M., Mendybaev, R.A., Christensen, J.N., Hutcheon, I.D., Williams, R.W., Sturchio, N.C. and Beloso Jr, A.D., 2006. Kinetic isotopic fractionation during diffusion of ionic species in water. Geochimica et Cosmochimica Acta, 70(2), pp.277-289.

Ridgwell, A. and Zeebe, R.E., 2005. The role of the global carbonate cycle in the regulation and evolution of the Earth system. Earth and Planetary Science Letters, 234(3-4), pp.299-315.

Riebe, C.S., Kirchner, J.W. and Finkel, R.C., 2004. Erosional and climatic effects on long-term chemical weathering rates in granitic landscapes spanning diverse climate regimes. Earth and Planetary Science Letters, 224(3-4), pp.547-562.

Rieman, W. and Walton, H.F., 1970. Ion Exchange in analytical chemistry Pergamon Press. Oxford, New York, p.296.

Roberts, J., Kaczmarek, K., Langer, G., Skinner, L.C., Bijma, J., Bradbury, H., Turchyn, A.V., Lamy, F. and Misra, S., 2018. Lithium isotopic composition of benthic foraminifera: A new proxy for paleo-pH reconstruction. Geochimica et Cosmochimica Acta, 236, pp.336-350.

Rosner, M., Ball, L., Peucker-Ehrenbrink, B., Blusztajn, J., Bach, W. and Erzinger, J., 2007. A simplified, accurate and fast method for lithium isotope analysis of rocks and

fluids, and δ7Li values of seawater and rock reference materials. Geostandards and Geoanalytical Research, 31(2), pp.77-88.

Rowley, D.B., 2002. Rate of plate creation and destruction: 180 Ma to present. Geological Society of America Bulletin, 114(8), pp.927-933.

Rudolph, W., Brooker, M.H. and Pye, C.C., 1995. Hydration of lithium ion in aqueous solutions. The Journal of Physical Chemistry, 99(11), pp.3793-3797.

Scarfe, 1979. Secondary minerals in some basaltic rocks from Deep Sea Drilling Project Legs 52 and 53, Hole 418A. In: T. Donnelly et al. (Editors), Init. Rept. DSDP. U.S. Govt. Printing Office, Washington, DC, pp.1243-1246.

Schauble, E.A., 2004. Applying stable isotope fractionation theory to new systems. Reviews in Mineralogy and Geochemistry, 55(1), pp.65-111.

Scholz, F., Hensen, C., De Lange, G.J., Haeckel, M., Liebetrau, V., Meixner, A., Reitz, A. and Romer, R.L., 2010. Lithium isotope geochemistry of marine pore waters–insights from cold seep fluids. Geochimica et Cosmochimica Acta, 74(12), pp.3459-3475.

Schramm, B., Devey, C.W., Gillis, K.M. and Lackschewitz, K., 2005. Quantitative assessment of chemical and mineralogical changes due to progressive low-temperature alteration of East Pacific Rise basalts from 0 to 9 Ma. Chemical Geology, 218(3-4), pp.281-313.

Sclater, J., Jaupart, C. and Galson, D., 1980. The heat flow through oceanic and continental crust and the heat loss of the Earth. Reviews of Geophysics, 18(1), pp.269-311.

Seton, M., Gaina, C., Müller, R.D. and Heine, C., 2009. Mid-Cretaceous seafloor spreading pulse: Fact or fiction?. Geology, 37(8), pp.687-690.

Seyfried Jr, W.E., Janecky, D.R. and Mottl, M.J., 1984. Alteration of the oceanic crust: implications for geochemical cycles of lithium and boron. Geochimica et Cosmochimica Acta, 48(3), pp.557-569.

Shannon, R.D., 1976. Revised effective ionic radii and systematic studies of interatomic distances in halides and chalcogenides. Acta Crystallographica Section A: Crystal Physics, Diffraction, Theoretical and General Crystallography, 32(5), pp.751-767.

Spencer, R.J. and Hardie, L.A., 1990. Control of seawater composition by mixing of river waters and mid-ocean ridge hydrothermal brines. Fluid-mineral interactions: A tribute to HP Eugster: Geochemical Society Special Publication, 19, pp.409-419.

Staudigel, H., 2014. Chemical fluxes from hydrothermal alteration of the oceanic crust. In Treatise on Geochemistry, Vol. 4: The Crust, ed. HD Holland, KKB Turekian, pp.583-606.

Staudigel, H., Gillis, K. and Duncan, R., 1986. K/Ar and Rb/Sr ages of celadonites from the Troodos ophiolite, Cyprus. Geology, 14(1), pp.72-75.

Staudigel, H., Hart, S.R. and Richardson, S.H., 1981. Alteration of the oceanic crust: processes and timing. Reports of the Deep Sea Drilling Project, 9, pp.10-12.

Staudigel, H., Plank, T., White, B. and Schmincke, H.U., 1996. Geochemical fluxes during seafloor alteration of the basaltic upper oceanic crust: DSDP Sites 417 and 418. Subduction: top to bottom, 96, pp.19-38.

Stein, C.A. and Stein, S., 1994. Constraints on hydrothermal heat flux through the oceanic lithosphere from global heat flow. Journal of Geophysical Research: Solid Earth, 99(B2), pp.3081-3095.

Stephen, R.A., Kasahara, J. and Acton, G.D., 2003. Explanatory notes. In Proc. ODP, Init. Reps., 200 (pp. 1-60). Ocean Drilling Program Colledge Station, TX.

Stewart, I.I. and Olesik, J.W., 1998. The effect of nitric acid concentration and nebulizer gas flow rates on aerosol properties and transport rates in inductively coupled plasma sample introduction. Journal of Analytical Atomic Spectrometry, 13(11), pp.1249-1256.

Stoffyn-Egli, P. and Mackenzie, F.T., 1984. Mass balance of dissolved lithium in the oceans. Geochimica et Cosmochimica Acta, 48(4), pp.859-872.

Sun, X., Higgins, J. and Turchyn, A.V., 2016. Diffusive cation fluxes in deep-sea sediments and insight into the global geochemical cycles of calcium, magnesium, sodium and potassium. Marine Geology, 373, pp.64-77.

Tan, S.H. and Horlick, G., 1987. Matrix-effect observations in inductively coupled plasma mass spectrometry. Journal of Analytical Atomic Spectrometry, 2(8), pp.745-763.

Tanner, S.D., 1992. Space charge in ICP-MS: Calculation and implications. Spectrochimica Acta Part B: Atomic Spectroscopy, 47(6), pp.809-823.

Tanner, S.D., 1995. Characterization of ionization and matrix suppression in inductively coupled ‘cold’plasma mass spectrometry. Journal of Analytical Atomic Spectrometry, 10(11), pp.905-921.

Teng, F.Z., McDonough, W.F., Rudnick, R.L., Dalpé, C., Tomascak, P.B., Chappell, B.W. and Gao, S., 2004. Lithium isotopic composition and concentration of the upper continental crust. Geochimica et Cosmochimica Acta, 68(20), pp.4167-4178.

Timofeeff, M.N., Lowenstein, T.K. and Blackburn, W.H., 2000. ESEM-EDS: An improved technique for major element chemical analysis of fluid inclusions. Chemical Geology, 164(3-4), pp.171-181.

Tomascak, P.B., Carlson, R.W., Shirey, S.B., 1999. Accurate and precise determination of Li isotopic compositions by multi- collector sector ICP-MS. Chemical Geology, 158(1), pp.145-154.

Tomascak, P.B., Langmuir, C.H., le Roux, P.J. and Shirey, S.B., 2008. Lithium isotopes in global mid-ocean ridge basalts. Geochimica et Cosmochimica Acta, 72(6), pp.1626-1637.

Torres, M.A., West, A.J. and Li, G., 2014. Sulphide oxidation and carbonate dissolution as a source of CO2 over geological timescales. Nature, 507(7492), pp.346-349.

Toyofuku, T., Matsuo, M.Y., De Nooijer, L.J., Nagai, Y., Kawada, S., Fujita, K., Reichart, G.J., Nomaki, H., Tsuchiya, M., Sakaguchi, H. and Kitazato, H., 2017. Proton pumping accompanies calcification in foraminifera. Nature Communications, 8(1), pp.1-6.

Turchyn, A.V. and DePaolo, D.J., 2019. Seawater Chemistry Through Phanerozoic Time. Annual Review of Earth and Planetary Sciences, 47, pp.197-224.

Turchyn, A.V. and Schrag, D.P., 2004. Oxygen isotope constraints on the sulfur cycle over the past 10 million years. Science, 303(5666).

Turchyn, A.V. and Schrag, D.P., 2006. Cenozoic evolution of the sulfur cycle: insight from oxygen isotopes in marine sulfate. Earth and Planetary Science Letters, 241(3-4), pp.763-779.

Vail, P.R., Mitchum Jr, R.M. and Thompson III, S., 1977. Seismic stratigraphy and global changes of sea level: Part 4. Global cycles of relative changes of sea level.American Association of Petroleum Geologists. 26, pp.82-97.

Veizer, J., Ala, D., Azmy, K., Bruckschen, P., Buhl, D., Bruhn, F., Carden, G.A., Diener, A., Ebneth, S., Godderis, Y. and Jasper, T., 1999. 87Sr/86Sr, δ13C and δ18O evolution of Phanerozoic seawater. Chemical Geology, 161(1-3), pp.59-88.

Verney-Carron, A., Vigier, N. and Millot, R., 2011. Experimental determination of the role of diffusion on Li isotope fractionation during basaltic glass weathering. Geochimica et Cosmochimica Acta, 75(12), pp.3452-3468.

Vigier, N. and Godderis, Y., 2014. A new approach for modeling Cenozoic oceanic lithium isotope paleo-variations: the key role of climate. Climate of the Past Discussions, 11(4), pp.635-645.

Vigier, N., Decarreau, A., Millot, R., Carignan, J., Petit, S. and France-Lanord, C., 2008. Quantifying Li isotope fractionation during smectite formation and implications for the Li cycle. Geochimica et Cosmochimica Acta, 72(3), pp.780-792.

Vigier, N., Rollion-Bard, C., Levenson, Y., Erez, J., 2015. Lithium isotopes in foraminifera shells as a novel proxy for the ocean dissolved inorganic carbon (DIC). Comptes Rendus Geosci. 347, pp.43-51.

Von Strandmann, P.A.P., Jenkyns, H.C. and Woodfine, R.G., 2013. Lithium isotope evidence for enhanced weathering during Oceanic Anoxic Event 2. Nature Geoscience, 6(8), p.668.

Watson, E.B., 2004. A conceptual model for near-surface kinetic controls on the trace-element and stable isotope composition of abiogenic calcite crystals1. Geochimica et Cosmochimica Acta, 68(7), pp.1473-1488.

Wenger, M. and Armbruster, T., 1991. Crystal chemistry of lithium: oxygen coordination and bonding. European Journal of Mineralogy, pp.387-400.

West, A.J., Galy, A. and Bickle, M., 2005. Tectonic and climatic controls on silicate weathering. Earth and Planetary Science Letters, 235(1-2), pp.211-228.

Wheat, C.G., Elderfield, H., Mottl, M.J. and Monnin, C., 2000. Chemical composition of basement fluids within an oceanic ridge flank: Implications for along-strike and across-strike hydrothermal circulation. Journal of Geophysical Research: Solid Earth, 105(B6), pp.13437-13447.

Wheat, C.G., McManus, J., Mottl, M.J. and Giambalvo, E., 2003. Oceanic phosphorus imbalance: Magnitude of the mid-ocean ridge flank hydrothermal sink. Geophysical Research Letters, 30(17), pp.1895-1899.

White, A.F., 1977. Sodium and potassium coprecipitation in aragonite. Geochimica et Cosmochimica Acta, 41(5), pp.613-625.

Wilschefski, S.C. and Baxter, M.R., 2019. Inductively Coupled Plasma Mass Spectrometry: Introduction to analytical aspects. The Clinical Biochemist Reviews, 40(3), p.115.

Wilson, D.S., Teagle, D.A.H., Acton, G.D. and 16 others, 2003. Proceedings of the Ocean Drilling Program, Vol. 206. Initial Reports. An in situ section of upper oceanic crust formed by superfast seafloor spreading. Ocean Drilling Program.

Yamaji, K., Makita, Y., Watanabe, H., Sonoda, A., Kanoh, H., Hirotsu, T. and Ooi, K., 2001. Theoretical estimation of lithium isotopic reduced partition function ratio for lithium ions in aqueous solution. The Journal of Physical Chemistry A, 105(3), pp.602-613.

Yoshimura, T., Tamenori, Y., Suzuki, A., Kawahata, H., Iwasaki, N., Hasegawa, H., Nguyen, L.T., Kuroyanagi, A., Yamazaki, T., Kuroda, J. and Ohkouchi, N., 2017. Altervalent substitution of sodium for calcium in biogenic calcite and aragonite. Geochimica et Cosmochimica Acta, 202, pp.21-38.

Yuan-Hui, L. and Gregory, S., 1974. Diffusion of ions in sea water and in deep-sea sediments. Geochimica et Cosmochimica Acta, 38(5), pp.703-714.

Zeebe, R.E., 2012. History of seawater carbonate chemistry, atmospheric CO2, and ocean acidification. Annual Review of Earth and Planetary Sciences, 40, pp.141-165.

Zhang, L., Chan, L.H. and Gieskes, J.M., 1998. Lithium isotope geochemistry of pore waters from Ocean Drilling Program Sites 918 and 919, Irminger Basin. Geochimica et Cosmochimica Acta, 62(14), pp.2437-2450.

Appendix A: Additional analytical details for Chapter 3

A.1. Sample preparation for chemical analysis

50 mg of calcite from the calcite growth experiments, was dissolved in 3 ml of 1 N HCl and then divided into a ~0.6 ml (equivalent to 10 mg powder) split for elemental analysis and a ~2 ml (equivalent to 32 mg powder) split for isotopic analysis. The splits of the initial and final solutions from the calcite growth experiments were diluted in 2% HNO_3; with a dilution factor of 2000, for elemental analysis and the source and sink solutions for the diffusion experiments were diluted 800 and 100 fold respectively and analysed directly. A split of 0.1 ml of the final solution from the calcite growth experiments was diluted in 3 ml 2% HNO_3 and 2 ml of it was separated for the isotopic analysis.

To prepare the calcite, and the solutions from the calcite growth experiments, for Li-isotopes analysis splits of these were dried and diluted into 0.2 ml, 0.5 N HCl for column chemistry that generally followed the method of Misra and Froelich (2009). The solutions were loaded into pre-calibrated, 15 ml micro-columns which were filled with 1.5 g (dry weight) of BIORAD AG 50W-x8 (200-400 mesh) resin. Lithium was eluted using 15 ml of 0.5 N HCl. The first 3.5 ml of solution was collected as pre-aliquot, the following 5 ml as the peak of Li, then the next 3.5 ml as the post-aliquot. The pre- and the post-aliquots were dried and diluted in 2% HNO_3 and analyzed to test the Li recovery and separation of other ions. The peaks were dried and diluted (to 1.4 ppb Li for calcite and 10 ppb for solution) in 2% HNO_3 for Li isotopic analysis.

A.2. ICP-MS elemental analysis

Elemental analysis for the solutions from both the calcite growth experiments and the diffusion experiments were performed using an Agilent 8800 triple quadrupole ICP-MS at the University of Victoria. The sodium content of calcite samples was measured using a regular calibration method modified from Eggins et al. (1997). The Na calibration solutions were prepared by mixing of standard single element solutions from NIST to match the matrix of calcite solutions and cover the range of Na of the calcite samples. To measure the Li content of calcite samples, a Li standard addition method was used. Two splits of calcite solutions (1.5 ml each), which were prepared for the concentration analysis (with dilution factor of 1000), were separated into two centrifuge tubes. One of the splits was spiked with 7.5 ppb Li. Both splits were spiked with internal standard solutions and both were diluted into 2% HNO_3 with the same dilution factor of 2. To measure the Ca and Na concentrations of the initial and final solutions from the calcite growth experiments and the Li content of solutions from both calcite and diffusion experiments, the usual calibration method was used. The calibration solutions were prepared to cover the expected range of Li, Na and Ca in the solutions.

The precision of the concentration analyses for the solutions from calcite growth experiments was estimated using the relative standard deviation of stock solutions containing 100 ppb Li, and 5 to 50 ppm Na and Ca giving 9 %, 5 % and 2 %,

respectively. The precision for Li and Na of calcite samples are 8 % and 9 % (2SD), respectively, which were obtained by multiple analysis of calcite samples with a wide range of Na (400 ppb to 5 wt%) and Li (50 ppb to 1000 ppb) concentrations. We aimed to determine precision of the Li in calcite data for a $CaCO_3$ matrix using a 99.999% pure $CaCO_3$ powder that was homogenized by grinding in an agate mortar. However, analysis of ten ~5 mg splits of this sample (MS-STD-2018-14-1 to 23-1; Supplementary Table D.1.3) show that Li in this material is not homogenously distributed. The total procedural blanks which were loaded into the columns and analysed along with samples contained 14 to 140 pg Li, 10 to 200 ng Na and 200 to 800 ng Ca (Supplementary Table D.1.1).

A.3. Li-isotope analysis using ICP-MS

Li-isotope analyses were performed using the same instrument as the elemental analyses. The instrumental conditions for isotope analysis are presented in Table A.1. Each analytical session started (and ended) with a block of 10 analyses of IRMM-016 and then samples and standards were alternately run. The data always showed smooth drift (the precision of the $^7Li/^6Li$ ratio of the standard IRMM-016 was always better than ±1 ‰) and so a polynomial curve, not higher than 3rd order, was fit through the IRMM-016 $^7Li/^6Li$ ratios and the value given by this curve at the time of each sample was used in calculating the δ^7Li of that sample:

$$\delta^7 Li = \left[\frac{\left(\frac{^7Li}{^6Li}\right)_{sample}}{\left(\frac{^7Li}{^6Li}\right)_{IRMM\text{-}016}} - 1 \right] \times 1000 \qquad \text{Eq. A.1}$$

Each sample was analyzed three to five times during an analytical session and the average of these is used, with the standard error of these taken as an estimate of the uncertainty (Supplementary Tables D.1.1, D.1.2 and D.1.3).

Table A.1. Instrumental conditions for Li-isotope analyses.

Instrument	Agilent 8800 Triple Quadrupole
Forward power	1350 W
Sample depth	8 mm
Carrier gas flow rate	0.74 L/min
Makeup gas flow rate	0.6 L/min
Dwell time mass 6	250 ms
Dwell time mass 7	50 ms
Sweeps per run	30
Runs per analysis	45
Typical sensitivity mass 6	11000 cps / ppb
Typical sensitivity mass 7	170000 cps / ppb

A.4. Total alkalinity measurements using an automated titrator

The total alkalinity of solutions that were prepared to start calcite growth experiments and the solutions extracted at the end of experiments were measured using an automated mini titrator (HI84531-Hanna Instruments). Alkalinity is an expression of solution's acid-neutralizing capacity and it determines by titration with standard acidic solution. The automated mini titrator instrument determines the alkalinity of solution by titration of the samples with strong acid solution to reach a fixed pH end point of 4.5 or 8.3. The end point is determined by the potentiometric input. Based on the Na concentration of the solutions, a range of alkalinity between 10 to 100 meq/l was expected. The instrument is designed to cover low range alkalinity between 0.6 to 8 meq/l, and it needs 50 ml solution for total alkalinity measurements. To provide 50 ml solution, a split of ~2 ml solution was diluted by a factor of 25. The exact weight of splits and diluted solutions were recorded, and precise dilution factors were calculated to obtain the actual alkalinity of solutions. Only the alkalinity of solutions with pH > 8.5 were within the detection limit of instrument. The accuracy and precision of the instrument was tested using multiple measurements of solutions prepared by mixing known amounts of $NaHCO_3$ and $CaCl_2$; therefore, the only source of alkalinity was HCO_3^-. The expected alkalinities were in good agreement with the measured values (Figure A.1). Maximum and average of the absolute difference between the measured and known alkalinity values were 14.0 % and 4.7 % respectively.

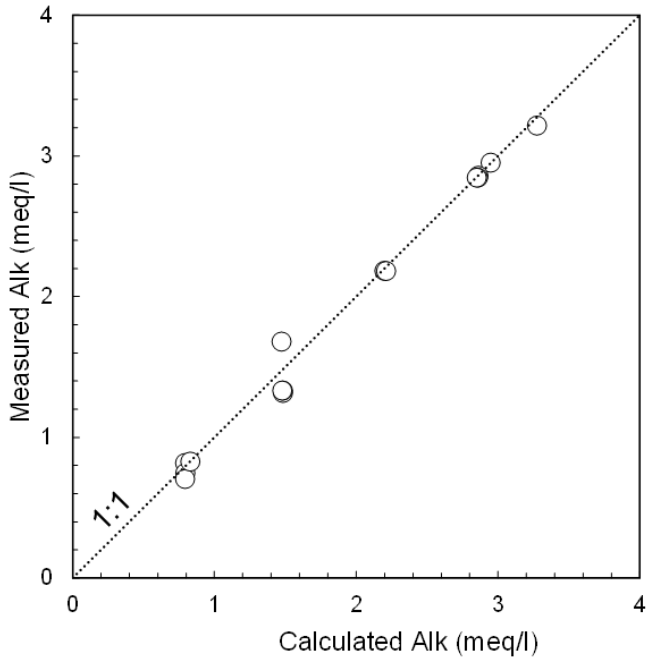

Figure A.1. The measured alkalinity plotted against the calculated alkalinity of solutions which were simple mixtures of $NaHCO_3$ and $CaCl_2$. The measurements were made immediately after making the solutions. The dashed line shows 1:1 line and it demonstrates good agreement between measured and expected values. The maximum difference between the measured and calculated alkalinity is 14.0 % and the average is 4.7 %.

A.5. SEM images

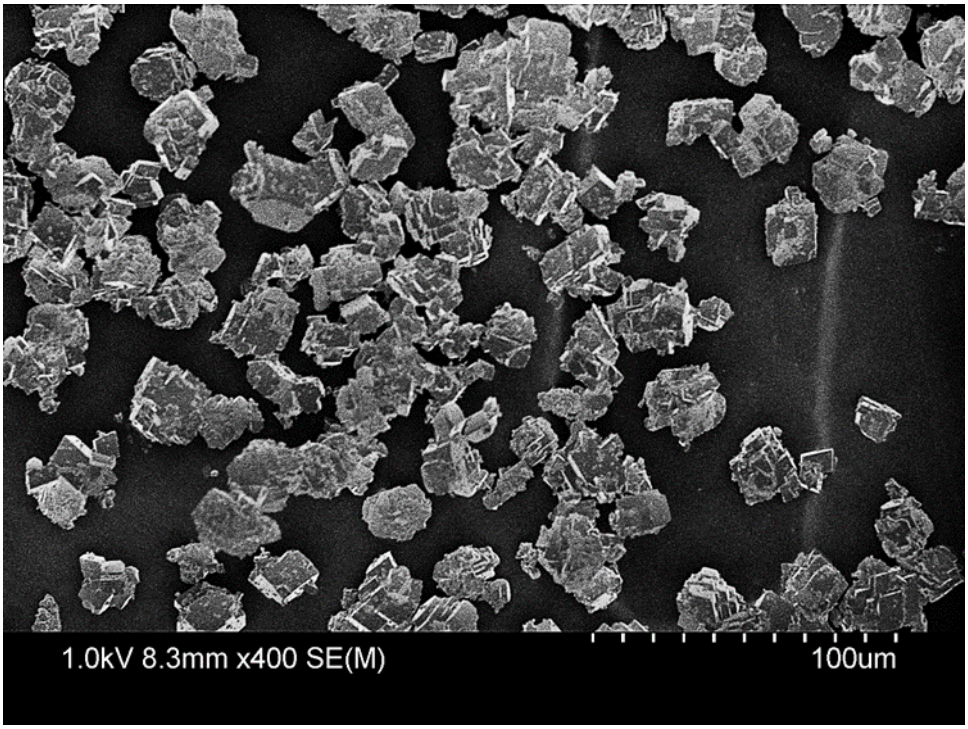

Sample ID. MS-VC2#A-4-2 (duration: 5 days, pH: 9.4, phase: vaterite-calcite mix)

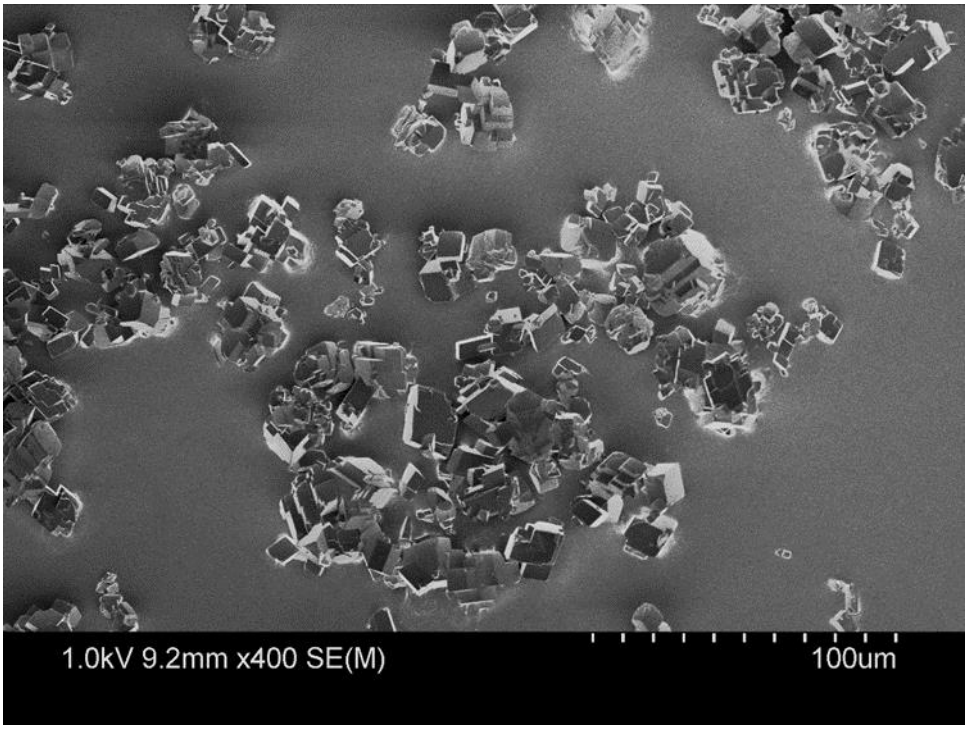

Sample ID. MS-VC2#A-5 (duration: 14 days, pH: 9.4, phase: pure calcite)

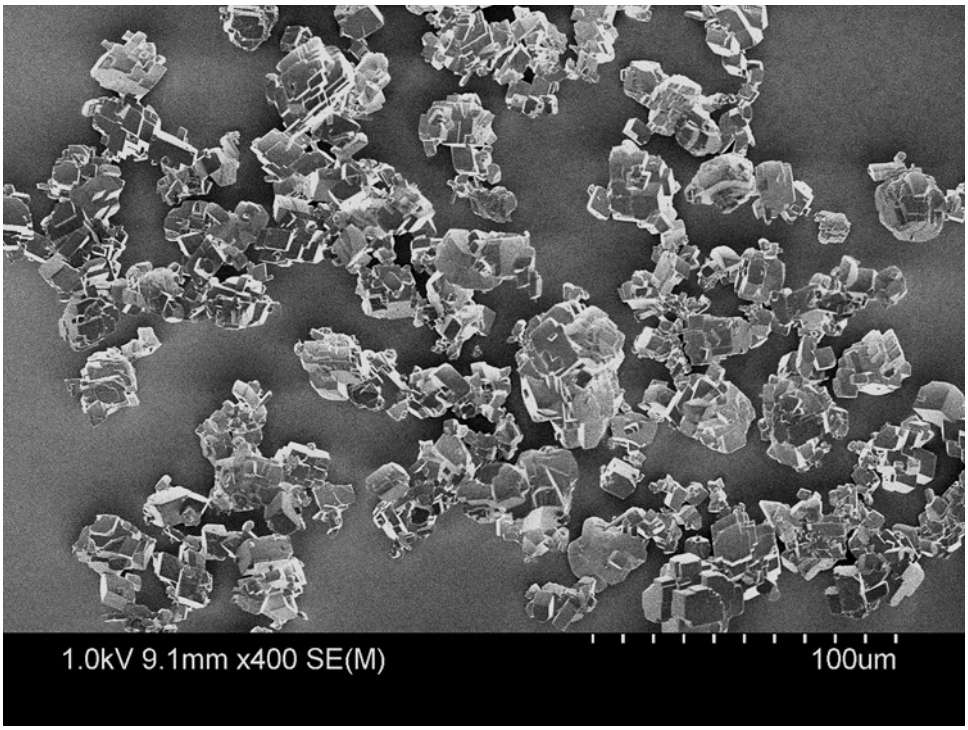

Sample ID. MS-VC2#A-6 (duration: 30 days, pH: 9.4, phase: pure calcite)

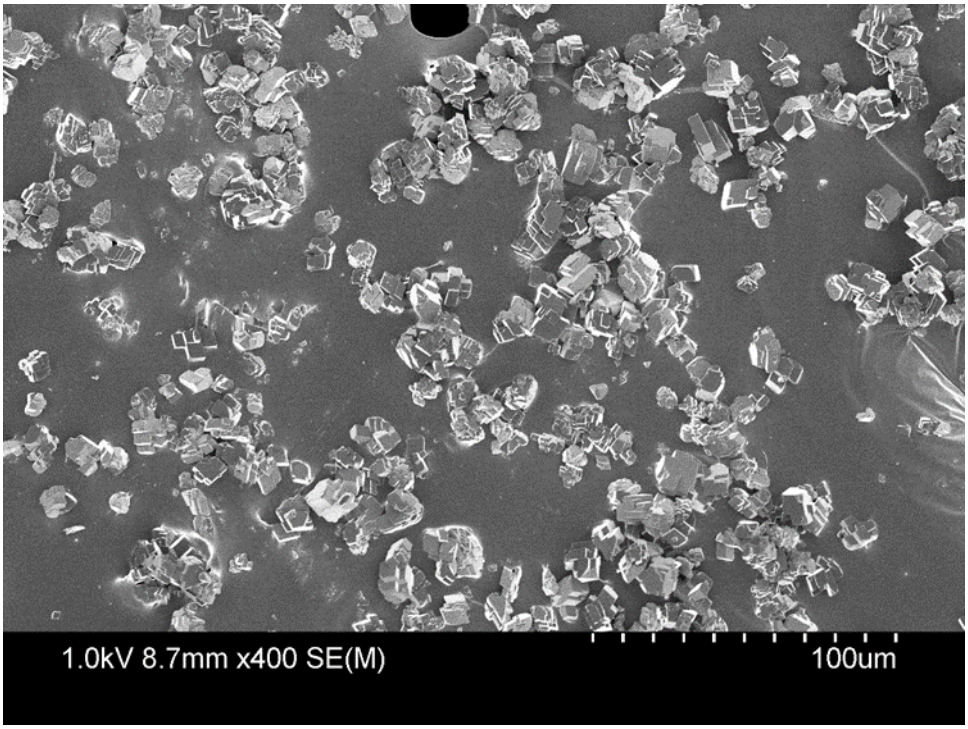

Sample ID. MS-VC2#A-2 (duration: 70 days, pH: 9.5, phase: pure calcite)

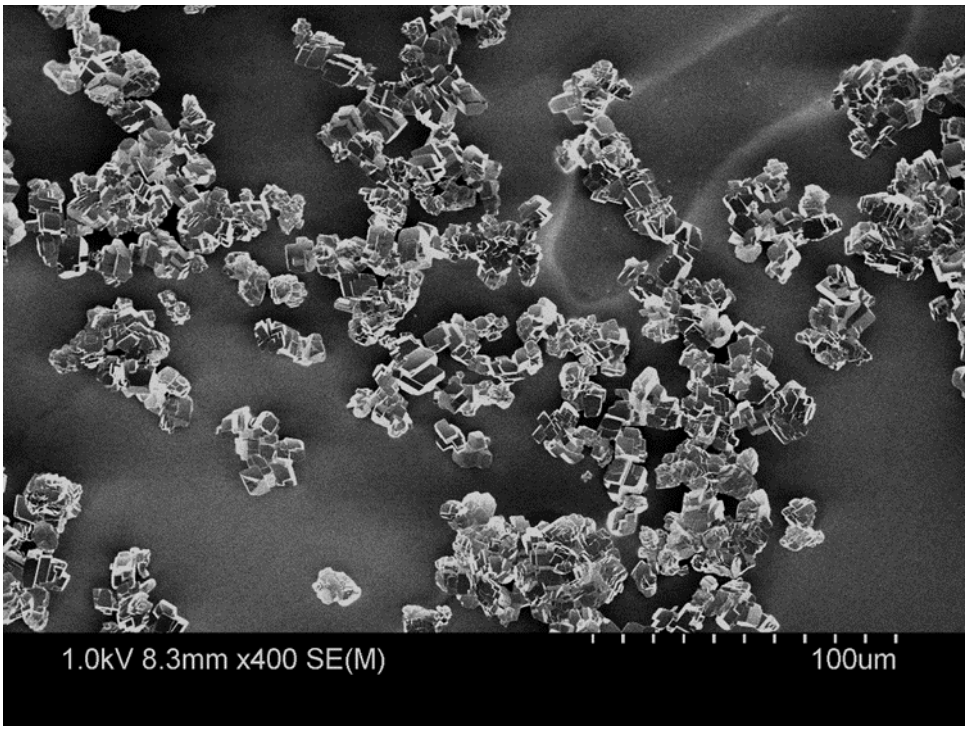

Sample ID. MS-VC2#A-3 (duration: 120 days, pH: 9.5, phase: pure calcite)

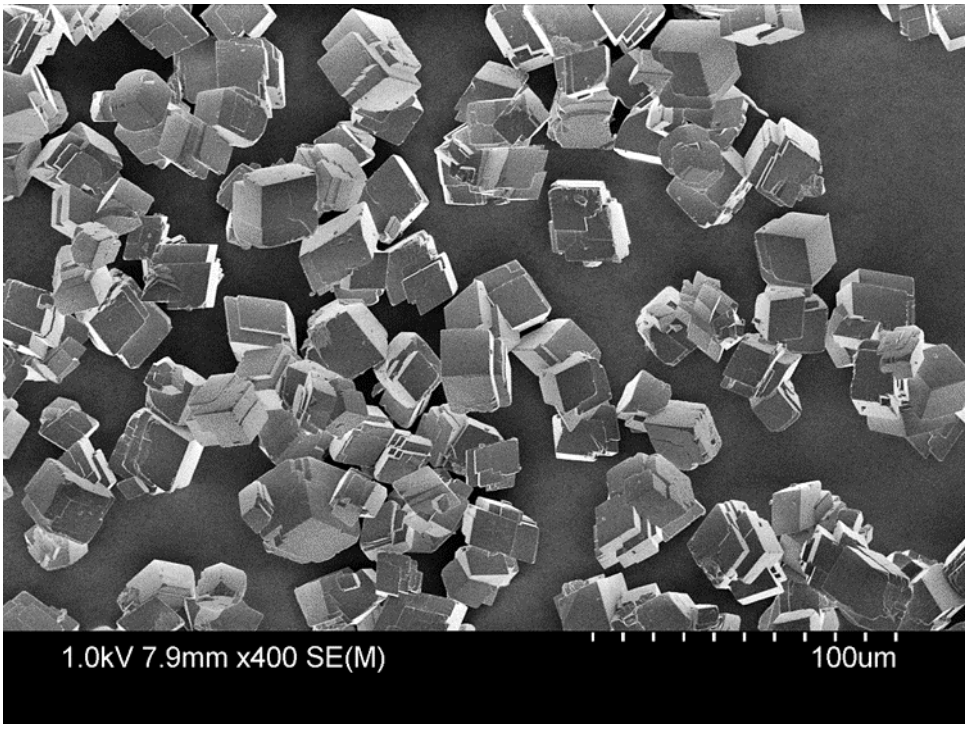

Sample ID. MS-VC2#D-4 (duration: 5 days, pH: 6.9, phase: pure calcite)

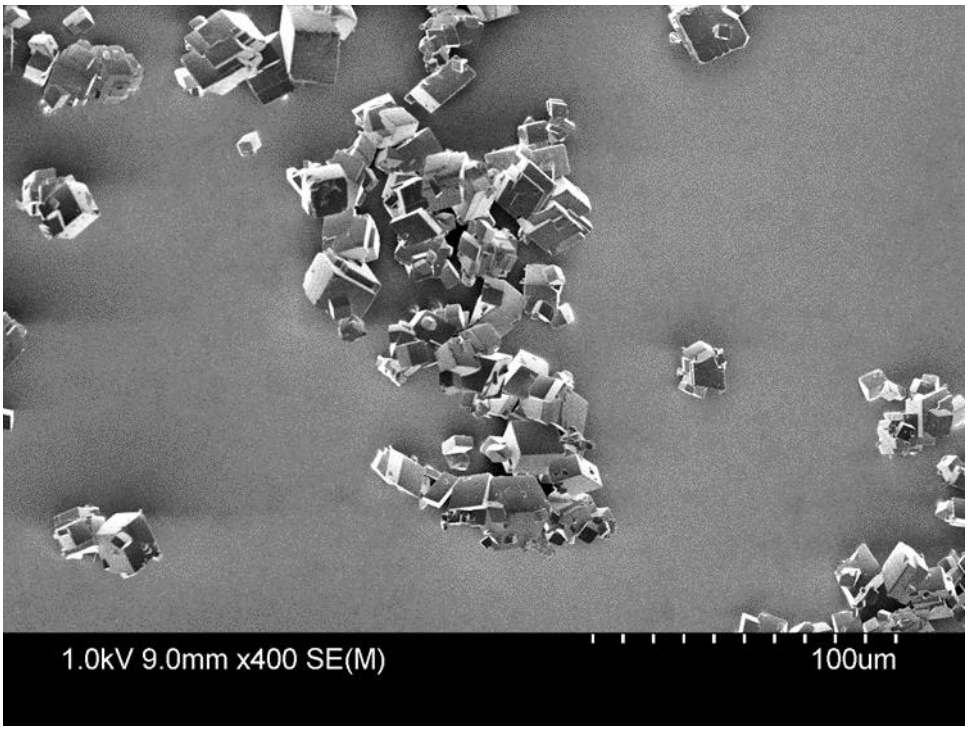

Sample ID. MS-VC2#D-5 (duration: 14 days, pH: 6.2, phase: pure calcite)

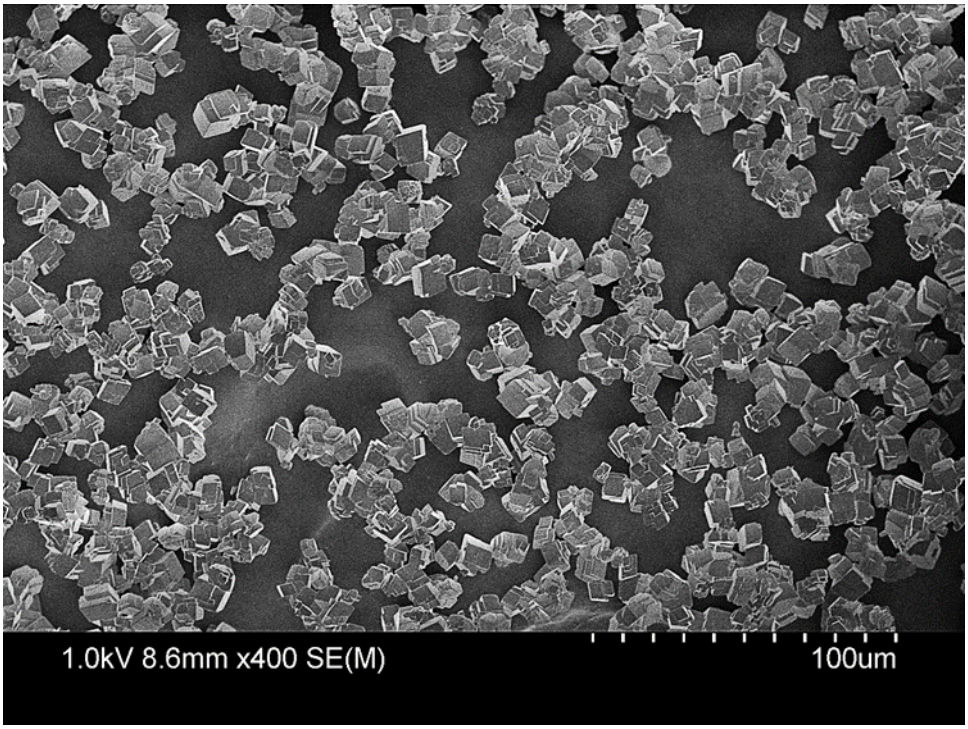

Sample ID. MS-VC2#D-3 (duration: 120 days, pH: 6.8, phase: pure calcite)

A.6. XRD analysis results

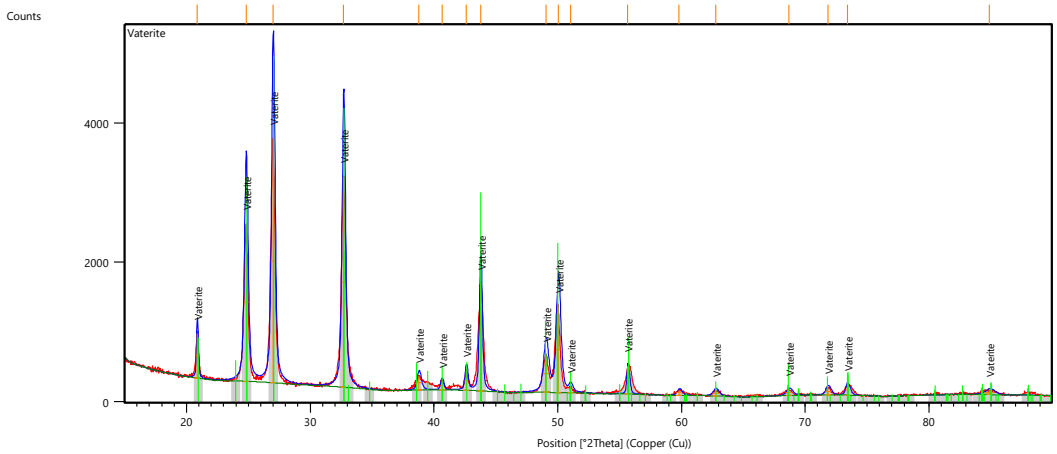

Sample ID. Vaterite

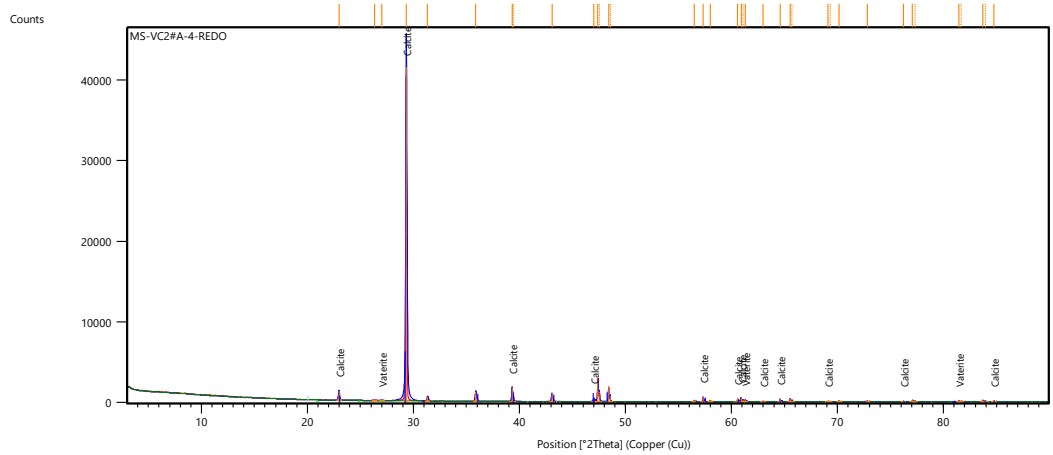

Sample ID. MS-VC2#A-4-2

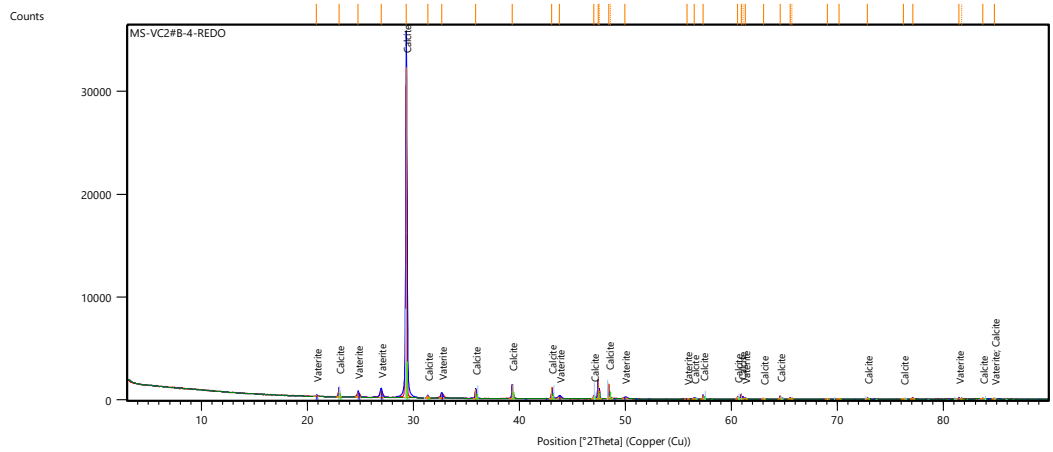

Sample ID. MS-VC2#B-4-2

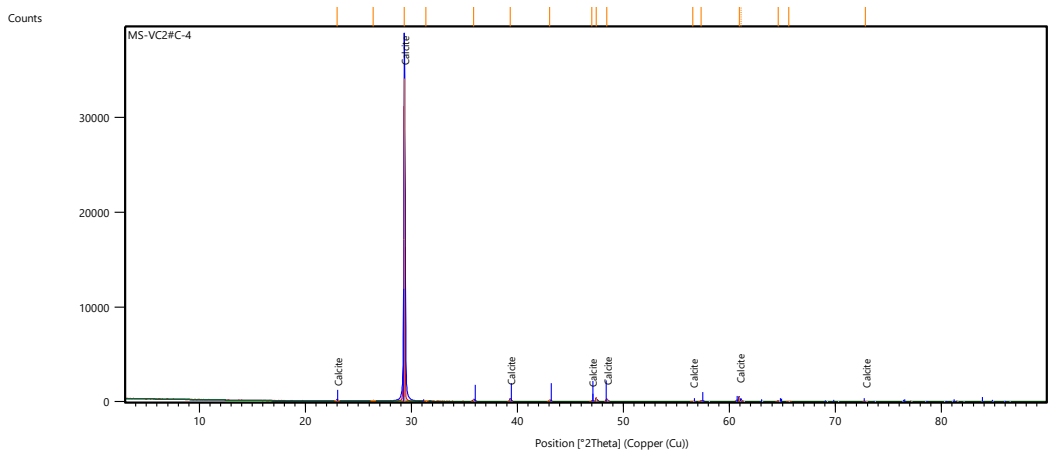

Sample ID. MS-VC2#C-4

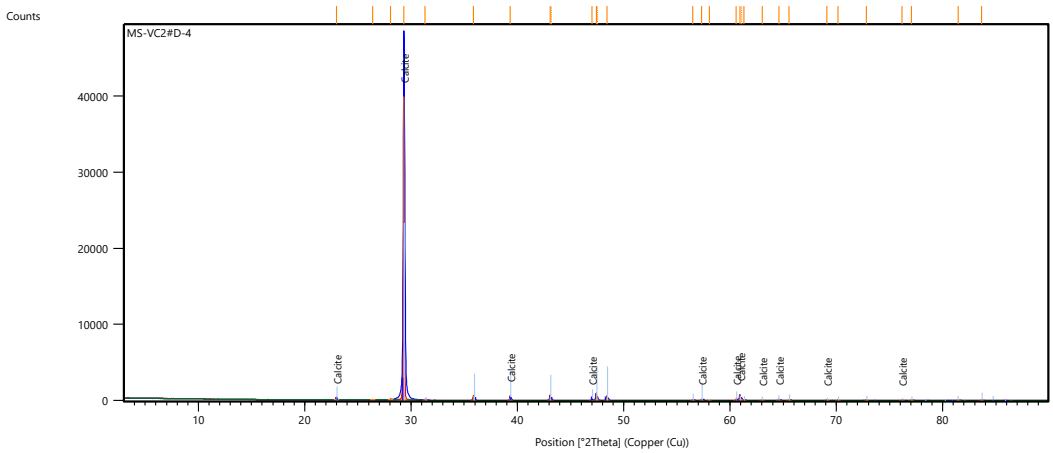

Sample ID. MS-VC2#D-4

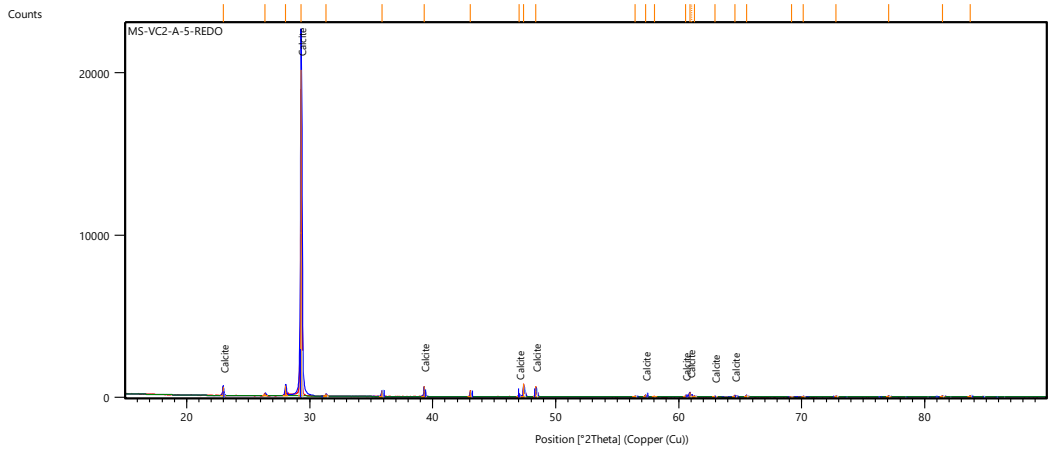

Sample ID. MS-VC2#A-5-2

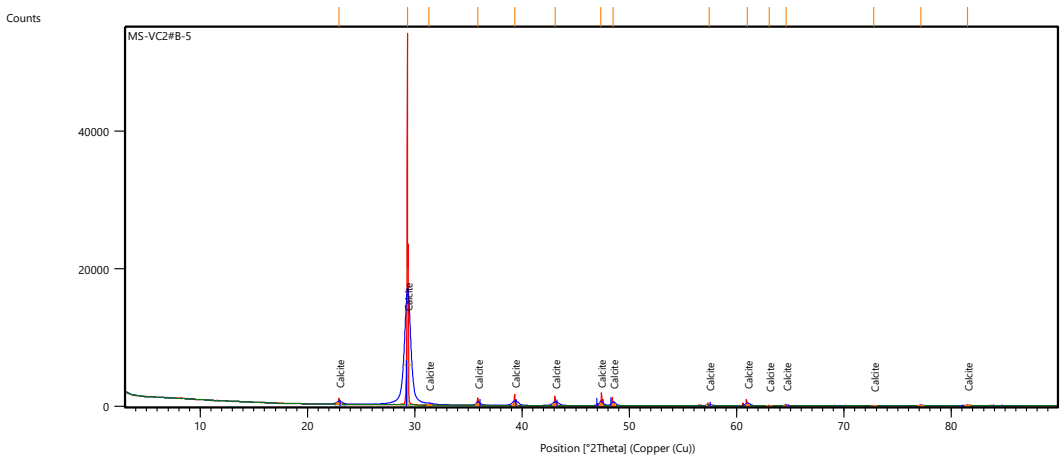

Sample ID. MS-VC2#B-5

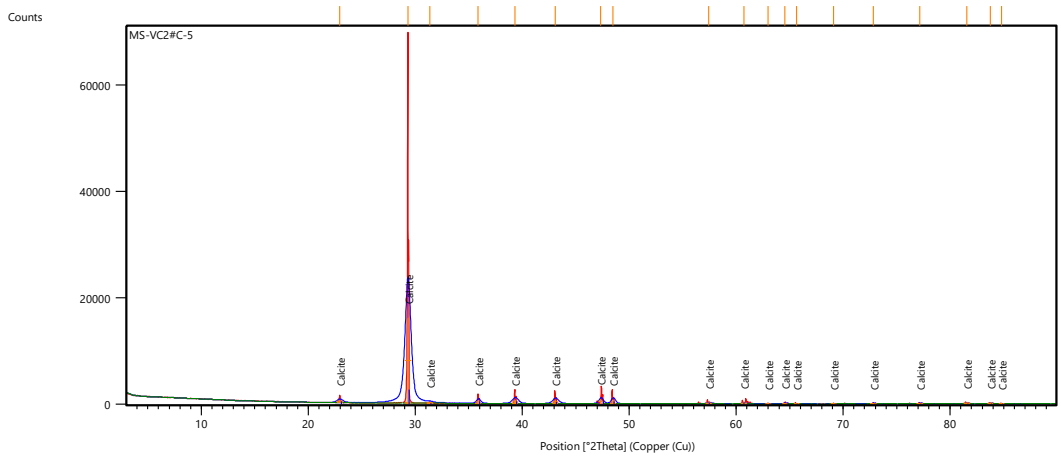

Sample ID. MS-VC2#C-5

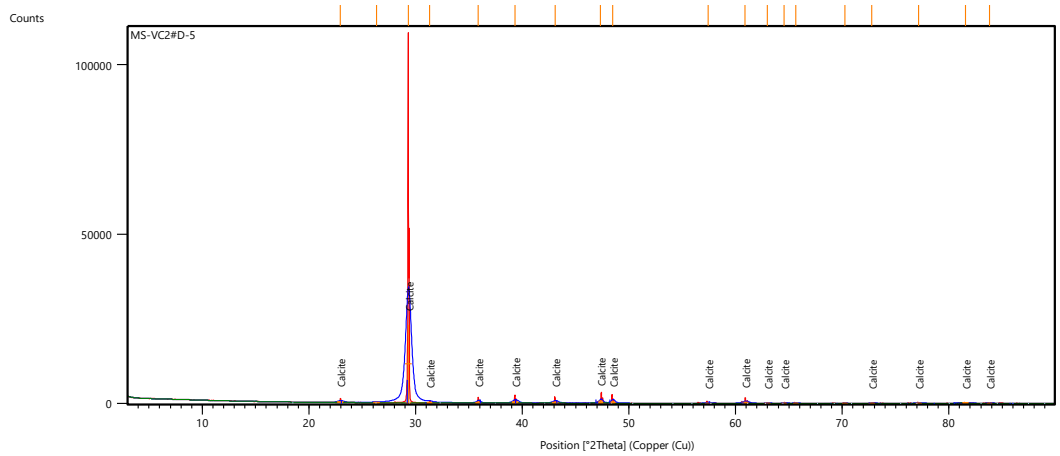

Sample ID. MS-VC2#D-5

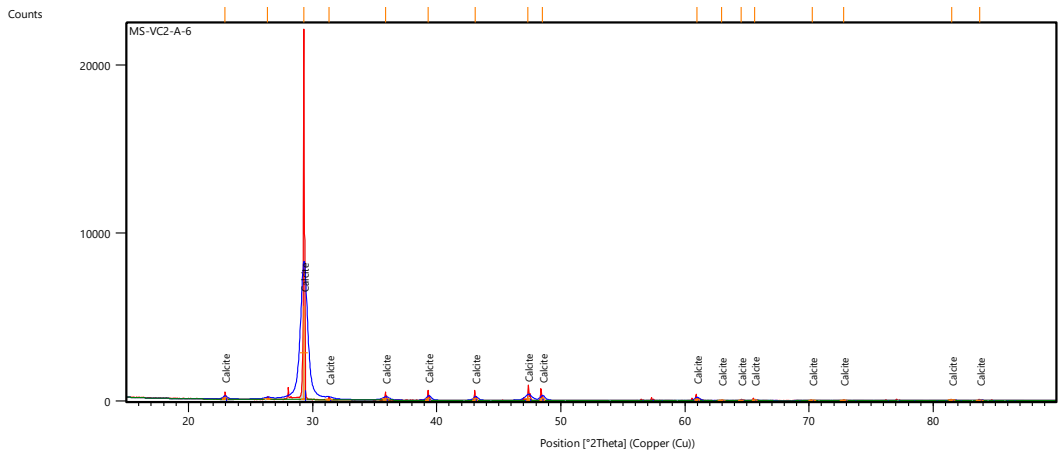

Sample ID. MS-VC2#A-6

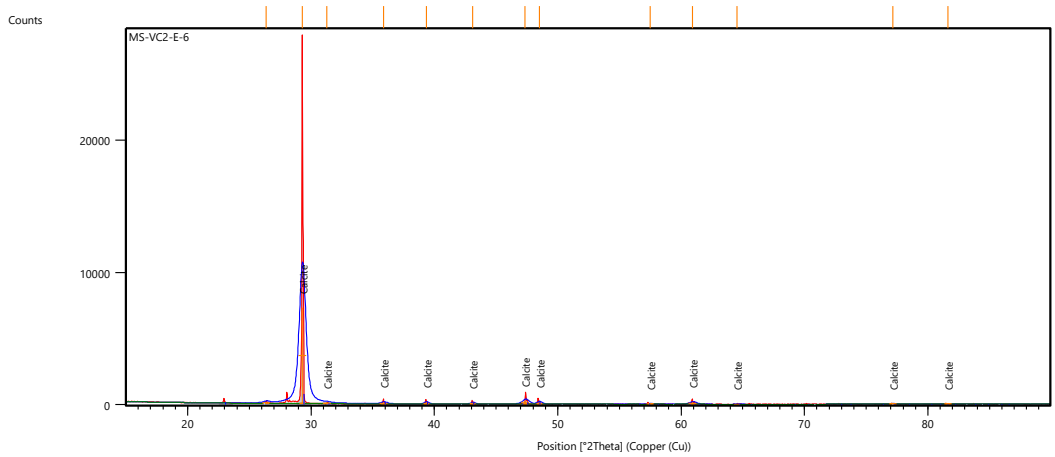

Sample ID. MS-VC2#E-6

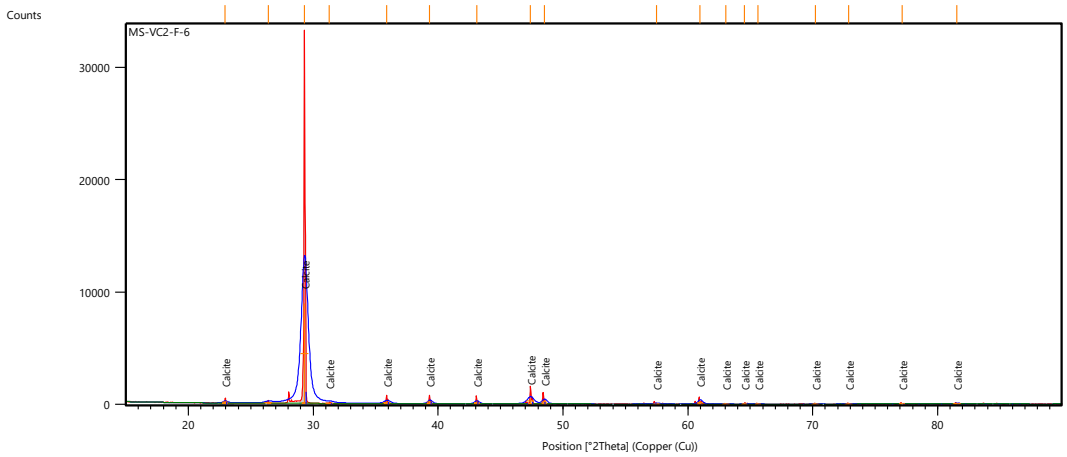

Sample ID. MS-VC2#F-6

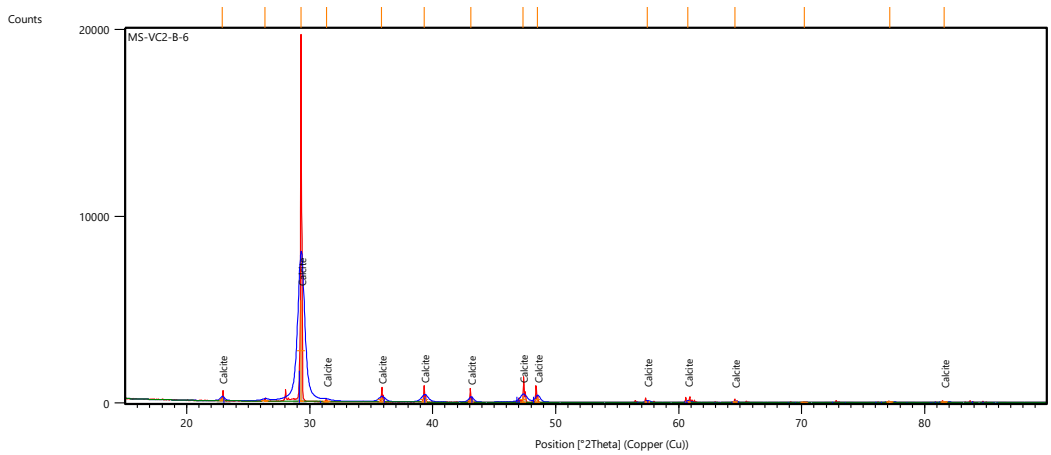

Sample ID. MS-VC2#B-6

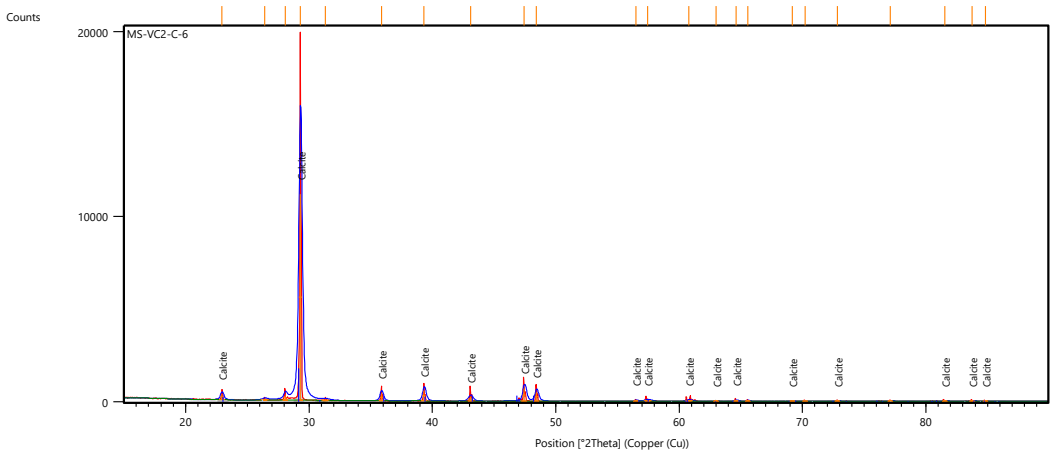

Sample ID. MS-VC2#C-6

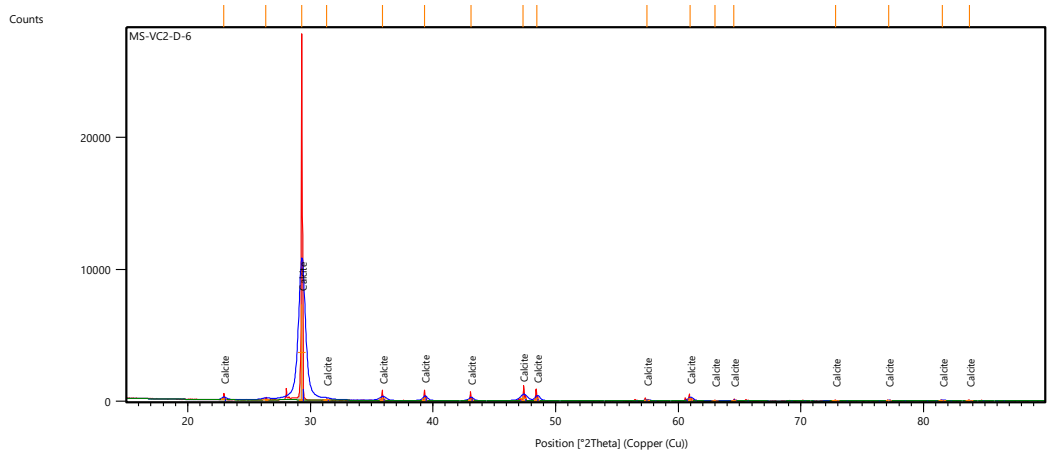

Sample ID. MS-VC2#D-6

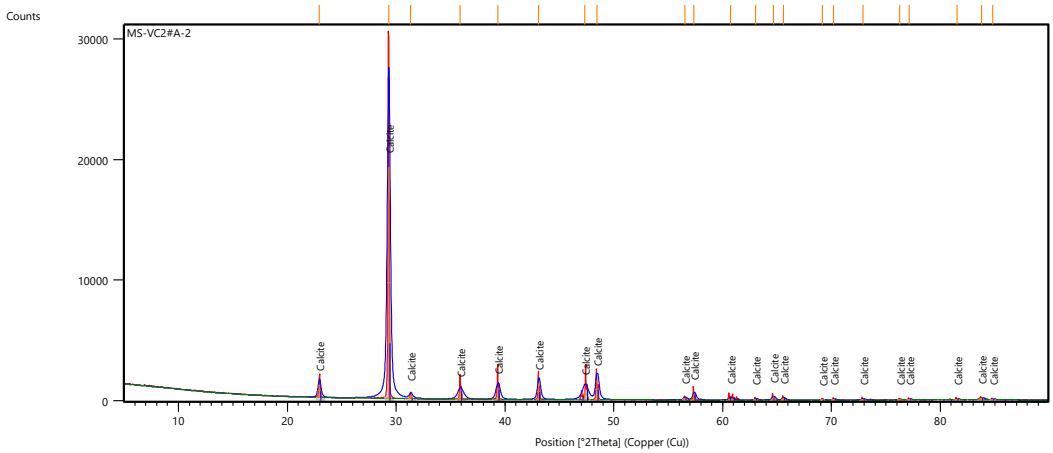

Sample ID. MS-VC2#A-2

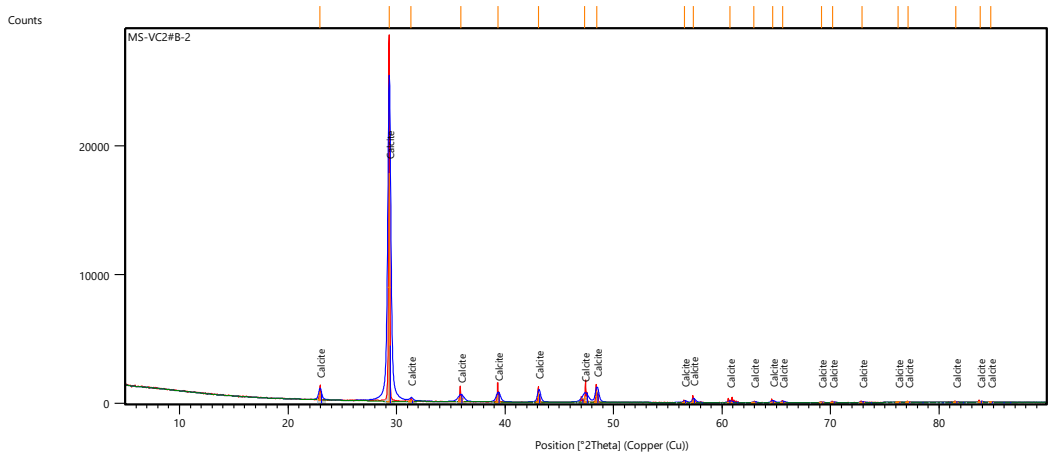

Sample ID. MS-VC2#B-2

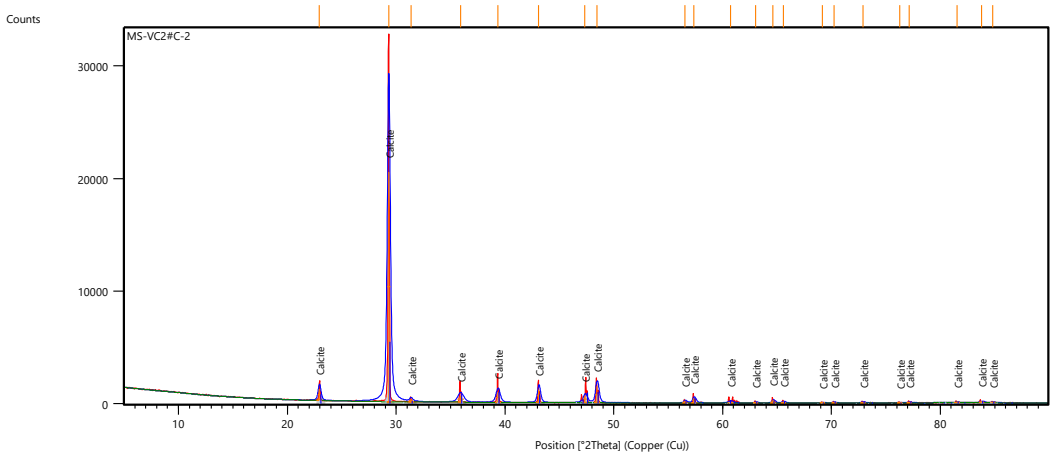

Sample ID. MS-VC2#C-2

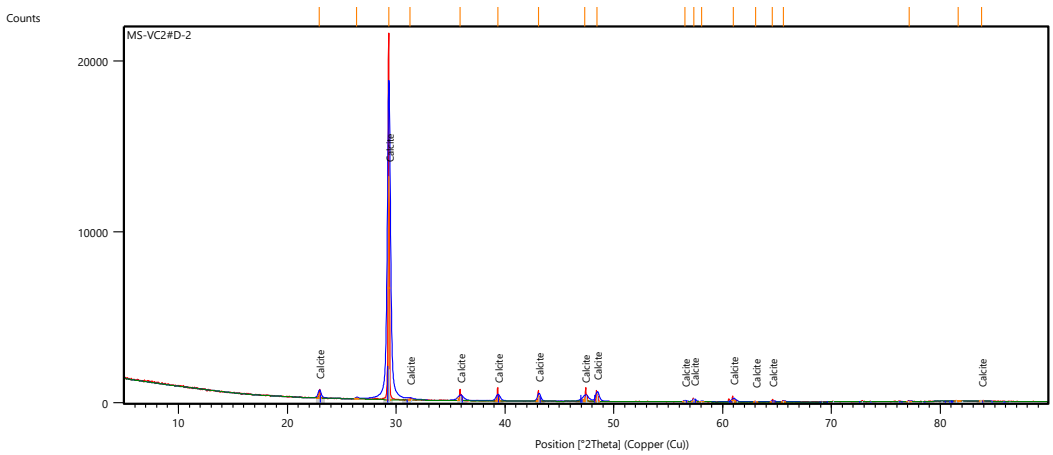

Sample ID. MS-VC2#D-2

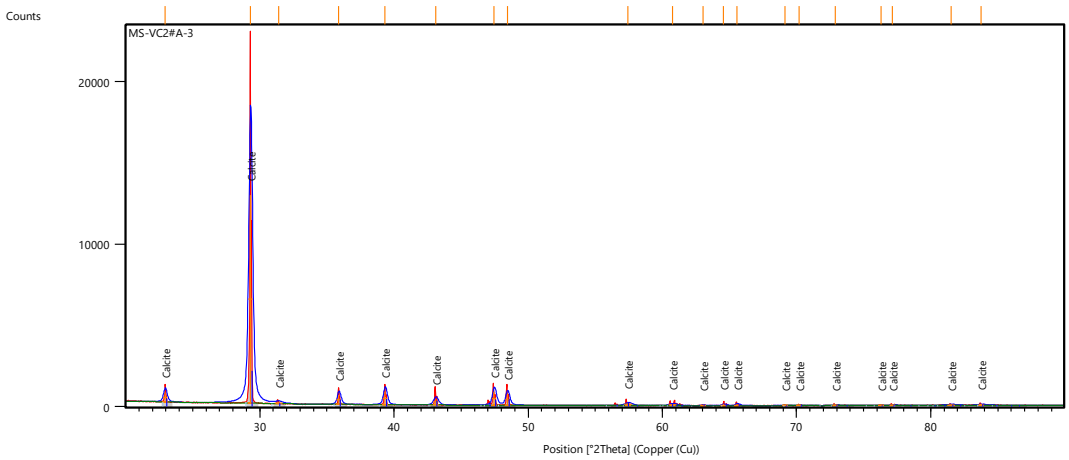

Sample ID. MS-VC2#A-3

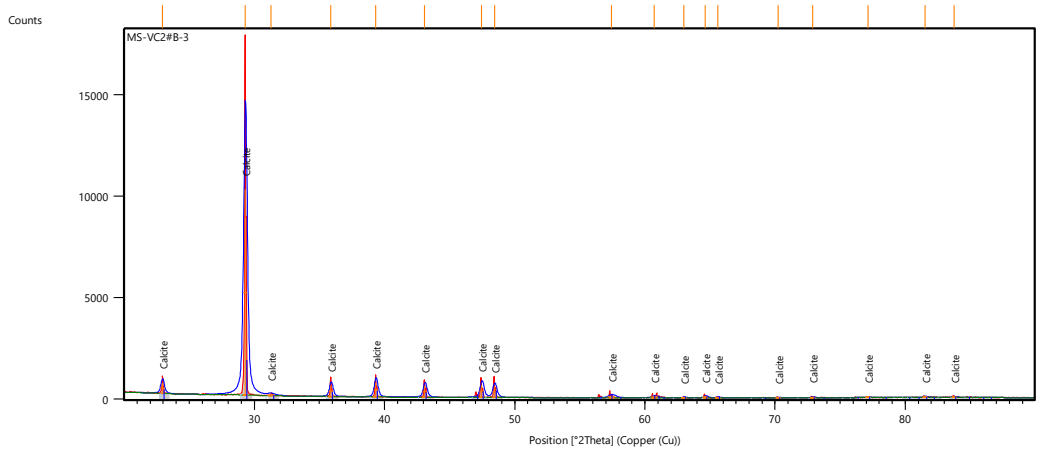

Sample ID. MS-VC2#B-3

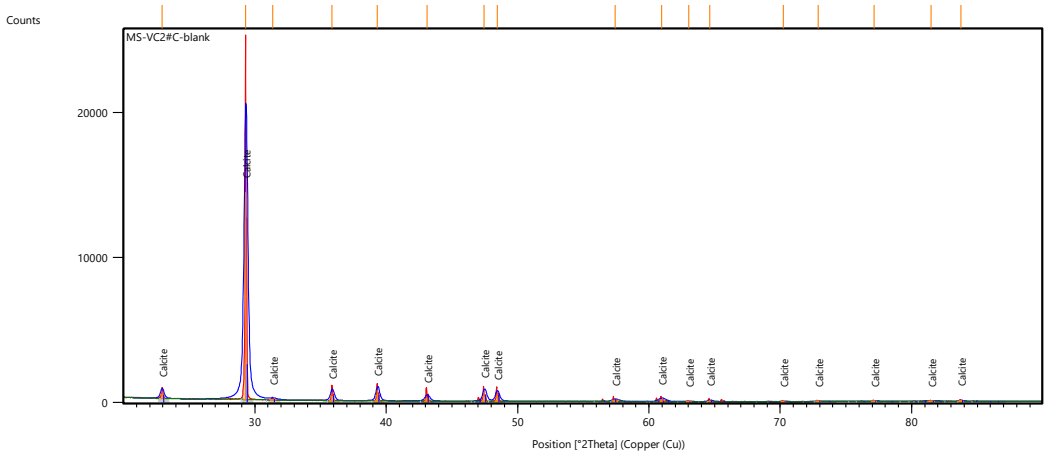

Sample ID. MS-VC2#C-blank

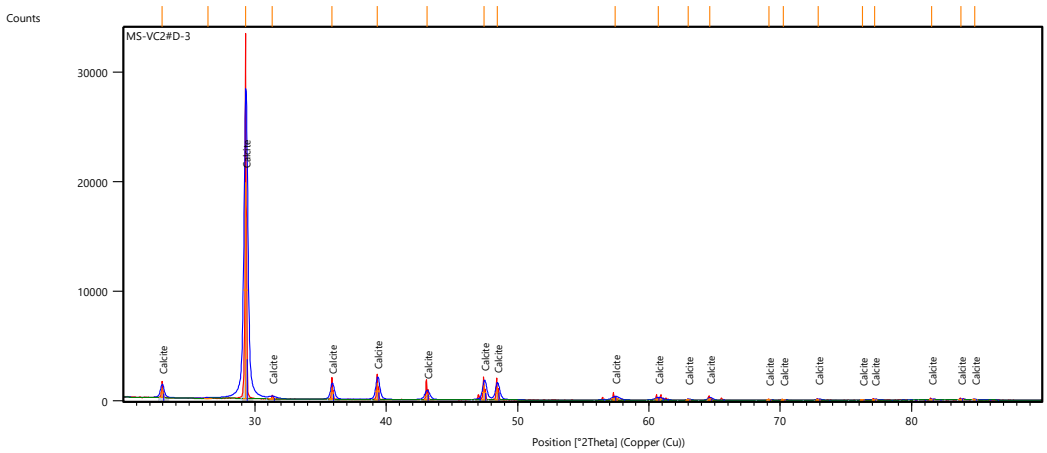

Sample ID. MS-VC2#D-3

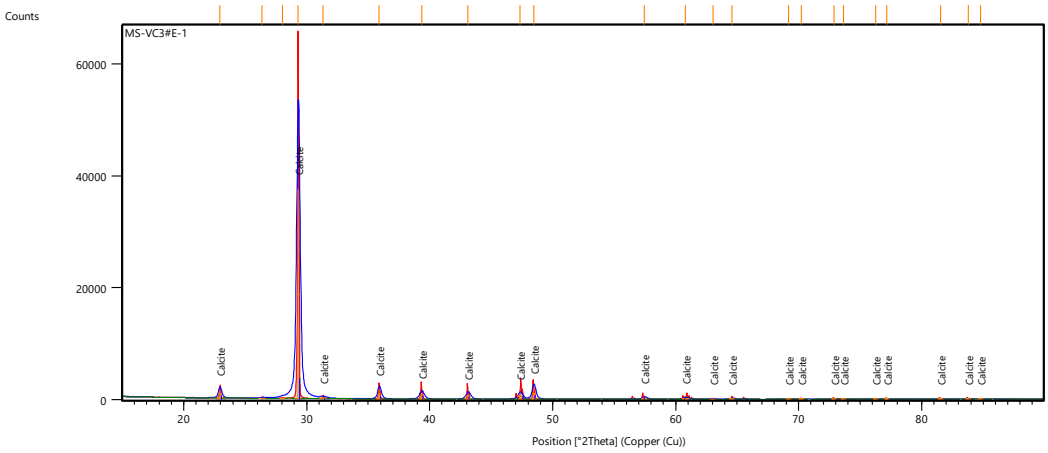

Sample ID. MS-VC3#E-1

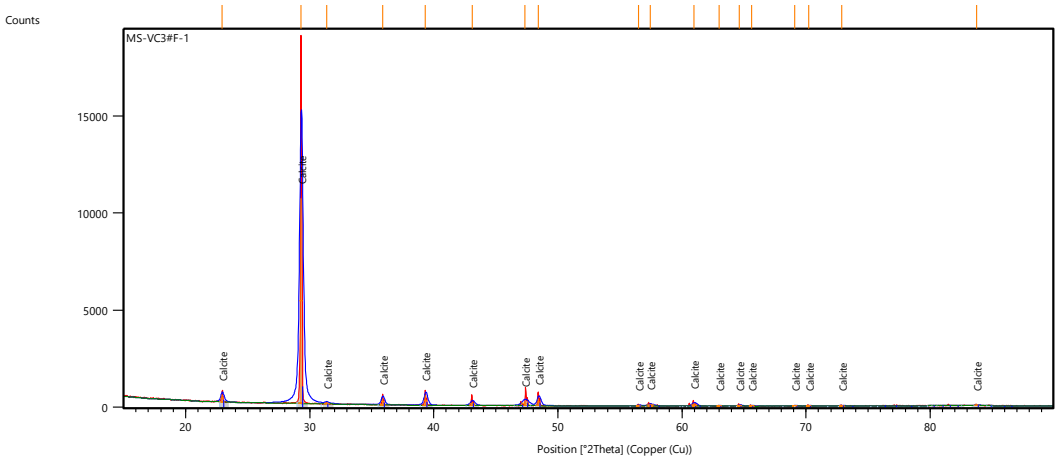

Sample ID. MS-VC3#F-1

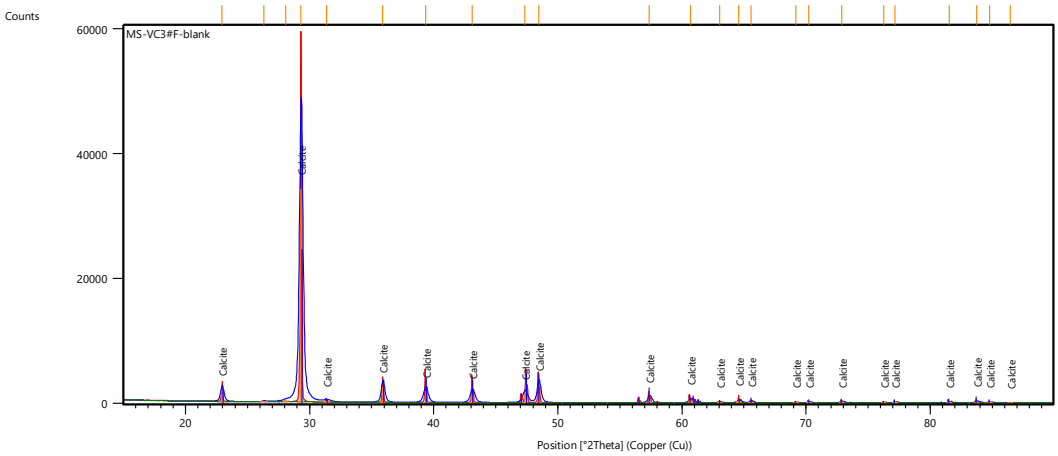

Sample ID. MS-VC3#F-blank

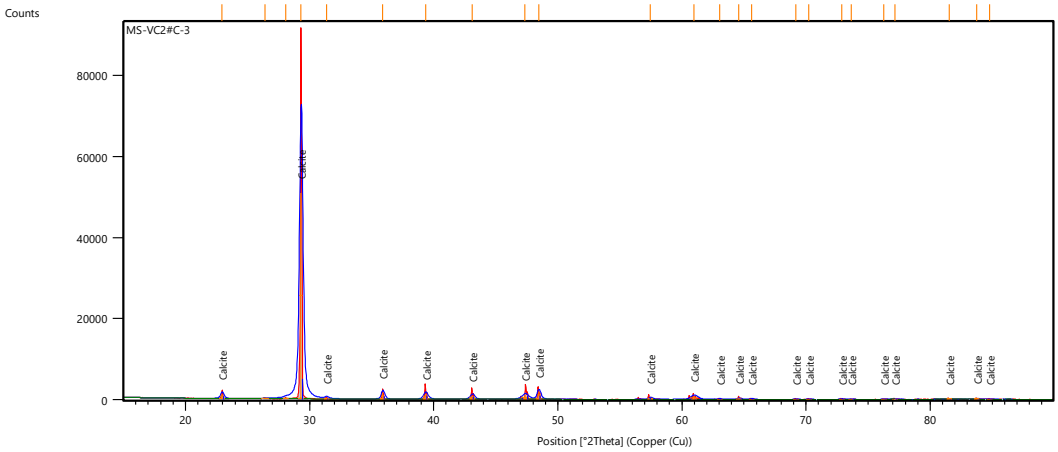

Sample ID. MS-VC2#C-3

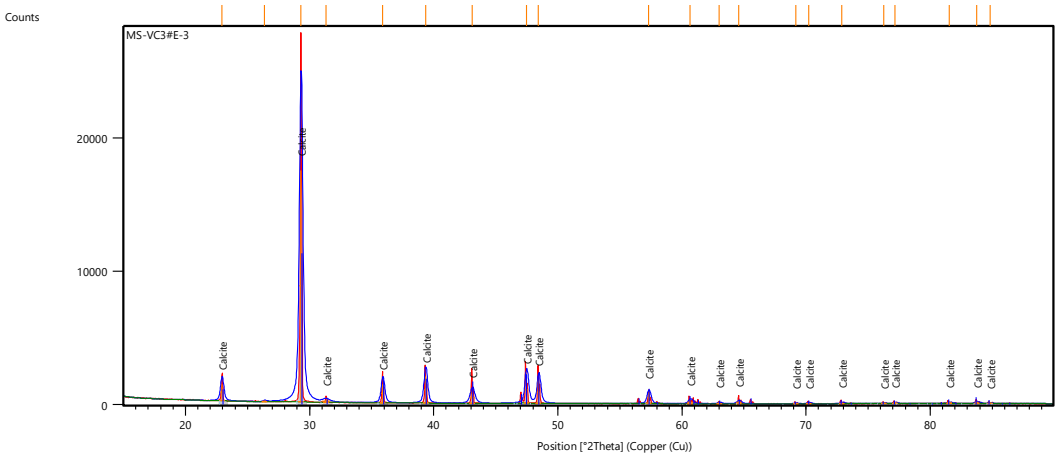

Sample ID. MS-VC3#E-3

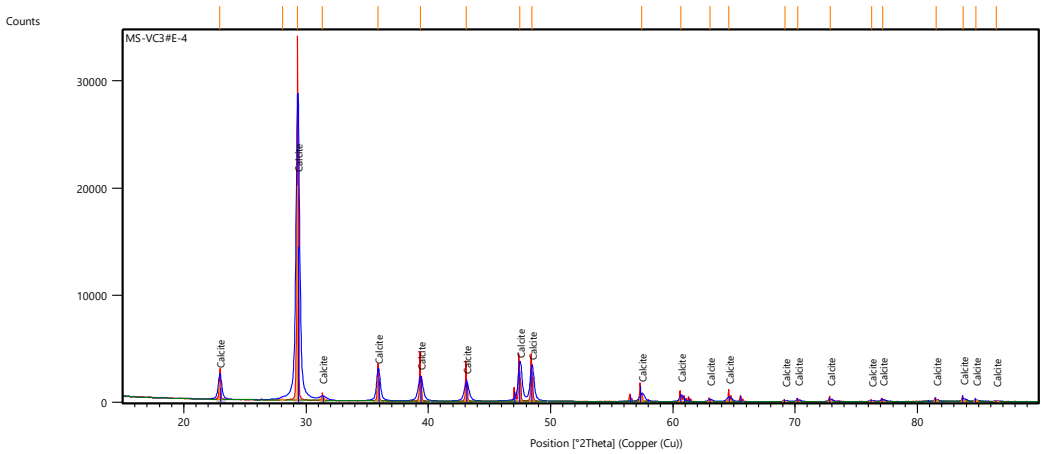

Sample ID. MS-VC3#E-4

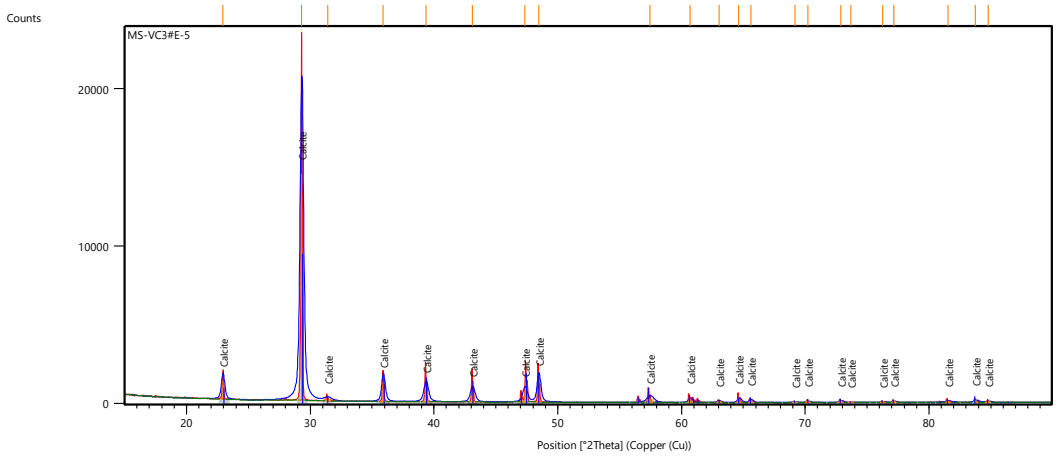

Sample ID. MS-VC3#E-5

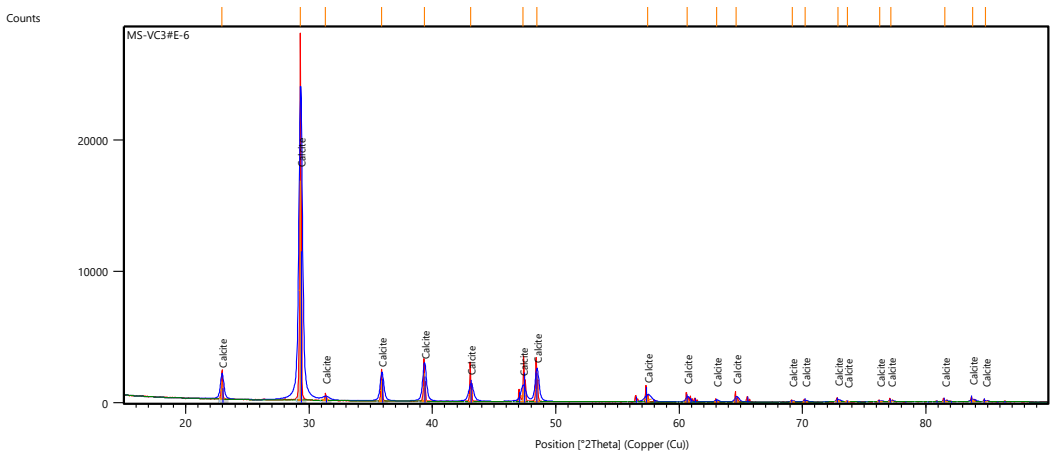

Sample ID. MS-VC3#E-6

Appendix B: Modeling of the evolution of the Li concentration and isotopic composition of altered oceanic crust during interaction with hydrothermal fluid at low temperatures

Hydrothermal alteration of basalts during interaction with hydrothermal fluid happens by dissolution of primary phases in the fresh basalts and precipitation of secondary minerals. Exchange of tracers between rock and fluid also happens during the dissolution and precipitation process. Secondary clay minerals take up Li from the fluid so that the Li concentration of the fluid changes as it moves through the porous medium of rocks. Also, Li isotopes fractionate between clay minerals and fluid, due to a higher tendency of ^{6}Li to be incorporated into clay minerals in preference to ^{7}Li. Therefore, the Li isotopic composition of a hydrothermal fluid changes as seawater interacts with fresh rocks. If the exchange of a trace element and its isotopes between solid and fluid occurs at a slower rate than the rate of transport of that tracer by fluid flowing through the porous medium of rocks, then rock and fluid cannot be at a full equilibrium conditions (e.g., Bickle, 1992; DePaolo, 2006). Therefore, to model the evolution of the composition of a hydrothermal fluid and the rock it reacts within an aquifer system, it is essential to include time dependent parameters. The presence of primary phases in even heavily altered rocks, shows that there is not complete equilibrium between fluid and rock. Hence, to predict the evolution of the composition of the hydrothermal fluid and altered rock, a model is required that accounts for both advective transport of the tracer and the rate of the tracer's exchange reactions.

In addition to advective transport of tracers, another kinetic process that affects the distribution of elements in the fluid is diffusion. As fluid-rock reactions occurs the fluid Li content decreases, therefore a gradient of Li concentration forms within the fluid which leads to diffusion of Li within the hydrothermal fluid. The importance of diffusive transport of Li can be assessed by comparing the length scales of diffusion versus advection. The diffusive length scale can be quantified as:

$$L_{\mathrm{diff,Li}} = \left(D_{\mathrm{Li}} t\right)^{1/2} \qquad \text{Eq. B.1}$$

where D_{Li} is the diffusion coefficient of Li in seawater and t is time. The D_{Li} depends on diffusivity of Li in seawater, porosity of the porous medium and the tortuosity coefficient which is in the range of 0.1 to 1.0 (Dullien, 1979):

$$D_{\mathrm{Li}} = D_{\mathrm{Li}}^{SW} \varphi_{aquifer} \theta \qquad 0.1 < \theta < 1.0 \qquad \text{Eq. B.2}$$

A study by Yuan-Hui and Gregory (1974) suggests that cation diffusion coefficients in seawater are 0 % to 8 % smaller than that of diffusion coefficients in pure water, at a given temperature (D^{0}_{Li}). Studies have shown that the alteration temperature within the upper oceanic crust was warmer during the Cretaceous compared with modern seawater (~20°C; e.g., Gillis and Coogan., 2011). Yuan-Hui and Gregory (1974) modelled Li diffusion coefficient in water at three temperatures of 0°C, 18°C and 25°C. The closest

temperature to the alteration temperature of Cretaceous oceanic crust is 25°C. To account for the maximum possible length scale of diffusion, it is assumed the Li diffusion coefficient in seawater is no different than that in water ($D^{sw}_{Li}= D^{0}_{Li}= 0.0325$ m^2.yr^{-1}; Yuan-Hui and Gregory, 1974). Therefore, for a maximum aquifer porosity of 0.1 (Lauer et al., 2018) and maximum tortuosity coefficient of 1.0, the D_{Li} would be 0.0033. The Li diffusion coefficient obtained from diffusion experiments, which were designed to evaluate the diffusion coefficient ratio of ^{7}Li to ^{6}Li as pH of aqueous solution changes at room temperature, is somewhat smaller than this (D_{Li}=0.0001 m^2.yr^{-1}; Chapter 2).

To compare the length scale of diffusion with the length scale of advection of Li, the latter is calculated for a range of fluid velocity in oceanic crust using the following equation:

$$Li_{adv,Li} = \omega_0 t \qquad \text{Eq. B.3}$$

Results show that the length of advection of Li (assuming a residence time of hydrothermal fluid in off-axis oceanic crust of ~20,000 yrs; Baker et al., 1991) is >2000 times larger than the length scale of diffusion of Li in seawater flowing through the upper oceanic crust (Table B.1). Therefore, I ignore diffusion in fluid-rock reaction modelling.

Table B.1. Parameters used to calculate the diffusion reaction length and length of advection for Li.

Symbol	Definition	Values	Unit	Ref
$\varphi_{aquifer}$	Maximum crustal aquifer porosity	0.1		Lauer et al. (2018)
θ	Tortuosity coefficient	0.1-1.0		Dullien (1979)
D^0_{Li}	Diffusion coefficient of Li in water	0.0325[a]	$m^2.yr^{-1}$	Yuan-Hui and Gregory (1974)
D^{sw}_{Li}	Diffusion coefficient of Li in seawater	0.0325[b]	$m^2.yr^{-1}$	Yuan-Hui and Gregory (1974)
t	Time	20000[c]	yr	Baker et al. (1991)
ω_0	Fluid velocity in porous rock medium	1-10	m/yr	Lauer et al. (2018)
$L_{diff,\mathrm{Li}}$	Reaction length for diffusive pore-fluid transport of Li (Eq. B.1)	8.06	m	
$L_{adv,\mathrm{Li}}$	Length of advection of Li (ω_0*t)	20000-200000	m	
$\boldsymbol{L_{adv,\mathrm{Li}}/ L_{diff,\mathrm{Li}}}$	Ratio of length of advection to diffusive transport of Li	**2481-24813**	m/m	

[a] At 25° C

[b] To calculate maximum possible diffusive length scale of Li, D^0_{Li} is assumed to be equal as D^{sw}_{Li} and D_{Li} (Eq. B.2) is calculated for tortuosity coefficient of 1.0.

[c] Suggested residence time of hydrothermal fluid in upper off-axis oceanic crust.

Two types of fluid flow models are discussed in the Chapter 4 (i.e., horizontal and vertical fluid flow). Considering that the mathematics of both models is the same, the following explanations are focused on the horizontal fluid flow model.

The following model from Bickle et al. (1992) is used to evaluate the variation in Li concentration and isotopic composition of bulk rocks with depth at Holes 417A, 417D and 418A. The first application of this model is to evaluate if fluid-rock reaction during lateral flow, with decreasing fluid flux with depth, can explain the observed variation in Li content and isotopic composition of bulk rock samples. The proposed model assumes that rocks have parallel fractures along which fluid flow pathways and interacts with fresh rocks (Figure B.1). Moreover, it has been assumed that advective transport of Li and Li exchange between solid and fluid are the only governing kinetic processes limiting solid-fluid exchange processes, ignoring diffusive transport of Li through the fluid. Change in the fluid flux is assumed to be due to a change in porosity and permeability of rocks with depth, while the gradient of temperature and pressure is assumed to be constant between recharging and discharging conduits.

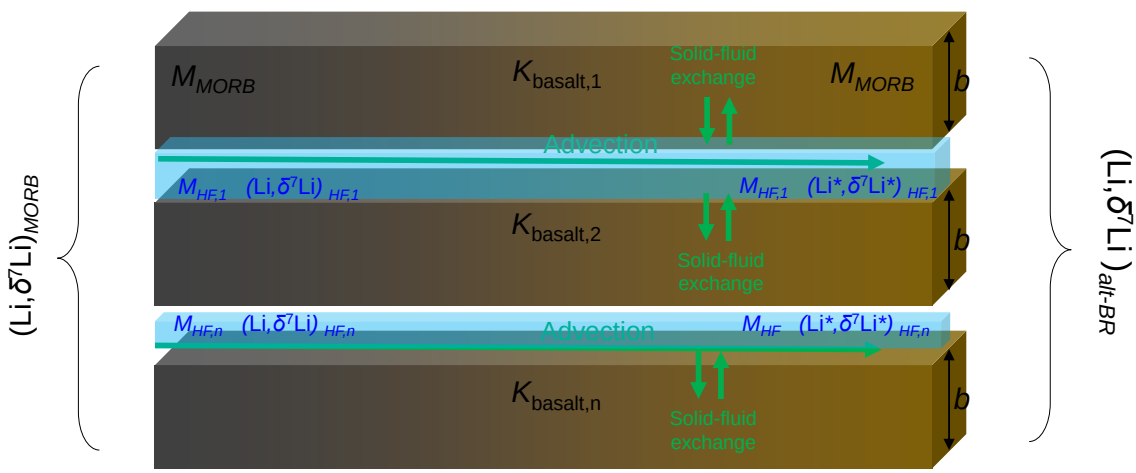

Figure B.1. Cartoon shows the conceptual model for the evolution of Li concentration and isotopic composition of hydrothermal fluid (*HF*) and altered mid ocean ridge basalt (*alt-BR*; *MORB* stands for fresh mid ocean ridge basalt). Mass (*M*) of basalt is assumed to stay unchanged but mass of hydrothermal fluid flowing through the fractures is assumed to decrease with depth. Fluid flows through fractures between parallel slabs of rocks with a thickness of *b*. Li exchanges between rock (with permeability of $K_{basalt,1}$ to $K_{basalt,n}$) and fluid while the linear kinetic processes of Li exchange rate and advection are limiting the exchange process.

Bear (1992) has shown that if the ratio of diffusive length of a tracer to the fracture spacing (*b*; distance between two parallel fractures, Figure B.1) is greater than unity, then one can assume the fluid flow is evenly distributed through the rock pore-space and is not localized along fractures or high-permeability zones. The calculated diffusive reaction length for Li gives a value of ~8 m, which means for $L_{Li}/b > 1$, a fracture spacing < 8 m is required. The upper basaltic sections at Holes 417A and 417D are reported as being highly fractured (Donnelly et al., 1979a and 1979b). For example, based on the radial fracture sizes, most pillows are reconstructed to have a size in a range of 0.3 to 0.5 m

(Donnelly et al., 1979a and 1979b), and considering that most pillows are internally fractured as well, fracture spacing in these cores is expected to be much less than 8 m. Therefore, it seems reasonable to assume an even distribution of fluid flux in the direction of fluid flow; which in this model is assumed to be horizontal.

The dimensionless Damköhler number (N_D; Boucher and Alvez, 1959) accounts for the relative rates of fluid-solid exchange (κ) to advective transport where:

$$N_D = \frac{\kappa h}{\omega_0} \qquad \text{Eq. B.4}$$

where ω_0 is fluid velocity and h is the length scale for kinetic exchange which depends on time and fluid velocity. Darcy's law states that, the fluid flux with a given viscosity (μ), which has laminar flow within a medium with a given permeability (k), depends on the gradient of pressure (∇p):

$$q = \frac{-k\nabla p}{\mu} \qquad \text{Eq. B.5}$$

Hence, for a given gradient of pressure, if permeability (and porosity) of the porous medium decreases, fluid flux decreases as well. The Darcy velocity (v) in a porous medium also depends on fluid flux and porosity of the medium:

$$v = \frac{q}{\varphi} \qquad \text{Eq. B.6}$$

If permeability decreases, porosity is also expected to decrease. Therefore, a decrease in fluid flux does not lead to a change in fluid velocity. Hence, N_D is independent of fluid flux and only depends on the exchange rate constant.

The differential equations governing concentration of a tracer in fluid, where diffusion is ignored and advection of fluid is the only governing kinetic process limiting tracer exchange between solid and fluid, are given by Lassey and Blattner, (1988):

$$\frac{\partial(\Phi' C_f + C_s)}{\partial t} + \Phi' \omega_0 \frac{\partial C_f}{\partial z} = 0 \qquad \text{Eq. B.7}$$

$$\frac{\partial C_s}{\partial t} = \kappa(C_s^* - C_s) \qquad \text{Eq. B.8}$$

$$\Phi' = \frac{\rho_f C_f \varphi}{\rho_s C_s (1-\varphi)} \qquad \text{Eq. B.9}$$

The analytical solution for Eq. B.7 and Eq. B.8 as a function of N_D are taken from Lassey and Blattner (1988):

$$z' = \frac{z}{h}$$
$$t' = \frac{\omega_0 t}{h} \qquad \text{Eq. B.10}$$

where z' and t' are dimensionless time and distance.
The dimensionless solutions of Eq. B.7 and Eq. B.8 for a tracer concentration in solid (*s*) and fluid (*f*) are:

$$C_s(z',t') = C_{s_0} + kd_{Li} C_{f_0} K\left\{N_D(t'-z'), \frac{N_D z'}{\Phi'}\right\} \qquad \text{Eq. B.11}$$

$$C_f(z',t') = C_{f_0} - K\left\{\frac{N_D z'}{\Phi'}, N_D(t'-z')\right\} \qquad \text{Eq. B.12}$$

$$K(x,y) = \int_0^x e^{(-u-y)} I_0(2\sqrt{uy})du \qquad \text{Eq. B.13}$$

To calculate the evolution of Li isotopic composition of fluid and rocks, solutions for concentrations given above can be used for each isotope of ^{6}Li and ^{7}Li. Knowing *Kd* of one of the isotopes, one can calculate *Kd* for the other isotope using the isotopic fractionation factor (α):

$$kd_{\mathrm{Li}} = \frac{\mathrm{Li}_s}{\mathrm{Li}_f} \qquad \text{Eq. B.14}$$

$$\alpha = \frac{(\frac{^7\mathrm{Li}}{^6\mathrm{Li}})_s}{(\frac{^7\mathrm{Li}}{^6\mathrm{Li}})_f} \qquad \text{Eq. B.15}$$

hence:

$$kd_{^7\mathrm{Li}} = kd_{^6\mathrm{Li}}\alpha \qquad \text{Eq. B.16}$$

To calculate α from apparent isotopic fractionation factor ($\Delta_{s\text{-}f}$) the following equation can be used:

$$\Delta_{s-f} = 1000 Ln(\alpha) \qquad \text{Eq. B.17}$$

Using the calculated Li concentration for each isotope and assuming natural abundances of Li isotopes (^{7}Li is 92.5 % and ^{6}Li is 7.5 %), δ^7Li can be calculated:

$$\delta^7\mathrm{Li} = \left[\left(\frac{(\frac{^7\mathrm{Li}}{^6\mathrm{Li}})_{sample}}{(\frac{^7\mathrm{Li}}{^6\mathrm{Li}})_{std}}\right) - 1\right] \times 1000 \qquad \text{Eq. B.18}$$

Models are run for variable time-integrated fluid flux (F_f) which is a function of the length scale for kinetic exchange, aquifer porosity and fluid density:

$$F_f = h * \varphi * \rho_f \qquad \text{Eq. B.19}$$

Parameters and given values to model the evolution of Li and Li isotopic composition in rocks are presented in the main text (Table 4.4). Models are only shown for the evolution of the Li concentration and isotopic composition of the rocks as these can be compared with the measured Li concentration and isotopic composition of samples from Holes 417A, 417D and 418A.

Appendix C: Additional analytical details

C.1. Lava samples

Lava samples from DSDP and ODP cores from the Atlantic (Holes 417A, 417D, 418A, 543A and 396B) and Pacific (Holes 597C, 1224F/D and 595B) ocean basins that formed 13.6 to 119 Myr ago were analysed for major and trace element and lithium isotopic compositions. Sample preparation (crushing, weighing, dissolution and column chromatography) for chemical analysis are described in the following sections. All reagents used were environmental grade, HPLC grade and 18.2 MΩ.cm Millipore DI.

C.1.1. Crushing samples

Samples were photographed and described prior to crushing. Sample numbers and the associated glue were ground off the samples. Samples were dried to evaporate moisture prior to crushing. Samples were placed in a beaker, covered with another beaker and dried in an oven at ~60°C over at least one night. A jaw crusher was used to break samples into pieces of <1 cm diameter. The jaw crusher was cleaned before using it. To powder crushed samples, a planetary agate mill was used for ~30 minutes at 480 RPM. If any lumps of the samples remained inside the instrument jars, the jars were placed back into the instrument without any changes in the settings, and the pulverizing process was continued for another 20 to 30 minutes.

C.1.2. Weighing samples

Around 100 mg of the pulverized rocks were weighed out into cleaned 15 ml screw top Teflon vials. Teflon vials easily accumulate negative charge on their surfaces. Electrostatic force can cause movement of small objects including the weighing pan of the digital balance leading to weighing inaccuracy. To eliminate the electric charge from the surface of Teflon vials, an antistatic gun (Zerostat Milty 3) and anti-static gloves were used. The gun releases positrons and discharges the negative charge of the Teflon vials. Vials were weighed before and after adding powders using a weighing balance outside of the clean labs. A weighing paper was used to transfer each sample powder from its bag into the Teflon vial. It was also possible to slowly transfer the powder from its main bag to the vials directly, without using weighing paper. However, because only a small amount of powder is needed, by direct transferring samples from its main bag, it is possible to transfer more powder. If more powder was transferred into a vial, it could not be returned into its main bag; otherwise, it would contaminate the whole batch of valuable samples. Hence, excess of powder must go to the waste.

C.1.3. Sample dissolution

Samples digestion started using 10:1 environmental grade concentrated HF and HNO_3 (5 ml of HF and 0.5 ml of HNO_3). Procedural blanks were also prepared with every batch of samples the same way as samples were prepared. Vials were placed in heating blocks

(i.e., they help with homogenous distribution of heat around the Teflon vials) on a hotplate with lids on at ~125°C for more than 48 hours to reflux and react with acids. It helps to break down the mineral structures and digest them. Vials were taken off the hotplate, cooled down and opened. Solutions were dried completely at ~150°C and re-digested in 1ml DI, 1 ml of concentrated HNO_3 and 1 ml of concentrated HCl on a hotplate at ~125°C over night followed by two steps of drying and re-digesting in 4 ml of 8 M HNO_3 for at least one day and finally in 4 ml of 1 M HNO_3. If the solutions were not perfectly clear at this stage, they were dried down and digested in 0.5 ml of concentrated HCl and refluxed over night at ~125°C. The HCl was then evaporated and the samples taken up again in 4 ml of 1 M HNO_3. Vials with 4 ml of sample solutions were weighed and a 0.5 ml split of the solutions were removed after shaking the vials well, and diluted in 2% HNO_3 to produce solutions with a dilution factor of 1000 for trace element analysis. The remaining 3.5 ml of solutions were kept in the vials for column chromatography. The 0.5 ml split of the solutions were transferred into a pre-cleaned and weighed 15 ml centrifuge tube. Tubes were cleaned by rinsing their inside with a few ml of 2% HNO_3, following by three times rinsing with DI, and left with lids off for at least 24 hours to dry.

C.1.4. Sample preparation for trace element and Li-isotopes analysis

Lithium was separated from the matrix of the remaining 3.5 ml of the dissolved sample. Teflon columns (30 cm long and 0.95 cm inner diameter) were filled with 7.5 g (dry weight) of BIORAD AG 50W-x8 (200-400 mesh). PTFE frit with 30 μm pore-size and 2.5 mm thickness was used to hold the resin inside the columns. Resin tends to leach styrene over time, hence it needs re-invigoration prior to use. To re-invigorate the resin, 5 column volumes (~100 ml) of 1 N HCl was poured through the resin followed by 10 column volumes (~200 ml) of DI. The resin was cleaned using 40 ml of 7 M HNO_3 followed by 15 ml of deionized H_2O (DI), 40 ml of 4 M HCl and a further 50 ml DI.

Ion-exchange resins need conditioning before loading samples to stimulate the ion exchange sites of the resin. For conditioning of the cation exchange resin, 25 ml of 20 % 0.1 M HNO_3 in 80 % methanol (0.1/80; by volume) was used. The mixture of nitric acid/methanol generates many air bubbles inside the resin. This is because the resin provides nucleation sites for mixtures of organic solution-water to release its dissolved air. To remove the air bubbles the following “back-washing” method was used.

The back-washing apparatus is a short (~8 cm) length of 1/8” PVC tubing (PVC is more resistant to nitric acid than Tygon tubing) with a 60 ml rubber-less syringe attached to one end and a knurled Teflon nut at the other end. The nut fits onto the base of the Teflon column, attaching the syringe to the column via the tubing. Inside of the back-washing apparatus was washed with 1 M HNO_3 in 80 % methanol (1/80; by volume) and 0.1/80. To remove the air bubbles after conditioning of the resin, the nut was removed from the back-washing tubing and 30 ml of 0.1/80 was drawn into the syringe. The nut slid back onto the end of the tubing and screwed onto the bottom of the stopcock. The 0.1/80 solution was slowly injected into the column, pushing the resin up into the reservoir of the columns. As the resin enters into the reservoir, it begins to sink. Before a

significant base of resin has settled to the bottom of the column, all air bubbles were dislodged by flicking the columns. Then, the nut was detached from the stopcock and the reservoir was rinsed with 0.1/80. The solution is then left to drain into a waste beaker.

To make 2L of 0.1/80, 200 ml DI was added to a pre-cleaned 2L bottle, followed by adding 200 ml 1 M HNO_3 and the mixture was well shaken. Then, 1600 ml methanol was slowly added to the bottle to make a solution with 80 % methanol and 0.1 M HNO_3. The mixture was shaken gently and stored in special box for flammable material in the clean lab. To make 2L of 1/80, 114 ml DI was added, followed by adding 286 ml 7 MHNO_3 and 1600 ml methanol. The used HNO_3 was environmental grade and the methanol was HPLC grade.

The 3.5 ml sample in 1 M HNO_3 was mixed with 0.5 ml of concentrated HNO_3 and 3.43 ml of methanol giving 1.55 M HNO_3 in a 46 % methanol matrix. 5.9 ml of this mixed solution was loaded into the columns. Li was collected by elution using 85 g of a solution of 1 M HNO_3 in 80 % methanol and collecting the aliquot released between 25 and 75 g. A 10 g aliquot before and after the peak was collected to test recovery of Li and ensuring that all of the loaded Li was collected in the peak aliquot. All aliquots were collected in Teflon beakers.

The pre, peak and post-aliquots were weighed after collection (empty beakers were weighed beforehand) and dried on hotplate. The dried material was rinsed from the inner surfaces of the Teflon beakers using 2 to 3 ml 2% HNO_3 and placed on a hotplate at 100°C to 120 °C for a few minutes. The pre and post aliquots were transferred into pre-weighed and rinsed 15 ml centrifuge tubes and diluted up to 5 ml using 2% HNO_3 and their weight was recorded. The peak aliquots were also transferred into pre-cleaned 15 ml centrifuge tubes after multiple rinses of the inner walls of the collecting beaker using 2% HNO_3. The peak aliquots were diluted in 10 ml of 2% HNO_3.

For Li-isotope analysis, all samples were prepared with the same Li concentration (e.g. 10 ppb). Hence, a split of the 10 ml peak aliquots was used (i.e., calculated based on the Li concentration of each sample) to make enough solution for the isotope analysis. Around 12 ml solution was usually enough for 5 Li-isotopic measurements of a sample using the ICP-MS.

For Li isotope analysis, the reason for preparing all samples with the same Li concentration, is to minimize the effect of the ICP-MS detector's dead-time. Dead-time is an effect that belongs to the ion counting detectors. Dead-time is an interval in time that after impact of an ion, the detector becomes blind to the further incoming ions. Dead-time is typically within a range of 10-60 ns, and hence, it is difficult to determine it accurately and precisely (e.g., Nelms et al, 2001). At high count rates this effect can lead to significant bias in the measured ion intensity. However, by keeping the concentration of all of the samples close to each other, the importance of the dead-time correction is minimized. The dead-time can be calculated by determining the best-fitting value that leads to a constant measured $^{7}Li/^{6}Li$ ratio with changing Li concentration using the standard correction equation:

$$I_t = \frac{I_0}{(1 - I_0 \tau)} \qquad \text{Eq. C.1}$$

where I_t is the count rate corrected for the dead-time, I_0 is the measured count rate with no dead-time correction applied and τ is the dead-time. The dead-time was determined by analysing solutions of variable lithium concentrations (3 to 20 ppb) a day prior to each Li-isotope analytical session.

C.2. Carbonate samples

Synthetic and hydrothermal carbonate samples were studied in this thesis. The procedures to prepare the carbonate samples for elemental and Li-isotopes analysis are explained in the following sections. All reagents used were environmental grade and 18.2 MΩ.cm Millipore DI and all Teflon vials were dedicated to carbonate analysis.

C.2.1. Consumables required

The following material were prepared prior to start samples dissolution:

- Tygon tubing, 4th smallest size with Science Store's code 12-C-23. Around 6 cm of Tygon tubing was required to prepare one sample loader
- Scalpel blade # 11 to fit # 13 handle
- Sterile 4.5 ml transfer pipettes
- 1 ml pipette tips; blue and colourless
- 5 ml and 15 ml centrifuge tubes. All centrifuge tubes were rinsed with DI and 2% HNO_3 and left to dry overnight.
- 0.5 N, 1 N and 6 N Environmental grade HCl
- 7 N Environmental grade HNO_3
- 2 N Environmental grade CH_3COOH

C.2.2. Sample preparation for trace and Li-isotopes analysis

To prepare natural carbonate samples, two 5 ml centrifuge tubes were cleaned and their weights were recorded. Using a weighing paper, 50 mg of uncrushed carbonate (or slightly less to avoid returning the extra samples into its jar) which were hand-picked under a binocular microscope and subsequently re-picked by a second person, were transferred into each of the centrifuge tubes and their weights were recorded. For the synthesized carbonates, only one centrifuge tube was needed because they do not need the following test for clay mineral contamination. ~75 % of centrifuge tubes with natural carbonate chips were filled with DI and shaken a few times. DI was decanted off carefully into a clean beaker, so that if any calcite spilt, it could be salvaged. This step was done twice, and the tube was filled with DI and left overnight to minimize the surface contamination of the samples. Finally, the DI water was decanted to the other

prepared centrifuge tube, and if no carbonate chips spilt, the DI was disposed into the sink.

Carbonate samples were dissolved in 3 ml of 1 N HCl. Acid reaction with carbonate is effervescent and quickly releases CO_2 gas, hence, the lid was quickly closed upon addition of the acid and the weight was recorded. Sample dissolutions was speeded up by inverting the tube and slowly opening the lid to release the pressure under the fume hood. The fully dissolved samples were split to two parts: (i) a volume equivalent to 10 mg powder and, (ii) a volume equivalent to 32 mg powder, for elemental and isotope analysis, respectively. Splits were transferred into 3 ml Teflon vials, their weights recorded, and placed on a hotplate at 150 °C with lids off to dry down. Samples were re-diluted in 0.2 ml 0.5 N HCl for isotope analysis, and the vial of samples for the concentration analysis were filled with 2 % HNO_3. The Teflon vials were placed on a hot plate with closed lids for at least a few hours to reflux. Vials were taken off the hot plate and cooled down. For trace element analysis, solutions were transferred into pre-washed and weighed 15 ml centrifuge tubes and diluted to 10 ml of 2 % HNO_3 (resulting a dilution factor of 1000). To measure the Li concentration of carbonate samples, standard addition method was used. To prepare samples for Li concentration analysis, two 15 ml centrifuge tubes were cleaned, labeled and weighed for each sample. Using a pipette, 0.5 ml of 2 % HNO_3 added to one tube followed by adding 1.5 ml of the sample solution with dilution factor of 1000, and then spiked with 1 ml of 7.5 ppb IRMM-016. The other tube was filled with 1.2 ml of 2 % HNO_3, 1.5 ml of the sample and 0.3 ml of 30 ppb internal standard solution (mixture of In, Re and Rh). The weight of each solution was recorded. To run samples on the ICP-MS, the un-spiked solution was analysed first following by the solution spiked with IRMM-016, so the difference in Li count rates between spiked and un-spiked solutions would account for the concentration of added Li, and was used to calculate the Li concentration of un-spiked solution. To measure the concentration of other elements, a series of matrix matched solutions were prepared in a way to cover the expected range of elements in the samples. The un-spiked solutions were used to measure the concentration of other elements in carbonate samples using matrix matched solutions as calibration solutions.

C.2.3. Column chromatography

C.2.3.1. Preparation of sample loader

Lithium was separated from the sample matrix for isotopic analysis, using 15 ml micro-columns (12.5 cm long, 4.7 mm outer and 3.2 mm inner diameters with 15 ml reservoir) filled with BIORAD AG 50W-x8 (200-400 mesh) broadly following the method of Misra and Froelich (2009). Resin was kept in the columns using PTFA frits with 3.2 mm thickness and 30 μm pore-size. To load samples into the columns a sample loader was needed. To prepare the sample loaders, 1 m of Tygon tubing was cut using a clean scalpel blade. One end of the Tygon tubing was attached to a 1 ml pipette tip. The pipette was set on 1 ml and ~5 ml of 2 % HNO_3 was drawn into the tubing. Then the tubing was rinsed with ~10 ml of DI. The tubing was cut into 6 cm pieces and placed in a clean bottle to wash the exterior of the tubing. Enough 2 % HNO_3 was added to the bottle to submerge

the tubing and left for an hour. Leaving the tubing with 2% HNO_3 longer than an hour was avoided, otherwise the tubing starts to react with the acid. The tubing was then rinsed with DI and left to dry. Finally, a 1 ml pipette tip (colourless tip) was attached to one end of each 6 cm tubing and stored to use for loading samples into the micro-columns.

C.2.3.2. Washing and conditioning columns

Prior to loading samples into the columns, if columns were filled with 0.5 N HCl, it was removed. To remove it, a transfer pipette was used after rinsing it with 0.5 N HCl. A small amount of 0.5 N HCl was left in the reservoir to avoid formation of air bubbles inside the columns. To wash the columns, the reservoir was filled with 6 N HCl and left to drain into a waste beaker. If any air bubbles formed in the column, they were removed using the sample loader tubing. The inside and outside of the sample loader tubing was rinsed with 0.5 N HCl before using it. Tips of the columns were also rinsed with 6 N HCl and 0.5 N HCl.

For back-washing and conditioning of the resin, a 125 ml bottle was prepared for each column which were filled with 0.5 N HCl and tips of the columns were submerged in the acid. A 1 ml pipette tip was attached to a pipette which was set on 1 ml. The outside of the pipette tip was rinsed with 0.5 N HCl. While the pipette lever was pushed down, the pipette tip was placed firmly into the column opening at the base of the reservoir. At the same time, a small amount of 0.5 N HCl was added to the reservoir to help make a seal between the pipette tip and the column. The lever was slowly released to create a vacuum in the pipette, helping the resin to rise and 0.5 N HCl to enter into the column from the bottle below. When the resin stopped moving upward, the pipette tip was slowly removed while the plunger was gently depressed to prevent liquid getting sucked into the pipette and touch the pipette filter. The resin and 0.5 N HCl were ejected into the reservoir. These later steps were repeated until the entire resin was transferred into the reservoir and the column was filled with 0.5 N HCl. The column was gently flicked to remove any air bubbles that were caught in the column frit. The 0.5 N HCl was left to drain into a waste beaker, and the inner walls of the reservoir were rinsed with 0.5 N HCl as most of the resin settled in the column. Then the reservoir was filled with 0.5 N HCl to drain into the waste beaker. To condition the resin, another 15 ml of 0.5 N HCl was added before the back-washed 0.5 N HCl was completely drained out of the columns. The 125 ml bottles of 0.5 N HCl were placed under the columns and condition solutions were left to drain into the bottles overnight. This way, the tips of the columns would not dry out.

C.2.3.3. Loading samples and elution

Tips of the columns were rinsed with 6 N HCl and 0.5 N HCl, and the respective containers to collect the pre-aliquot were placed under the columns. The pipette was set to 250 µl and a sample loader tubing was attached to it. The inside and outside of the sample loader were rinsed 3 times with 0.5 N HCl. Sample solution was drawn from the digestion Teflon vial into the sample loader and inserted into the column, above the resin bed. The pipette plunger was slowly pushed while the pipette was simultaneously being raised to keep the sample loader tip just above the top of the liquid. The sample loader

was disposed of, and the solution was let to fully flow into the resin. A new sample loader was attached to the pipette and 300 µl of 0.5 N HCl was loaded into the columns the same way as the sample was loaded (the first rinse). The 0.5 N HCl was let to drain fully to rinse the sample residue from the walls of columns into the resin. This later step was repeated with a new sample loader (the second rinse). A third clean sample loader was used to fill column with 800 µl of 0.5 N HCl following the same way as the first and second rinse, and then the reservoir was directly filled with 15 ml 0.5 N HCl to elute the sample.

When the pre-aliquot container was filled with 3.5 g of eluant the peak vial replaced it; 15 ml Teflon vials dedicated for carbonates were used to collect Li. Lithium was separated by collecting the next 5 g of eluant draining off the columns. The rest of the eluant (~4 g) was collected as the post-aliquot. Weights of collected aliquots and their containers were recorded. To prepare the collected Li for isotope analysis, the solution was dried on hot plate at ~125 °C and re-diluted in 0.3 ml of 2 % HNO_3 and left to reflux for ~ 1 hour at ~125 °C. The vial was taken off the hot plate and, after cooling, the solution was transferred into a pre-cleaned and weighed 15 ml centrifuge tube. This latter step was repeated with another 0.3 ml of 2 % HNO_3 to rinse the samples from the Teflon vial. The required 2 % HNO_3 volume to dilute samples to 1 or 2 ppb Li (i.e., depending on the required volume for the Li-isotopes analysis and the initial Li concentration of carbonate samples) was calculated and added to the 15 ml tubes. The centrifuge tube was shaken and weighed before the isotope analysis.

C.3. Cleaning Teflon ware

To clean Teflon vials and beakers, the following method was used. Vials were rinsed with DI first and any remaining material was removed using Kimwipes. However, toward the end of this thesis, lab protocols were changed and using Kimwipe was banned in clean labs due to contaminating clean labs with some trace metals (other than Li). Hence, Kimwipes were replaced with clean labs cloth wipes. Vials were then rinsed with DI again and ~ 2 to 5 ml of 6 N HCl was added to each vial with lids on. Vials were placed on a hot plate at ~125 °C to reflux overnight. The 6 N HCl was discarded and the vials were rinsed with DI at least 3 times. This latter step was repeated with ~ 2 to 5 ml of 7 N HNO_3. Vials and lids were placed on hot plate to dry at ~125 °C for ~ 15 minutes. The cleaned and dried vials were stored in clean Ziplock bags for re-use.

Appendix D: Supplementary Tables

This appendix contains:

D.1 Supplementary Tables for Chapter 3

D.2 Supplementary Tables for Chapter 4

D.3 Supplementary Tables for Chapter 5